TESIS DE LA UNIVERSIDAD DE ZARAGOZA
2021
146

Natalia Martín Hernández

The use of long-term high.spatial resolution Normalized Difference vegetation Index (NDVI) to determine different environmental processes in Spain

Director/es
Vicente Serrano, Sergio Martín
Beguería Portugués, Santiago

ISSN 2254-7606

Prensas de la Universidad
Universidad Zaragoza

ISSN 2254-7606

Universidad Zaragoza
1542

Tesis Doctoral

THE USE OF LONG-TERM HIGH.SPATIAL RESOLUTION NORMALIZED DIFFERENCE VEGETATION INDEX (NDVI) TO DETERMINE DIFFERENT ENVIRONMENTAL PROCESSES IN SPAIN

Autor

Natalia Martín Hernández

Director/es

Vicente Serrano, Sergio Martín
Beguería Portugués, Santiago

UNIVERSIDAD DE ZARAGOZA
Escuela de Doctorado

2019

The use of long-term high-spatial resolution Normalized Difference vegetation Index (NDVI) to determine different environmental processes in Spain

Autor/a:

Natalia Martín Hernández

Director/es:

Sergio Martín Vicente Serrano y Santiago Beguería Portugués

Universidad de Zaragoza

Facultad de Filosofía y Letras

Departamento de Geografía y Ordenación del Territorio

2018

Los directores de la tesis doctoral, el Dr. Sergio M. Vicente Serrano, Investigador Científico del Instituto Pirenaico de Ecología (Consejo Superior de Investigaciones Científicas) y el Dr. Santiago Beguería Portugués, Científico Titular de la Estación Experimental de Aula Dei (Consejo Superior de Investigaciones Científicas)

CERTIFICAN

Que la memoria titulada "*The use of long-term high-spatial resolution Normalized Difference vegetation Index (NDVI) to determine different environmental processes in Spain*" ha sido realizada bajo su dirección por Dª. Natalia Martín Hernández en el marco del Programa de Doctorado en Ordenación del Territorio y Medio Ambiente del Departamento de Geografía y Ordenación del Territorio de la Universidad de Zaragoza.

Y para que conste y en cumplimiento de la normativa vigente, firman el presente informe en Zaragoza, a 29 de Noviembre de 2018.

Fdo. Dr. Sergio M. Vicente Serrano Fdo. Dr. Santiago Beguería Portugués

A mis padres

Agradecimientos

En primer lugar, quiero agradecer a mi director de tesis Sergio M. Vicente Serrano del Instituto Pirenaico de Ecología (CSIC), que haya compartido sus conocimientos, sus ideas, su visión aplicada y consejos a futuro. También quiero agradecerle toda su ayuda, sobre todo en los momentos más difíciles. En segundo lugar, a mi codirector de tesis Santiago Beguería Portugués de la Estación Experimental de Aula Dei (CSIC) por sus explicaciones (sobre todo con R), por su visión metodológica, sus consejos constructivos, y toda su ayuda. A ambos, os agradezco todo lo aprendido tanto a nivel profesional como personal. Gracias también a José Carlos González Hidalgo, por su tutorización desde la Universidad de Zaragoza. Y gracias al Gobierno de Aragón por la concesión del Contrato Predoctoral de Personal Investigador en Formación (2014 – 2018), es decir, la beca DGA.

Quiero dar las gracias a todas las personas del Instituto Pirenaico de Ecología (CSIC), por hacerme sentir una más durante estos cuatro años. Gracias a las personas del grupo de investigación y de los otros grupos, por todo lo aprendido. Gracias a todas las personas que han contribuido de alguna manera en el desarrollo de esta tesis. A los del despacho 3 de la sede en Zaragoza: Javi, Fergus, Makki, Esteban, Marina, Paco, Fernando y demás compañeros que hemos coincidido días o años, a todos, mil gracias por trabajar juntos compartiendo risas. A todas y todos los "IPErinos y Auladeis" que he tenido la suerte de conocer, por los grandes momentos vividos. Y gracias especialmente a Ana y a Miquel.

También quiero dar las gracias a las personas que he conocido durante las estancias de investigación por su acogida. De los quince días en Toulouse (Francia), *je remercie Laurent, Manuela et Fabrice pour les réunions sur les méthodes et les résultats avec le café en main. Et Manuela, en plus, merci pour l'inoubliable dîner français avec de la nourriture asiatique, parlant en italien*.

De los tres meses en Lund (Suecia): *I want to thank Lars for those tutorials in which he began to draw before the technical words in English could hinder his explanation. To Hongxiao, Cai, Jonas and the other members of the Remote Sensing group for their help, meetings and field activities. To Tanya, Yanzi, Olive and Minchao for the shared laughter as ¡little potatoes! To Karlis, Kristiina and Guido for enjoying Scania excursions*.

También quiero hacer mención a aquellos "colegas" de profesión que he conocido o reencontrado en los congresos (EGU y RAQRS V, 2017). La oportunidad de hablar sobre conocimientos adquiridos y dudas compartidas, fue muy enriquecedora tanto a nivel personal como profesional. Gracias también a todas las mujeres científicas que he conocido estos años.

Gracias a mis masinas y masinos, por todos los momentos que seguimos sumando. A las viejas y nuevas amistades en Zaragoza. Eva, mil gracias. *A la meva gent de Barcelona, gràcies per totes les xerrades durant l'any 2017. A les "Geonenes i geonens", gràcies pels riures i les calçotades. També a l'Adry, l'Elena i en Sergio, perquè l'afecte (i la música) poden amb tot.*

Por último, agradezco a toda mi familia el apoyo y cariño recibido. A mi hermano y mi cuñada, por regalarme los dos momentos más felices de estos últimos cuatro años: la llegada de *mis sobris*. Quiero mencionar a mi *"tíoEmilio"* y decirle ¡viva la Geografía! Dar infinitas gracias a mis padres, por creer en mí siempre y ser mi mayor apoyo. A mi otra familia, agradezco todo el cariño a pesar de las dificultades que nos han acompañado estos años. Y a mi pareja, mil gracias por las fuerzas, los abrazos, por todo.

Abstract

This doctoral thesis has processed the 1.1-km spatial resolution NOAA–AVHRR afternoon images available over the last three decades (1981 – 2015) to obtain a NDVI dataset for peninsular Spain and the Balearic Islands that is called Sp_1Km_NDVI. The method included calibration with post-launch calibration coefficients, geometric and topographic corrections, cloud removal, temporal filtering and semi-monthly composites by maximum NDVI-value. In addition, the thesis compared the new Sp_1km_NDVI dataset with other existing global NDVI datasets.

In order to assess the comparison, the Mann-Kendall and Theil-Sen statistics were used to calculate the slope and the significance of the NDVI trends, finding that the annual NDVI trends from the Sp_1km_NDVI product resemble the other three datasets (GIMMS3g, SMN and MODIS) and showing where the spatial patterns in seasonal NDVI trends are similar or not. In addition, the Sp_1km_NDVI dataset allowed achieving changes in the inter-annual variability of NDVI values at longer and continuous temporal coverage than MODIS and higher spatial resolution than GIMMS3g and SMN. The new dataset provided information about vegetation activity for climate change research in this part of the Mediterranean region, stressing the complex spatial changes in the NDVI as a consequence of different land intensification and extensification processes and illustrating a dominant positive NDVI trend over the study period.

The PhD thesis also studied links between tree-ring growth and gross primary production for a variety of forest types under different environmental conditions. The NOAA-AVHRR satellite imagery data were combined with dendrochronological records and climate data at a fine spatial resolution (1.1 km^2) to analyse the interannual variability of tree-ring growth and vegetation activity for different forest biomes from 1981 to 2015. Specifically, the links between the Normalized Difference Vegetation Index (NDVI) and tree-ring width indices (TRWi) and a variety of environmental conditions, represented by climatic variables (air temperature, precipitation, evapotranspiration and water balance), mean NDVI and elevation were assessed. The impact of these variables on tree growth was assessed by means of the Predictive Discriminant Analysis (PDA). Results reveal a general positive and significant relationship between inter-annual variability of the NDVI at a high spatial resolution (1.1 km^2) and tree-ring growth. Maximum correlations between NDVI and tree-ring growth were recorded when cumulative NDVI values were considered, in some cases covering long

time periods (6-10 months), suggesting that tree growth is mainly related to Gross Primary Production (GPP) at annual scale. The relationship between tree-ring growth and inter-annual variability of the NDVI, however, strongly varies between forest types and environmental conditions.

Finally, drought impacts on the NDVI were analysed since drought is one of the main natural hazards affecting vegetation activity in Spain, which causes important impacts on crops, noticeably decreases yield in crop lands, but it also affects forest growth and the frequency of forest fires. This thesis determined possible differences in the sensitivity to drought determined by the presence of different land cover types and climate conditions and analysed the drought time scales at which vegetation activity is responding to drought severity. The results have showed that in large areas of Spain the vegetation activity is strongly determined by the interannual variations of drought. During the summer dry season, more than 90% of land areas show significant positive correlations between the NDVI and drought. Nevertheless, there are important seasonal and spatial differences in which the land cover and aridity conditions play an important role. The thesis also found that the time scale at which drought is measured is very relevant to understand the different seasonal impacts and it informs on the different seasonal and land cover differences in the NDVI sensitivity to drought.

Resumen

En esta tesis doctoral se han procesado imágenes de los satélites NOAA-AVHRR de 1,1 km de resolución espacial, disponibles durante las últimas tres décadas (1981 - 2015) para obtener una base de datos del índice de vegetación NDVI, para la España peninsular y las Islas Baleares, llamada Sp_1Km_NDVI. El método incluye la calibración de la información con los coeficientes calibrados posteriores al lanzamiento de cada satélite, correcciones geométricas y topográficas, una eliminación de nubes, el filtrado temporal de las series y la obtención de compuestos quincenales mediante el valor máximo del índice NDVI de las imágenes. Además, la tesis compara la nueva base de datos Sp_1km_NDVI con otras bases de datos existentes.

Para llevar a cabo la comparación, se han utilizado métodos estadísticos como el análisis de la significación de tendencias mediante el test de Mann-Kendall y la magnitud de cambio mediante la regresión de Theil-sen. Se ha comprobado que las tendencias anuales del producto Sp_1km_NDVI se asemejan a las de los otros tres conjuntos de datos (GIMMS3g, SMN y MODIS). Se ha analizado si los patrones espaciales de las tendencias estacionales son similares o no. Además, el conjunto de datos SP_1km_NDVI permite visualizar los cambios en la variabilidad interanual de los valores de NDVI a una cobertura temporal más larga y continua que la base de datos MODIS y a una resolución espacial más alta que los productos GIMMS3g y SMN. La nueva base de datos proporciona información sobre la actividad de la vegetación, útil para investigar los procesos de cambio climático en esta región mediterránea, mostrando los complejos cambios espaciales en el NDVI como consecuencia de los diferentes procesos de intensificación y extensificación e identificando una tendencia positiva dominante del NDVI durante el periodo de estudio.

En el presente trabajo también se han estudiado los vínculos entre el crecimiento de los anillos de los árboles y la producción primaria bruta en distintos tipos de bosques, bajo diferentes condiciones ambientales. La base de datos satelital del índice NDVI se ha combinado con registros dendrocronológicos y datos climáticos para analizar la variabilidad interanual del crecimiento de los anillos de los árboles y la actividad vegetal en distintos biomas forestales desde 1981 y hasta 2015. Concretamente, se ha evaluado la relación entre el NDVI y los índices de anchura de los anillos de los árboles (TRWi), poniendo en relación los resultados con una variedad de condiciones ambientales, representadas por variables climáticas (temperatura del aire, precipitación, evapotranspiración y balance hídrico), el valor NDVI medio y la elevación. El impacto de estas variables en el crecimiento de los árboles se ha evaluado mediante un Análisis Discriminante. Los

resultados revelan la existencia de una relación positiva y significativa entre la variabilidad interanual del NDVI y el crecimiento de los anillos de los árboles. Cuando se han considerado los valores NDVI acumulados, en algunos casos cubriendo periodos largos de tiempo (6 – 10 meses), se han registrado las mayores correlaciones entre el NDVI y el crecimiento de los anillos de los árboles. Esto sugiere que el crecimiento de los árboles está relacionado principalmente con la Producción Primaria Bruta (PPB) a escala anual. Sin embargo, la relación entre el crecimiento de los anillos de los árboles y la variabilidad interanual del NDVI depende mucho del tipo de bosque y de las condiciones ambientales.

Finalmente, se han analizado los impactos de la sequía en el NDVI, ya que la sequía es uno de los principales riesgos naturales que afectan la actividad de la vegetación en España, lo que provoca importantes impactos en los cultivos, disminuye notablemente el rendimiento de las cosechas, y también afecta al crecimiento forestal y a la frecuencia de los incendios forestales. En esta parte de la tesis se han detectado diferencias en la sensibilidad de la vegetación a la sequía. Esa sensibilidad viene determinada por los distintos tipos de cubiertas vegetales y por las condiciones climáticas medias. Se han podido identificar los periodos en los que la actividad vegetal ha respondido a una mayor severidad de la sequía. Los resultados han demostrado que, en grandes áreas de la España peninsular, la actividad de la vegetación está fuertemente determinada por las variaciones interanuales de la sequía. De hecho, durante la estación estival, más del 90% de la superficie muestra correlaciones positivas significativas entre el NDVI y las condiciones de sequía. Sin embargo, existen importantes diferencias estacionales y espaciales en las que el tipo de cubierta y las condiciones de aridez juegan un papel importante. En esta tesis también se ha mostrado que la escala temporal a la que se mide la sequía es muy relevante para entender los diferentes impactos estacionales, e informa sobre la sensibilidad del NDVI a la sequía a nivel estacional y en diferentes coberturas vegetales.

Contents

List of figures

List of tables

List of abbreviations

NDVI	Normalized Difference Vegetation Index / *Índice de Vegetación de Diferencia Normalizada*
AVHRR	Advanced Very High Resolution Radiometer
NOAA	National Oceanic Atmospheric Administration
GIMMS3g	Global Inventory Monitoring and Mapping Studies
MODIS	Moderate Resolution Imaging Spectroradiometer
SMN	Smoothed NDVI
VHP	Vegetation Health Product
NASA	National Aeronautics and Space Administration
TRWi	Tree Ring Width index
PDA	Predictive Discriminant Analysis
GPP	Gross Primary Production / (PPB: *Producción Primaria Bruta)*
MEDOKADS	Mediterranean Extended Daily One-km Data Set
NPP	Net Primary Production
STAR	Center for Satellite Applications and Research
NESDIS	Environmental Satellite Data and Information Service
MVC	Maximum Value Composite
HRPT	High Resolution Picture Transmission
CREPAD	*Centro de Recepción, Proceso, Archivo y Distribución de Imágenes de Observación de la Tierra*
INTA	Spanish National Institute of Aerospace Technology
DN	Digital Numbers
TOA	Top of the Atmosphere
BFAST	Breaks For Additive Seasonal and Trend
SeaWiFS	Sea-viewing Wide Field-of-view Sensor
NCEP	National Center for Environmental Prediction
NCAR	National Center for Atmospheric Research
TOMS	Total Ozone Mapping Spectrometer
AOT	Aerosol Optical Thickness

1. Introduction

1.1. The use of remote sensing data to identify vegetation processes

Among the possible information sources to analyse in depth land-cover processes, earth observation data allows obtaining spatial and temporal information about dynamics and evolution of environmental variables. Different vegetation indices can be calculated with spectral radiometric information. On one hand, these indices are closely related to different vegetation features, while they can give indications on the trees' primary above-ground productivity on the other hand. Among all these indices, the most common is the Normalized Difference Vegetation Index (NDVI), which shows strong relationship with photosynthetically active radiation (Myneni *et al.*, 1995), the leaf area index (Baret and Guyot, 1991; Carlson and Ripley, 1997) and the total green biomass (Cihlar et al., 1991; Gutman, 1991; Tucker et al., 1983; Wylie et al., 2002). The NDVI has widely been used for several purposes, including the analysis of vegetation trends (Herrmann et al., 2005; Zhou et al., 2001) and their relationships with climate variability and droughts (Kogan, 1997; Vicente-Serrano, 2007).

The NDVI is related with net primary production (NPP) and several studies have used NDVI data as key input in NPP models (e.g., Nemani et al., 2003; Zhao and Running, 2010), but NDVI is not a direct metric of the NPP. What the NDVI really represents is the gross primary production (GPP); in other words the vegetation photosynthetic activity or the photosynthetically active radiation obtained by vegetation (Myneni *et al.*, 1995). Part of this energy obtained by vegetation is consumed in respiration processes, and the remaining is the NPP, which includes the primary and secondary growth but also the activity of the flowers, fruits, etc. The tree-ring growth can be considered a good summary of these variables (Grissino-Mayer and Fritts, 1997). Therefore, the NDVI can be employed to assess the possible links between primary production and secondary forest growth variability (Kaufmann et al., 2008; Vicente-Serrano et al., 2016; Pasho and Alla, 2015).

In Spain, different studies have used remote sensing imagery to assess possible changes on vegetation activity and other land cover processes. They have been based on high-spatial resolution images (e.g. Landsat) (Serra et al., 2008; Lasanta and Vicente-Serrano, 2012; Martinez del Castillo et al., 2015) but also low-spatial resolution images like NOAA-AVHRR (Alcaraz-Segura et al., 2010; Julien et al., 2011). The

main problem is that the studies based on high spatial resolution images cover small areas but the studies based on low spatial resolution images do not allow identifying in detail the processes given the coarse resolution of the data. For example, del Barrio et al. (2010) used 1 km MEDOKADS archive (Koslowsky et al., 2005), to analyse changes in the vegetation activity and rain use efficiency between 1989 and 2000. The same dataset was used by Stellmes et al. (2013) and Hill et al. (2008) between 1989 and 2004 to determine vegetation changes in Spain, but they only focussed on natural vegetated areas, determining processes related to the rural exodus and forest fires. The studies focusing on longer periods have been based on very coarse datasets. For example, Gouveia et al. (2016) analysed the evolution of the Normalized Difference Vegetation Index (NDVI) in the Iberian Peninsula from 1981 to 2012 but used data at $64km^2$ of spatial resolution obtained from the Global Inventory Modelling and Mapping Studies (GIMMS) dataset (Tucker *et al.*, 2005), which has not the necessary spatial details given the characteristic spatial complexity of the landscape and natural vegetation in this Mediterranean region.

The need of determining the changes in the land conditions over the whole Iberian Peninsula contrasts with the type of studies available that are partial from a spatial and temporal perspective. For this reason, this thesis considers necessary to use the available historical records of satellite imagery to determine long-term trends in the vegetation processes with the sufficient spatial resolution to detect changes in the complex Mediterranean region and the images from the Advanced Very High Resolution Radiometer (AVHRR) data from the National Oceanic and Atmospheric Administration (NOAA) polar-orbiting satellites are the longest and continuously available record to monitor vegetation since they are available from 1981 to the present. They have been widely used to retrieve NDVI and to develop vegetation activity databases (Gutman and Masek, 2012; Beck et al., 2011). This thesis has used the entire historical dataset of daily NOAA-AVHRR images available from 1981 over the peninsular Spain and the Balearic Islands to develop a NDVI dataset useful to assess different environmental processes: i) long-term vegetation activity trends, ii) the relationship between vegetation activity and tree-ring growth and iii) the impact of drought on vegetation activity.

1.2. Vegetation trends

The Mediterranean region is one of the main environmental hotspots for the twentieth-one century. The climate models predict strong changes in the climate characterised by the decrease of precipitation and the

strong increase of temperature (Giorgi and Lionello, 2008), being Spain one of the most affected areas. These changes are expected to have strong influence on hydrological processes and the availability of water resources in the region (García-Ruiz *et al.*, 2011). Moreover, climate processes have already been observed during the last decades in the region, which were characterised by increased temperatures (Gonzalez-Hidalgo *et al.*, 2016), decreased relative humidity (Vicente-Serrano *et al.*, 2014a) and strong increase of the atmospheric evaporative demand (Vicente-Serrano *et al.*, 2014c).

In addition to climate processes, really the most relevant environmental modification in Spain is related to the land cover change. In Spain there are very rapid and generalized land cover change processes (Hill *et al.*, 2008). These processes are very diverse and are characterised to be the result of land extensification or intensification practices (Lasanta and Vicente-Serrano, 2012), but also biophysical factors play an important role (Serra *et al.*, 2008). The slopes of the Mediterranean mountains are characterised by a general abandonment during the twentieth century given the margination of the traditional economic activities and the general collapse of the mountain agriculture and livestock (Garcia-Ruiz and Lasanta-Martinez, 1990; García-Ruiz et al., 1996; Lasanta et al., 2017). These areas have been affected by strong revegetation processes, some of them given an intense policy of reforestation (Ortigosa *et al.*, 1990), but also as a consequence of the natural recolonization (Poyatos et al., 2003; Lasanta-Martínez et al., 2005; Lasanta and Vicente-Serrano, 2007), which was favoured by the low rates in the use of the territory. On the contrary, other regions have been affected by land intensification processes given the increase of urban and touristic areas (Gallardo and Martínez-Vega, 2016), but also by the agricultural changes, with the development of new irrigation polygons with the purpose of producing high added-valued agricultural products (Pinilla, 2006). In addition to extensification and intensification of land areas, in Spain there is strong complexity since there are also some processes, which are not clearly visible in the landscape but which are being observed using satellite imagery from earth observation systems. In some areas, land degradation processes are being recognised (del Barrio et al., 2010; Vicente-Serrano et al., 2012), in others, the loss of pasture lands in high elevations as a consequence of the advance of shrublands (Sanjuán *et al.*, 2018), the forest decline as a consequence of climate aridification and more frequent droughts (Camarero *et al.*, 2015), forest fires (Díaz-Delgado et al., 2002; Moreno et al., 2014; Viedma et al., 2015), changes in the type of cultivation as a consequence of the European Agrarian Policy (Lasanta and Marín-Yaseli, 2007), etc. Therefore, although

there are studies that have analysed recent land cover change processes in Spain, they are usually geographically partial (e.g., Lasanta and Vicente-Serrano, 2012), or they do not cover the variety of processes that are affecting the country, which are strongly complex (Serra et al., 2014; Martínez-Fernández et al., 2015).

1.3. Connection with tree-ring growth

Climate plays a paramount role, controlling the inter-annual variability of both gross primary production (GPP) and secondary growth of trees -secondary growth is the increase in the diameter of the roots, stems and branches, while primary growth consists of longitudinal growth- (Barber et al., 2000; Ciais et al., 2005; Nemani et al., 2003). Under a changing climate scenario, the impacts of climate extreme events (e.g. droughts, heat waves) on tree growth appear as a main concern. Numerous studies have confirmed climate influence on forest GPP (e.g. Granier et al., 2007; Zhao and Running, 2010) and their secondary growth as well (e.g. Camarero et al., 2015; Orwig and Abrams, 1997; Vicente-Serrano et al., 2014). Nevertheless, the response of vegetation activity, as regards GPP and secondary growth, to climate variability can differ significantly over contrasting forest biomes, as a function of regional-scale climate characteristics, land cover, topographical gradient, etc. (Bhuyan et al., 2017; Gazol et al., 2018; Montserrat-Martí et al., 2009; Tognetti et al., 2007).

Growth efficiency can differ among populations of the same species living under different climate conditions (Peguero-Pina *et al.*, 2007). For example, del Castillo et al. (2015) indicated that leaf activity and radial growth of the Aleppo pines have different response patterns to precipitation in eastern Spain. More recently, Gazol et al. (2018) confirmed that the resilience of forests to the occurrence of drought events in Spain is different considering the leaf activity or the tree-ring growth. As such, it is important to assess the possible links between climate determinants and both GPP and secondary tree growth. This assessment is also necessary for a better understanding of the influence of different projected scenarios of climate change on forest growth and productivity (Sánchez-Salguero *et al.*, 2017).

Nonetheless, as opposed to the long-term time-series of secondary growth of trees obtained using dendrochronological techniques (Grissino-Mayer and Fritts, 1997), long-term measurements of GPP are not widely available. This temporal inconsistency makes it difficult to directly assess the relationship between

GPP and secondary growth across different biomes. However, with the advancement in remote sensing instruments and techniques, vegetation information derived from different satellite platforms, which extends back to the early 1980s, can be a valuable resource as a reliable surrogate for GPP data of trees.

Several studies have already found positive and significant relationships between NDVI and radial secondary growth (tree-ring width) across different forest types worldwide (e.g. Alla et al., 2017; Coulthard et al., 2017; Leavitt et al., 2008; Liang et al., 2009; Lopatin et al., 2006; Malmström et al., 1997). Nonetheless, these relationships are complex and widely varies across different climate regions, forest types and biomes (Bhuyan et al., 2017; Gazol et al., 2018) and they are characterized by contrasting responses according to the period of the year in which NDVI is recorded and averaged (Vicente-Serrano *et al.,* 2016). According to Gough et al. (2008), the cumulative NDVI values over determined periods can be seen as better proxies of the total NPP, which strongly determines secondary growth.

The existing studies focusing on the links between NDVI and secondary growth are usually based on the Global Inventory Monitoring and Mapping Studies (GIMMS3g) dataset, which is the key reference for temporal homogeneity of NDVI data at global level (Pinzon and Tucker, 2014; Tucker et al., 2005). Nonetheless, the utility of the GIMMS3g NDVI is mainly constrained by its very low spatial resolution (ca. 8 km). While this low spatial resolution may not be critical in boreal homogeneous landscapes, given that the same forest typology can dominate over large areas, this resolution remains questionable in more heterogeneous areas, hindering the comparison between GIMMS3g NDVI and site tree-ring width series. These limitations increase as the complexity of the landscape does, such as the case of the Mediterranean-type ecosystems, where vegetation exhibits strong spatial heterogeneity. Over an individual pixel of the GIMMS3g (64 km^2), very different vegetation types with different local climate conditions may predominate, which makes the corresponding NDVI values less representative of those characterizing the forest of interest. Therefore, the global patterns of response of tree-ring growth to NDVI time-scales, described in Vicente-Serrano et al. (2016), cannot be completely representative of the highly-diverse Mediterranean region. For a better understanding of these underrepresented regions, the use of a high-spatial resolution NDVI dataset is preferable. This thesis analyses the relationships between NDVI and tree-ring width series, as reliable proxies of primary production and secondary growth, respectively. To accomplish this task, a very dense network of tree-ring width chronologies (n = 566 forests) is employed, covering 16

dominant forest tree species. This dataset is useful for understanding the diverse climatic and environmental conditions found across the peninsular Spain and the Balearic Islands.

1.4. Drought impacts on vegetation activity

Drought is one of the most relevant climate phenomena, which affect the interannual variability of the surface fluxes (Baldocchi et al., 2004; Fischer et al., 2007; Hirschi et al., 2011), including vegetation respiration (Ciais *et al.*, 2005), net primary production (Reichstein et al., 2007; Zhao and Running, 2010), primary and secondary forest growth (Allen *et al.*, 2015) and crop yield (Lobell et al., 2015; Asseng et al., 2015). Recent studies have suggested an increased impact of the drought events on vegetation, including increased forest mortality under different environmental conditions (Allen et al., 2010; Allen et al., 2015; Breshears et al., 2005), and the decrease of the vegetation activity with higher rates of tree decay (Carnicer et al., 2011; Restaino et al., 2016). Nevertheless, the analysis of the drought impacts on vegetation is usually difficult given low data availability. On the one hand, data on forest conditions and growth is very partial and restricted to small number of forests sampled by means of tree-ring (Grissino-Mayer and Fritts, 1997), or it does not have the necessary temporal frequency to assess drought impacts as happens for example with the official forest inventories, (Jenkins *et al.*, 2003). Crop data is also partial, aggregated to administrative levels and it does not provide information on the activity of the vegetation over different periods of the year, but usually only the annual yield (e.g., http://faostat.fao.org; https://quickstats.nass.usda.gov/#AF9A0104-19EF-3BFE-90D2-C67700892F3E). To solve these problems, a growing number of studies have analysed the impact of drought on vegetation by means of remote sensing data (Ji and Peters, 2003; Wan et al., 2004; Rhee et al., 2010; Zhao et al., 2017).

Remote sensing allows quantifying vegetation conditions given the different spectral response of the healthy and dry vegetation biomass since the electromagnetic signal received in the visible and near-infrared parts of the spectrum are different (Knipling, 1970). Given the available necessary spectral information recorded by sensors on board of different satellite platforms, it is possible to calculate vegetation indices (Tucker, 1979), which merge the spectral information obtained in different regions of the electromagnetic spectrum to determine vegetation conditions. Different studies have used vegetation indices to develop drought-related metrics (Kogan, 1997; Mu et al., 2013), but also to determine the effect of climate droughts on the vegetation

conditions (Vicente-Serrano et al., 2013; Zhang et al., 2017). In general, the results indicate that drought impacts can be well recorded by means of vegetation indices, identifying the complex influences that can be recorded as a function of the type of vegetation, the bioclimatic conditions, the severity of the drought events, etc. (Vicente-Serrano, 2007; Bhuiyan et al., 2006; Quiring and Ganesh, 2010; Ivits et al., 2014).

In Spain, drought is one of the most important natural hazards, which causes different impacts. As a consequence of the semiarid climate conditions that characterise a large part of the territory, Spain is highly vulnerable to drought events since precipitation shows a high interannual variability and the climate drought events are very frequent (Vicente-Serrano, 2006). Moreover, the increased atmospheric evaporative demand observed in the last decades (Vicente-Serrano *et al.*, 2014b), has caused an increase in the severity of droughts in comparison to the expected severity only related to precipitation deficits (Vicente-Serrano et al., 2014a; González-Hidalgo et al., 2018). Hydrological impacts of droughts are usually recorded, which are characterised by the decrease in streamflow and reservoir storages (Lorenzo-Lacruz et al., 2010; Lorenzo-Lacruz et al., 2013). Moreover, droughts cause important impacts on crops, noticeably decreasing yield in arable non-irrigated lands (Austin et al., 1998; Páscoa et al., 2017), but also compromising the water need of irrigated crops (Iglesias *et al.*, 2003), which show a high productivity and added economic value. Moreover, droughts strongly affect forest growth (Camarero et al., 2015; Gazol et al., 2018; Peña-Gallardo et al., 2018), and under the current rural abandonment and natural revegetation scenarios (Lasanta et al., 2017; Hill et al., 2008), the droughts driven the interannual variability and frequency of forests fires (Pausas, 2004; Pausas and Fernández-Muñoz, 2012).

Although drought is the main drivers of vegetation activity in Spain, there are not still studies covering the entire Spanish territory and a long time period to determine the possible differences in the impacts of drought on different land cover and vegetation types. Different studies have used remote sensing imagery and vegetation indices to analyse the spatial and temporal variability and trends in vegetation activity in Spain (Julien et al., 2011; Stellmes et al., 2013; del Barrio et al., 2010). Nevertheless, very few studies have related the temporal dynamic of the satellite-derived vegetation activity with climate variability and drought (e.g., Udelhoven et al., 2009; Vicente-Serrano et al., 2006; Gouveia et al., 2012; Mühlbauer et al., 2016). For example, González-Alonso and Casanova (1997) analysed the spatial distribution of droughts in 1994 and 1995 and showed that most affected areas coincided with those that received precipitation below the 75%.

García-Haro et al. (2014) analysed seven years of NDVI data obtained from MODIS satellite images, which was compared with the Standardized Precipitation Index (SPI) and showed important spatial differences in the response of the NDVI to the drought index. Vicente-Serrano (2007) and Contreras and Hunink (2015) analysed NDVI data in semiarid regions of northeast and south-east Spain, respectively, and showed important seasonal differences in the vegetation response to drought indices but also an important role of time scale of the drought indices. This thesis develops a complete analysis of the response of vegetation to drought using a long (1981-2015) and high spatial resolution (1.1 km^2) NDVI dataset over the whole peninsular Spain and Balearic Islands.

1.5. Objectives

The objectives of this study were related to the three main topics analysed but also to the development of the basic dataset to develop the different analysis:

i) to develop a high spatial resolution and long-temporal coverage NDVI dataset for Spain,

ii) to compare the developed NDVI dataset using other global widely used NDVI datasets that contain information at more coarse resolution or that cover shorter periods,

iii) to determine long term (1982-2014) NDVI trends over Spain and to know the land cover types that have experienced the most notable changes of vegetation activity.

iv) to determine the relationships between NDVI and tree-ring width for different tree species representing different forest biomes in Spain

v) to assess the relative contribution of tree species and environmental conditions to the different patterns of relationships observed between NDVI and tree-ring width.

vi) to determine possible differences in the sensitivity to drought determined by the presence of different land cover types and mean climate conditions and

vii) to know the drought time scales at which vegetation activity is responding to the drought severity.

2. Data and methods

This section describes the database obtained in this study and the steps taken to develop it, based on the processing of NOAA-AVHRR satellite images. The specific methodology used in each chapter is described in the corresponding sections.

2.1. Remote sensing datasets

The entire available record of daily afternoon passes from the NOAA-AVHRR satellites from 1981 to 2015 - more than 30 years- at the spatial resolution of 1.1 km at nadir were used. From this information a semi-monthly NDVI dataset was created after a careful procedure that includes the radiometric calibration, image georreferencing, cloud removal, etc. and that is detailed in depth below.

For comparison purposes three widely used NDVI datasets that are developed at different spatial resolutions and that cover different periods were used: the Global Inventory Modelling and Mapping Studies (GIMMS3g), the Smoothed NDVI (SMN) and the MODIS NDVI product called MOD13A3.

The GIMMS3g is the NDVI dataset most widely used worldwide. Several studies have analysed NDVI trends using this product in different regions and at the global scale (Beck et al., 2011). The dataset consists in semi-monthly maximum NDVI value composite images at 8-km of spatial resolution for the period 1981 – 2015 (that is the latest version of GIMMS NDVI3g product that was actualized until 2015, not the older version GIMMS NDVI). It has been corrected for cloud cover, atmospheric perturbations, sensor degradation, inter-satellite differences and solar and viewing angle effects due to satellite drift (Tucker et al., 2005, Pinzon and Tucker, 2014). Data is available at https://ecocast.arc.nasa.gov/data/pub/gimms/3g.v1/; last accessed October 2017.

The Smoothed Normalized Difference Vegetation Index (SMN) is a product used to obtain the Vegetation Health Product (VHP) by the NOAA. The images are re-processed datasets derived from AVHRR data in GAC (Global Area Coverage) format at a weekly time scale and at 4-km of spatial resolution. The SMN dataset is smoothed for cloud removal and adjusted using the Empirical Distribution Function (EDF) statistical technique in order to correct sensor degradation, satellite orbital drift and to reduce the possible effect of aerosols (Kogan *et al.*, 2011). This data is provided by the Center for Satellite Applications and Research (STAR) from the Environmental Satellite Data and Information Service (NESDIS) server

(https://www.star.nesdis.noaa.gov/smcd/emb/vci/VH/vh_ftp.php; last accessed October 2017). The SMN data contain weekly composites of seven Julian days, starting on Thursday and ending on Wednesday, nearly 52 weeks per year. The files between the 35th week of September 1981 to the 32th week of June 2015 were downloaded. The dataset contains five weekly gaps in the study period due to problems with the AVHRR platform or other measurement errors (Latifovic et al., 2012; Gutman and Masek, 2012). Due to the SMN data have weekly temporal resolution a monthly composites using a Maximum Composite NDVI rule were created (Holben, 1986).

MODIS satellites were launched in 2000 and provide daily images with a spatial resolution of 250 m. The MOD13A3.005 product has been used to provide monthly NDVI images with 1x1-km^2 spatial resolution (Huete *et al.*, 2002). These images were resampled from 1-km^2 to 1.1-km^2 to correspond with the database created for this thesis, (https://lpdaac.usgs.gov/dataset_discovery/modis/modis_products_table/mod13a3; last accessed October 2017).

2.2. Development of the NDVI dataset from the daily NOAA-AVHRR satellite imagery

The NOAA-AVHRR dataset used in this study contains daily images acquired by the AVHRR sensor on-board the polar-orbiting satellites NOAA-7-9-11-14-16-18 and -19. The images were captured during the afternoon passes of the satellite in an ascending mode. The historical daily NOAA-AVHRR dataset comprise more than 10,000 images spanning the period from July 1981 to June 2015 and covering the entire Iberian Peninsula and the Balearic Islands.

The images used in this study were acquired from different sources, including: the Dundee Satellite Reception Center (images from 1981 to 1986), the European Spatial Agency (images from 1986 to 1997), and by the High Resolution Picture Transmission (HRPT) antennae (images from 1998 onwards), located at the *Centro de Recepción, Proceso, Archivo y Distribución de Imágenes de Observación de la Tierra* (CREPAD) and coordinated by the Spanish National Institute of Aerospace Technology (INTA) in its Canaries Space Centre (Maspalomas, Gran Canaria). The dataset is obtained from approximately 2TB of information at the mentioned HRPT format. The processing routine for each daily image included the data import, the radiometric calibration, geometric and topographic corrections, cloud removal and NDVI calculation. The files had different formats from 1981 so the software developed allows to i) read all the

format files automatically and verify if each file is completed; ii) discard the files: if are damaged, if an image was acquired before 10:00 am or after 16:00 pm, if it is full of clouds or if it is affected of bad scan lines. Once the images were read and converted to a common format, the digital numbers (DNs) of the Channels 1 (Red) and 2 (Near infrared) were geocoded using control points, which are identified automatically (Baena-Calatrava, 2002). Control points correspond to 97 coast-line fragments and specific invariant locations from a good quality cloud-free image of the study area. The geocoding algorithm uses these fragments as a moving window looking for the higher correlation values in the image. Images were geocoded to a coordinate system ED50-UTM zone 30°N over an area bounded between 34°22'N and 44°12'N and 11°7'W and 4°16'E.

Geocoded Channels 1 and 2 DNs were transformed to top-of-the atmosphere reflectances. Following the recommendations by the NOAA User's Guide (http://noaasis.noaa.gov/NOAASIS/ml/calibration.html; last accessed November 2017), the coefficients proposed by Nagaraja Rao and Chen (1995) were used to calibrate the NOAA -7,-9 and -11 images and NOAA-14 was calibrated according to Rao and Chen (1999). NOAA-16, -18 and -19 images were calibrated according to the NOAA-KLM user's guide (https://www1.ncdc.noaa.gov/pub/data/satellite/publications/podguides/N-15%20thru%20N-19/pdf/0.0%20NOAA%20KLM%20Users%20Guide.pdf; last accessed 4th September 2018) and considering revised post-launch calibration coefficients available at: http://noaasis.noaa.gov/NOAASIS/ml/calibration.html; last accessed November 2017. The values of calibrated Channel 1 and 2 radiances (L) in W/(m^2 sr μm) were transformed to top-of-the-atmosphere reflectances ρTOA_λ, according to:

$$\rho TOA_\lambda = \frac{\pi \cdot Lsat_\lambda \cdot d^2}{ESUN_\lambda \cos\theta_s}$$

where ρTOA_λ is the TOA reflectance for band λ, d is the earth–sun distance in astronomical units, $ESUN_\lambda$ is the mean solar exoatmospheric irradiance for band λ, and θ_s is the solar zenith angle in degrees.

In addition, the thermal bands 4 and 5 were also calibrated since they were needed to remove the cloud coverage from each image. Details on the calibration and processing the thermal bands can be found at Azorin-Molina et al. (2013) and Khorchani et al. (2018). Clouds were removed using the algorithm developed by Azorin-Molina et al. (2013), which was fully validated for the atmospheric conditions of the

Iberian Peninsula and separates between cloud, snow-ice and clear ground pixels to compute the daily cloud masks. The pixels with observation angles higher than 50º were removed to avoid any geometric and radiometric problems related to the view angle of the satellites since high observation angles tend to reduce the NDVI values (Gutman, 1991).

Between 1981 and 2015 the channels 1 and 2 of the AVHRR sensors on board of the different NOAA satellites have slightly different spectral response functions, which may have an impact on the obtained top-of-the-atmosphere reflectances. To diminish this problem, the procedure described in Trishchenko et al. (2002) and Trishchenko (2009) was used to normalize the TOA reflectance in the Channel 1 and Channel 2 obtained by the different satellites to the NOAA-9 satellite. Finally, before NDVI calculation, a topographic correction was applied to each image using a Digital Elevation Model (DEM) at the resolution of 1.1 km to correct the effects of lighting on the ground by means of a non-lambertian model (Riaño *et al.*, 2003). The NDVI was obtained from topographically corrected TOA reflectances in Channels 1 and 2:

$$NDVI = \frac{\rho_2 - \rho_1}{\rho_2 + \rho_1}$$

where ρ_2 and ρ_1 are the reflectance values for bands 2 and 1.

Daily NDVI images were composited in semi-monthly periods (two per each month: from 1st day of the month to the 15th, and from 16th to the end of the month) using the maximum NDVI recorded in the period, with the aim of reducing uncertainty (Holben, 1986; Latifovic et al., 2005).

To fill gaps in the series, which can be originated from clouds and large observation, a linear regression model was used, considering the NDVI values before and after each gap as predictors. This procedure was applied iteratively to account for all gaps existing in the series. Then, in order to reduce residual noise presented in the series, data of each series was filtered following Quarmby et al. (1993):

NDVI = Max{NDVI(n),(NDVI(n-1)+NDVI(n+1))/2}

According to this approach, only low NDVI values are filtered, given that high values are less affected by atmospheric contamination and residual noise (Gutman, 1991).

After processing the entire semi-monthly complete NDVI dataset over the Iberian Peninsula, a temporal inhomogeneity in the semi-monthly NDVI time-series was found using the Breaks For Additive Seasonal and Trend (BFAST) method (Verbesselt *et al.*, 2010), coinciding with the change between the AVHRR/2

and AVHRR/3 instruments (Figure 1). The same problem was identified by Pinzon and Tucker (2014) for the GIMMS3g dataset, and was caused by the existence of two different AVHRR sensors: the AVHRR/2 instrument that spans July 1981 to November 2000 and the AVHRR/3 instrument from November 2000 to the present. Latifovic et al. (2012) also stressed the differences between the AVHRR/2 and AVHRR/3 measurements that must be corrected.

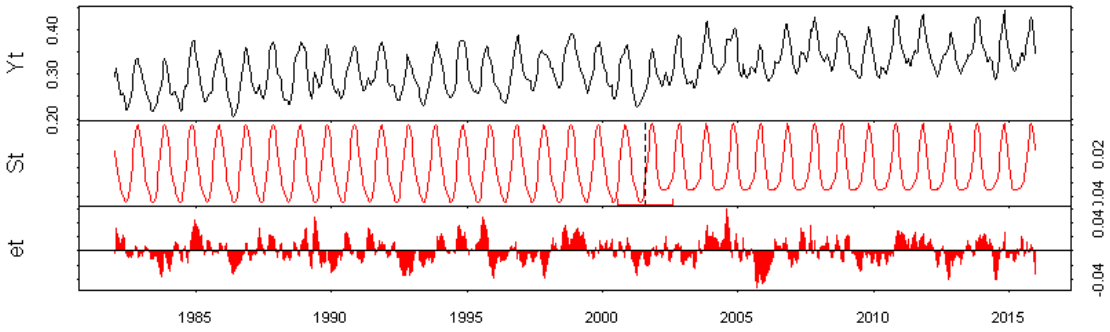

Figure 1: Average evolution of the semi-monthly NDVI for Spain decomposed in trend, seasonality and residual components using BFAST method.

Pinzon and Tucker (2014) developed a methodology to correct this problem by means of images of the SeaWIFS satellite. They obtained pixel-per-pixel coefficients of correction coefficients and applied them to correct the GIMMS3g dataset from 2000. This approach could not be applied here to correct the NDVI dataset since the SeaWIFS data was not available. To solve the problem it was assumed that the existing inhomogeneity problems between the AVHRR/2 and AVHRR/3 instruments sensors are systematic and affect equally to the entire images, independently of the land cover type. Therefore, the average ratio between the average semi-monthly series of the developed NDVI dataset and the average semi-monthly series of the GIMMS3g $NDVI_{3g}$ dataset between 2000 and 2015 were calculated over the whole peninsular Spain and Balearic Islands and used the average semi-monthly coefficients to correct the entire images. Figure 2 shows the average GIMMS3g and the average NDVI series developed for the territory before and after the correction. The dataset developed in this study has been called Sp_1km_NDVI and it has been compared with other global NDVI datasets before its use to analyse NDVI trends across the peninsular Spain and Balearic Islands.

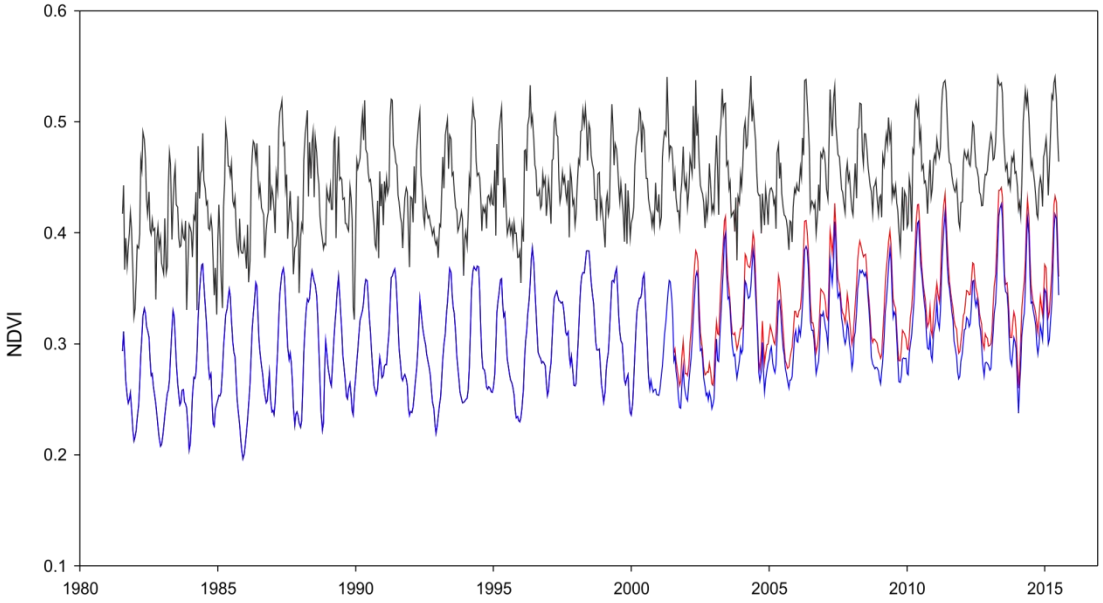

Figure 2: Evolution of the semi-montlhy GIMMS3g dataset (black), the original inhomogeneous developed semi-monthly NDVI (red) and the homogeneous Sp_1km_NDVI (blue)

2.3. Comparison with other NDVI datasets

In order to compare the Sp_1km_NDVI dataset with the other three products, the Sp_1km_NDVI dataset was adapted to different spatial and temporal resolutions to match with the spatial or temporal resolution of the other products. First the 1.1-km^2 Sp_1km_NDVI was resampled to 4-km^2 and 8-km^2 with the purpose of being compared with SMN and GIMMS3g datasets, respectively. The first images captured by the AVHRR/2 sensor begin in July 1981 and the images from the AVHRR/3 sensor were processed until June 2015. To make the comparison between the Sp_1km_NDVI dataset and the GIMMS3g and SMN datasets, the analyses has been done over the entire years, from 1982 to 2014. The monthly MODIS NDVI product was resampled from 1-km^2 to 1.1-km^2 to match with the Sp_1km_NDVI dataset and the decade from 2004 to 2014 selected for comparisons. The spatial comparisons were based on the annual and seasonal scales (Winter: DJF, Spring: MAM, Summer: JJA, Autumn: SON). Pearson's r correlation was used for the comparisons between the average regional series of the four datasets but also the pixel-per-pixel correlations at the different spatial resolutions.

The signification of the observed trends during the different periods of analysis was also compared. For this purpose a modified Mann–Kendall trend test was used, which returns the corrected p values after accounting

for temporal pseudoreplication (Hamed and Rao, 1998). Significant trends were set at p-value < 0.05. To determine the magnitude of the trends the Theil-Sen slope estimator was used.

2.4. Spatial patterns of average NDVI

Figure 3 show the seasonal and annual NDVI averages obtained from the four NDVI datasets for the corresponding temporal periods. The averages are adapted from the Sp_1km_NDVI dataset for the different periods and spatial resolutions of the other datasets and the results show high agreement with the GIMMS3g, SMN and MODIS data. Although using the same spatial resolution that the GIMMS3g and SMN, the Sp_1km_NDVI shows a lower spatial filtering and allows to identify more details at the local scale than the other two datasets. On the contrary, at the 1,1-km spatial resolution the spatial detail of the average values is similar to that observed with MODIS. All the maps show the highest NDVI values in the northwest of the peninsular Spain and these values decrease towards the southeast part. Seasonally, each pair of maps also shows a similar variability in the NDVI. For example, on spring there is an increase in the NDVI values in the western half of the peninsular Spain and on summer, there are a general decrease of the NDVI in the south.

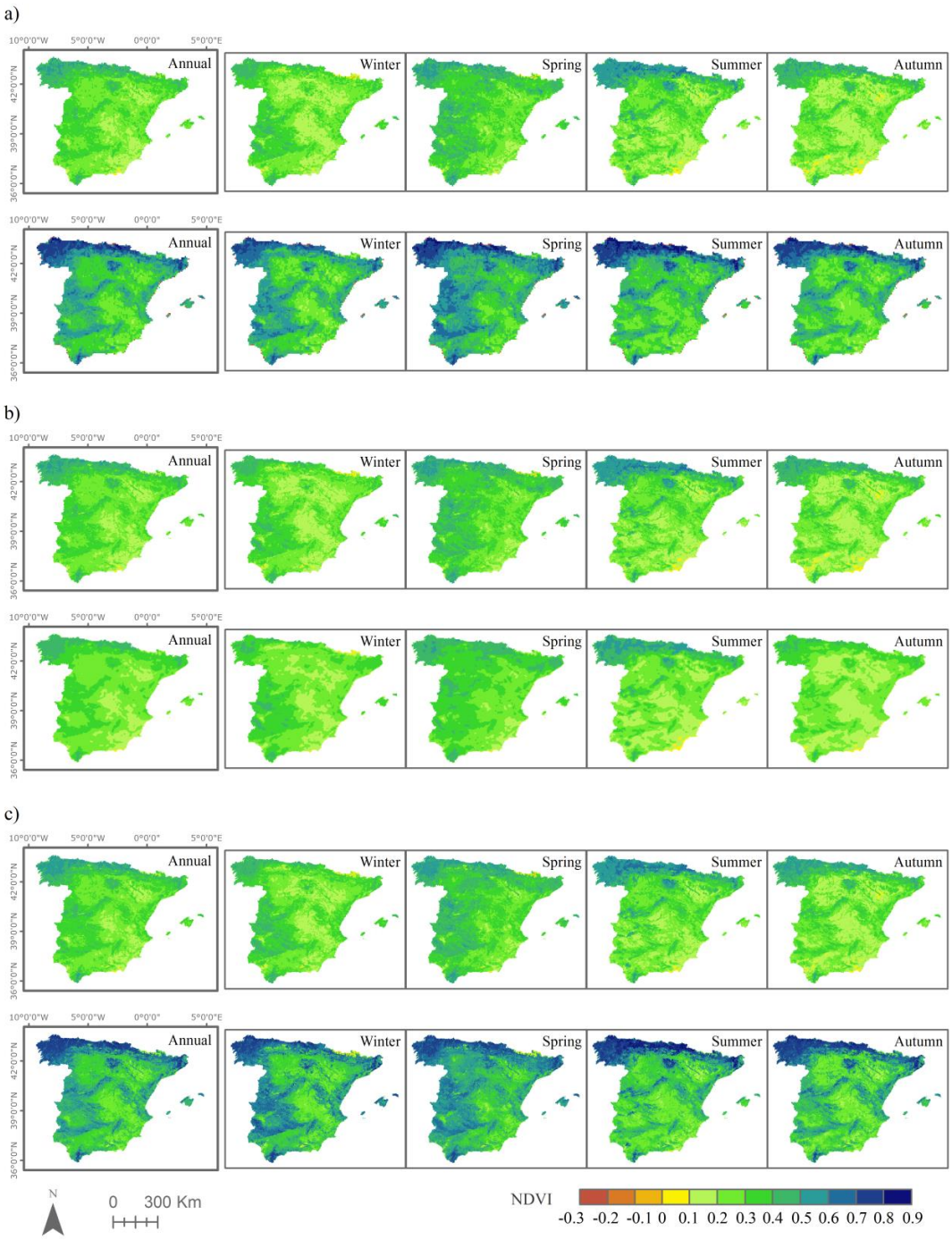

Figure 3: Spatial distribution of the average seasonal and annual Sp_1km_NDVI in comparison to the 8 km^2 1982-2014 GIMMS3g (a), 4 km^2 SMN 1982-2014 (b) and 1 km^2 2004-2014 MODIS. The original 1.1 km^2 spatial resolution of the Sp_1km_NDVI was resampled to the spatial resolution of the other datasets.

Figure 4 shows different scatterplots representing the relationship between the average values of the Sp_1km_NDVI and the three other NDVI datasets. All these plots show a strong positive relationship between the average NDVI values from the developed Sp_1km_NDVI dataset and the GIMMS3g, SMN and MODIS seasonal and annual average values. With the exception of the GIMMS3g dataset in spring, the

correlations are higher than 0.8, and even higher than 0.9 considering the SMN and the MODIS datasets. The magnitude of the NDVI values is similar between the SMN and the Sp_1km_NDVI but NDVI values tend to be higher with the GIMMS3g and the MODIS datasets. The difference tends to be higher for the high NDVI values but in all of the cases the relationship is clearly linear.

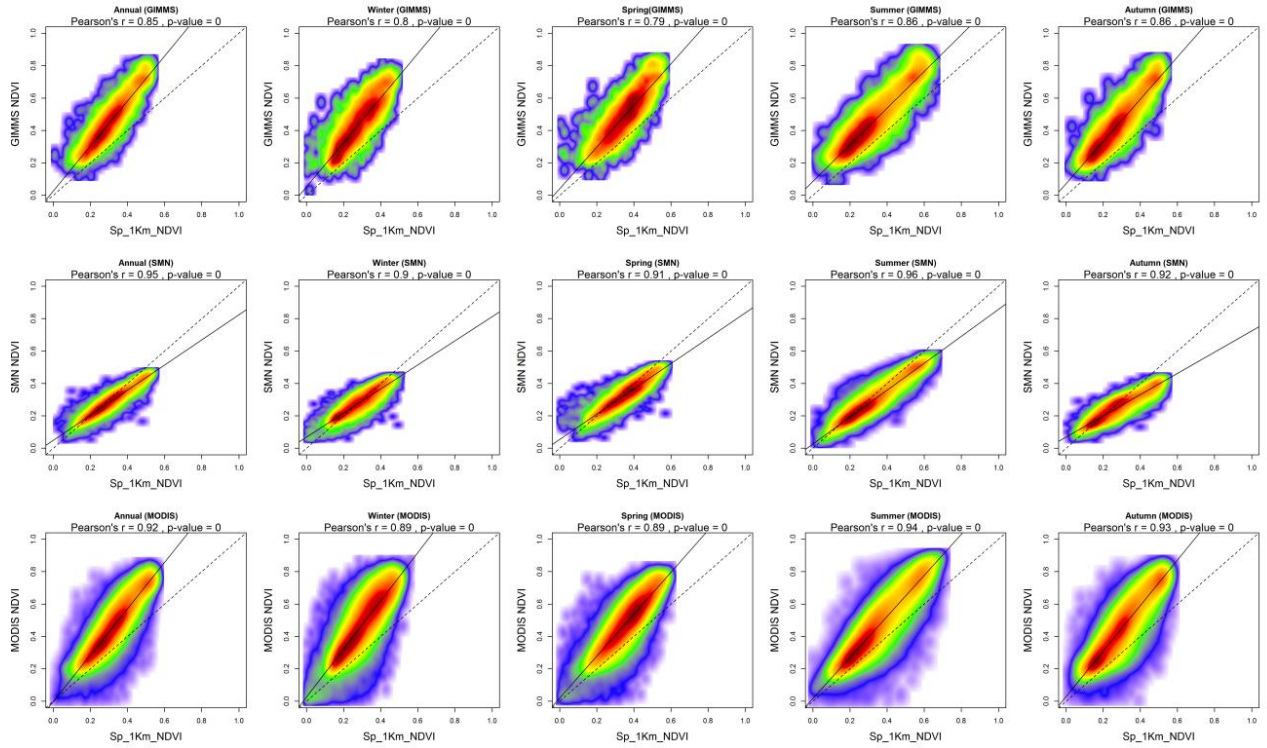

Figure 4: Relationship between average annual and seasonal NDVI obtained with the Sp_1km_NDVI and the other three datasets. Upper row represents the relationship between Sp_1km_NDVI and GIMMS3g3g, the middle row between Sp_1km_NDVI and SMN and the bottom line between Sp_1km_NDVI and MODIS. The colors represent the density of points: red shows high density and blue low density. Given the high number of points the significance of correlation was obtained by means of 1000 random samples of 30 cases from which correlations and p-values were obtained. The final significance was assessed by means of the average of the obtained p-values.

2.5. Comparison of the temporal evolution of the different NDVI datasets

Figure 5 shows the average evolution of the NDVI series from the developed Sp_1km_NDVI and the other three NDVI datasets for the whole peninsular Spain and Balearic Islands. The series are showed at the semi-monthly temporal scale to be compared with the available temporal resolution of the GIMMS3g dataset and the monthly resolution to match with SMN and MODIS NDVI. The different series reproduce well the expected annual cycles of vegetation activity in Spain, and some recent years characterised by low vegetation activity as a consequence of drought events are clearly recorded in the different datasets (e.g., 1995, 2005 and 2012).

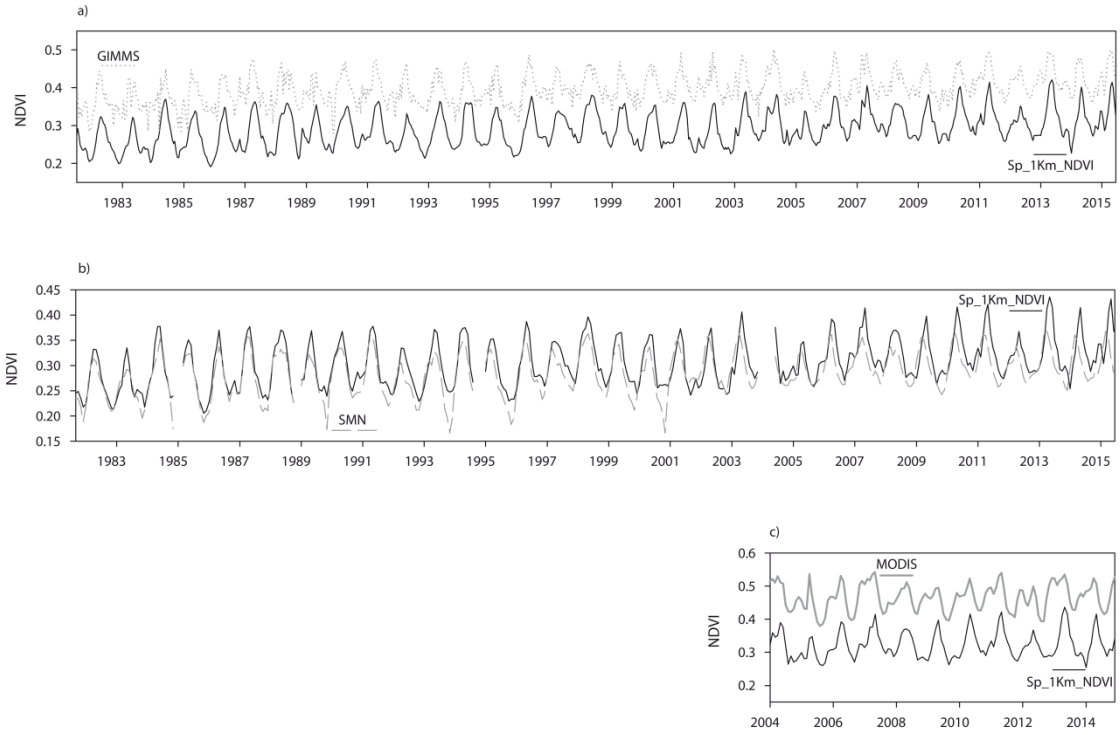

Figure 5: Average NDVI time series for Spain for a) semi-monthly Sp_1km_NDVI and GIMMS3g, b) monthly Sp_1km_NDVI and SMN and c) monthly Sp_1km_NDVI and MODIS.

The correlation among the series is statistically significant between the different datasets. The Pearson's r correlations between the Sp_1km_NDVI and the GIMMS3g, SMN and MODIS are 0.84, 0.85 and 0.67, respectively. The correlation between GIMMS3g and SMN and MODIS is 0.84 and 0.69, respectively, and finally, the correlation between SMN and MODIS is 0.69. These strong correlations are not determined by the strong seasonality of the NDVI series since there is a strong agreement between the seasonal and annual series of the different datasets (Figure 6; Table 1).

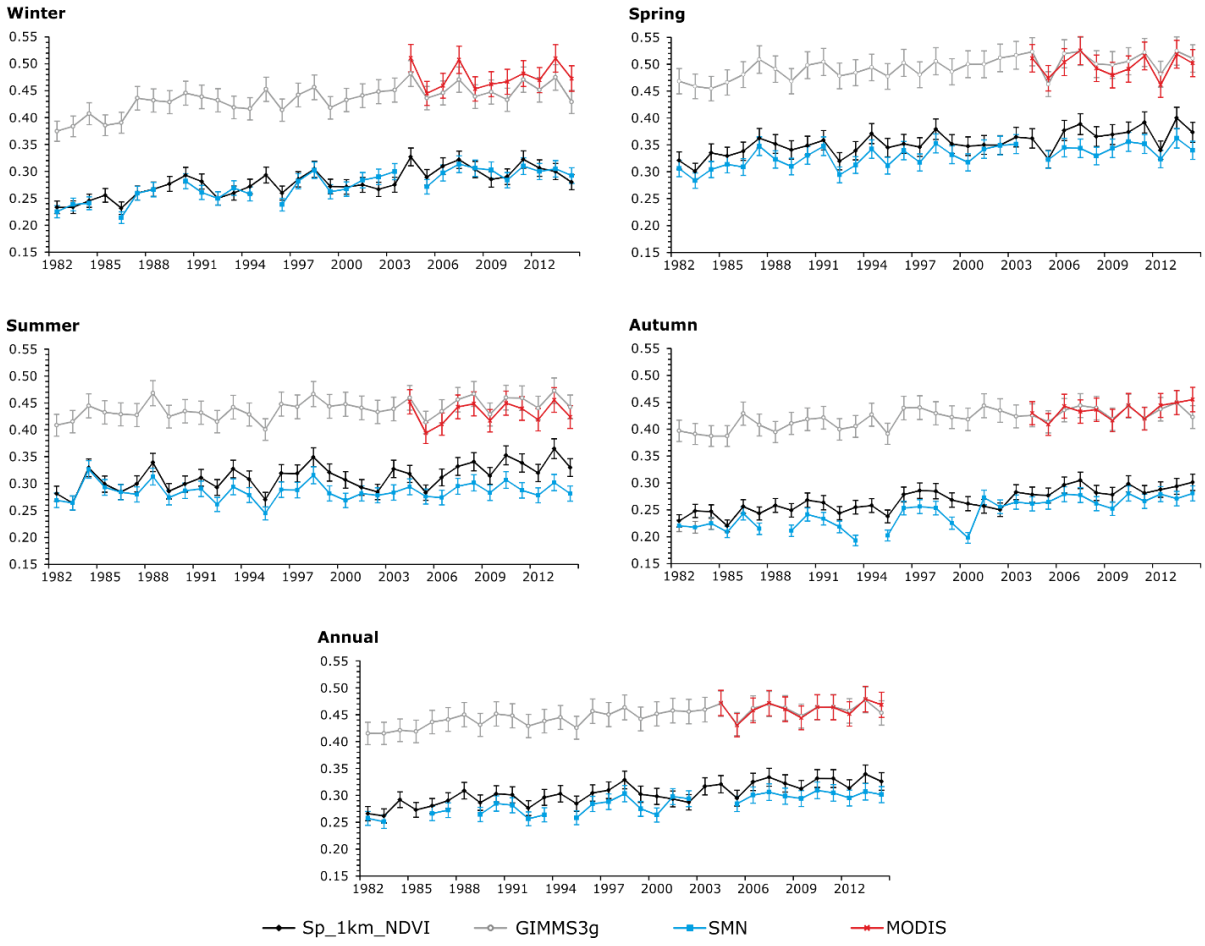

Figure 6: Seasonal and annual averages and standard deviation NDVI values from the four datasets (Sp_1km_NDVI, GIMMS3g, SMN and MODIS).

Table 1: Temporal correlation between the seasonal and annual average NDVI series obtained from the different datasets. All correlations are statistically significant at $p < 0.05$.

	Winter	Spring	Summer	Autumn	Annual
Sp_1km_NDVI vs. GIMMS3g	0.87	0.86	0.89	0.76	0.89
Sp_1km_NDVI vs. SMN	0.89	0.87	0.76	0.82	0.89
Sp_1km_NDVI vs. MODIS	0.58	0.83	0.85	0.73	0.91
GIMMS3g vs. SMN	0.89	0.87	0.78	0.78	0.90
GIMMS3g vs. MODIS	0.85	0.90	0.97	0.66	0.92
SMN vs. MODIS	0.62	0.70	0.90	0.72	0.91

Temporal correlation between the different datasets show some spatial differences (Figure 7) although with very few exceptions, the correlations are high and statistically significant between the different seasonal and annual NDVI values obtained with the Sp_1km_NDVI and the other three different datasets.

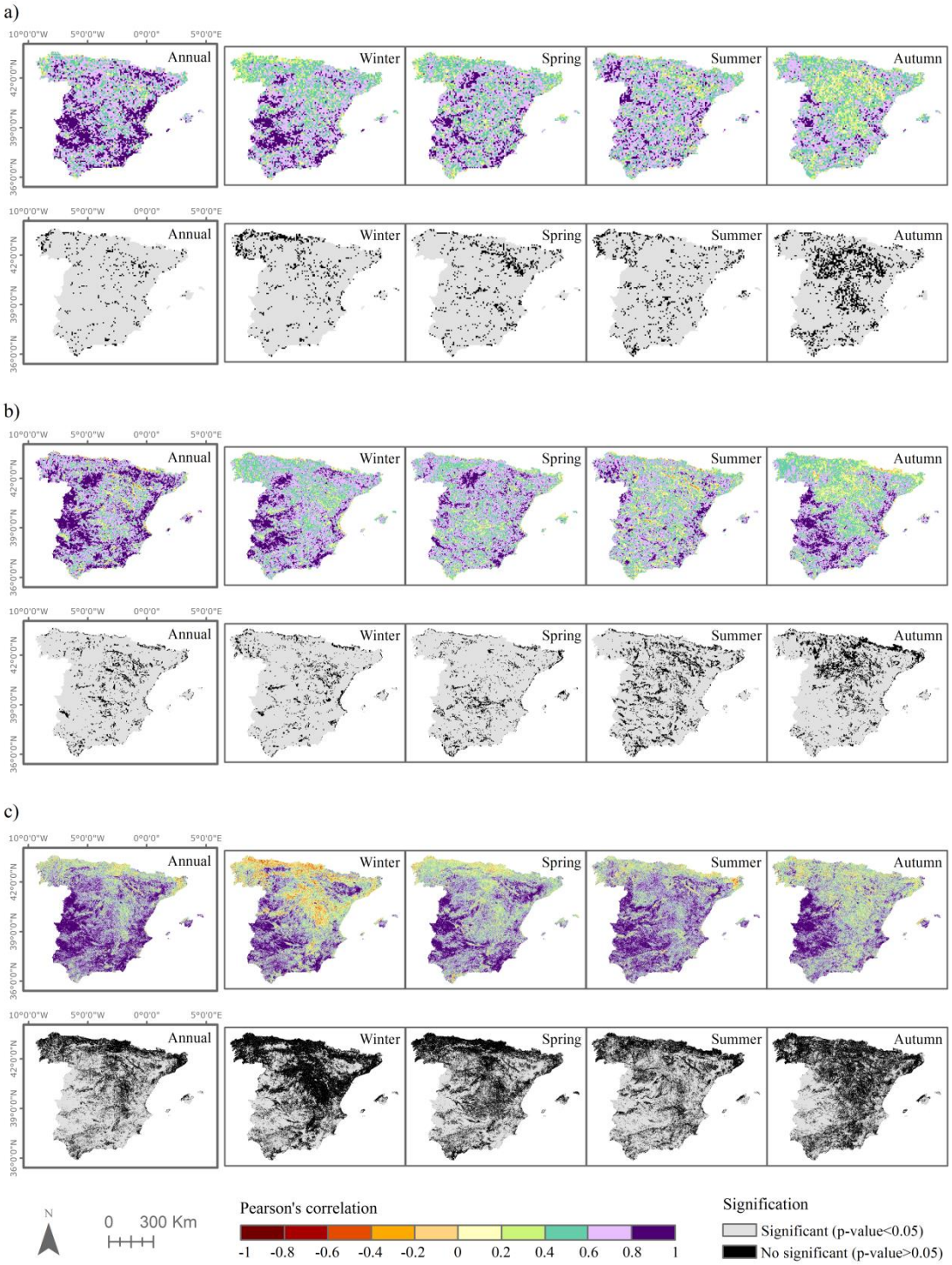

Figure 7: Spatial distribution of the annual and seasonal Pearson's r correlation between Sp_1km_NDVI and 8 km^2 GIMMS3g dataset for 1982-2014 (a), 4 km^2 SMN 1982-2014 (b) and 1 km^2 2004-2014 MODIS (c). The original 1.1 km^2 spatial resolution of the Sp_1km_NDVI was resampled to the spatial resolution of the other datasets by means of an average algorithm. The statistical significance of the Pearson's r correlation is shown for each dataset.

The GIMMS3g dataset seasonal correlations tend to be higher than 0.6 and at the annual scale they are higher than 0.8 in large areas of Spain (See also Supplementary Figure 1). Similar patterns are obtained in comparison with the SMN dataset, although in summer the correlations decrease noticeably showing large

areas of Spain characterised by non-significant correlations. This pattern is also identified in central and norther areas in autumn. With MODIS NDVI, correlations tend to be higher than with the other two datasets, but given the shorter temporal sample, the percentage of areas showing significant correlations decreases.

Figure 8 shows the comparison of the spatial distribution of the NDVI changes obtained from the Sp_1km_NDVI and the other three NDVI datasets. Comparison of the trends refers to the common periods and the corresponding spatial resolutions. In relation to the GIMMS3g dataset, the spatial patterns of the NDVI changes at the annual scale identified with the Sp_1km_NDVI show the main increases in areas of northeast, coinciding with the development of some irrigated lands. This is not well reproduced with the GIMMS3g dataset. On the contrary, the main NDVI decrease recorded in areas of southwest and southest are recorded in both datasets. The strong decrease recorded in the Guadalquivir valley (Southwest) in spring is well recorded by the two datasets but also the decrease observed in some areas of the central Spain in summer. Nevertheless, the strong NDVI increase identified in summer in areas of northeast given replacement of drylands by highly active irrigated crops in summer is not recorded by the GIMMS3g dataset. The comparison of the NDVI changes with the SMN dataset show more differences than the obtained with GIMMS3g NDVI. The NDVI changes are more pronounced with the SMN dataset in the different seasons and at the annual scale. Finally, the comparison of the NDVI trends between the Sp_1km_NDVI and the MODIS NDVI shows some similarities in the spatial patterns of the NDVI changes, but also strong differences in the magnitude of these changes across peninsular Spain and Balearic Islands. These spatial differences explain why the spatial agreement of the NDVI magnitude of change is not high among datasets.

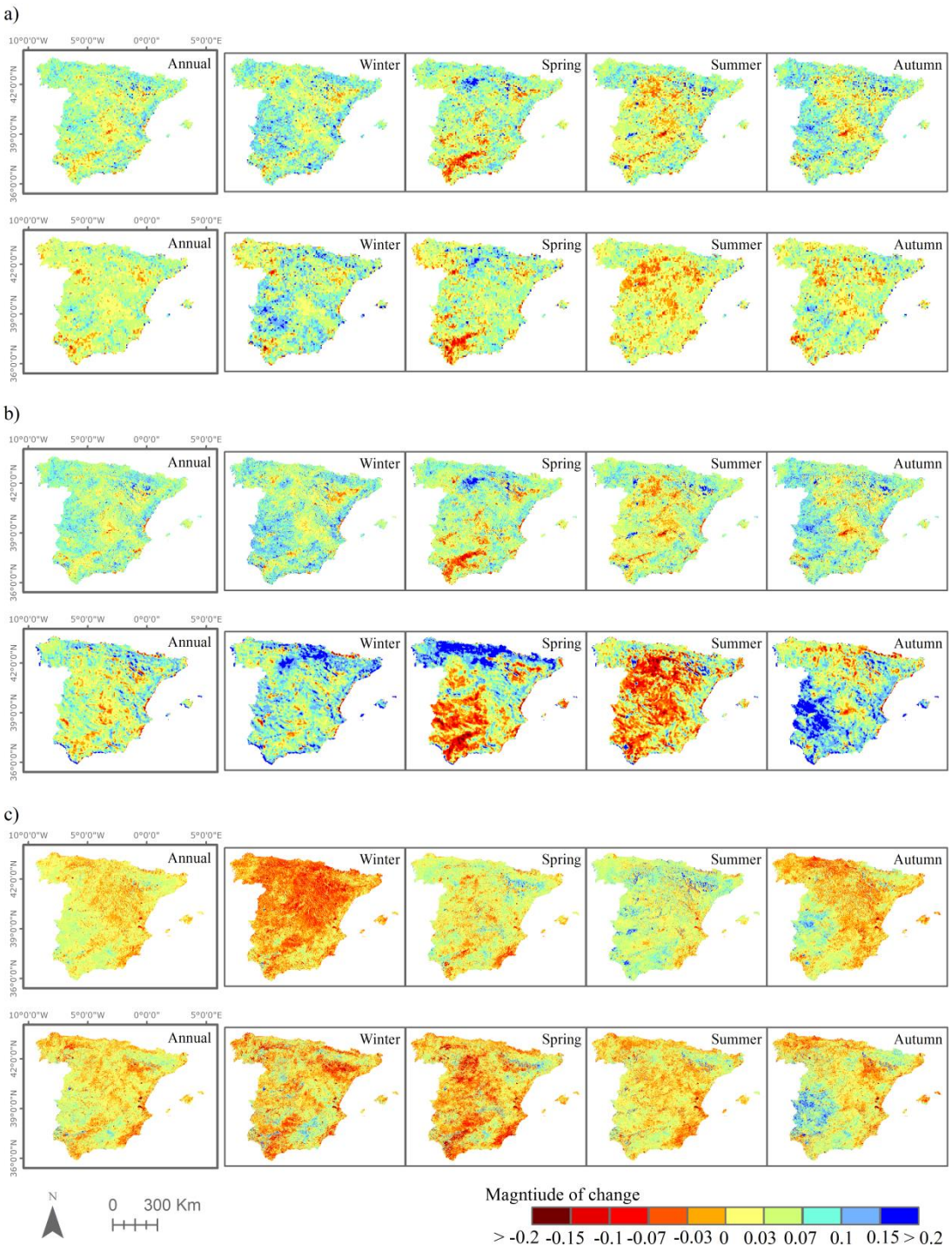

Figure 8: Spatial distribution of the annual and seasonal magnitude of change of the NDVI for the Sp_1km_NDVI and 8 km^2 GIMMS3g dataset for 1982-2014 (a), 4 km^2 SMN 1982-2014 (b) and 1 km^2 2004-2014 MODIS (c). The original 1.1 km^2 spatial resolution of the Sp_1km_NDVI was resampled to the spatial resolution of the other datasets.

The relationship of the spatial patterns of the NDVI change is higher considering the period 2004-2014 with the MODIS dataset. On the contrary, the spatial agreement is low considering both GIMMS3g and SMN datasets (Supplementary Figure 2).

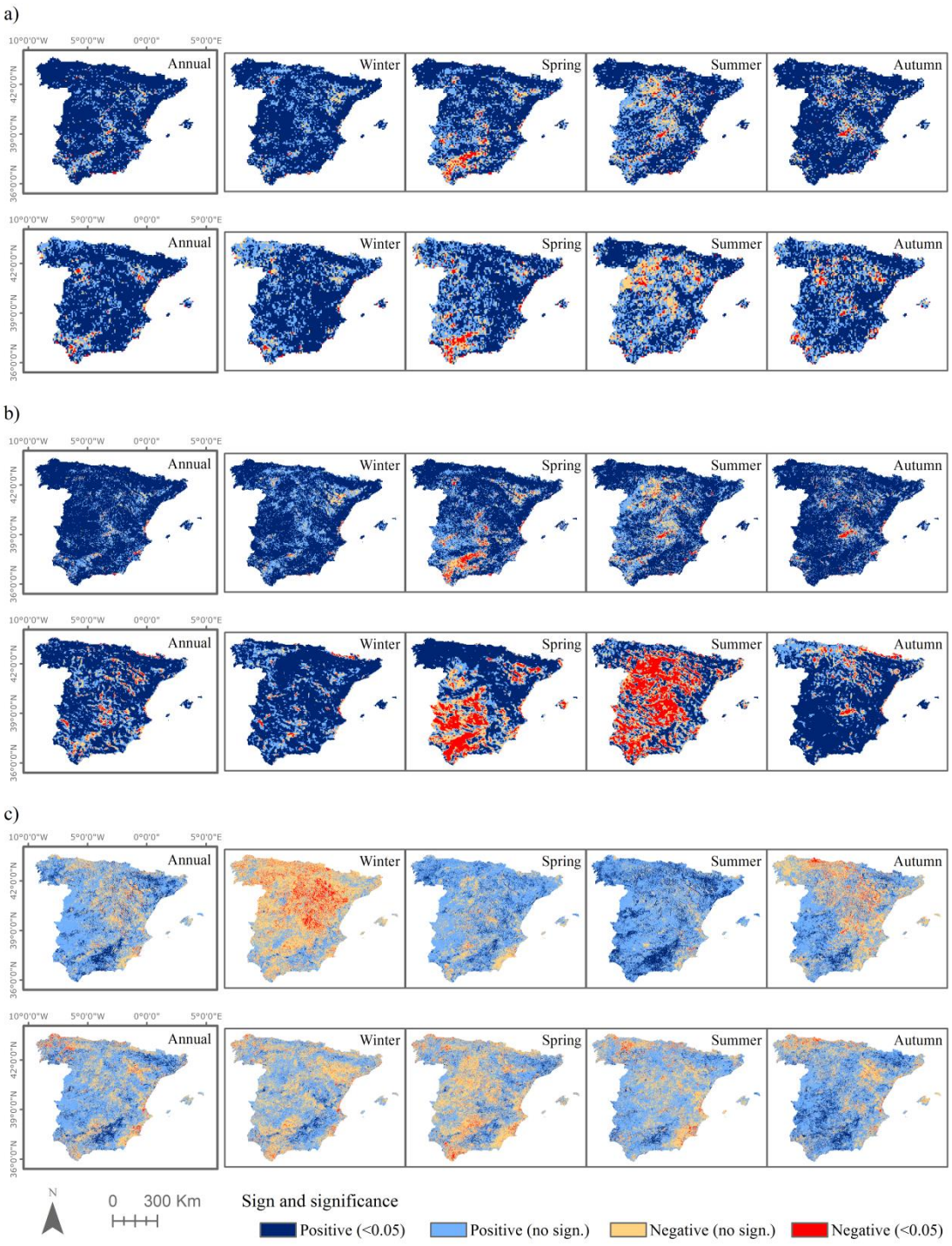

Figure 9: Spatial distribution of the annual and seasonal sign and significance of the NDVI trends comparing between Sp_1km_NDVI and 8 km^2 GIMMS3g dataset for 1982-2014 (a), 4 km^2 SMN 1982-2014 (b) and 1 km^2 2004-2014 MODIS (c). The original 1.1 km^2 spatial resolution of the Sp_1km_NDVI was resampled to the spatial resolution of the other datasets.

Nevertheless, although the magnitude of the change in the NDVI shows some differences between the Sp_1km_NDVI and the other three NDVI datasets, the signification of the observed NDVI trends shows high agreement among the Sp_1km_NDVI and the GIMMS3g and MODIS datasets, mostly at the annual

scale (Figure 9). Both GIMMS3g and Sp_1km_NDVI show dominant positive and significant NDVI trends between 1982 and 2014. In contrast, the SMN dataset shows strong differences with large areas showing negative and significant NDVI trends in spring and summer that were not identified with the Sp_1km_NDVI and the GIMMS3g datasets. Thus, with the exception of the annual SMN, the coefficients of contingency that measure the spatial agreement in the sign of the NDVI trends show similar values considering the different datasets, which showed high agreement with the trend patterns obtained with the Sp_1km_NDVI (Supplementary Tables 1 and 2).

3. High spatial resolution 1981-2015 NDVI changes in Spain

3.1. Methodology for the analysis of NDVI changes using the Sp_1km_NDVI

Trends from the Sp_1km_NDVI dataset were assessed for the 1981-2015 period at the original 1.1 km spatial resolution. For this purpose the modified Mann–Kendall trend test and the Theil-Sen slope estimator were also used, as described above. In addition to the remote sensing information, an official land cover map for 1980, developed by the Ministry of Agriculture of Spain (https://www.mapama.gob.es/es/cartografia-y-sig/publicaciones/agricultura/mac_1980_1990.aspx; Last access: 04/09/2018) was used. This was used to detect the land cover classes affected by changes in recent decades. The map is available in vector format at the spatial scale of 1:50,000. The map was transformed to a raster format at the spatial resolution of 1.1 km, covering the same spatial area that the daily NOAA-AVHRR images. The rasterization was performed using a criterion of majority (Figure 10).

Thanks to this data, the signification and magnitude of the trend at seasonal and annual scale using the Sp_1km_NDVI dataset was analysed and provided a summary for the whole peninsular Spain and the Balearic Islands but also for the different land cover types existing at the beginning of the study period to determine the influence of the land cover type on the NDVI.

Moreover, the NDVI trends were compared with climatic variables to determine if there is a relationship between the NDVI trends and the average precipitation, temperature and aridity (precipitation minus reference evapotranspiration) in peninsular Spain and the Balearic Islands. The climatic datasets have been obtained from average gridded meteorological variables at the same spatial resolution that the NOAA-AVHRR data. Details on the climate dataset can be found at Vicente-Serrano et al. (2017).

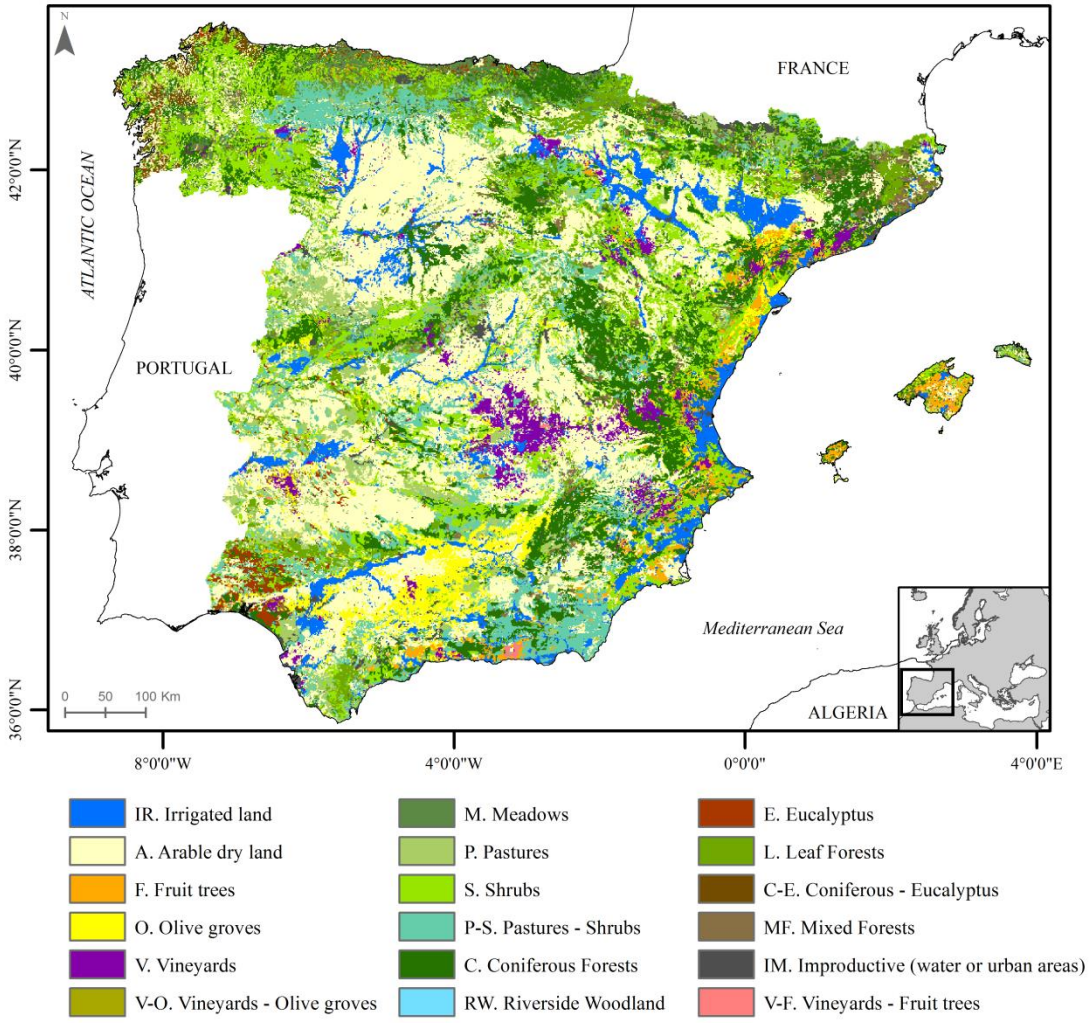

Figure 10: Spatial distribution of the main land cover categories recorded in Spain at the beginning of the decade of 1980.

3.2. Patterns of NDVI changes

Figure 11 shows the 1.1 km NDVI trends between 1981 and 2015 in Spain at the seasonal and annual scales obtained with the Sp_1km_NDVI dataset. At the annual scale the changes are less spatially contrasted in comparison to what is found at the seasonal scale. At the annual scale, the changes are dominantly positive (the average magnitude of change for the annual NDVI in the period 1981-2015 was 0.056) (Supplementary Figure 3). Nevertheless, although the general pattern indicates a dominant NDVI increase across the country, there are also regions that have showed a general NDVI decrease. This is clearly evident in the eastern Mediterranean coastland, areas of central Spain, sectors of the Ebro basin and also large areas of Southwest and also the Southeast Spain. For example, the areas of greenhouses of Southeast Spain are well characterised by strong NDVI decrease since 1982. At the same time, there are also some areas characterised

by a strong NDVI increase in the East, Northwest Pyrenean area but mostly in areas of the Ebro basin in which large irrigated lands have been created.

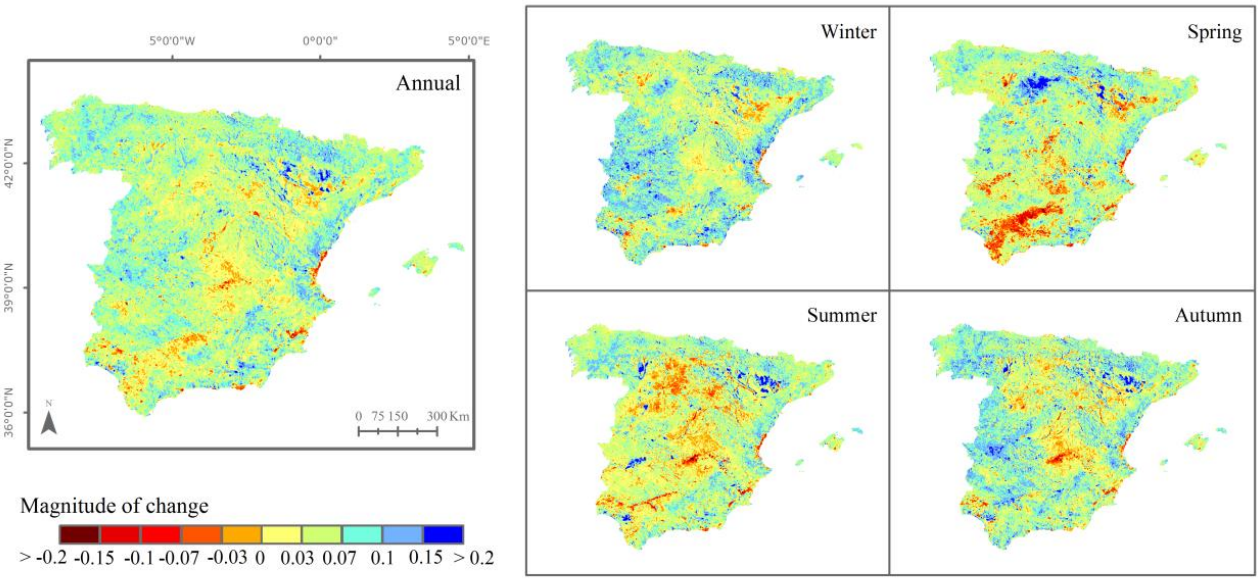

Figure 11: Magnitude of change of the 1.1 km^2 NDVI trends for Spain (1982-2014).

At the seasonal scale there are more spatial contrasts, although the magnitude of change has also been dominantly positive (winter: 0.065 NDVI units/34 years, spring: 0.05 NDVI units/34 years, summer: 0.045 NDVI units/34 years and autumn: 0.06 NDVI units/34 years). In winter there is a dominant NDVI trend across the territory although there are not large areas characterised by strong NDVI changes. On the contrary, in spring and summer the Sp_1km_NDVI dataset identifies important changes in large regions. In spring there is a general decrease of NDVI values in the Guadalquivir valley but also in areas of Western and in central peninsular Spain, in some sectors of the Ebro basin and also in the East of the Mediterranean coastland. In summer, the main positive changes are identified in some small areas of West Spain and the Ebro basin, but also strong decrease of the NDVI is recorded in large areas of central peninsular Spain. Thus, in the Duero basin there are large areas affected by negative changes of the NDVI.

There are dominant positive and significant NDVI trends at the annual and seasonal scales (Figure 12). Thus, the 95.1% of Spain shows positive annual NDVI trends, and 79.6% positive and significant trends (Table 2). Only 4.85% of Spain shows negative trends and thus in less than the 1% of the territory the trends are negative and statistically significant. There are some seasonal differences in the sign of the NDVI trends.

Summer is the season that records a lower percentage of positive and significant trends (57.1%), showing a 13.3% of negative trends.

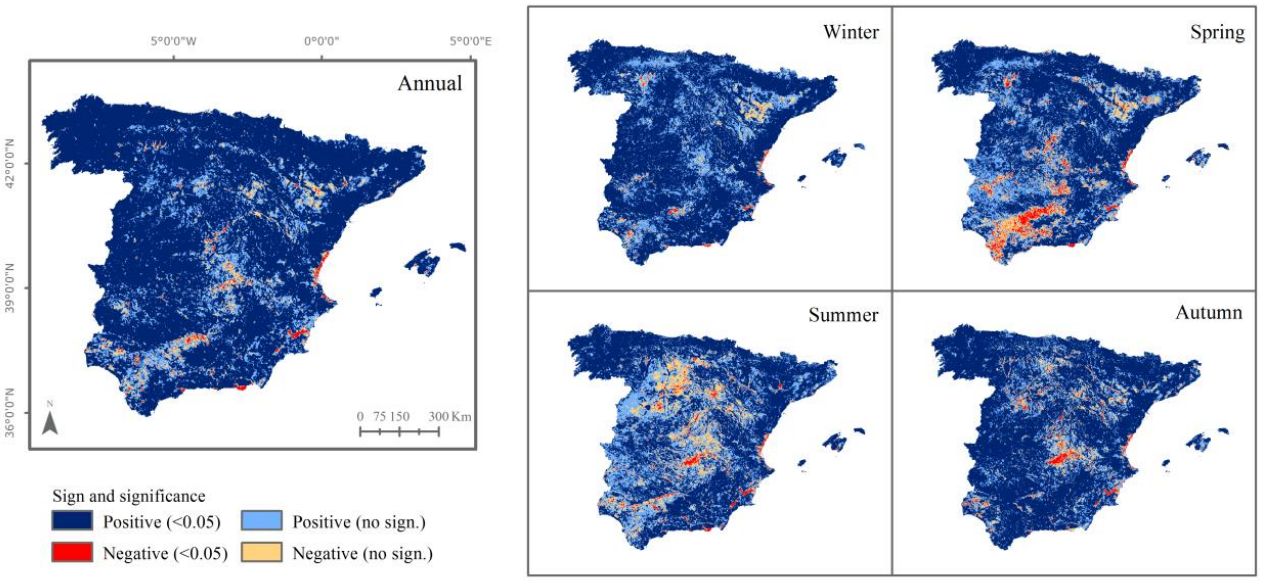

Figure 12: Sign and significance of the 1.1-km^2 NDVI trends for Spain (1982-2014).

Table 2: Percentage of surface area affected by significant and non-significant NDVI trends at seasonal and annual scales

	Negative ($p < 0.05$)	Negative ($p > 0.05$)	Positive ($p > 0.05$)	Positive ($p < 0.05$)
Annual	1	4	16	80
Winter	0.5	4	22	74
Spring	3	9	26	62
Summer	2	11	30	57
Autumn	2	6	19	74

3.3. Connection with land cover and average climate conditions

There are not important differences in the recorded NDVI changes between 1981 and 2015 as a function of the average climatic conditions. There are not significant correlations between the average annual precipitation and the recorded annual and seasonal NDVI magnitude of change. The same pattern is identified with the average temperature and the aridity (Supplementary Figures 4 and 5).

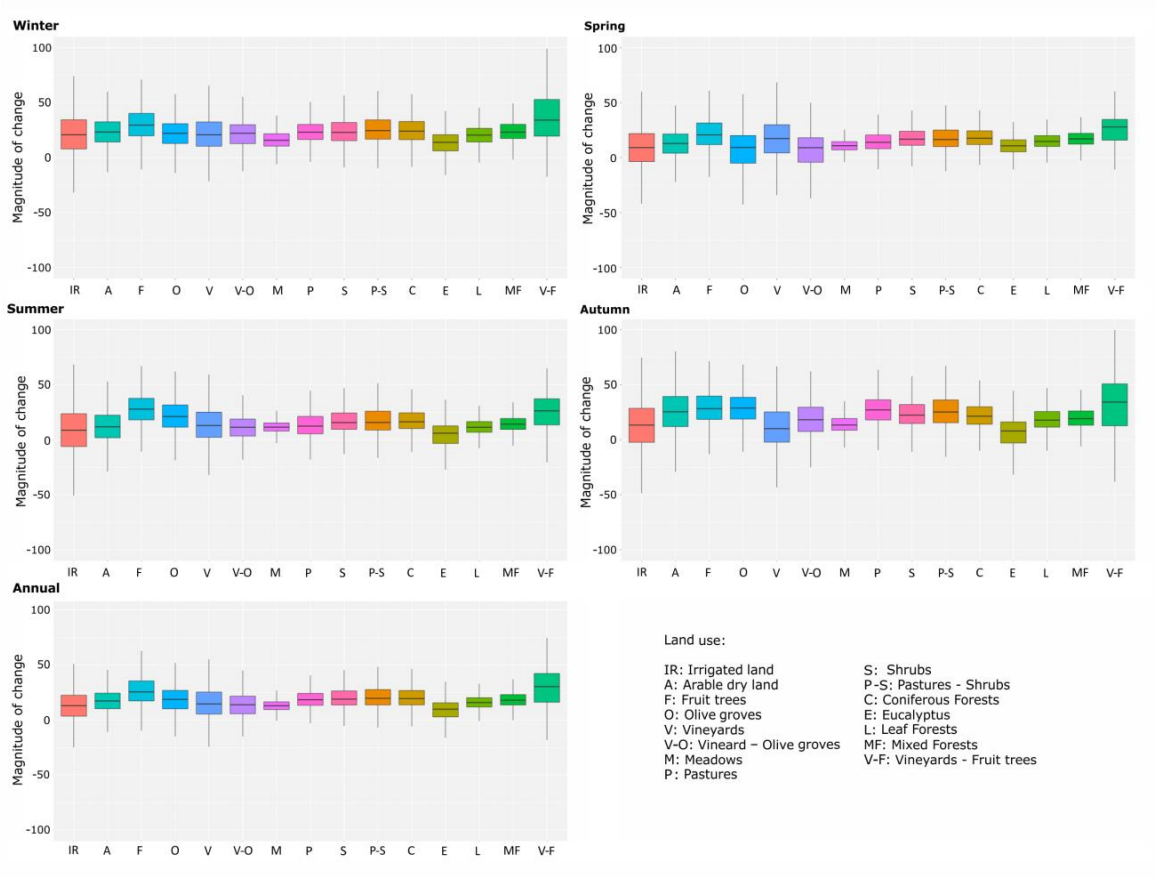

Figure 13: Box plots showing the seasonal and annual NDVI magnitude of change for the main land cover types

The magnitude of NDVI change observed in the different 1982 -first year complete of the serie- land cover types is showed in Figure 13. The changes are showed in percentage values instead of NDVI units to be comparable among land cover types that may show very different average values. In general, all the analysed land cover types in 1982 have showed an increase of the NDVI. At the annual scale, the mean magnitude of change in percentage is positive in the different land cover classes. Maximum increase is found in irrigated vineyards and fruit-tree plantations. In general, the coniferous forests show a higher average increase than deciduous and mixed forests, and similar to the observed trend in shrubs and pastures. These patterns tend to be repeated at the seasonal scale but spring shows lower differences in the magnitude of change and between the different land cover types, in comparison to the other seasons of the year.

Nevertheless, although analysing the magnitude of the changes it is difficult to extract relevant differences among the land cover categories, the percentage of surface area for the different land covers that is affected by significant trends show some noticeable differences (Table 3). The different land cover types show a dominance of positive significant trends at the annual scale. Nevertheless, there are important differences

between the surface with positive and significant trends at the annual scale in the irrigated lands (54.5%), the arable dry lands (72.4%), and the shrubs and forests (86-92%). These percentages strongly vary at the seasonal scale. In spring and summer, the months in which higher vegetation activity is recorded in the study area the differences among land cover types clearly emerge. In spring more than 30% of the irrigated lands showed a negative trend (10.79% statistically significant), and in summer, the period of higher activity of this land cover type, the negative trends were recorded in the 35% of the irrigated lands, with 13.5% of the lands showing a significant trend. The exceptions are the irrigated fruit and vineyard plantations, in which the areas characterised by positive and significant trends clearly dominate.

In the arable dry lands, olive grows and vineyards a percentage around 50% showed positive and significant trends in spring, which is the season of a higher activity in these land cover types, and percentages higher than 15% (and > 30% in the case of the olive grows) of the land area in 1982 covered by these land uses showed negative trends. On the contrary, these percentages are far from those found in spring in shrub areas and other forest types, with positive and significant trends higher than 75%, and with negative trends in areas lower than 5%. This pattern is also reproduced in summer months in which natural vegetation areas characterised by forests and shrubs show a dominant positive trend. A particular behaviour was observed in the Eucalyptus forest, which showed a lower percentage of positive and significant trends and even in summer a high percentage of surface was characterised by negative trends.

The connection between the magnitude of change of the NDVI observed between 1981 and 2015 in each land cover type and the average climate conditions is showed in Supplementary Figures 6 to 20. In general, the relationships are not statistically significant, which suggest that the average climate conditions recorded in each region are not a noticeable factor that may explain the patterns of NDVI trends recorded in peninsular Spain and the Balearic Islands during the time period analysed.

Table 3: Seasonal and annual significance of the NDVI trends (1982-2014) for the different land cover types, in %.

Annual	**IR**	**A**	**F**	**O**	**V**	**V-O**	**M**	**P**	**S**	**P-S**	**C**	**E**	**L**	**MF**	**V-F**
Neg. (<0.05)	6.98	0.54	0.18	1.69	1.37	0.62	0.34	0.54	0.15	0.35	0.12	3.22	0.11	0.11	0.67
Neg. (no sign.)	12.05	5.17	0.82	5.51	11.26	8.14	1.18	2.26	1.49	1.49	1.59	16.18	1.52	0.65	9.53
Pos. (no sign.)	26.45	21.90	11.48	17.62	27.14	30.70	5.57	13.74	9.30	11.26	8.24	32.07	8.49	6.98	14.63
Pos. (<0.05)	54.52	72.39	87.52	75.19	60.24	60.54	92.91	83.46	89.06	86.90	90.05	48.52	89.88	92.26	75.17
Winter	**IR**	**A**	**F**	**O**	**V**	**V-O**	**M**	**P**	**S**	**P-S**	**C**	**E**	**L**	**MF**	**V-F**
Neg. (<0.05)	4.20	0.28	0.05	1.61	0.25	0.49	0.24	0.32	0.08	0.18	0.10	1.76	0.03	0.01	0.67
Neg. (no sign.)	9.89	4.90	0.88	5.18	6.49	3.70	1.97	2.44	2.08	1.78	1.63	12.19	1.87	0.98	4.66
Pos. (no sign.)	29.65	27.13	13.23	21.11	31.72	26.39	19.99	24.63	15.87	20.22	11.43	31.18	19.34	10.22	15.52
Pos. (<0.05)	56.26	67.69	85.85	72.10	61.54	69.42	77.80	72.61	81.97	77.82	86.83	54.87	78.76	88.79	79.16
Spring	**IR**	**A**	**F**	**O**	**V**	**V-O**	**M**	**P**	**S**	**P-S**	**C**	**E**	**L**	**MF**	**V-F**
Neg. (<0.05)	10.79	4.59	0.54	10.81	5.22	10.11	0.63	1.93	0.31	1.02	0.16	0.77	0.24	0.13	1.11
Neg. (no sign.)	20.30	13.65	4.53	21.81	13.84	22.56	3.15	6.90	2.88	4.62	2.14	10.34	2.05	1.11	6.21
Pos. (no sign.)	31.15	32.25	23.47	25.86	27.01	32.80	19.37	36.57	19.22	28.64	13.07	39.91	21.19	10.46	17.96
Pos. (<0.05)	37.76	49.51	71.46	41.52	53.93	34.53	76.85	54.60	77.59	65.72	84.63	48.97	76.52	88.29	74.72
Summer	**IR**	**A**	**F**	**O**	**V**	**V-O**	**M**	**P**	**S**	**P-S**	**C**	**E**	**L**	**MF**	**V-F**
Neg. (<0.05)	13.47	2.00	0.39	0.74	4.92	3.21	0.33	1.23	0.51	0.77	0.46	5.22	0.70	0.86	2.00
Neg. (no sign.)	21.75	19.16	1.87	6.54	15.98	14.06	2.41	10.42	4.77	6.12	4.18	27.30	7.32	3.97	11.53
Pos. (no sign.)	28.65	38.28	16.09	25.05	34.50	45.25	14.95	41.31	23.53	28.51	18.27	35.59	26.98	21.13	19.96
Pos. (<0.05)	36.13	40.56	81.65	67.67	44.61	37.48	82.31	47.03	71.19	64.60	77.10	31.89	65.01	74.03	66.52
Autumn	**IR**	**A**	**F**	**O**	**V**	**V-O**	**M**	**P**	**S**	**P-S**	**C**	**E**	**L**	**MF**	**V-F**
Neg. (<0.05)	10.86	1.27	0.25	0.62	8.84	3.08	0.23	1.07	0.41	0.44	0.30	8.61	0.38	0.19	4.43
Neg. (no sign.)	17.26	7.87	2.20	3.24	20.26	9.25	3.27	2.97	2.93	3.25	2.76	21.85	4.35	2.30	9.98
Pos. (no sign.)	25.73	22.85	18.89	12.99	29.35	30.09	23.10	17.04	13.31	15.99	12.07	31.80	14.42	12.41	18.63
Pos. (<0.05)	46.15	68.01	78.65	83.15	41.55	57.58	73.40	78.92	83.36	80.32	84.87	37.73	80.85	85.09	66.96

4. Linking tree-ring growth and satellite-derived NDVI in multiple forests. Temporal-scale matters.

4.1. Datasets description and methods

In addition to the NDVI data described above, this thesis used tree-ring width information obtained using dendrochronological methods, covering most of the forested areas in the peninsular Spain and the Balearic Islands (Figure 14), which were provided by different research teams in Spain. The samples were processed by these teams following the same approach: for each forest, at least 10-15 healthy, dominant or codominant trees were selected and cored at 1.3 m using increment borers to obtain 2-3 cores per tree. For each sampled stand, latitude, longitude and mean elevation were recorded. Wood samples were sanded until rings were clearly visible and then visually cross-dated. Tree-ring width was measured to the nearest 0.01 mm using binocular microscopes and measuring device systems (Lintab, F. RinnTech., Germany; Velmex Inc., USA). The accuracy of visual cross-dating and measurements was checked using the COFECHA program, which uses moving correlations between each individual tree-ring series and the mean site series to check the cross-dating accuracy (Holmes, 1983).

Tree-ring width measurements were converted into residual indices using standard dendrochronological protocols (Fritts, 1976). Specifically, the individual series of tree-ring widths were detrended using a negative exponential curve and residuals were obtained by dividing the observed values by the fitted ones. Finally, the individual standardized series were averaged into site mean chronologies of tree-ring width indices (hereafter TRWi) using bi-weight robust means. The mean site-level chronology represents the average growth series of a variable number of trees of the same species growing at the same site. Overall, the low- to mid-frequency variability was removed, while keeping the high-frequency variability and the first-order autocorrelation since no autoregressive modelling was performed. Table 1 lists the number of forests with dominant species in the available dataset. The species with a higher number of sampled stands are *Pinus halepensis* (117 forests), followed by *Pinus sylvestris* (76) and *Pinus nigra* (66). While the dataset is dominated by conifers, it is also characterized by a good sampling of Fagaceae (*Fagus sylvatica* -9%-, *Castanea sativa* -1.8%-, besides several *Quercus* species -17.5%-). Spatial distribution of the species considered in this study can be found in Supplementary Figure 21.

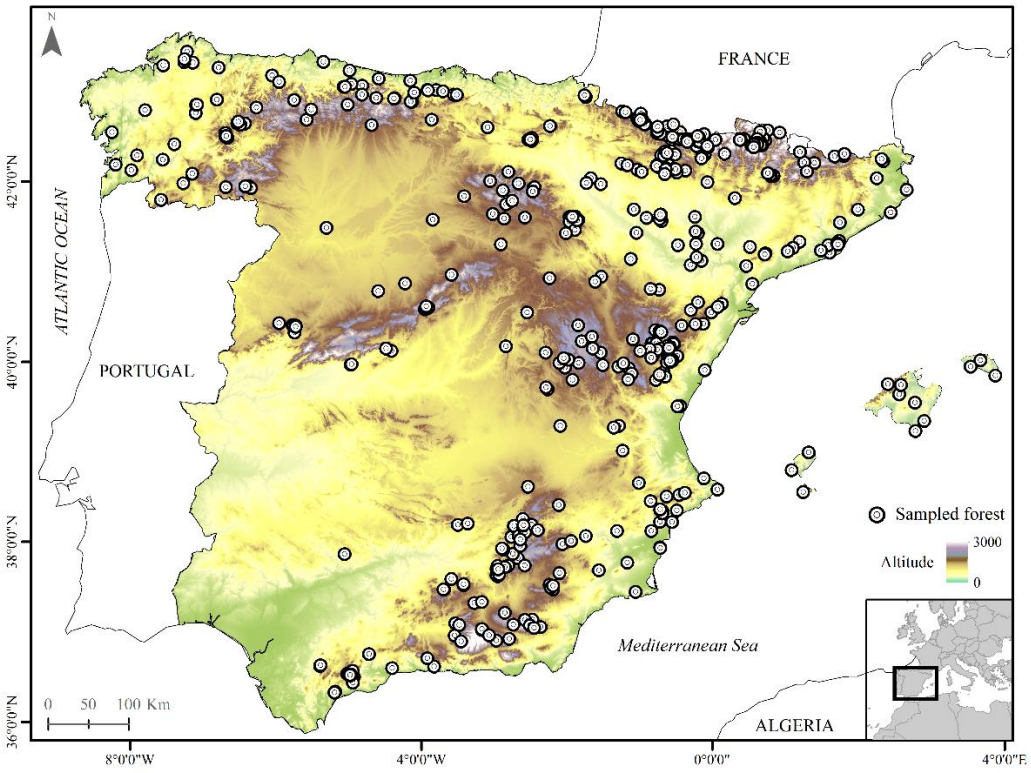

Figure 14: Spatial distribution of the tree-ring dataset available in the peninsular Spain and the Balearic Islands. Each point represents a sampled forest.

The NDVI data was also processed since it can be affected by trends in the time series as a consequence of different factors including CO_2 fertilization (Donohue *et al.*, 2013), and forest densification (Vicente-Serrano *et al.*, 2004). For this reason, and to be comparable with the available de-trended tree-ring series, the semi-monthly NDVI series were detrended. For this purpose a linear regression analysis was used to fit NDVI (dependent variable) with time (independent variable). The residuals of the model were summed to the average of the entire semi-monthly period to have detrended NDVI series. To quantify the NDVI-TRWi associations, Pearson correlation coefficients between the annual TRWi and the detrended semi-monthly NDVI series were calculated at each forest site. Since the cumulative NPP over long periods can give better estimations of tree-ring width than that of shorter periods (Gough et al., 2008; Zweifel et al., 2010), it was preferred to correlate the annual TRWi with the NDVI summarized at different time scales (for NDVI time scales, it is referred to the average NDVI over the previous n biweekly periods). This is simply because linking TRWi with semi-monthly NDVI can give less reliable results (see Vicente-Serrano et al., 2016). In contrast, the use of the cumulative past NDVI conditions (referring to NDVI time scales), usually provides

better relationship with tree-ring growth, as observed in different studies (Arzac et al., 2016; Pasho et al., 2011; Vicente-Serrano et al., 2014).

Table 4: Tree species, abbreviations and number of sampled forests. The annual water balance was defined as the difference between precipitation and the reference evapotranspiration (ETo).

Tree species (code)	Number of forests	Mean NDVI	Mean Annual Temperature (ºC)	Annual Precipitation (mm)	Annual Water Balance (mm)
Abies alba (ABAL)	48	0.32	13.06	1441.08	486.46
Abies pinsapo (ABPN)	15	0.26	17.64	1469.77	296.28
Castanea sativa (CASA)	10	0.43	17.53	928.83	-139.96
Fagus sylvatica (FASY)	51	0.39	14.72	1213.45	283.87
Juniperus thurifera (JUTH)	16	0.28	17.21	690.61	-397.87
Pinus halepensis (PIHA)	117	0.26	19.99	600.31	-617.18
Pinus nigra (PINI)	66	0.29	17.06	753.91	-344.72
Pinus pinaster (PIPI)	20	0.32	18.78	705.39	-454.55
Pinus pinea (PIPN)	9	0.27	20.10	551.33	-665.18
Pinus sylvestris (PISY)	76	0.32	14.74	959.48	-36.94
Pinus uncinata (PIUN)	39	0.23	10.18	1445.58	576.37
Quercus faginea (QUFA)	19	0.36	16.82	976.20	-125.80
Quercus ilex (QUIL)	5	0.31	17.42	786.00	-338.58
Quercus petraea (QUPE)	7	0.41	15.67	1062.21	114.98
Quercus pyrenaica (QUPY)	34	0.40	16.22	878.32	-142.55
Quercus robur (QURO)	34	0.46	16.22	1484.47	594.25

NDVI time scales refer to average NDVI over the previous *n* semi-monthly periods (i.e., two per month). Then the TRWi series were correlated with the 24 NDVI semi-monthly series at time scales varying from 1 to 48 semi-monthly periods (i.e., two years). The NDVI values were considered not only for the corresponding year, but for the previous year as well to account for any possible lag effect, given that tree-ring growth may be impacted by tree activity and climate conditions during the previous year (Fritts, 1976). For each site chronology (mean TRWi series), 2304 correlations were calculated (48 semi-monthly periods × 48 time-scales). This procedure allowed for determining whether the TRWi are linked more to the semi-monthly NDVI values of the previous and/or the corresponding year and also define the period with strongest correlation in the two years.

The high diversity in the patterns of correlations between the TRWi and the NDVI series was summarized using a S-mode Principal Component Analysis (PCA; (Richman, 1986)). A correlation matrix was used to calculate the Principal Components (PC), and the components were obtained from the original correlation coefficient values using the weight coefficients of each forest in each component. The number of retained components was defined based on the percentage of the total explained variance following the results of the scree-plot. The PC loadings were mapped. They summarize the correlation between the TRWi and NDVI for each particular component, as well as the general pattern that represents a number of forests. Finally, each forest was classified by means of a maximum loading rule.

Different sources of information were used to assess the influence of different biophysical and climate conditions on the links between the TRWi chronologies and NDVI variations at different time-scales. First, the tree species dominating the forest was assessed and their corresponding average NDVI values. Second, this thesis focused on the role played by a range of climatic variables (e.g. annual precipitation and mean air temperature). In this regard, the impact of water balance, defined as the difference between precipitation and reference evapotranspiration (ETo), was assessed. The ETo was calculated following the FAO-56 Penman-Monteith equation (Allen *et al.*, 1998). The climate data were provided at a grid resolution similar to that of the NDVI using a newly developed weekly gridded dataset for Spain (Vicente-Serrano *et al.*, 2017b).

In order to summarize the role of these climatic and environmental conditions and explain the relationship between the TRWi and the NDVI time-scales, the average values for these geographical variables corresponding to each forest were obtained. The contribution of these explanatory variables to the spatial differences in the TRWi responses to NDVI at different time scales was illustrated by means of different box plots and quantified using a Predictive Discriminant Analysis (PDA), which explains the value of a dependent categorical variable based on its relationship to one or more predictors (Hair et al., 1995; Huberty, 1994). PDA allowed assessing which predictors contributed more to the PCs that summarized the TRWi-NDVI dependency. The tree species were included in the PDA as a binary variable, so each tree species was included in the analysis as an individual variable.

4.2. Patterns of relationship between NDVI and TRWi

Figure 15 summarizes the maximum Pearson correlation between NDVI and TRWi, the semi-monthly period at which the maximum correlation is recorded and the NDVI time-scale at which the maximum correlation is recorded. The results are provided for each tree species. In general, the maximum correlations do not show clear differences among tree species, albeit with slightly higher correlations found for *Pinus halepensis* forests. Notably, the maximum correlation between NDVI and tree-ring growth is recorded at shorter time-scale (< 10 semi-monthly cumulative periods). Nevertheless, although the magnitude of correlations and time-scale at which maximum correlation is recorded are quite similar among all species, there are important differences in the semi-monthly period at which maximum correlation is recorded. For instance, in fir species (*Abies alba* and *A. pinsapo*) highest NDVI-TRWi correlations appear much earlier than those observed for tree species located in drier areas (*P. halepensis, P. pinaster, P. nigra, Juniperus thurifera,* and *Quercus ilex*). Species predominating in cold and often wet mountainous areas (e.g. *P. sylvestris* and *P. uncinata*) show the strongest response earlier than species located in drier areas.

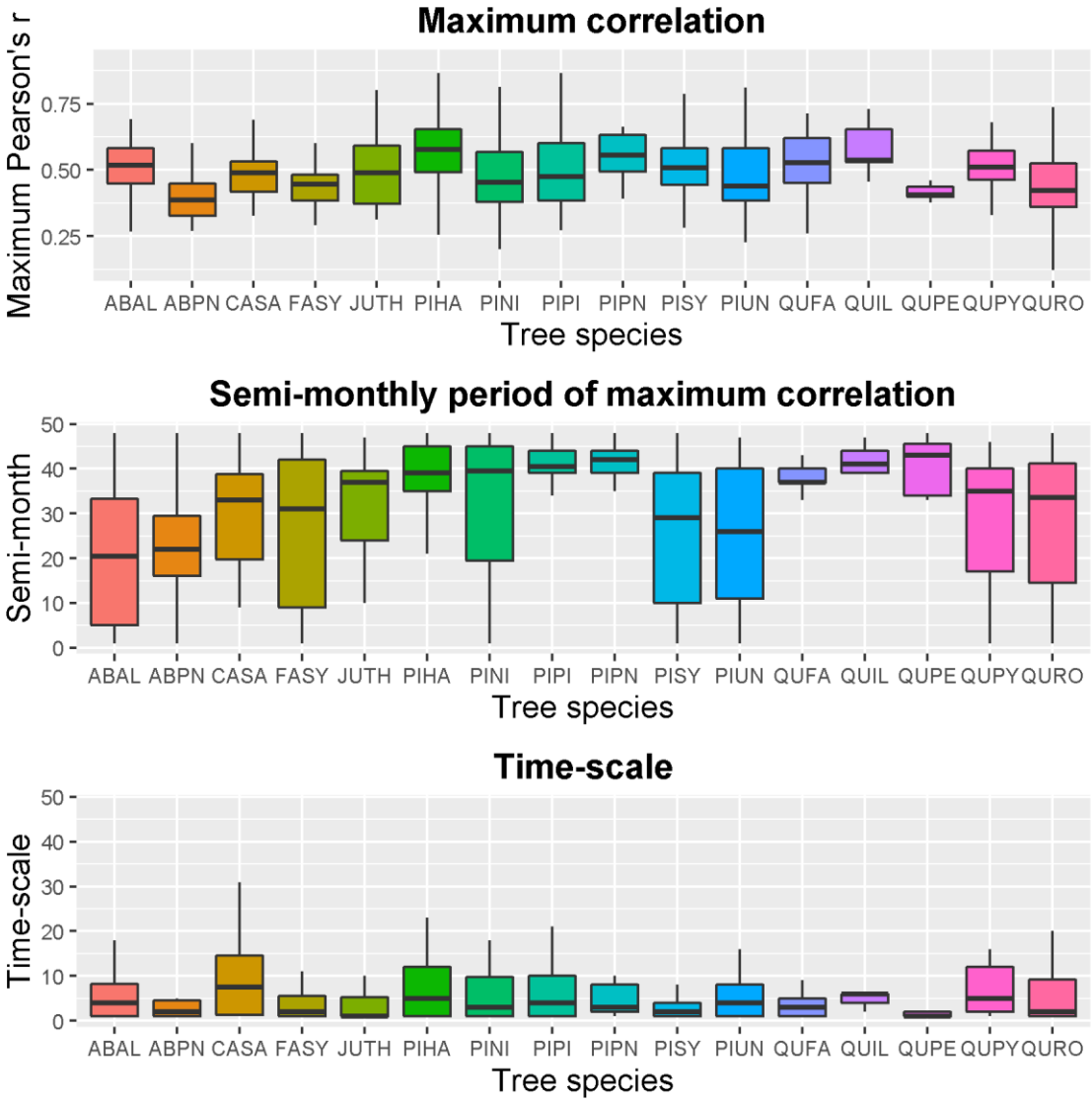

Figure 15: [Upper] Box plots showing the maximum Pearson correlation obtained between the NDVI series at different time scales and the indexed tree-ring width series for each tree species; [central] the semi-monthly period at which the maximum correlation is recorded, and [lower] the NDVI time-scale (in semi-months) at which the maximum correlation is recorded. All codes of species correspond to those listed in Table 1. For each box plot, the central solid line indicates the median. The whiskers represent the 10th and the 90th, while the 25th and the 75th are plotted as the vertical lines of the bounding boxes.

The principal component loadings show different patterns of correlation between the cumulative NDVI and the annual TRWi (Figure 16). The first Principal Component (PC1) represents the highest percentage of the total explained variance (42.1%), with the maximum correlations between NDVI and TRWi found considering NDVI at time-scales of 10-20 semi-monthly periods at the semi-monthly period 45 (i.e. second half of November). There is a coherent pattern, with NDVI-TRWi correlations that increase in agreement with higher NDVI cumulative periods with the maximum for NDVI values from March to November of the

year in which the growth is recorded. The second Principal Component (PC2; 13.1% of total variance) also shows a coherent pattern, with the maximum correlation recorded NDVI time scale throughout 15-20 semi-monthly periods, but in the semi-monthly period 26 (second half of January). This means that the cumulative NDVI values between June of the previous year to January of the year of tree-ring formation show the highest correlation with TRWi. The third Principal Component (PC3; 10.1% of total variance) shows the maximum correlation between NDVI and TRWi around the semi-monthly period 34 (first half of March) considering a cumulative NDVI in a period between November and March. Finally, the remaining Principal Components (PC4-PC6) explain low percentages of the total variance (<7%), suggesting random patterns, which are quite difficult to interpret.

Figure 17 shows the spatial distribution of the PC loadings corresponding to each PC. PC1 almost shows higher loading values over a high percentage of all forests, summarizing the general pattern of relationships between TRWi and NDVI in the whole Spain. Furthermore, the importance of PC1 is three times higher than the PC2. In comparison to PC1, PC2 shows higher loadings for a lower number of forests, but they are distributed across different regions of Spain. PC3 shows higher loadings for forests located mainly in the Pyrenees (northeastern Spain), whereas PC4 high loadings are distributed along the Pyrenean, besides other forests located in different regions of the country. As opposed to other PCs, both PC5 and PC6 do not reveal clear spatial patterns, with a lower percentage of forests and even very distant forests (PC6).

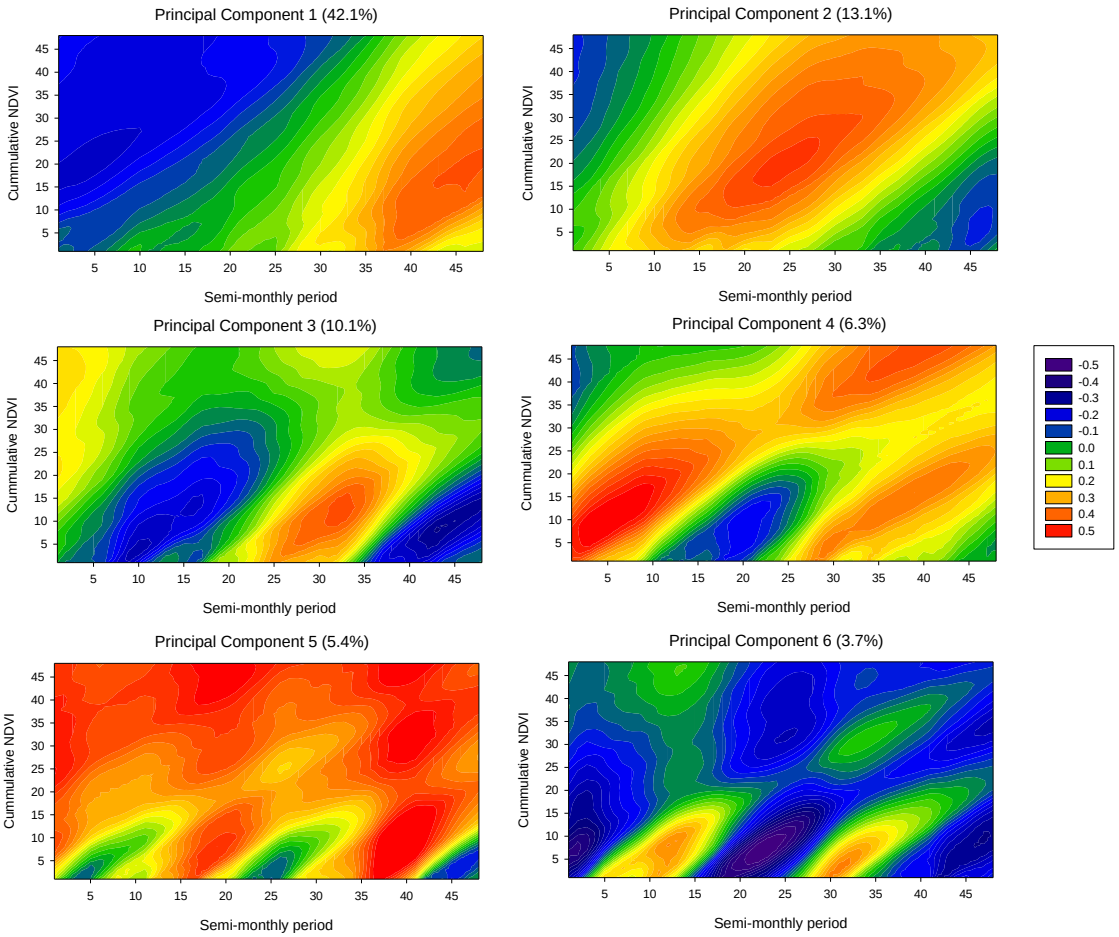

Figure 16: Principal Component loadings extracted representing the main patterns of NDVI-TRWi correlations. The percentage of the variance represented by each component is shown between brackets. The values of the components are represented in the original variable (correlation).

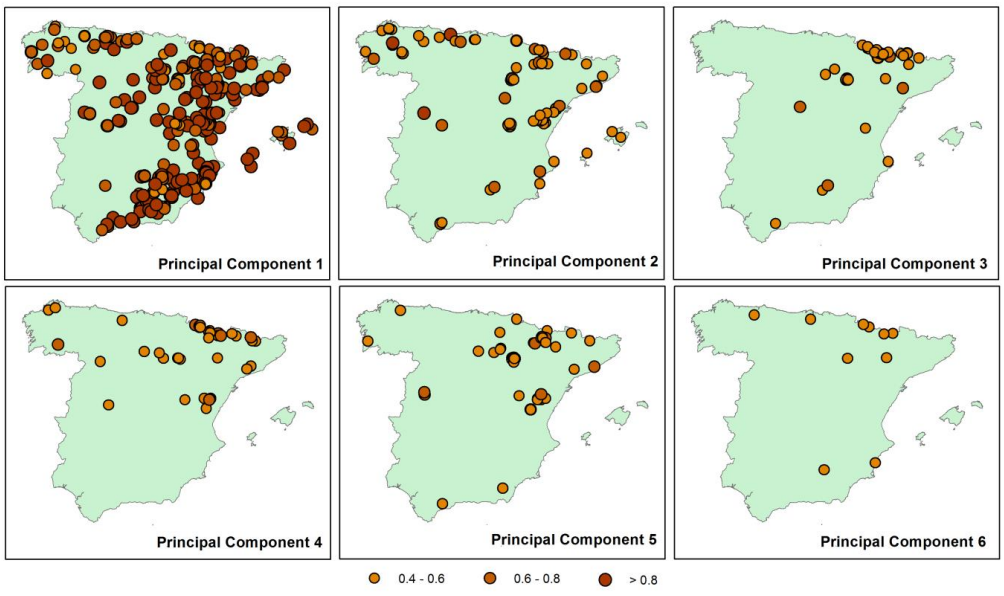

Figure 17: Spatial distribution of the Principal Component loadings for the six principal components extracted. Only significant loadings are shown.

The patterns of the relationship between NDVI time scales and the TRWi is presented in Figure 18. PC1 shows higher loadings than other components, suggesting that this pattern represents a high percentage of forests in Spain. Nevertheless, higher PC loadings are found for evergreen conifers, mainly living in semi-arid to drought-prone areas (e.g. *P. halepensis*, *P. pinaster*, *P. pinea* and *J. thurifera)*. The pine species that dominate in colder and more humid regions (e.g. *P. sylvestris* and *P. uncinata*) show lower load values. Among the oak species, the evergreen *Q. ilex* exhibits the highest loadings. The remaining PCs show lower loadings, but with some interesting patterns. For example, PC2 shows higher loadings for *C. sativa* and *Q. robur*. Similarly, PC3 indicates higher loadings for *A. alba*, *P. uncinata* and *F. sylvatica*, which prevail in cool and wet conditions or in moist and temperate regions. A cluster analysis of forests according to the maximum loading rule shows that PC1 accounts for 304 forests, in comparison to other PCs (e.g. PC5 [69], PC2 [66] and PC4 [64]) (Table 5). Notably, PC1 covers the majority of pine forests, apart from *P. sylvestris* and *P. uncinata*, which are also well-presented in PC3 and PC5. The highest percentage of *A. alba* is recorded in PC3, while *F. sylvatica* shows a higher percentage in PC4.

Table 5: Percentage of species represented by each PC following the maximum loading rule.

	PC1 (304)	PC2 (66)	PC3 (38)	PC4 (64)	PC5 (69)	PC6 (22)
ABAL	12.5	8.3	35.4	20.8	10.4	12.5
ABPN	53.3	13.3	6.7	0.0	20.0	6.7
CASA	40.0	30.0	0.0	0.0	30.0	0.0
FASY	39.2	17.6	2.0	31.4	3.9	5.9
JUTH	75.0	18.8	0.0	0.0	6.3	0.0
PIHA	83.8	6.0	0.9	0.9	6.0	2.6
PINI	68.2	10.6	4.5	3.0	9.1	4.5
PIPI	90.0	5.0	0.0	0.0	5.0	0.0
PIPN	100.0	0.0	0.0	0.0	0.0	0.0
PISY	42.1	9.2	10.5	13.2	23.7	1.3
PIUN	25.6	12.8	10.3	35.9	12.8	2.6
QUFA	52.6	10.5	0.0	5.3	26.3	5.3
QUIL	100.0	0.0	0.0	0.0	0.0	0.0
QUPE	57.1	28.6	14.3	0.0	0.0	0.0
QUPY	32.4	20.6	2.9	11.8	29.4	0.0
QURO	35.3	20.6	2.9	17.6	8.8	8.8

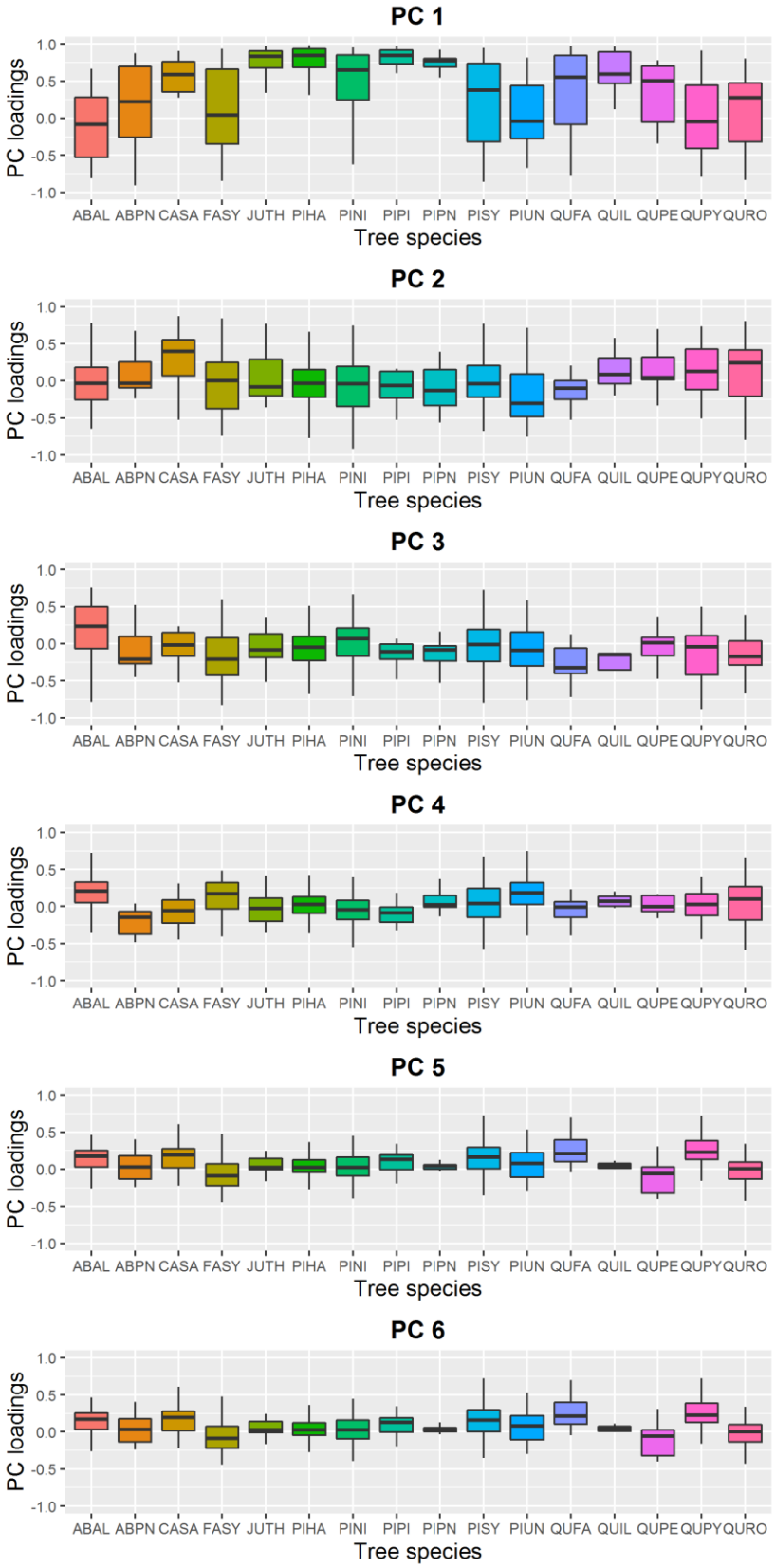

Figure 18: Box plots showing PC loadings for the different tree species. For each box plot, the central solid line indicates the median. The whiskers represent the 10th and the 90th, while the 25th and the 75th are plotted as the vertical lines of the bounding boxes. All codes of species correspond to those listed in Table 4.

4.3. Factors explaining the different patterns of the NDVI-TRWi relationship

Here this thesis presents the comparison between the different PC groups of link between the TRWi and the NDVI time scales and the different environmental characteristics (e.g. air temperature, precipitation, etc.) of the forests included in each PC group. Supplementary Figure 22 summarizes the average monthly NDVI in the different PC groups. As depicted, there are no clear differences between PC groups during the cold season. Nevertheless, during the warm season, there are significant differences between PC1 and the remaining groups. The average NDVI values of PC1 are lower than those of other PCs during summertime (JJA), indicating that forests represented by this component tend to show lower average NDVI values than other forests. Notably, the highest average NDVI values are recorded for PC3 during summer season.

In addition to lower average NDVI values, the forests represented by PC1 correspond to climates with higher air temperature (Supplementary Figures 23 and 24), compared to other PCs. This feature is more pronounced during the warm season. Results also reveal that PC2 shows higher average maximum and minimum air temperatures than PC3 and PC4. These PCs exhibit the lowest averages of air temperature, especially for minimum air temperature. For ETo, PC1 incorporates forests located in dry-warm areas, with higher ETo values than other PCs. This is mostly observed during the warm season, given that ETo is a limiting factor of forest growth in Spain (Supplementary Figure 25). On the contrary, PC3 and PC4 groups correspond to forests located in areas characterized by lower ETo values.

Considerable differences in the average precipitation values recorded for the different PC groups were found (Supplementary Figure 26). PC1 represents not only the forest group characterized by the lowest NDVI values, highest temperatures and ETo, but it is also the group of forests characterized by the lowest average annual precipitation. PC2 is also characterized by low average precipitation values throughout the year. In contrast, PC3 and PC4 are characterized by forests located in areas with higher average precipitation values, even during the dry season. Finally, the water balance, defined as the difference between precipitation and ETo, is summarized for the different forest groups (Supplementary Figure 27). PC1 and PC2 correspond to forests characterized by negative water balance, especially from March to September. This suggests that the forests corresponding to PC1 are located mainly in sites with semi-arid climate conditions. On the other hand, PC3 and PC4 show the higher values for water balance during the warm season.

Overall, these results suggest that TRWi link with NDVI time-scales for the large sample of forests analysed is controlled mainly by the dominant tree species in every forest and the climatic characteristics. This is noticeably confirmed with the Predictive Discriminant Analysis (PDA) that accounts for the relative contribution of each factor to TRWi-NDVI dependency. Table 6 shows the centroids of the groups obtained through a PCA corresponding to the first three functions of the PDA and the percentage of variance explained by each of these functions. The first function shows the highest predictive power, representing 52.8% of the total variance of the PDA. The second and third functions represent 19.7% and 12% of predictive power, respectively. The first function suggests negative values for PC1 and positive values for the remaining components, with the highest values found for PC3. The second function shows its maximum values for PC3 (positive) and PC4 (negative), which means that this function extracts some features of the independent variables that maximize the characteristics of the forests represented by these two components.

Table 6: Centroids of the groups obtained through a principal components analysis corresponding to the first three functions of the Predictive Discriminant Analysis (PDA). The variance explained by each PDA is shown in parentheses.

	PDA 1 (52.8%)	PDA 2 (19.7%)	PDA 3 (12.0%)
Component 1	-0.583	0.039	-0.060
Component 2	0.305	-0.063	0.530
Component 3	1.533	0.792	-0.243
Component 4	0.818	-1.045	-0.057
Component 5	0.568	0.209	-0.406
Component 6	0.479	0.490	1.133

The structure matrix of the three predictive discriminant functions indicates the correlation values of each predictor variable with the three discriminant functions (Table 7). Function 1 shows negative values for the presence of *P. halepensis* forests with negative values of PC1 in the first function. This suggests that the response between TRWi and the different time-scales of the NDVI is favored in semi-arid (positive values of the climate water balance during the growing season) *P. halepensis* forests located in low elevations (given positive value of elevation in PDA1 = 0.43), low average NDVI values during the period of vegetation activity (positive values of the NDVI from June and October in PDA1), high average temperature and ETo values across the year (negative values of these variables in PDA1) and low precipitation (positive values in PDA1). These conditions are completely the opposite to forests characterized by PC3, which show high positive values for the first PDA function. This indicates that PC3 pattern is more common in mountain cool-

wet *A. alba* and *P. uncinata* forests, which show positive values in the first PDA function, located at high elevations, with high average NDVI values during the growing season (June to October) but negative during winter months with snow coverage and low vegetation activity. In addition, the climate characteristics of PC3 pattern are markedly different from those of PC1, given that this pattern is mainly identified in forests characterized by low temperatures and ETo and general humid conditions.

The second PDA function has lower predictive capacity, but with positive values for PC3 and negative values for PC4. A negative value for this second function is obtained for *F. sylvatica* forests, indicating that PC4 pattern is dominant in forest of this species. This pattern is mainly characterized by low temperatures and ETo and high precipitation and climate water balance. In the same context, PC2 is better discriminated by the third PDA function, with a value of 0.53. This PC does not show a clear connection with any forest type, although with the positive values found for temperate *Q. robur* forests across wet areas. This pattern is favored by positive average NDVI values during the warm season and positive values of precipitation during the cold season.

Table 7: Structure matrix of the first three components of the Predictive Discriminant Analysis (PDA). The table shows the correlation values of each predictor variable with the three discriminant functions. The variables most representative in each of the functions are in bold.

Variable type	VARIABLES	FUNCTION 1	FUNCTION 2	FUNCTION 3
Tree species	ABAL	0.254	0.169	-0.049
	ABPN	-0.065	0.08	0.084
	CASA	0.067	-0.005	-0.037
	FASY	0.111	**-0.496**	0.294
	JUTH	-0.121	0.019	-0.018
	PIHA	**-0.458**	0.158	-0.081
	PINI	-0.048	0.021	-0.162
	PIPI	-0.075	-0.033	0.052
	PIPN	-0.157	0.028	-0.071
	PISY	0.071	0.025	-0.086
	PIUN	0.27	-0.276	-0.076
	QUFA	-0.022	0.042	-0.045
	QUIL	0.026	0.016	-0.028
	QUPE	0.093	0.068	0.046
	QUPY	0.136	0.152	0.024
	QURO	0.114	0.132	0.29
Topography	ELEVATION	**0.427**	-0.253	-0.239
Monthly NDVI values	NDVI JAN.	-0.16	0.248	0.066
	NDVI FEB.	-0.146	0.275	0.131
	NDVI MAR.	-0.091	0.311	0.147
	NDVI APR.	-0.012	0.285	0.168
	NDVI MAY.	0.253	0.223	0.227
	NDVI JUN.	**0.513**	0.1	0.275
	NDVI JUL.	**0.527**	-0.01	0.205

Variable type	VARIABLES	FUNCTION 1	FUNCTION 2	FUNCTION 3
Monthly mean minimum temperatures	T. MIN. MAY.	**-0.646**	0.33	0.104
	T. MIN. JUN.	**-0.661**	0.33	0.053
	T. MIN. JUL.	**-0.66**	0.33	-0.014
	T. MIN. AUG.	**-0.659**	0.326	-0.018
	T. MIN. SEP.	**-0.651**	0.298	0.035
	T. MIN. OCT.	**-0.622**	0.279	0.094
	T. MIN. NOV.	**-0.601**	0.246	0.138
	T. MIN. DEC.	**-0.582**	0.219	0.156
Monthly evapotranspiration	ETo JAN.	**-0.402**	0.11	-0.025
	ETo FEB.	**-0.609**	0.253	-0.008
	ETo MAR.	**-0.681**	0.351	-0.018
	ETo APRIL	**-0.693**	0.376	-0.008
	ETo MAY.	**-0.66**	0.398	-0.047
	ETo JUN.	**-0.595**	0.393	-0.111
	ETo JUL.	**-0.518**	0.367	-0.193
	ETo AUG.	**-0.513**	0.379	-0.152
	ETo SEP.	**-0.624**	0.391	-0.067
	ETo OCT.	**-0.648**	0.349	-0.03
	ETo NOV.	**-0.5**	0.187	-0.022
	ETo DEC.	-0.318	0.041	-0.038
Monthly precipitation	PRECIP JAN.	0.349	-0.006	0.331
	PRECIP FEB.	0.275	0.018	0.331
	PRECIP MAR.	0.396	-0.05	0.339
	PRECIP APR.	**0.582**	-0.149	0.252

	NDVI AUG.	**0.694**	0.007	0.329
	NDVI SEP.	**0.673**	0.028	0.279
	NDVI OCT.	**0.544**	0.083	0.258
	NDVI NOV.	0.177	0.187	0.153
	NDVI DEC.	-0.093	0.258	0.028
Monthly mean maximum temperatures	T. MAX. JAN.	**-0.648**	0.313	0.187
	T. MAX. FEB.	**-0.671**	0.359	0.19
	T. MAX. MAR.	**-0.674**	0.388	0.17
	T. MAX. APR.	**-0.677**	0.397	0.141
	T. MAX. MAY.	**-0.67**	**0.417**	0.098
	T. MAX. JUN.	**-0.654**	**0.428**	0.045
	T. MAX. JUL.	**-0.634**	**0.412**	-0.032
	T. MAX. AUG.	**-0.638**	**0.418**	-0.004
	T. MAX. SEP.	**-0.666**	**0.406**	0.097
	T. MAX. OCT.	**-0.68**	0.385	0.154
	T. MAX. NOV.	**-0.667**	0.335	0.176
	T. MAX. DEC.	**-0.644**	0.286	0.18
Monthly mean minimum temperatures	T. MIN. JAN.	**-0.593**	0.232	0.159
	T. MIN. FEB.	**-0.617**	0.271	0.156
	T. MIN. MAR.	**-0.62**	0.298	0.139
	T. MIN. APR.	**-0.638**	0.328	0.148

	PRECIP MAY.	**0.684**	-0.264	0.118
	PRECIP JUN.	**0.663**	-0.298	0.001
	PRECIP JUL.	**0.65**	-0.328	0.024
	PRECIP AUG.	**0.544**	-0.367	-0.033
	PRECIP SEP.	**0.545**	-0.292	0.059
	PRECIP OCT.	**0.435**	-0.132	0.24
	PRECIP NOV.	**0.444**	-0.097	0.315
	PRECIP DEC.	0.302	0.001	0.305
Monthly climatic water balance	BALANCE JAN.	0.385	-0.02	0.321
	BALANCE FEB.	0.348	-0.022	0.309
	BALANCE MAR.	**0.504**	-0.128	0.294
	BALANCE APRIL	**0.653**	-0.229	0.192
	BALANCE MAY	**0.705**	-0.323	0.098
	BALANCE JUN.	**0.672**	-0.359	0.051
	BALANCE JUL.	**0.631**	-0.374	0.115
	BALANCE AUG.	**0.572**	-0.4	0.045
	BALANCE SEP.	**0.605**	-0.344	0.066
	BALANCE OCT.	**0.517**	-0.188	0.219
	BALANCE NOV.	**0.485**	-0.115	0.303
	BALANCE DEC.	0.328	-0.004	0.299

5. Impact of drought variability on remote sensing vegetation activity in Spain: a high spatial resolution analysis from 1981 to 2015

5.1. Datasets and methods

Given strong seasonality of vegetation activity, and also given different vegetation types the NDVI magnitude is not spatially and temporally comparable in the peninsular Spain and the Balearic Islands. For this reason, the data from the Sp_1Km_NDVI dataset was temporally standardized (sNDVI) with the purpose of having series with comparable magnitudes and characterized by an average equal to zero and a standard deviation equal to one. For this purpose, a log-logistic distribution was used, which has showed better performance than others to obtain standardized series of different physical variables (Vicente-Serrano and Beguería, 2016). Moreover, to avoid that land cover changes could disturb the temporal relationship between drought severity and NDVI and after testing different thresholds, the areas that showed a decrease in the annual NDVI higher than 0.05 units and an increase higher than 0.15 units between 1981 and 2015 were removed from analysis. There are also other areas that although more gradual, they also show NDVI changes, mostly characterised by a positive NDVI trend in large areas of Spain as a consequence of rural exodus and natural revegetation processes (Hill et al., 2008; Vicente-Serrano et al., 2018). To avoid an influence of these dominant positive trends, we have detrended the standardized NDVI series by means of a linear model, adding to the residuals the average over the entire period.

For the quantification of the drought variability a high spatial resolution gridded meteorological variable available was used for peninsular Spain and the Balearic Islands. This dataset matches the spatial resolution and the temporal frequency and coverage of the NDVI data. The dataset includes the following climate variables: precipitation, maximum and minimum air temperature, relative humidity, sunshine duration and wind speed. This dataset has been based on a careful quality control and homogenization of the complete meteorological daily series of the Spanish Meteorological Agency (AEMET). Details of the dataset and the methodological approach used for gridding and data validation can be found at Vicente-Serrano et al. (2017). Using the gridded dataset, the atmospheric evaporative demand (AED) was calculated. The physically based FAO-

56 Penman-Monteith equation was used for calculations (Allen *et al.*, 1998). With the gridded data of precipitation and AED at the semi-monthly temporal resolution from 1981 to 2015, we calculated the Standardized Precipitation Evapotranspiration Index (SPEI) (Vicente-Serrano *et al.*, 2010) at time scales of 1- to 48- semi-monthly periods, which cover the common 1- to 24-month time scales. The SPEI is one of the most widely used drought indices worldwide and it has showed advantages regarding others to identify drought impacts in a number of socioeconomic (Bachmair et al., 2015; Stagge et al., 2015), agricultural (Peña-Gallardo *et al.*, 2018a) and environmental (Vicente-Serrano et al., 2012; Bachmair et al., 2018) drought impacts. Regarding other drought indices, like the Palmer Drought Severity Index (PDSI), the SPEI has the advantage of being calculated on different time scales, but it has also advantages regarding the Standardized Precipitation Index (SPI) (McKee *et al.*, 1993) since in addition to the precipitation, it includes the AED, which is essential in the current climate change scenario in which the AED has noticeably increased in the last decades in Spain (Vicente-Serrano *et al.*, 2014b). Vicente-Serrano et al. (2014a) showed that including AED in the drought quantification explains better streamflow variability than using precipitation alone.

The use of different drought time scales is absolutely essential to quantify the response of different hydrological and environmental systems to drought (Vicente-Serrano et al., 2011; Vicente-Serrano et al., 2013). The time scale refers to the period in which antecedent climate conditions are accumulated and it allows to determine accurately the drought impacts since different hydrological systems show different responses to the time scales of climate variability (López-Moreno et al., 2013; Barker et al., 2016) but also ecological and agricultural systems show strong differences in the response to different time scales of climatic droughts (Pasho et al., 2011; Peña-Gallardo et al., 2018b) given different biophysical conditions, but also the different strategies of vegetation types to cope with water stress (Chaves et al., 2003; McDowell et al., 2008), which are strongly variable in complex Mediterranean ecosystems. The influence of drought on vegetation activity and forest growth is extremely difficult to be assessed, due to is related to complex and not well-known physiological strategies (Chaves et al., 2003), and also related to the different specific resistance and vulnerability to drought (Gazol et al., 2017; Gazol

et al., 2018), which makes absolutely necessary to use drought indices that can be calculated on flexible time scales since it is not known a priori the most suitable period at which the NDVI is responding. Semi-monthly SPEI data was also de-trended to be compared with the de-trended sNDVI so both datasets have the same units (standardized anomalies) with no trends in the different series.

Finally, a new land cover map was used with the purpose of determining the possible influence of land cover on the response of the NDVI to drought severity. For this purpose the official CORINE land cover for 2000 (https://land.copernicus.eu/pan-european/corine-land-cover) was selected date because it corresponds approximately to the mid of the analysed period and it can be more representative for the long analysed period.

Pearson's correlation coefficients were used to determine the relationship between the interannual variability of the sNDVI and the SPEI. This was analysed for each semi-monthly period of the year. The correlation between the sNDVI with the SPEI was calculated at time-scales between 1- and 48-semi-month time scales. Significant correlations were set at $p < 0.05$. Since it is not known a priori what the time scale is which maximum correlation is identified, the maximum correlation found between the sNDVI and the different SPEI time scales was retained, independently of the time scale at which this maximum correlation is recorded. In addition, the time scale at which the maximum correlation is recorded was also retained to determine possible spatial and seasonal differences and differences among the land cover categories.

The correlations obtained, but also the time-scales at which the relationship is obtained, were related to the average climate conditions, including the aridity (precipitation minus AED) and the average temperature. These data were obtained from the average values of the climate gridded dataset described above.

5.2. General Influence of the SPEI on the sNDVI

Figure 19 shows an example of the spatial maps of the Pearson's r correlations between the sNDVI and the SPEI at the time-scales of 1-, 3-, 6- and 12-months (2-, 6-, 12- and 24-semi-

monthly periods). The results are showed for the second semi-monthly period of each month between April and July. The maps clearly illustrate the different response of the NDVI to the drought time scales. This stress the need of considering different drought time scales to know the climate cumulative period that mostly affects vegetation activity. In this case, it is evident that the 6-month time scales are more relevant to explain vegetation activity in large areas of Southest and Southwest of Spain during the second half of April, but vegetation activity is more determined by the 12-month SPEI in the Ebro basin (northeast). In the 2nd period of May the 6-month and 12-month SPEI seem to produce similar results but in June and July the 12-month outperforms the results obtained with the 6-month SPEI. Supplementary Figures 28 to 31 show different density plots illustrating how the magnitude of correlations obtained over Spain between the SPEI and the sNDVI show strong changes as a function of the analysed semi-monthly period but also as a function of the SPEI time scale. These plots clearly illustrate how correlations tend to be higher during the warm season (May to August) and at time scales between 6 and 24 months.

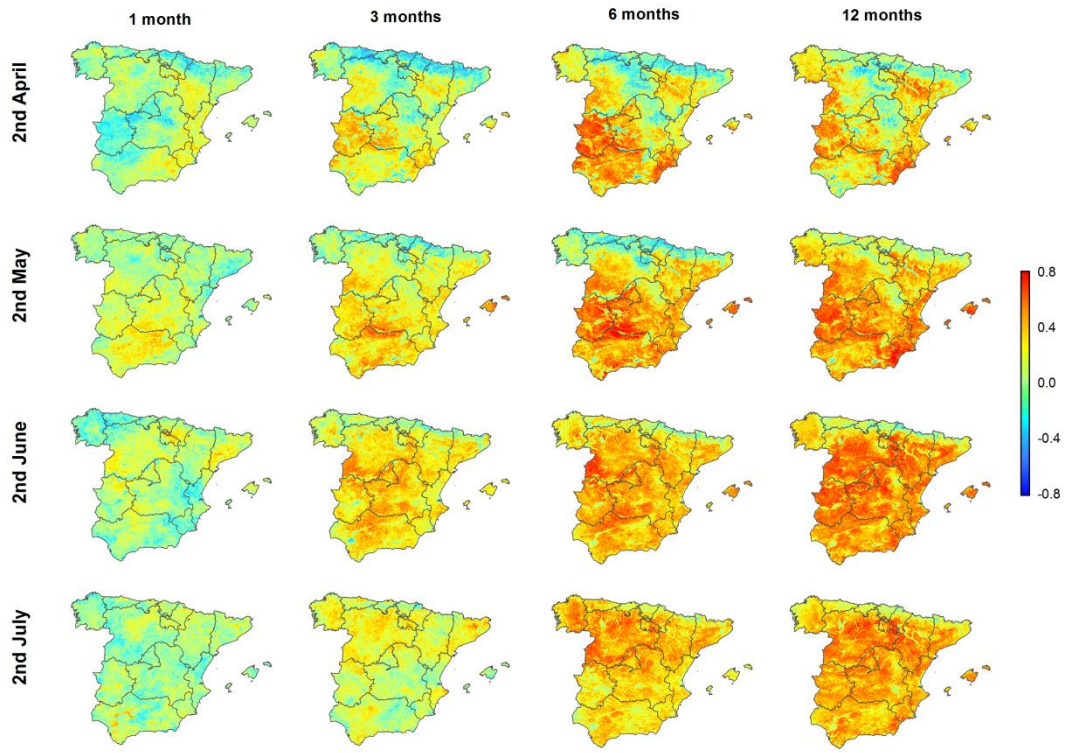

Figure 19: Examples for different semi-monthly periods on the spatial differences in correlation between the sNDVI and different SPEI time scales.

Figure 20 summarizes the response of the NDVI to drought by means of the calculation of the maximum correlation between the sNDVI and the SPEI, independently of the SPEI time scale. The maps show strong seasonality and important spatial differences. The main sensitivity of the NDVI to drought is recorded during the warm season (May to August), in which the highest correlations are found. On the contrary, between September and April the sensitivity of vegetation to drought is lower, although in some areas (e.g. the Southeast Mediterranean coastland) the sensitivity remains relevant throughout the entire year. Table 8 shows a summary, with the percentage of Spain showing significant or non-significant correlations during the different semi-monthly periods. It illustrates how positive and significant correlations are dominant across the country, but also how there is a relevant seasonal component since during the warm season a high percentage of Spain shows positive and significant correlations. Between the second half of the month of May to the second of September more than the 80% of the study domain shows positive and significant correlations between the sNDVI and the SPEI. Between 2nd June and 1st August, more than 90% of Spain shows positive and significant correlations. Figure 21 summarizes the average correlations between SPEI and sNDVI over the whole Spain, clearly showing how from the 1st April period (7th) the response of the sNDVI to the SPEI increases noticeably until July (13th), month in which the maximum average correlation is recorded. From August to December correlations slowly decrease.

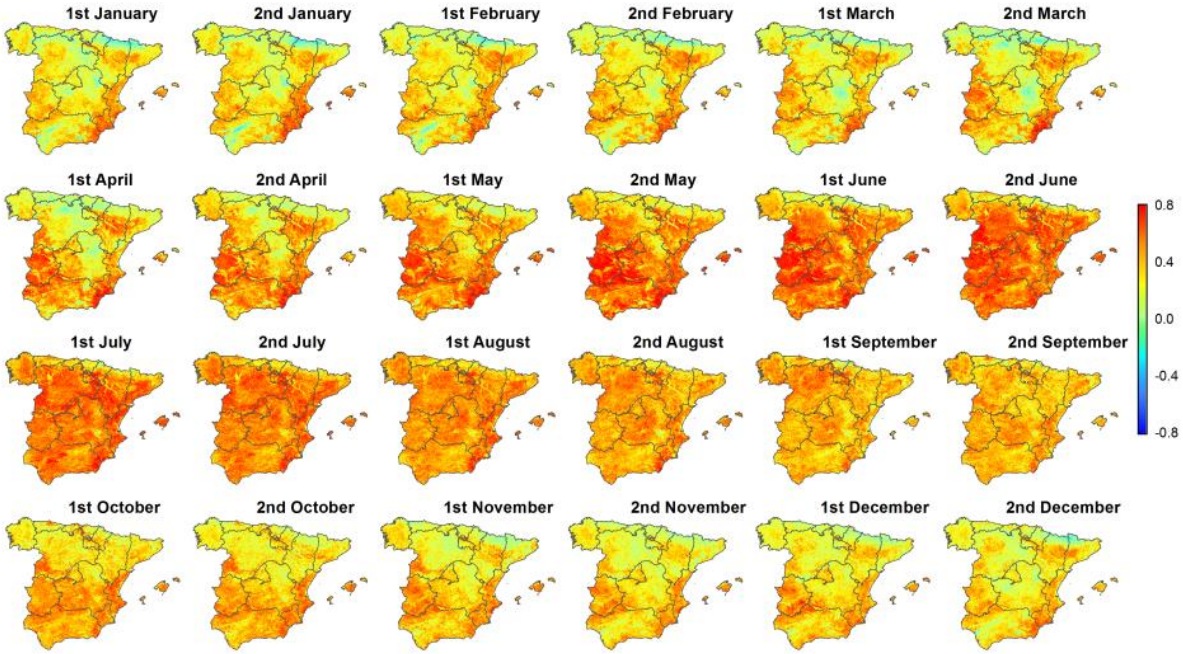

Figure 20: Spatial distribution of the maximum correlation between the sNDVI and the SPEI during the different semi-monthly periods.

Table 8: Percentage of the total surface area in Spain showing positive or negative, significant or non-significant Pearson's r correlations between the sNDVI and the SPEI.

	Neg. ($p < 0.05$)	Neg. ($p > 0.05$)	Pos. ($p > 0.05$)	Pos. ($p < 0.05$)
1st Jan	0.3	9.8	41.3	48.6
2nd Jan	0.4	8.7	40.2	50.7
1st Feb	0.3	7.5	39.9	52.3
2sd Feb	0.1	7.5	39.0	53.4
1st Mar	0.2	8.9	41.6	49.4
2sd Mar	0.2	11.3	38.2	50.3
1st Apr	0.0	7.6	34.9	57.5
2sd Apr	0.0	3.4	27.0	69.7
1st May	0.0	1.6	19.0	79.4
2sd May	0.0	0.9	14.2	84.9
1st Jun	0.0	1.2	10.8	88.0
2sd Jun	0.0	0.5	7.4	92.0
1st Jul	0.0	0.3	5.3	94.4
2sd Jul	0.0	0.1	4.5	95.4
1st Aug	0.0	0.1	5.9	94.1
2sd Aug	0.0	0.2	10.6	89.2
1st Sep	0.0	0.6	14.0	85.4
2sd Sep	0.0	0.4	16.9	82.6
1st Oct	0.0	1.5	24.5	74.0
2sd Oct	0.0	1.9	31.1	67.0
1st Nov	0.0	4.5	35.6	59.8
2sd Nov	0.0	4.8	41.8	53.4
1st Dec	0.0	4.4	38.9	56.7
2sd Dec	0.2	5.9	43.1	50.8

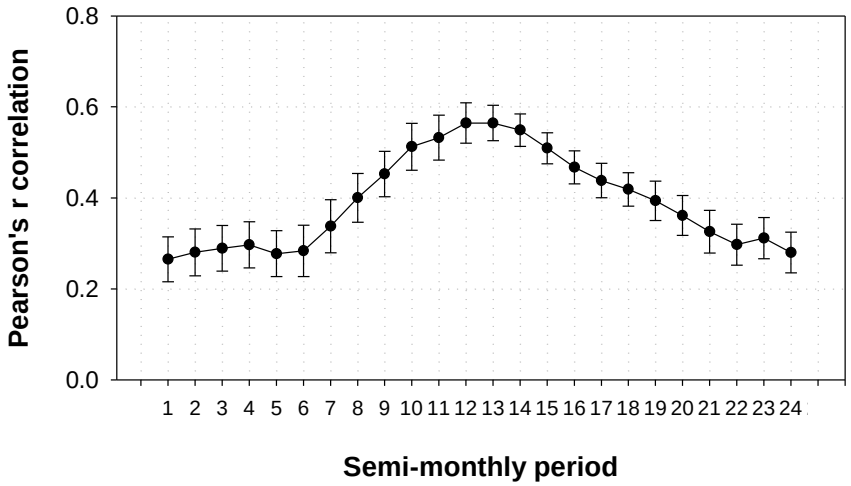

Figure 21: Average and standard deviation of the Pearson's r correlation coefficient between the sNDVI and the SPEI in Spain.

The response of the sNDVI to different times scales of the SPEI show strong complexity. Figure 22 shows the spatial distribution of the SPEI time scale at which maximum correlation is found between the SPEI and the sNDVI in each one of the 24 semi-monthly periods of the year. There are very important spatial and seasonal differences, which are masked with the estimated average values of the SPEI time scale recorded for the different semi-monthly periods (Figure 23), which are quite similar (oscillating between 18 and 22 semi-monthly periods -9 to 11 months-) throughout the year. In general, the areas and periods with higher correlations between the sNDVI and the SPEI are recorded at time scales between 7 and 24 semi-months (3-12 months) and this pattern is mostly recorded between May and July (Supplementary Figure 32), the period in which the sNDVI variability is more sensitive to the SPEI. Nevertheless, there are not general patterns that suggest a dominance of the maximum correlations associated to a certain SPEI time scale (Supplementary Figure 33) and this pattern is not driven by the presence of different land cover since the different boxplots are quite similar among the different land cover types (Supplementary Figures 34 to 44).

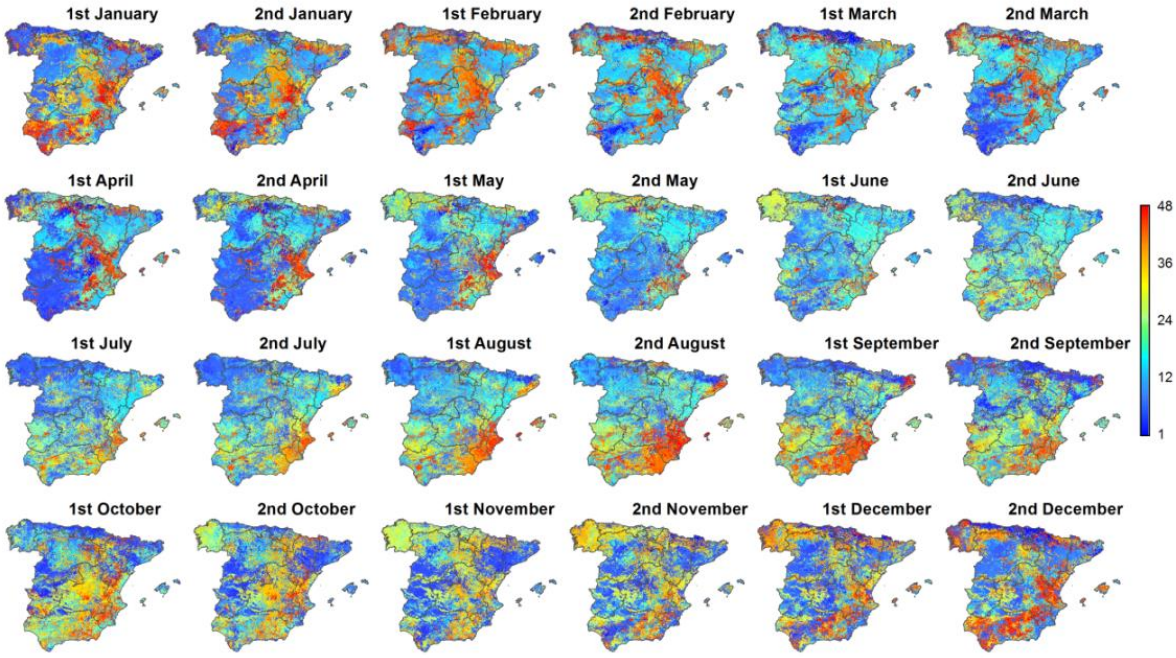

Figure 22: Spatial distribution of the SPEI time scales at which the maximum correlation between sNDVI and SPEI is found in each one of the semi-monthly periods.

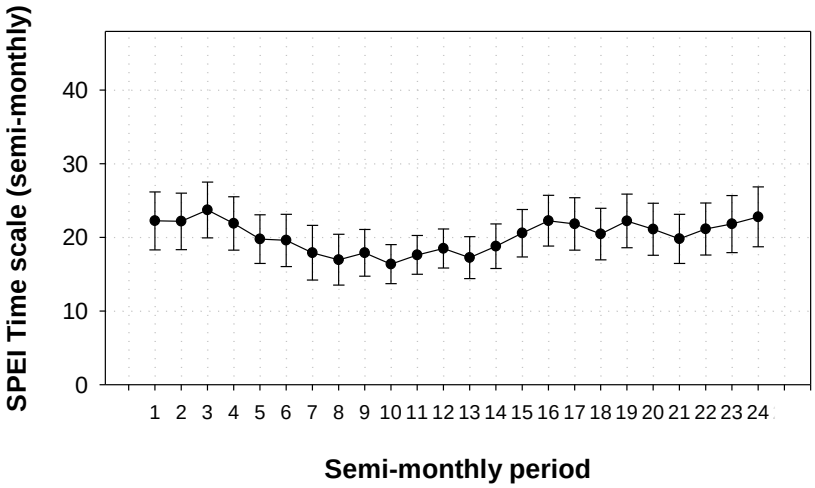

Figure 23: Average and standard deviation of the SPEI time scale at which the maximum Pearson's r correlation coefficient between the sNDVI and the SPEI is found in Spain.

5.3. Land cover differences

There are relevant differences in the magnitude and seasonality of the Pearson's r correlation coefficients considering different land cover types. Figure 24 shows the average and standard error of the average maximum Pearson's r coefficients between the sNDVI and the SPEI for the different land cover types and the 24 semi-monthly periods. It shows strong differences among

the magnitude of correlations but also in the period of the year in which these correlations are recorded. The non-irrigated arable lands show a clear increase in the magnitude of the correlations between April to June, in which a peak of significant correlation is recorded but a decrease in the magnitude of correlations to the end of the year. The majority of the surface of this land cover shows positive and significant correlations between May and September (Supplementary Table 3), with percentages close to 100%. On the contrary, irrigated lands do not show so clear signal of response to the drought variability during the warm season and although a seasonal pattern is also recorded, this is much less pronounced than the recorded for non-irrigated arable lands. In any case, irrigated areas characterized by positive and significant correlations between sNDVI and SPEI are dominant during summer months (Supplementary Table 4).

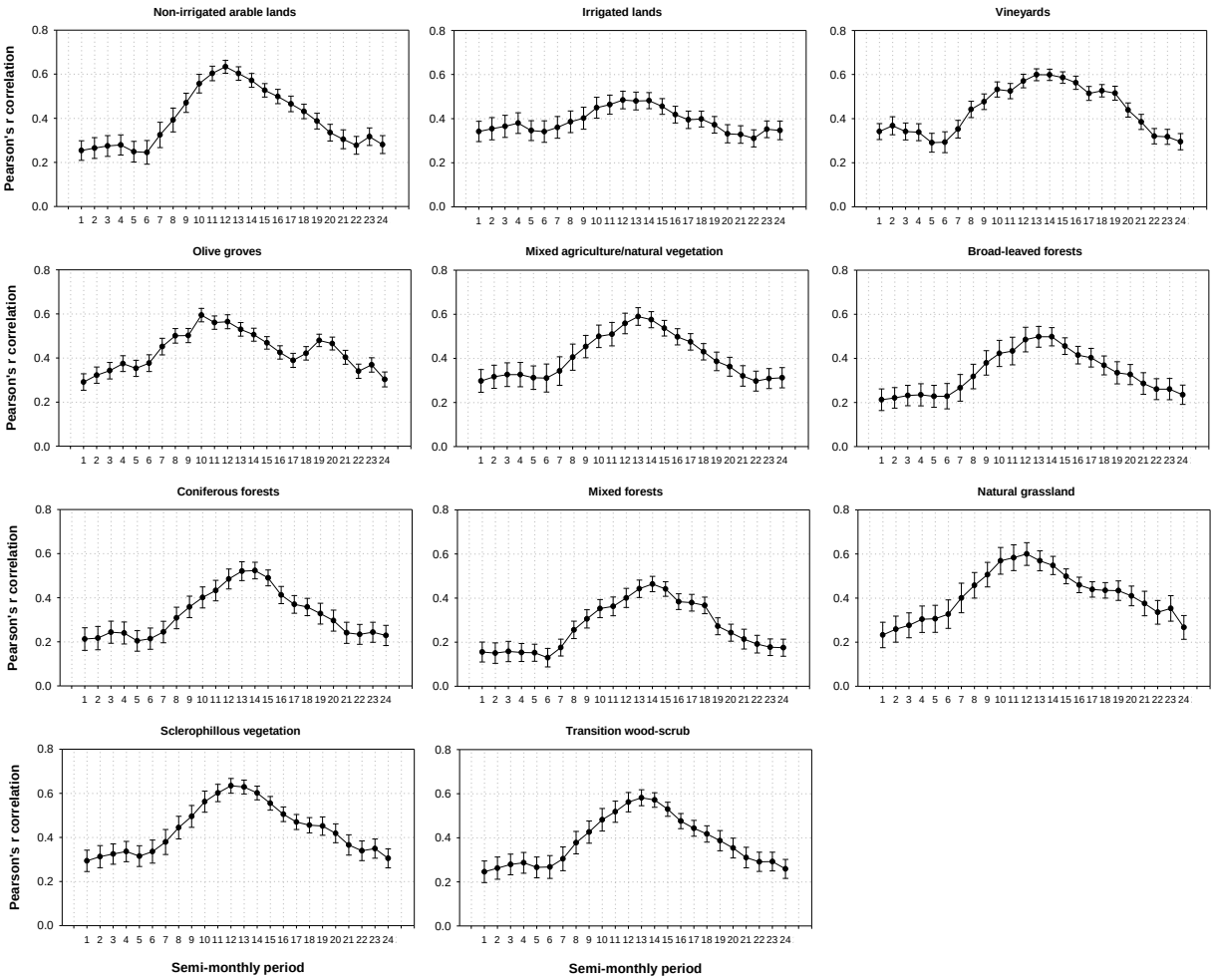

Figure 24: Average and standard deviation of the Pearson's r correlation coefficient between the sNDVI and the SPEI in the different land cover types analysed.

Vineyards also show a clear seasonal pattern. Nevertheless, the peak of maximum correlations is displaced in comparison to that observed in the non-irrigated arable lands in July and August, but also high average correlation values are recorded until October. Thus, between May and October high percentage of vineyards shows positive and significant correlations between the sNDVI and the SPEI (Supplementary Table 5). Olive groves show a peak of correlation between the sNDVI and the SPEI in the second half of May, followed by a decrease in the magnitude of the correlations to September, showing also an increase of the magnitude of correlations in October, which suggest a quasi bi-modal peak of response, also observed in the percentage of the surface area showing significant correlations (Supplementary Table 6). The dominant areas of natural vegetation clearly show a unimodal pattern of response of the sNDVI to the SPEI, with peaks of maximum correlation during the active summer season. The peak of maximum correlations tends to be recorded in July and August for the different forest types but earlier (June) for the natural grasslands and the areas of sclerophillous vegetation. Mixed forests tend to show a lower magnitude in the correlation values than the broad-leaved and the coniferous forests. In any case, the majority of the area covered by these types of land cover show positive and significant correlations between the sNDVI and the SPEI during summer months (Supplementary Tables 7 to 13).

The SPEI time scales at which the maximum correlations between the sNDVI and the SPEI are found vary among the different land cover types (Figure 25). For non-irrigated arable lands the SPEI time scale showing maximum correlation with the sNDVI is recorded in average at time scales between 11 and 21 semi-monthly periods. During the period in which higher correlations are recorded (May-June), the crops respond mostly to the climate conditions recorded between December and June. Irrigated lands show a clear seasonal pattern. Maximum correlations tend to be recorded at time scales between 12-18 semi-monthly periods (6-months) between November and May but in the summer season the time-scales with maximum correlations between sNDVI and SPEI increase to 25-28 semi-monthly periods. Vineyards also show certain seasonality, responding to longer time-scales at the end of the summer. In general, natural

vegetation areas show less seasonality in the SPEI time scales that mostly control interannual sNDVI variability. They oscillate between 30 semi-monthly periods in the cold season to 20 semi-monthly periods during the warm season in the different forest types, sclerophillous vegetation areas and the areas of transition wood-scrub. Exceptions are natural grasslands, which tend to show a response to shorter SPEI time-scales (20 semi-monthly periods in winter and 15 in spring and early summer).

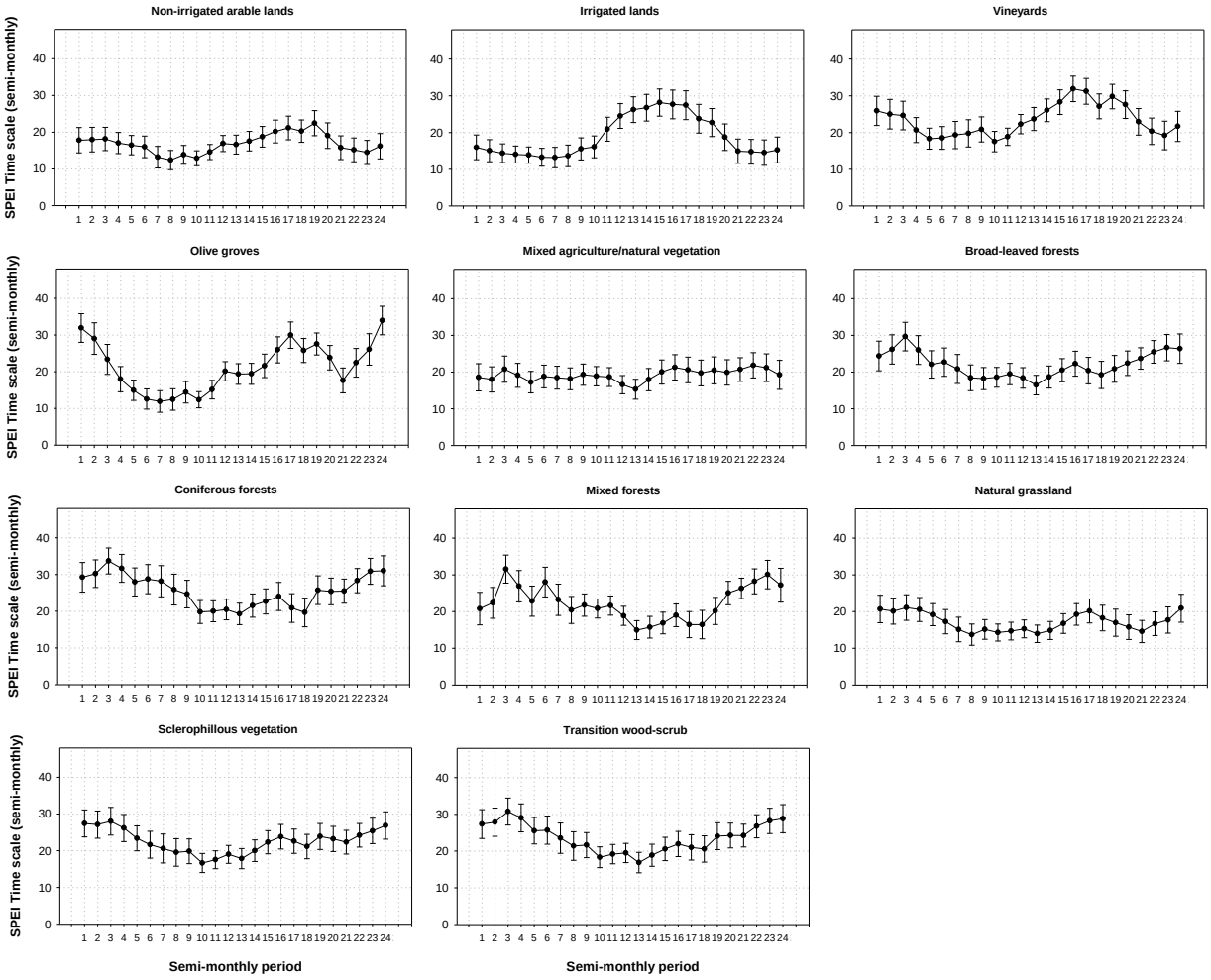

Figure 25: Average and standard deviation of the SPEI time scale at which the maximum Pearson's r correlation coefficient between the sNDVI and the SPEI in the different land cover types analysed.

5.4. Influence of average climate conditions

The sensitivity of the sNDVI to the SPEI variability is strongly related to the average climate conditions, summarized by the climate aridity and the mean air temperature. Figure 26 shows the relationship between the spatial distribution of the aridity and the spatial distribution of the maximum correlation between the sNDVI and the SPEI. It clearly shows that for most of the

semi-monthly periods of the year there is a significant negative relationship between the aridity and the maximum correlation between sNDVI and SPEI, which means that vegetation activity in arid sites is mostly controlled by the SPEI variability. Significant relationships have been found from December to June. Nevertheless during the warmest months (July and August), there is not a significant relationship between the sensitivity of the sNDVI to the SPEI and the aridity conditions. A similar pattern is observed with the analysis of the relationship with the average temperature (Figure 27). There are general positive and significant relationships between March and June, but there is not a control of the spatial correlation patterns by the average air temperature during the summer season.

These general patterns strongly vary as a function of the land cover (Supplementary Figures 45 to 55). In the non-irrigated arable lands, there are strong negative relationships between the sNDVI/SPEI correlation and the spatial distribution of aridity between March and May, coinciding with the period of higher vegetation activity in this land cover type, and also with the period of higher average correlations between sNDVI and the SPEI, suggesting that non-irrigated arable lands located in the most arid areas are more sensitive to drought variability than those located in humid regions. The correlations observed in irrigated lands, vineyards and olive groves are not significantly related with aridity in any period of the year. Nevertheless, in the different natural vegetation categories the relationships are negative and statistically significant during large periods. The mixed agricultural/natural vegetation areas show a significant relationship between October and July and very negative coefficients are recorded at the beginning of the summer season (< -0.7). Broadleaved and coniferous forests, scrubs and pasture lands also show a negative relationship between the spatial patterns of the sNDVI/SPEI correlations and the patterns of aridity.

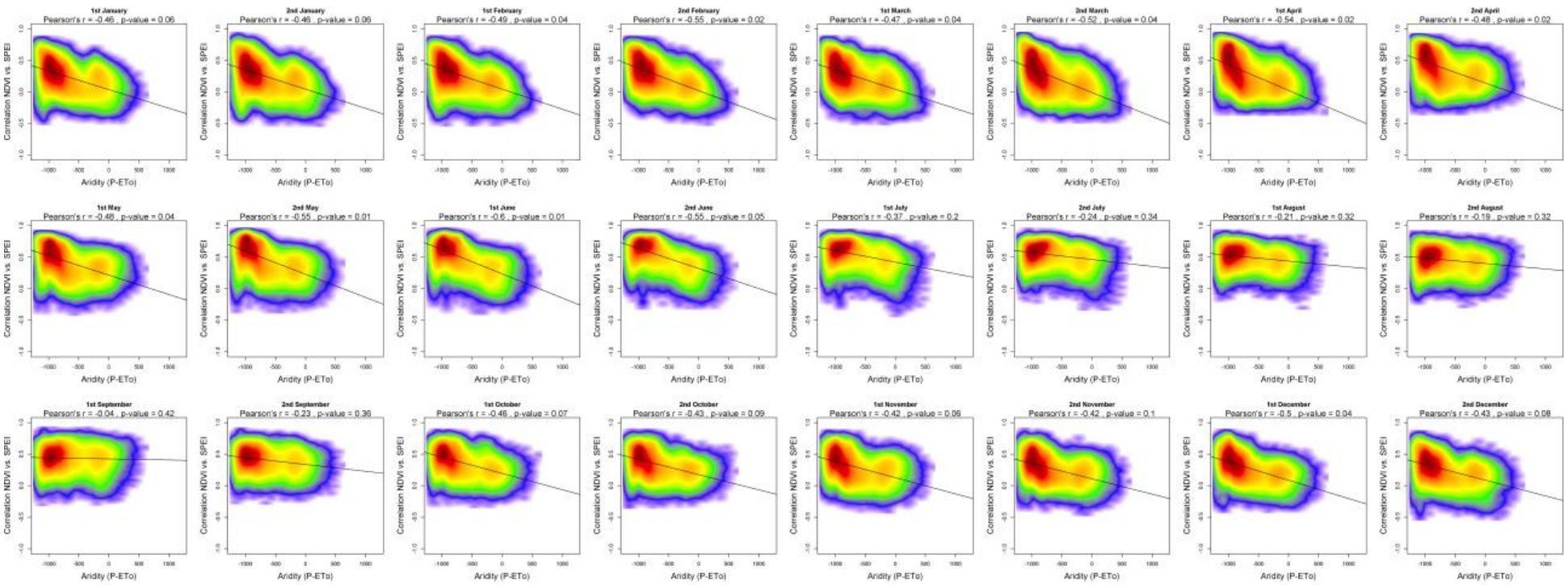

Figure 26: Scatterplots showing the relationships between the maximum correlations obtained between the sNDVI and the SPEI and the climate aridity (Precipitation minus Reference Evapotranspiration). Given the high number of points the signification of correlation was obtained by means of 1000 random samples of 30 cases from which correlations and p-values were obtained. The final signification was assessed by means of the average of the obtained p-values.

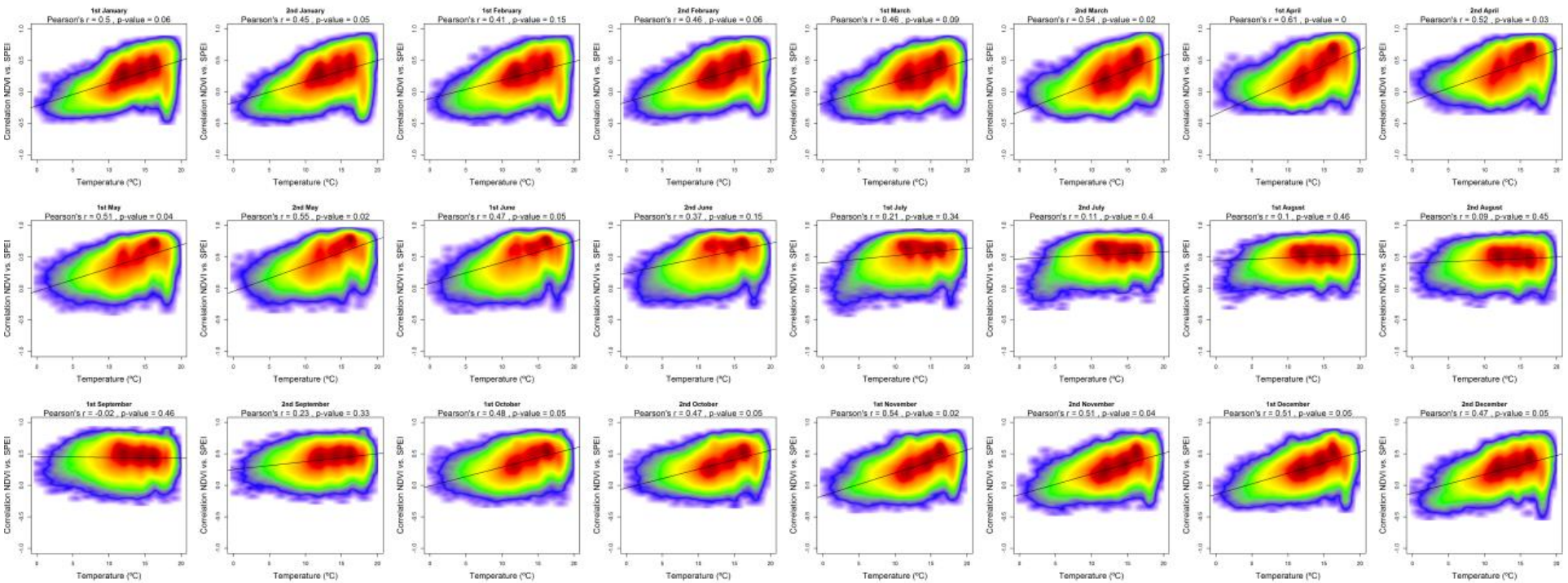

Figure 27: Scatterplots showing the relationships between the maximum correlations obtained between the sNDVI and the SPEI and the average air temperature. Given the high number of points the signification of correlation was obtained by means of 1000 random samples of 30 cases from which correlations and p-values were obtained. The final signification was assessed by means of the average of the obtained p-values.

The relationship between sNDVI vs. SPEI correlations and the average air temperature over the entire peninsular Spain and Balearic Islands shows that in spring the control of the sNDVI by the SPEI is correlated with the air temperature, so the warmer areas are those in which the sNDVI is more controlled by drought (Figure 26). Moreover, during the warm season this pattern disappears and the spatial patterns of correlations between sNDVI and SPEI do not show any control by the average temperature. The connection of the NDVI-SPEI relationships with average temperature also varies among different land cover types (Supplementary Figures 56 to 66). For example, in the non-irrigated arable lands there is a positive and significant relationship between March and April, which means that areas in which the interannual variability of the sNDVI is more controlled by the SPEI tend to coincide with average warmer conditions. As observed for aridity, the relationship between the SPEI and the sNDVI in irrigated lands is not sensitive to the spatial patterns of the average temperature. This pattern is also recorded for vineyards and olive groves. Nevertheless, the areas of natural vegetation show a clear relationship between the sNDVI and the SPEI correlations and the spatial distribution of temperatures. In the mixed agriculture/natural vegetation areas there is a significant positive spatial association between the sNDVI and the SPEI between October and May. On the contrary, in summer months the association is not statistically significant. The general association during spring and the lack of association during summer is recorded in other natural vegetation classes like the broad-leaved and coniferous forests, natural grasslands, sclerophillous vegetation and transition wood-scrubs.

It was also analysed if there is an association between the time-scales at which the maximum sNDVI/SPEI correlation is recorded, the aridity (P-ETo) and the average air temperature. The results are very complex. Figure 28 shows different box-plots (one for each semi-monthly period) in which the values of land aridity are indicated for SPEI time scales at which the maximum correlation between the sNDVI and the SPEI has been found. In general, during the cold season there are no appreciable patterns. In spring (semi-monthly periods 6th to 11th), it seems that the less arid areas tend to record correlations at long time-scales (25-42 semi-

monthly periods). Nevertheless, also the regions that record the maximum correlations at short time scales (1-6 months) tend to show less aridity than areas that record maximum correlations at time scales between 7 and 24 semi-monthly periods. It means that the most arid areas mostly respond to the SPEI time scales between 6 and 12 months, but more humid sites are responding to short (1-3 months) or long (> 12 months) SPEI time-scales.

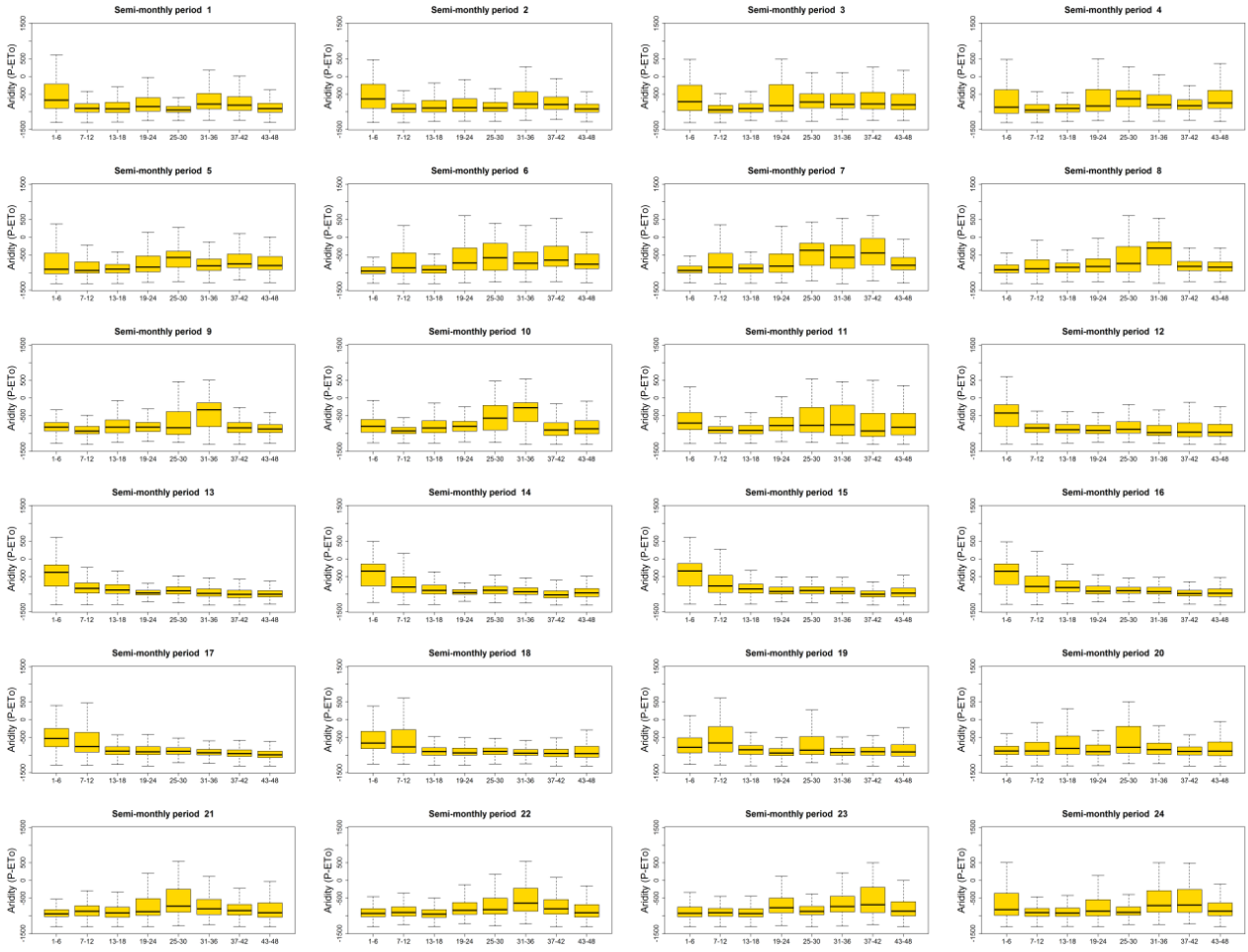

Figure 28: Box plots showing the climate aridity values as a function of the SPEI time scales at which the maximum correlation between sNDVI and SPEI has been found

Nevertheless, also the regions that record the maximum correlations at short time scales (1-6 months) tend to show less aridity than areas that record maximum correlations at time scales between 7 and 24 semi-monthly periods. It means that the most arid areas mostly respond to the SPEI time scales between 6 and 12 months, but more humid sites are responding to short (1-3 months) or long (> 12 months) SPEI time-scales. Nevertheless, this pattern completely changes during the summer season (from June to September), in which the interannual variability of the

sNDVI in the arid areas is mostly determined by the SPEI recorded at time scales higher than 6 months (12 semi-monthly periods). On the contrary, the most humid regions tend to respond to short SPEI time scales (< 3 months).

This general pattern is highly dependent of the land cover type since it cannot be identified in some land covers although it is evident in others (Supplementary Figures 67 to 77). In the non-irrigated arable lands there are not important differences of aridity as a function of the SPEI time-scale that recorded the maximum correlation with the sNDVI. Moreover, this pattern is independent of the semi-monthly period considered. In the vineyards summer months also show a general response of the sNDVI to short SPEI time scales in areas characterized by lower aridity conditions, but this pattern is not identified in the olive groves. The differences in aridity as a function of the SPEI time scale that showed stronger correlation with sNDVI are more evident in natural vegetation. Areas characterized by mixed agriculture/vegetation areas show high complexity in winter and spring with not clear patterns in relation to the SPEI time-scales that show the maximum correlations. Nevertheless, in summer months there is a clear pattern characterized by a dominant correlation recorded at shorter time scales in the most humid areas, whereas the most arid sectors tend to respond to very long SPEI time-scales (> 12 months). This pattern is clearly recorded from June to September. The pattern is not so well identified in the broad-leaved forests although the response to short SPEI time scales seems to be more frequent in the less arid broad-leaved forests. On the contrary, coniferous forests, sclerophylous vegetation and the transition wood-scrub show a relationship between the aridity and the average SPEI time-scales at which maximum correlation with the sNDVI is recorded during summer months. Natural grassland areas show a completely different pattern between spring and summer months since in spring the grasslands located in the most arid sites show dominant correlation at short SPEI time scales. On the contrary, from July to September, these areas follow the same pattern observed in other natural vegetation areas, characterized by maximum correlations recorded at short SPEI time scales under less arid conditions.

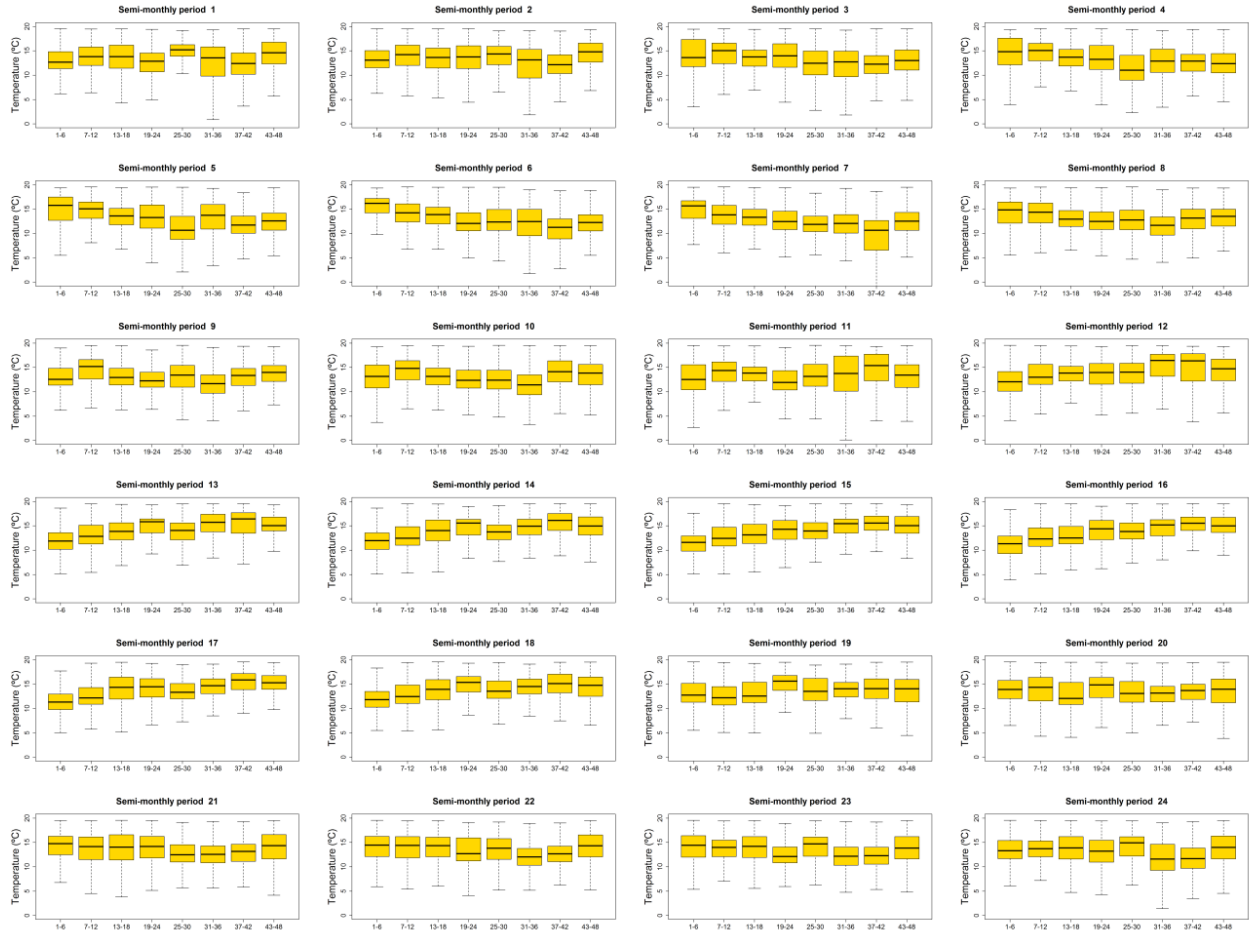

Figure 29: Box plots showing the air temperature values as a function of the SPEI time scales at which the maximum correlation between sNDVI and SPEI has been found

There is also a certain relationship between the spatial distribution of the average temperature and the SPEI time scales at which maximum correlation between sNDVI and SPEI is recorded (Figure 29). In early spring, short SPEI time scales are dominant in the warmest areas, whereas dominant long SPEI time scales are recorded in colder regions. Nevertheless, from June to September is recorded the opposite pattern, characterized by dominant short SPEI time scales in cold sites and long SPEI time scales in warm areas. These patterns show strong differences among vegetation types, but the natural vegetation areas tend to reproduce the general behavior (Supplementary Figures 78 to 88).

The spatial distribution of the different land cover types analysed in this study (excluding the irrigated lands in which the anthropogenic factors are determinant) show a clear gradient determined by the climate aridity. Mixed forest are located in the most humid areas and

vineyards, olive groves, non-irrigated arable lands and the sclerophyllous natural vegetation are located in the most arid sites (Figure 30). Nevertheless, it is also found a gradient of these land cover types related with the sensitivity to drought. Therefore, the land cover types located under more arid conditions show a higher response of the NDVI to the SPEI than those located under more humid bioclimatic conditions. For example, the mixed forests show lower correlations than the different crop types but also than the rest of the vegetation areas. Thus, there is a linear relationship between the climate aridity in which each land cover is located and the maximum response of the sNDVI to the SPEI. This pattern is identified during the different semi-monthly periods of the year, although the differences are much more important in spring and autumn. In summer months the differences in correlation are smaller between the different land cover categories, independently of the aridity conditions.

There are also differences in the average SPEI time scale at which the maximum sNDVI vs. SPEI correlation is obtained but in this case the pattern is more complex, with noticeable seasonal differences in the pattern of relationship with the climate aridity of the different land cover types (Figure 30). In spring and late autumn the land cover types located in more arid conditions tend to respond to shorter SPEI time scales than the land cover types located in more humid sites. Nevertheless, this pattern is not recorded at the beginning of the summer (June) but it changes in late summer and early autumn, in which the most arid land cover types (vineyards and olive groves) tend to respond at longer SPEI time scales than the different forest types (mostly the mixed forests) usually located under more humid conditions.

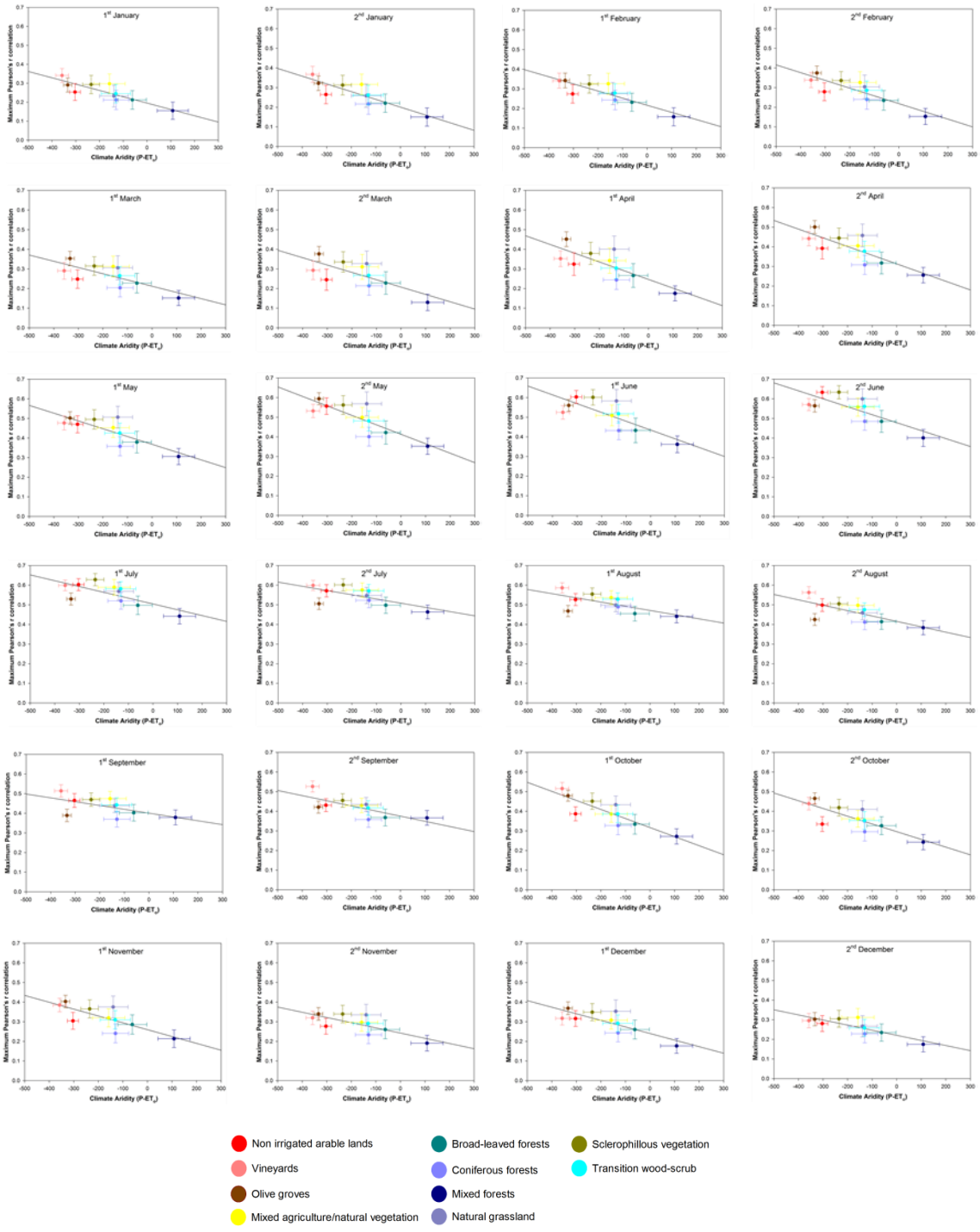

Figure 30: Scatterplots showing the relationship between the mean annual aridity and the maximum correlation found between the sNDVI and the SPEI in the different land cover types analysed in this study. Vertical and horizontal bars represent ¼ of standard deviation around the mean values.

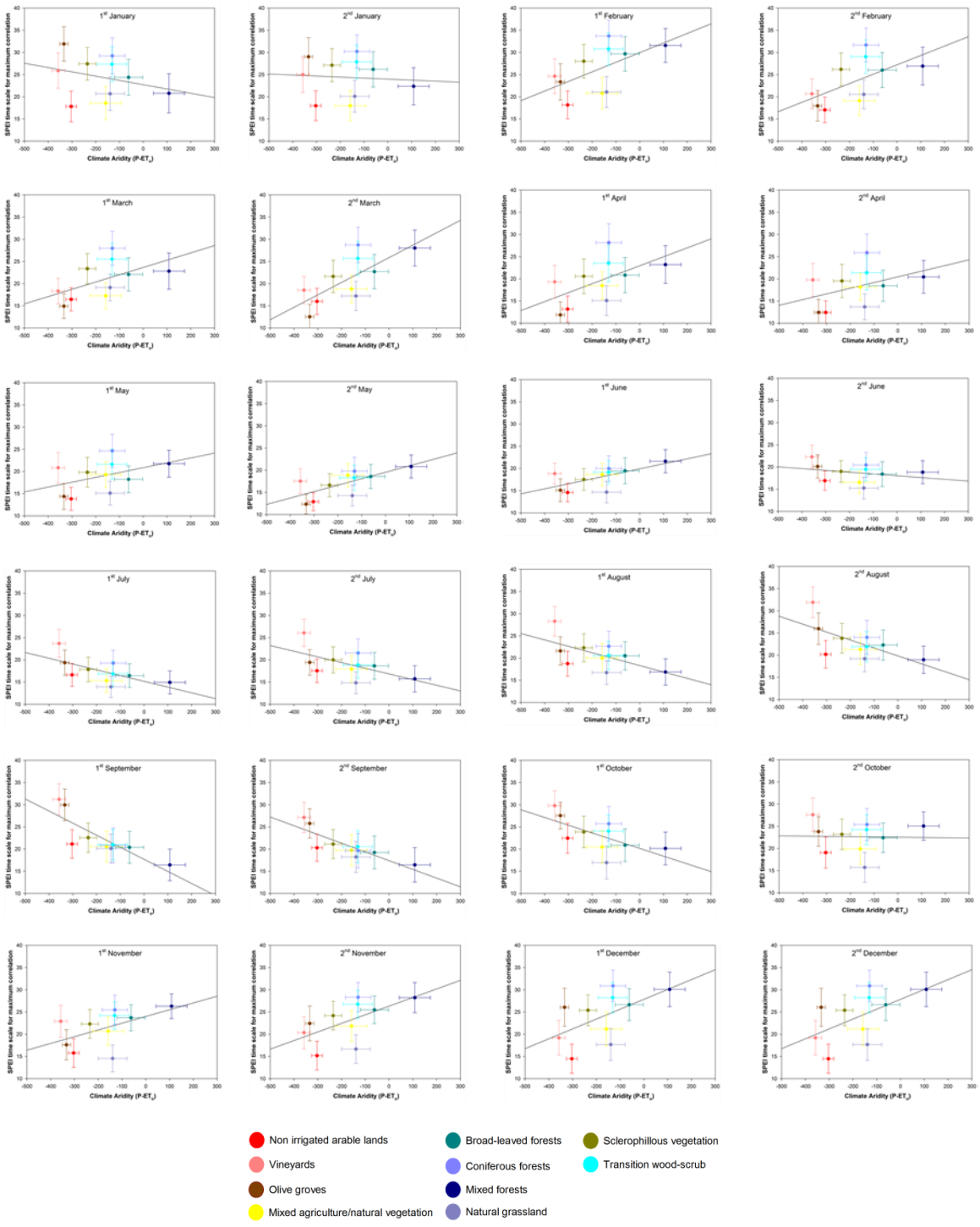

Figure 31: Scatterplots showing the relationship between the mean annual aridity and the SPEI time scale at which the maximum correlation is found between the sNDVI and the SPEI in the different land cover types analysed in this study. Vertical and horizontal bars represent ¼ of standard deviation around the mean values.

6. Discussion

6.1. Development of the Sp_1km_NDVI dataset

The developed NDVI dataset described in this study has been based on a standard methodology, in which accurate post-launch calibration coefficients, and a cross-calibration among satellites and sensors has been used following the specifications of different technical documents. Cloud cover removal has been also carefully applied and also topographic correction to diminish the role of the complex topographic conditions in Spain. Atmospheric correction to the images was not applied as observed in other datasets [e.g., Kaufman et al., 1997 and Vermote et al., 2002 for the MODIS NDVI or (Pinzon and Tucker, 2014) for the GIMMS3g dataset]. Although different attempts were made to correct atmospherically the images using the Second Simulation of the Satellite Signal in the Solar Spectrum (6S) code (Vermote *et al.*, 1997), non-reliable results were found given the topographic complexity and the coarse spatial resolution data necessary to use the correction model. For example the ozone concentration levels available from Total Ozone Mapping Spectrometer (TOMS) data were available at 1.25°×1.00° spatial resolution (http://toms.gsfc.nasa.gov/ozone/ozone_v8.html) and missing data existed for 1994-1996. For other more critical variables like the column water vapor available data from NCEP reanalysis (Kalnay *et al.*, 1996) is even available at lower spatial resolution (2.5º x 2.5º). Using data at this coarse resolution caused a high uncertainty of the atmospheric correction in areas with high elevation gradients in short distances (> 1000 m in 50 km), which are very common in Spain, and resulted in strong underestimation or overestimation of the surface reflectances. In addition to the lack of high-resolution data for atmospheric parameters, the most critical parameter for atmospheric correction is not available (i.e., the Aerosol Optical Thickness –AOT-) since there is not a network of sun photometer in Spain to be operatively used for the atmospheric correction of remote sensing imagery. Although various methods have been developed to obtain reliable estimations of AOT from satellite imagery (e.g. Kaufman et al., 1997; Liang et al., 2001), the AVHRR sensor does not have short-wave visible information data

useful to apply these procedures in opposition to the MODIS images (Huete *et al.*, 2002). Therefore, given existing uncertainties to apply an accurate atmospheric correction to the daily images and the over- or under- estimations in the atmospheric correction obtained in several of the daily scenes, it was decided to use top-of-the-atmosphere (TOA) reflectance to calculate the NDVI. It is known that the NDVI from non-atmospherically corrected reflectance is reduced in comparison to TOA reflectances given aerosol scattering, atmospheric Rayleigh scattering in the visible region and atmosphere molecular absorption in the near infrared region (Arino *et al.*, 1997). This would explain the higher NDVI values in the GIMMS3g and the MODIS NDVI datasets, which show an atmospheric correction, in comparison to the NOAA-SMN and the developed Sp_1km_NDVI, which are not atmospherically corrected. Nevertheless, although this could have an influence if the NDVI data is used to force vegetation or land-surface models, it has not an impact for the objective of our study, which was to analyse temporal trends and relationships of the NDVI with tree-ring and drought. Moreover, it is also not expected that the NDVI dataset is biased by atmospheric influences since the daily images were grouped to semi-monthly composites, which strongly reduce the possible atmospheric influences (Holben, 1986; Gutman, 1989).

More important than the effect of the use of an atmospheric correction approach was the existence of possible temporal inhomogeneities in the NDVI series caused by the change of sensor between the AVHRR/2 and AVHRR/3 instruments (Pinzon and Tucker, 2014). Although a cross-calibration procedure was applied to reduce the different spectral response functions of the different sensors by normalizing them to the spectral response of the NOAA-9 satellite (Trishchenko et al., 2002), a bias was still observed in the resulting NDVI series due to the replacement of AVHRR/2 by AVHRR/3 in satellites launched after November 2000. Although several trend analysis have been developed using NDVI data from AVHRR images that combined the AVHRR/2 and the AVHRR/3 sensors, showing coherent and robust NDVI trends (Heumann et al., 2007; Beck and Goetz, 2011; Stellmes et al., 2013), Pinzon and Tucker (2014) illustrated how this problem may have some residual effects, particularly in some land cover types. Analysing average NDVI over the whole peninsular Spain and Balearic Islands, a change

in the seasonality from 2000 was found that mostly affect to the winter season NDVI values so it was decided to apply a correction following Pinzon and Tucker (2014). It was not possible to establish a pixel per pixel comparability using SeaWIFS data, but the application of global average correction coefficients using the GIMMS3g dataset as reference, allowed reducing the possible temporal inhomogeneity in the data. Although non-physically based, the elimination of temporal inhomogeneities in geophysical series using statistical approaches and reference series is a common approach and highly necessary e.g. in climate change quantification (Peterson *et al.*, 1998). Therefore, the series and the obtained results are more robust applying this kind of statistical correction.

6.2. Comparison of the developed Sp_1km_NDVI with other global NDVI products

The comparison of the developed Sp_1km_NDVI with other globally available datasets has allowed validating the performance of the NDVI dataset to analyse trends of NDVI across the peninsular Spain and the Balearic Islands. There is a good agreement between the spatial patterns of the average NDVI obtained with the Sp_1km_NDVI and the other three datasets. Moreover, the temporal variability over the entire territory closely resembles the other different datasets. The general increasing NDVI trends at the seasonal and annual scales and the interannual anomalies show high agreement among the different datasets, which showed in general high temporal correlations. Moreover, the correlations obtained between the Sp_1km_NDVI and the other three NDVI datasets was comparable to the magnitude of correlations existing among the other three global datasets. Existing studies analyzing the comparability of different NDVI datasets have provided varied results (Brown et al., 2006; Fensholt et al., 2009; Baldi et al., 2008), but in general all of them stress an agreement in the temporal dynamic of NDVI datasets even if they were obtained from different sensors (Ouaidrari et al., 2003; Brown et al., 2006; Stellmes et al., 2010; Song et al., 2010; Yin et al., 2012). Nevertheless, although the average NDVI time series closely agree among the different datasets, the spatial analysis have showed that although correlations between the Sp_1km_NDVI dataset and the other three datasets are positive and statistically significant in

the majority of areas, there are spatial and seasonal differences in the magnitude of the correlations, but also in the spatial patterns of the magnitude of change of NDVI. Other studies have shown that there are also problems of spatial scale, as databases tend to lose spatial variability with increasing pixel size (Tarnavsky *et al.*, 2008), and that the spatial differences in the agreement of the NDVI trends can be found in very different vegetation types from equatorial, arctic and arid areas (Fensholt and Proud, 2012). For example, Fensholt et al. (2009) analysed three NDVI datasets in the Sahel between 2002 and 2007, which were derived from different sensors and showed that the three data products did not exhibit identical patterns of NDVI trends. This pattern may also be identified with datasets obtained from the same satellite imagery, but also between different versions of the same dataset as observed by Jiang et al. (2013) with the GIMMS dataset. Baldi et al. (2008) used three global NDVI datasets obtained from NOAA-AVHRR images in South America and found large differences in the percentage of surface area affected by positive and negative trends as a function of the dataset. Alcaraz-Segura et al. (2010) compared four different global NDVI datasets obtained from NOAA-AVHRR sensors between 1982 and 1999 in Spain, and showed that even using datasets created from the same satellite imagery, different spatial patterns of NDVI can be obtained. Here it is showed that in general terms the spatial patterns of NDVI trends obtained with the Sp_1km_NDVI tend to agree more with the patterns obtained with the GIMMS3g and the MODIS NDVI datasets but large spatial differences are found in comparison with the SMN, which in general provides non-reliable trends in comparison to the other datasets. In any case, although the magnitude of the NDVI change shows some divergences among datasets, it is showed that the signification of the trends shows high spatial agreement with comparable patterns and a dominant positive and significant NDVI trends both in the GIMMS3g and Sp_1km_NDVI datasets for 1982-2014. Moreover, there are also some local features identified in the trends obtained from the different images that allow to assess with robustness the quality of the datasets since for example, there are well known land cover changes well recognized with NDVI data in summer months given the transformation of dry agricultural lands to irrigated lands in the decades of 1980, 1990 and 2000 (Lasanta and Vicente-Serrano, 2012). These cause

a dramatic increase of the vegetation activity, and they are well recognized by intense positive trends in the Sp_1km_NDVI in summer months, but they are masked in the GIMMS3g dataset, probably as a consequence of the original spatial resolution of the dataset (Tarnavsky *et al.*, 2008). Therefore, the identification of these well-known abrupt trends in the Sp_1km_NDVI provides strong confidence to analyse long-term NDVI trends and relationship with other variables in comparison to other datasets.

6.3. Long term NDVI trends in peninsular Spain and the Balearic Islands from 1982 to 2014

This study has analyzed for the first time high spatial resolution vegetation activity for a recent period covering 34 years between 1981 and 2015. Although previous studies had analyzed high spatial resolution trends in vegetation activity over Spain, they had been based on short periods (< 15 years) (Hill et al., 2008; Stellmes et al., 2013; del Barrio et al., 2010), or were based on low spatial resolution (Vicente-Serrano and Heredia-Laclaustra, 2004; Julien et al., 2011). Although the vegetation trends can be affected by the study period and the starting date (Giner *et al.*, 2012), the majority of the existing studies based on satellite imagery agree with a general increase of the vegetation activity across Spain considering shorter periods (Hill et al., 2008; del Barrio et al., 2010) or lower spatial resolutions (Alcaraz-Segura et al., 2010; Militino et al., 2018). Here it is also identified a general positive and significant NDVI trend, which is dominant across the entire Spain. Thus, at the annual scale, close to 80% of the region has showed positive and significant NDVI trends, although there are some seasonal differences, with the highest percentage of surface recorded in winter (75%) and the lowest in summer (57%). There are very few areas recording negative trends at the annual scale (< 5%). Although in the majority of the regions with positive and significant changes the magnitude of the identified change has not been very important (< 0.05 NDVI units over the study period), the monotonic character of the trend explains the dominant positive and significant trends throughout Spain. Moreover, there is not an important control by the bioclimatic conditions (summarised by the climatology) and the existing land cover categories at the beginning of the study period, although there is an increase in NDVI favoured by wetter and colder conditions.

Nevertheless, although the positive and significant NDVI trends are dominant over the entire Spain, the magnitude of changes in the NDVI shows important spatial but also seasonal differences across Spain. It is difficult to interpret the observed change over the whole Spain but there are some patterns that can be connected to well-known land cover changes and processes. At the annual scale there are large areas that show intense positive changes, which are mostly identified in spring, summer and autumn. They mostly correspond to localized areas that have been affected by strong transformation of the land cover, mostly from non-irrigated agricultural lands to irrigated lands (Stellmes *et al.*, 2013). The most intense development of new irrigated lands was recorded in the decades of 1950s and 1960s (Lasanta, 2009; Lecina et al., 2010), but the processes also continued in the decades of 1980, 1990 and 2000, in which more than 800.000 Ha of new irrigated lands were created in Spain, favoured by the dense network of reservoirs located in mountain areas. The irrigated lands were created in dry cultivated flat areas characterised by high climate aridity and very low vegetation coverage in summer months after the crop harvesting. This would explain the strong increase in the NDVI after transformation since in the new irrigated lands usually species of a high leaf area index are planted (e.g. corn), strongly increasing the photosyntethic and the NDVI in comparison to previous dry land cultivations.

In addition to the new irrigated lands there are also other areas that have experienced an important increase of the vegetation coverage. For example, in spring there are large cereal areas in the North of the Iberian Peninsula that have showed an increase in the magnitude of the NDVI. This pattern is difficult to interpret since these areas have not been affected by changes in the land cover type, but processes related to the improvement of the cereal varieties in the last decades (Álvaro et al., 2008; Sanchez-Garcia et al., 2012), together to the bioclimatic conditions and the recent climate trends could explain that in areas of the Duero basin and in Navarra the NDVI of the cereal areas have noticeably increased in spring. These areas are characterised to be one the coldest cultivated areas of Spain, in which precipitation availability is not usually a constrain so the observed strong temperature increase recorded in the last decades (Gonzalez-

Hidalgo et al., 2016; Vicente-Serrano et al., 2017) could have favoured a higher vegetation activity.

Other large areas also show an NDVI increase although not so intense that in managed agricultural areas. This pattern is identified annually but also over the different seasons of the year, but it is affecting the majority of mountain areas of Spain. The process of land margination and rural depopulation of the mountain areas of Spain has been widely described in a number of studies (Terres et al., 2015; Kuemmerle et al., 2016). Mountain areas suffered an abandonment of the traditional primary activities (agriculture and livestock) as a consequence of the environmental constrains and the low economic viability of the exploitations (Lasanta *et al.*, 2017). The main consequence of these processes have been the development of natural revegetation process that have transformed the old cultivated field under terraces and cultivated slopes in areas covered by dense shrubs and/or forests (Lasanta-Martínez *et al.*, 2005). Also at high elevations there is an altitudinal increment of the tree-line, mostly as a consequence of the decrease of the livestock pressure since the transhumant flocks that used the mountain pastures during summer months have practically disappeared (Batllori and Gutiérrez, 2008; Ameztegui et al., 2016). Therefore, the forest landscapes are currently dominant in the majority of the mountainous systems of Spain (Lasanta and Vicente-Serrano, 2007; Améztegui et al., 2010) mostly as a consequence of the described management changes. In these areas, forest densification but also changes in the vegetation types continues in the last decades (Vicente-Serrano *et al.*, 2006a). Thus, the land cover types that have showed the highest percentage of positive and significant NDVI trends are areas of forests and shrublands, which are mostly located in mountain areas. Mountain areas of Spain are water towers in which surface runoff is generated and in which there is a positive climate balance (Precipitation minus Reference Evapotranspiration). These climatic characteristics would favour that abandoned field have been naturally colonised in few decades. Thus, although human management changes have had main role to explain the positive NDVI trends (Vayreda *et al.*, 2016), the observed temperature increase would have also favoured the vegetation activity as suggested in the Pyrenees (Vicente-

Serrano *et al.*, 2004), since in these areas water availability is not the main vegetation constrain, but temperature.

There are also other areas that have showed a strong vegetation decrease. This is identified in few areas but it is necessary to stress that among the land cover categories, the irrigated lands show a high percentage of negative trends (35%) in summer months, the season in which this land cover type is characterised to record the highest vegetation activity. For example, it is clearly identified a reduction of the NDVI in areas of the historical irrigated lands in the Guadalquivir and Ebro rivers. This pattern may respond to a recent phenomenon, which is characterised by a certain margination of the old irrigated lands, which are active since centuries ago. Given historical evolution, old irrigated lands are characterised to be formed by smaller fields than the new irrigated lands, in which mechanization is easier, which allows an economic viability of the exploitations in comparison to the traditional irrigated lands. In these lands the rural depopulation and the socioeconomic changes have also contributed to the abandonment of some fields (Lasanta, 2009), which would contribute to explain the observed NDVI increase in large old irrigated areas of Spain.

There are also areas in the South Spain that have showed an important decrease of the NDVI in the last decades during spring. These areas are characterised by cereal and olive crops, in which the increased land aridity recorded in general in Spain (Vicente-Serrano et al., 2017) could explain this behaviour since in these areas water availability is the main constrain in comparison to temperature and radiation factors.

There is another relevant process that explains a strong decrease of the NDVI in some areas, which is related to the urban expansion and the development of tourist infrastructures in areas close to the Mediterranean coastland. The neighbour areas around largest cities like Madrid and Barcelona have showed a decrease of the NDVI in the last three decades as a consequence of the urban growth (Marraccini et al., 2015; Gallardo and Martínez-Vega, 2016). The Mediterranean coastland in the region of Valencia is an excellent example of strong tourism growth (Palazón *et al.*, 2016), which is clearly appreciated in the maps of NDVI trends, with a

fringe close to the coastland in which the NDVI decrease has been recorded in the different seasonal maps and annually.

Finally, it is also identified a vegetation decrease in some natural vegetation areas of Spain, in some cases it can be due to recurrent forest fires in which the resilience capacity is clearly diminished (Díaz-Delgado *et al.*, 2002), and the landscape homogenised (Van Leeuwen *et al.*, 2010), but the decrease is mostly in semiarid areas of the Ebro basin, the Southeast and also in central Spain, which were not affected by forest fires. It is suggested that in areas affected by high human pressure during the last centuries as a consequence of overgrazing and/or intensive land cultivation, land degradation processes can be recorded (del Barrio *et al.*, 2010). The mentioned semiarid areas could be affected by this kind of processes, which would affect small sectors of the driest areas of Spain. In any case, different studies have suggested that land degradation would be a very localised problem in Spain (del Barrio et al., 2010; Gouveia et al., 2016), only affecting very local areas characterised by strong past human pressure and very limited environmental constrains (Vicente-Serrano *et al.*, 2012b).

The identification of a general positive signal even in areas in which precipitation is low under a scenario in which temperature (Gonzalez-Hidalgo *et al.*, 2016), and the atmospheric evaporative demand (Vicente-Serrano *et al.*, 2014b) have strongly increased during the last decades seems to be contradictory, since environmental conditions have tended to be more limited for the vegetation growth. Although the magnitude of the NDVI increase is not important in the majority of the country, it is true that vegetation activity is not generally decreasing as it could be expected. In mountain humid areas this is mainly consequence of land management changes as discussed above. In the natural areas located in sub-humid and semi-arid regions there is also a decrease in the human pressure but also physiological factors related to a higher atmospheric CO_2 fertilization could have a role. Different studies have suggested that under enriched CO_2 concentrations, plant stomatal conductance would be reduced and the water requirements would be lower (Ainsworth and Long, 2005). Thus, it is suggested that increased CO_2 could be behind the general increase of vegetation activity in several semiarid regions of the world (Donohue *et*

al., 2013), but also the reduced vulnerability of vegetation to water limitations and drought (Peñuelas *et al.*, 2018).

6.4. Tree-ring and NDVI relationships

This is the first time that the relationship between the interannual variability of the tree-ring growth (TRWi) and the GPP has been established for a variety of forest types under different environmental conditions across Spain. The innovation of this work is mainly related to the high spatial resolution (1.1 km^2) of all input data (NDVI, climatic data) used for this analysis. This detailed spatial information is extremely important to account for the local-scale environmental signals influencing the growth of these tree species and to reduce the noise associated to other vegetation types. The high-resolution spatial data used to conduct a study in peninsular Spain and the Balearic Islands is also reinforced by a high temporal (semi-monthly) resolution of the NDVI dataset, combined with a dense network of tree rings across different forest ecosystems. (see Gazol et al., 2018).

The obtained results are also important to compare GPP and secondary growth in complex and heterogeneous landscapes, which is a typical feature of the Mediterranean region. Although numerous studies have already compared the NDVI with tree-ring growth over homogeneous forest types, particularly in high-latitude regions (e.g. Lopatin et al., 2006); Kaufmann et al., 2008; Kaufmann et al., 2004), these studies employed coarse resolutions data (64 km^2), mainly the GIMMS dataset. This dataset has frequently been employed to assess the relationships between vegetation activity and tree-ring growth in complex landscapes (e.g. Coulthard et al., 2017; Vicente-Serrano et al., 2016). However, there remains a degree of uncertainty in results obtained based on the GIMMS dataset, particularly at the regional scale. This uncertainty originates mainly from the very low spatial resolution of this product, where different cover types can predominate within an individual pixel. This study accounted for this kind of uncertainty by considering a high-resolution NDVI dataset.

Overall, the findings suggest a positive and significant relationship between the interannual variability in NDVI and the secondary growth measured by means of tree-ring growth series

(TRWi). Similar average correlations were found among all different forest types. Although this finding seems coherent with what has been evidenced using data of lower spatial resolutions (e.g. Berner et al., 2013; Kaufmann et al., 2008; Vicente-Serrano et al., 2016), the results based on high spatial resolution and long-term coverage of the NDVI data confer more reliability to these results. The magnitude of the maximum correlation between the TRWi and the semi-monthly NDVI series is quite similar between the semi-arid *P. halepensis* lowland forests and the wet-cool *A. alba* mountain forests. Similar maximum correlations were also found for other tree species from xeric and mesic sites (Coulthard *et al.*, 2017). This suggests that, irrespective of the forest type and the tree species, secondary growth is favored by a high GPP, leading to higher carbon sinks. There are few experimental studies that have tackled this issue by comparing the relationship between GPP and secondary growth in forest ecosystems, and in general they show agreement between both variables (Babst et al., 2014a; Poulter et al., 2013) both in cold and humid forests (Krause et al., 2012, Kraus et al., 2016) and in warm and xeric areas (Tognetti et al., 2007).

This study demonstrates that the maximum correlations found between NDVI and tree-ring growth are recorded considering cumulative NDVI values, in some cases covering long time periods (6-10 months). This suggests that tree growth is strongly related with GPP at annual scales, since wood production would be the result of accumulating the surplus of synthesized carbohydrates during long periods (Cuny *et al.*, 2015). Secondary growth and carbon storage would reflect long-lasting cumulative production (Gough *et al.*, 2008), as carbon must first be used for primary growth in order to form shoots, buds, leaves and fine roots (Stoy *et al.*, 2009). Moreover, temporal lags may be expected due to particular physiological processes. One example can be found during xylogenesis, where there is a delay from the expansion to the lignification of wood cells (Cuny *et al.*, 2015). Over Spain, the observed patterns stress that the highest positive and significant correlations between NDVI and TRWi across the different analyzed forests are obtained for long time spans of NDVI accumulation.

Albeit this general positive and significant correlation of TRWi with cumulative NDVI values, it is found that the magnitude of this relationship strongly varies between forest types and

environmental conditions (Gazol *et al.*, 2018). There are some dominant patterns of cumulative NDVI-TRWi correlations in the different forest types of Spain. These patterns are very coherent in the shape of this relationship, but also in the characteristics of the tree species involved. As regards the dominant pattern, it is characterized by the highest correlation recorded with a 10-month cumulative NDVI period in November of the year in which the tree-ring is formed. This robust signal was mainly recorded in evergreen tree species located in the semiarid and sub-humid regions of Spain. It represents conifers, such as *P. halepensis, P. pinaster, P. nigra, P. pinea* and *J. thurifera,* but also the evergreen oak *Q. ilex,* which is able to inhabit drought-prone areas. These species are characteristics of semi-arid to dry Mediterranean climates. Although they record low average precipitation and climate water balance values, these species show a very good acclimatization to these dry conditions. Even during the strong summer dryness that characterizes their area of distribution, these species are relatively drought tolerant (Zavala *et al.,* 2000), while the GPP during these long periods would affect the annual tree-ring growth (Camarero *et al.*, 2010). The significant contribution of summer season to explaining forest growth is also recorded in oak species from dry Mediterranean and sub-Mediterranean areas (*Q. faginea* and *Q. pyrenaica*), also represented by this pattern of response. Irrespective of summer dryness occurrence, these species form part of the annual tree-ring and carry out other growth processes (e.g. bud and acorn development) in summer (Montserrat-Martí *et al.*, 2009).

Other patterns of the NDVI-TRWi relationship represent fewer areas and specific tree species, but with well-defined seasonal patterns. The second pattern summarizing the NDVI-TRWi relationship is characterized by the highest correlation considering the NDVI between June of the previous year and January of the current year. This pattern is much less representative than the first one, with no clear representation of any forest type. The only exception corresponds to *C. sativa* forests, which are characterized by higher average NDVI values, lower temperatures and moister conditions than those drawn in the first pattern, representative of broadleaf hardwood species (Babst et al., 2014a; Kagawa et al., 2005; Richardson et al., 2013; Skomarkova et al., 2006). Different studies revealed that the vegetation activity and the NPP over the previous growing season may be important for explaining the forest growth during the

following growth season. For example, Babst et al. (2014a) and Babst et al. (2014b) suggest that carbon sequestered after June/July in temperate forests is mostly used for cell-wall thickening processes and/or stored in above- and below-ground nonstructural carbohydrate reserves, which would support next year spring tree-ring growth (Skomarkova *et al.*, 2006). This process implies a lagged use of synthesized carbohydrates in wood formation, explaining why the primary production of deciduous trees would affect the secondary growth during the following growing season (Kagawa et al., 2005; Richardson et al., 2013).

The third pattern of the NDVI-TRWi relationship show forests related to the cumulative NDVI during the winter and spring season of the current year. This kind of response is mostly represented by the *A. alba* forests located in the Pyrenees, where lower temperatures and higher precipitation values are recorded. The fourth pattern is also mostly characterized by the Pyrenean forests of *A. alba* and *F. sylvatica*, albeit with a positive influence of the summer NDVI on TRWi and an influence of the NDVI recorded during the first part of the previous year. These patterns of response are questionable, given that most active vegetative period of these tree species dominating in cold sites is recorded in late spring and summer (Macias *et al.*, 2006). Nevertheless, several studies have also suggested that the conditions during the prior summer, autumn and winter periods can be relevant to explaining tree-ring growth of these species in Spain (e.g. Hayles et al., 2007; Rozas et al., 2015; Sánchez-Salguero et al., 2013). Kraus et al. (2016) analyzed leaf and xylem phenology at different elevation ranges in Norway spruce forests of the Alps, demonstrating that the length of the xylem cell growth period does not show significant differences, as a function of either elevation or colder conditions, which seem to lead a longer period of cell maturation in spruce. Furthermore, the Pyrenean silver fir forest growth is sensitive to cold conditions in late winter (February) as well as to dry-warm conditions in the previous early autumn (September). As such, both prior cold and dry conditions can negatively affect subsequent tree-ring formation, NDVI and the NPP in this species (Vicente-Serrano *et al.*, 2015b).

It seems that phenology of the different tree species contributes significantly to the different patterns of relationship between NDVI and tree-ring growth (e.g. Boulouf Lugo et al., 2012;

Čufar et al., 2008). The main patterns of response found in this study are characteristics of species/regions, with very different tree life cycles driven by temperature. In general, in the forests located in cold areas the tree-ring growth responds to the cumulative NDVI over shorter periods than in the coniferous forests located in more temperate and arid areas. This feature has been identified by Vicente-Serrano et al. (2016) at the global scale, especially in the Alps and the high latitudes of North America, in which low air temperature, and short photoperiod constrain the periods of vegetation activity and subsequently limit the duration of tree-ring formation to the boreal summer (Vaganov et al., 1999; Kaufmann et al., 2004; Bergeron et al., 2007). Nevertheless, it is also stressed that although there is a clear positive signal between NDVI and TRWi, the magnitude of the correlations usually does not exceed 0.5 in the majority of cases. This finding indicates that GPP and tree-ring growth can be decoupled in a number of years. Also, it suggests that the drivers of vegetation activity can differ as well as the response of the primary production and secondary growth types to some stress factors. There are very few studies that have analyzed the different response of the GPP and secondary growth to climate variability with respect to climate stressors, and even their results are quite contradictory. Recently, Gazol et al. (2018) analyzed the response of the NDVI and the tree-ring growth to the four outstanding droughts, which affected Spain since the 1980s. They found that tree-ring growth is more determined by drought severity than NDVI. Newberry (2010) analyzed the effects of climate on carbon isotope discrimination ($\delta^{13}C$) in leaves and wood of *Pinus edulis* forests in North America, concluding that that $\delta^{13}C$-climate relationship was stronger for leaf than for tree-ring cellulose, especially at the xeric sites. Del Castillo et al. (2015) and Pasho and Alla (2015) showed contradictory for the Aleppo pine forests in northeastern Spain and Albania, respectively. Overall, these results stress that the magnitude of the correlations between the NDVI and the tree-ring growth is quite similar across different forest types. Nonetheless, very high spatial and temporal diversity in the responses of forest secondary growth to NDVI time scales in the peninsular Spain and the Balearic Islands has been found, with clear distinction between tree species and environmental conditions. As such, the obtained results can contribute not only to determine sensitive periods in vegetation activity affecting

forest growth, but also to assess the possible sensitivity of the GPP and secondary growth to climate change processes.

6.5. Magnitude of drought influence on NDVI

This study has also analysed the response of the vegetation activity to drought variability. The results have showed that in large areas of Spain the vegetation activity is strongly determined by the interannual variations of drought. During the summer dry season, more than 90% of land areas show significant positive correlations between the NDVI and the SPEI. This generalised response of the NDVI to drought is also characteristic of other sub-humid and semiarid climate areas like Northeast Brazil (Barbosa *et al.*, 2006), the Sahel (Herrmann *et al.*, 2005), Central Asia (Gessner *et al.*, 2013), Australia (De Keersmaecker *et al.*, 2017) or California (Okin *et al.*, 2018), among others. Nevertheless, in Spain noticeable spatial and seasonal differences in the response of the NDVI to the interannual drought variations have been found, and the time scale at which the drought is measured has a relevant role to explain the spatial and the seasonal differences.

There is an important seasonal component of the drought influence on the NDVI since the strongest signal is recorded during the warm season. In summer the majority of the areas show a positive and significant correlation between the NDVI and the SPEI. This seasonal pattern would be driven by two factors. The first one is the phenology that characterizes the majority of land cover types in Spain. During the cold season there are areas that do not show any vegetation activity (e.g., the pastures and the non-permanent broad leaf forests), but also the coniferous forests, shrubs and cereal crops show a very low activity. This would explain that independently of the recorded drought conditions the sensitivity to drought would be low in winter. In Spain, the atmospheric evaporative demand is very low in winter as a consequence of low temperature (Vicente-Serrano *et al.*, 2014c); so in this period the water demand by the vegetation respiration is small, explaining the low sensitivity to the soil water availability. Thus, studies have showed that the soil water recharge is mostly recorded in winter months given low water consumption by vegetation (Austin *et al.*, 1998). Once temperatures increase in spring,

the vegetation is more sensitive to drought since the photosynthetic activity, from which the NDVI ultimately depends (Myneni *et al.*, 1995), is highly determined by soil water availability. The positive spatial relationship found between the sensitivity of the NDVI to the SPEI and mean temperature reinforces this issue since in spring even colder areas tend to show low correlations between the NDVI and the SPEI. Warmer temperatures in summer cause the dominant peak of vegetation activity (with some exceptions like the cereal cultivations, dry pastures and shrubs, which record the maximum vegetation activity in spring). This would explain why in summer the sensitivity of the NDVI to drought tends to be maximum in the majority of Spain, but it would also be favoured by the characteristic dryness of the Mediterranean climate in summer.

In any case, substantial seasonal differences have been found in the response of the NDVI to drought, and in the magnitude of the correlation between the NDVI and the SPEI, as a function of the land cover. This is the general behaviour identified at the global scale (Vicente-Serrano *et al.*, 2013), but also at regional and local scales using NDVI data (Ivits et al., 2014; Zhao et al., 2015; Gouveia et al., 2017; Yang et al., 2018). Non-irrigated arable lands, natural grasslands and sclerophyllous vegetation show an earlier response to drought, in late spring and early summer. This is determined by the phenology of these land covers, which usually reach the maximum vegetation activity in late spring with the purpose of avoiding avoid the summer dryness. The root systems of herbaceous species are not very deep, so they depend on the water storage in the most superficial soil layers (Milich and Weiss, 1997), and they could not survive during the long and extreme summer dryness in which the surface soil layers are mostly depleted (Martínez-Fernández and Ceballos, 2003). This would explain an earlier and stronger sensitivity to drought also showed in other world semiarid regions (Liu et al., 2017; Yang et al., 2018; Bailing et al., 2018). On the contrary, maximum correlations between the NDVI and the SPEI are recorded during summer months in the forests but also in wood cultivations like vineyards and olive groves. In this case, the maximum sensitivity to drought coincides with the maximum temperature and atmospheric evaporative demand (Vicente-Serrano *et al.*, 2014c). This pattern would be indicative to a different adaptation strategy of the trees in comparison to

the herbaceous vegetation since whilst herbaceous cover would adapt to the summer dryness generating the seed bank before the summer (Peco et al., 1998; Russi et al., 1992), the trees and shrubs would base the adaptation on deeper root systems, translating the drought sensitivity to the period of highest water demand and water limitation.

In addition to the seasonal differences among land cover types, it is showed in Spain that herbaceous crops show a higher correlation between the NDVI and the SPEI than most of natural vegetation types (with the exception of the sclerophyllous vegetation). This behaviour could be explained by three different factors: i) the highest adaptation of natural vegetation to the characteristic climate of the region in which drought is a frequent phenomenon (Vicente-Serrano, 2006), ii) the deeper root systems that allow shrubs and trees to obtain water from the deep soil and iii) the common location of cultivated lands in drier areas than natural vegetation. Different studies have showed that the vegetation of dry environments tend to respond in more depth to drought than sub-humid and humid vegetation (Schultz and Halpert, 1995; Abrams et al., 1990; Nicholson et al., 1990; Herrmann et al., 2016). Vicente-Serrano et al. (2013) analysed the sensitivity of the NDVI in the different world biomes and showed a clear spatial gradient in the sensitivity to drought, which was more important in arid and semiarid regions. In this study we have showed a clear control in the response of the NDVI to drought severity by the climate aridity across Spain. Thus, there are significant correlations between the spatial distribution of the climate aridity and the sensitivity of the NDVI to drought, mostly in spring and autumn. This could be explained because humid environments show a water surplus as surface runoff, so not all the water available would be used by vegetation and this characteristic would make the vegetation less sensitive to climate drought. Drought indices are relative metrics in comparison to the long term climate with the purpose of making comparable drought severity between areas of very different climate characteristics (Mukherjee *et al.*, 2018). This means that in humid areas the corresponding absolute precipitation can be sufficient to cover the vegetation water needs although drought indices inform on below-of-the-average conditions. On the contrary, in arid regions a low value of a drought index is always representative of limited water availability, which would explain the closer relationship between the NDVI and the SPEI.

This thesis also explored if the general pattern found between humid and semi-arid regions is also affected by the land cover type and found that the behaviour in the non-irrigated arable lands is the main type to explain the global pattern. Herbaceous cultivations show that aridity has clear control of the response of the NDVI to drought during the period of vegetation activity. Nevertheless, after the common harvest period (June) this control by aridity mostly disappears. This is also observed in the grasslands and in the sclerophyllous vegetation, and it could be explained by the low vegetation activity of the herbaceous and shrub species during the summer, given the phenological strategies to cope with water stress with the formation of the seeds before the period of dryness (Chaves *et al.*, 2003). The limiting aridity conditions that characterises the regions in which these vegetation types inhabit would also contribute to explain this phenomenon. On the contrary, the forests, both broad-leaved and permanent also show a control by aridity in the relationship between the NDVI and the SPEI during summer months since these land cover types show the peak of the vegetation activity during this season.

In any case, it is also remarkable that the spatial pattern of the NDVI sensitivity to drought in forests is less controlled by aridity during the summer season, curiously the season in which there are more limiting conditions. This could be explained by i) the possible NDVI saturation under high levels of leaf area index (Carlson and Ripley, 1997) since once the tree tops are completely foliated, the electromagnetic signal is not sensitive to additional leaf growth. This could explain the less sensitive response of the forests to drought in comparison to land cover types characterised by lower leaf area (e.g. shrubs or grasslands). Nevertheless, it does not seem that this issue may explain the decreased relationship with aridity in summer since the dominant coniferous and broad-leaved forests in Spain are usually not characterised by a 100% of leaf coverage (Castro-Díez et al., 1997; Molina and del Campo, 2012) so it is not expected to find large signal saturation problems, ii) the physiological strategies of forests to cope with drought since experimental studies have suggested that interannual variability of the secondary growth could be more sensitive to drought than the sensitivity observed by the photosytetic activity and the leaf area (Newberry, 2010). This could be a forest strategy to optimise the storage of carbohydrates, suggesting that in dry years they would prioritize the development of an

adequate foliar area in relation to the wood formation in order to maintain respiration and photosynthetic processes. The recent results by Gazol et al. (2018) and Peña-Gallardo et al. (2018b) seem to confirm this issue since they showed a higher sensitivity to drought in tree-ring growth than that found for the NDVI, being this behaviour independent of the forest species, iii) other more complex issues related to dominant forest species and species richness as observed in forests of Northeast Spain (Lloret *et al.*, 2007), and iv) ecosystem physiological processes since it is suggested that independently of the vegetation types and environmental conditions, the vegetation would tend to the same water use efficiency in periods of water stress (Huxman *et al.*, 2004), which would explain that independently of aridity conditions the response of the NDVI to drought would be similar. Here it has been shown that in different land cover types located under different environmental conditions the sensitivity of the NDVI to the SPEI seems to converge to similar values (correlations) during summer months.

6.6. Drought influence on different time scales

A relevant finding of this study has also been that the response of the NDVI is highly dependent of the time scale at which drought is measured. Pioneer studies demonstrated that the accumulation of the precipitation deficits during different time periods is essential to determine the influence of drought on the NDVI (Malo and Nicholson, 1990; Liu and Kogan, 1996; Lotsch et al., 2003; Ji and Peters, 2003; Wang et al., 2003) since soil moisture is more dependent of the precipitation and the atmospheric evaporative demand over previous cumulative periods (Scaini *et al.*, 2015). Moreover, the different morphological, physiological and phenological strategies would explain that different vegetation types respond to varied drought time scales. This pattern has been identified using NDVI and different time scales of a drought index (e.g., Ji and Peters, 2003; Vicente-Serrano, 2007), but it is also identified by other variables like the tree-ring growth (Pasho et al., 2011; Arzac et al., 2016; Vicente-Serrano et al., 2014a). In this study it is also showed a high spatial diversity in the SPEI time scale at which vegetation is showing the maximum correlation with the NDVI, but also seasonal differences and a noticeable control by the dominant land cover types and the aridity conditions.

In a global study, Vicente-Serrano et al. (2013) illustrated gradients related to the sensitivity of the world biomes to drought, which are driven by the time scale at which the biome is responding to drought in a gradient of aridity. The response to these different time scales suggested different strategies to cope with drought but also different vulnerabilities to the water deficits. In Spain, this study has showed that the NDVI is mostly responding to the SPEI at time scales around 20 semi-monthly periods (10 months), with some few seasonal differences (shorter in spring and early autumn than in late summer and autumn), although there are noticeable differences among land cover types. In general, during the periods of highest vegetation activity, the herbaceous land covers (non-irrigated arable lands and grasslands) respond to shorter SPEI time-scales than the different forest types, also during the periods of highest vegetation activity in summer. This can be connected with the different root depths discussed above, which would make the herbaceous covers more dependent on the weather conditions recorded during short periods. These vegetation types could not reach deep soil levels, which would depend on climate conditions recorded during longer periods (Changnon and Easterling, 1989; Berg et al., 2017). On the contrary, the tree root systems would access to these deeper levels, having the capacity of softening the effect of short-term droughts, but they would be more vulnerable to long droughts that ultimately would affect deep soil moisture levels. This pattern has been recently observed in south East Spain comparing herbaceous crops and vineyards (Contreras and Hunink, 2015) but also by Okin et al. (2018) in California, who showed that the different response to drought time scales between scrubs and chaparral herbaceous vegetation would be explained by the soil water depletion at different levels.

Although the general patterns are described above, we have also found some relevant seasonal patterns. For example, irrigated lands respond to long SPEI time scales (> 15 months) during summer months, whilst in spring and autumn they are responding to time scales below 7 months (14 semi-monthly periods). This behaviour is clearly connected to the water management of these areas. In spring they do not receive irrigation and vegetation activity is determined by the water stored in the soil. On the contrary, summer irrigation depends on the water stored in the dense net of reservoirs existing in Spain, some of them with a multiannual capacity. Water

availability in the reservoirs usually depend on the climate conditions recorded during long periods (one or two years) (López-Moreno et al., 2004; Lorenzo-Lacruz et al., 2010), which determine water availability for irrigation and it would explain why the NDVI in irrigated lands depends to long SPEI time scales. Vineyards and olive groves also respond to long SPEI time-scales during the summer months. These cultivations are highly resistant to drought stress (Quiroga and Iglesias, 2009), but under extreme summer dryness even these adapted cultivations would be sensitive to severe droughts. Finally, in comparison to other natural vegetation, mixed forests show response to shorter SPEI time scales. This could be explained by the low resistance of these forest species to water deficits, such as, for example, the different fir species located in humid mountain areas, (Camarero et al., 2011; Camarero et al., 2018).

This study has also showed that the climate aridity has also a certain role to explain the response of the NDVI to the SPEI time scales. In Spain the range of the mean aridity recorded by the mean land cover types is much lower than that observed at the global scale for the world biomes (Vicente-Serrano *et al.*, 2013). Therefore, there are not clear patterns in the response of the land cover types to the aridity gradients and the SPEI time scales at which the maximum correlation between the NDVI and the SPEI is found. Nevertheless, it is also found clear seasonal differences between the cold and warm season and, more importantly, that during summer dryness the land cover types located in the most arid regions (vineyards and olive groves), the NDVI shows response to long SPEI time scales in opposition to the most humid forests, which tend to respond to shorter time scales. This stresses that not only mean aridity but also the degree of vulnerability to different duration water deficits (well quantified by the drought time scales) may have an important role to explain the spatial distribution of the main land cover types in Spain.

7. Conclusions

Satellite images are widely used in environmental sciences to respond to the challenges by spatial and temporal land changes due to both climate change and human activities. This thesis has provided information to understand recent changes in vegetation activity of peninsular Spain and the Balearic Islands in the last three decades, how these changes are related with tree-ring growth and also how a natural hazard, such as drought, influences this vegetation activity.

Regarding the creation of the Sp_1km_NDVI database:

1. The availability of daily NOAA-AVHRR satellite images has allowed to work with long time series. In spite of having had to discard those daily images that presented problems during their capture or that were totally covered by the clouds, by means of an exhaustive revision, the quantity of available data and the temporal scale of analysis offer very suitable information to carry out studies that analyze the vegetal activity in Peninsular Spain and the Balearic Islands.
2. Atmospheric correction is not considered an essential aspect in this case, due to the characteristics of the AVHRR sensor and the option of creating semi-monthly composite images to minimize the effect of atmospheric noise has been shown to be effective.
3. Regarding the inhomogeneity between the AVHRR/2 and AVHRR/3 sensors, the statistical correction used is considered enough to guarantee the temporal homogeneity of the dataset created.
4. Since NOAA-AVHRR images are used to obtain NDVI products, any dataset has been developed specifically for peninsular Spain and the Balearic Islands at 1.1 km resolution and covering the period 1981 - 2015. This fact makes these data an original, novel and useful product for the analysis of the vegetation activity.

As for the comparison between the NDVI databases:

5. The temporal dynamic of the developed dataset and the other three compared products is similar. Spatial analysis shows differences between the datasets related to the magnitude of change, but the patterns are comparable in the case of trend significance, except for the SMN.
6. In general, there is an increase of the NDVI values over the period analysed.
7. The database obtained makes it possible to quantify changes in vegetation cover, which are related to transformations in agricultural lands more clearly than considering the datasets characterized by lower spatial resolution (GIMMS3g and SMN). The dataset also shows the changes recorded for the long term better than the MODIS short-term information.

Conclusions obtained related to the long-term NDVI trends:

8. NDVI trends show a dominant increase in peninsular Spain and the Balearic Islands over the three decades analysed.
9. The magnitude of the NDVI changes shows spatial and temporal differences. The most important changes characterized by a strong greatest increase of the NDVI correspond to agricultural areas. They are mostly driven by human activities: transformations from dry to irrigated areas; but they may also be favored by climatic factors (e.g. the increase in temperature observed in recent decades).
10. The increase in the NDVI in mountainous areas is mostly due to the abandonment of land and rural margination that have led to the revegetation of slopes and increase the density of forests. Forests have shown the greatest increase in vegetation activity in recent decades. Factors such as temperature increase in areas characterized by a positive climate balance have favored this trend.
11. The decrease in vegetation activity is mostly restricted to small, highly localized areas. This process is mostly due to anthropogenic factors such as the abandonment of small old irrigated lands, the increased aridity in some cereal and olive crops, the urban expansion around large cities, especially on the coast, and possibly soil degradation in some specific areas.

12. An increase in vegetation activity has been observed over the last few decades in some areas where temperatures and atmospheric evaporative demand have also increased, which is surprising because both variables tend to limit vegetation activity. A future research line could be to investigate if the concentrations of CO_2 in the atmosphere have influenced this increase.

Regarding the relationship between NDVI and tree ring growth:

13. The greatest positive and significant correlations between the interannual variability of the NDVI and the secondary growth, measured by the growth rates of the tree rings (TRWi) are found in long NDVI cumulative periods (6 - 10 months).
14. Regardless of forest type, a high GSP favors secondary growth in forests.
15. The magnitude of correlations between NDVI and tree ring growth is quite similar between different forest types.
16. The responses of secondary forest growth to the NDVI time scales are diverse spatially and temporally.
17. There are dominant patterns in the NDVI and TRWi relationship in perennial tree species from semi-arid and sub-humid regions, and also in oak species from Mediterranean drylands, taking into account a cumulative NDVI of 10 months. There is also another relationship pattern with an accumulated NDVI at 8 months, characteristic of broadleaf species. The third pattern is represented by *A. alba* forests in the Pyrenees. And the fourth pattern also represents the Pyrenean forests of *A. alba* and *F. sylvatica*.

The conclusions in relation to the influence of droughts on the NDVI are:

18. The interannual variability of the NDVI in the peninsular Spain and the Balearic Islands has been strongly determined by the interannual variations of drought in the last three decades according to the relationship analysed between the NDVI and the SPEI.

19. The seasonal component influences the NDVI. The relationship between vegetation activity and drought is most marked in summer, when the temperature is highest, and mostly in forests, which are more active in summer months.
20. Seasonal differences have been found in the response of the NDVI to drought and in the magnitude of the correlation depending on the land cover.
21. It is observed that arable crops have a higher correlation between NDVI and SPEI than most natural vegetation types.
22. There are significant correlations between the spatial distribution of aridity and the sensitivity of the NDVI to drought, especially in spring and autumn.
23. The sensitivity of the NDVI to drought is not as controlled by aridity, in the case of forests, in summer.
24. In different types of land cover, under different environmental conditions, the sensitivity of the NDVI to SPEI shows similar correlations during the summer months.
25. NDVI's response to drought depends on the time scale at which the drought is measured. This is probably due to different morphological, physiological and phenological strategies of different vegetation types that respond differently to water stress conditions.
26. In peninsular Spain and the Balearic Islands, the NDVI responds in average to the SPEI on 10-month time scales, although there are spatial differences depending on the type of soil, as herbaceous coverages respond to shorter time scales than forests.
27. Climatic conditions recorded over longer periods also influence the vegetation's response to drought.
28. Water management and aridity in certain areas also influence the NDVI and SPEI relationship.
29. Mixed forests respond to shorter SPEI time scales than natural vegetation.

7. Conclusiones

Las imágenes de satélite son una herramienta muy utilizada en las ciencias ambientales para dar respuesta a los retos que nos plantean los cambios espaciales y temporales debidos tanto al cambio climático como a las transformaciones que resultan de las actividades humanas. Esta tesis ha aportado información para comprender qué cambios se han dado en la actividad vegetal de la España peninsular y las Islas Baleares en las últimas tres décadas, cómo esos cambios pueden estar relacionados con el crecimiento de los árboles y también, cómo influye en la actividad vegetal un riesgo climático como la sequía, tan presente en esta región mediterránea.

Respecto a la creación de la base de datos Sp_1km_NDVI:

1. Disponer de imágenes satelitales diarias NOAA-AVHRR ha permitido tener información suficiente para poder trabajar con series temporales largas. A pesar de haber tenido que descartar aquellas imágenes diarias que presentaban algún problema durante su captura o que estaban totalmente cubiertas por las nubes, mediante una revisión exhaustiva, la cantidad de datos disponibles y la escala temporal de análisis ofrece información muy adecuada para realizar estudios que analicen la actividad vegetal en la España Peninsular y las Islas Baleares.
2. La corrección atmosférica no se considera un aspecto imprescindible en el desarrollo de la presente base de datos, debido a las características del sensor AVHRR y, además, al procedimiento de creación de imágenes compuestas semi-mensuales para minimizar el efecto del ruido atmosférico ha mostrado ser eficaz.
3. Respecto a la inhomogeneidad entre los sensores AVHRR/2 y AVHRR/3, la corrección estadística utilizada se considera suficiente para poder trabajar con la base de datos creada.
4. Desde que se utilizan las imágenes NOAA-AVHRR para obtener productos NDVI, no se ha presentado hasta ahora una base de datos desarrollada específicamente para la España peninsular y las Islas Baleares a 1,1 km de resolución y que abarque el periodo

1981 – 2015. Lo que hace de estos datos un producto original, novedoso y útil para el análisis de la actividad vegetal.

En cuanto a la comparación entre las bases de datos NDVI:

5. La dinámica temporal de la base de datos desarrollada y de las otras tres bases de datos comparadas es similar. El análisis espacial muestra más diferencias entre las bases de datos respecto a la magnitud de cambio, pero los patrones son comparables en el caso de la significación de las tendencias, resultando la base de datos SMN la más dispar.
6. Los patrones espaciales se asemejan y la variabilidad temporal, con un incremento general de los valores NDVI a lo largo del periodo analizado.
7. La base de datos obtenida permite localizar fácilmente cambios conocidos en la cubierta vegetal, que son debidos a la transformación de las tierras agrícolas, de forma más clara que las bases de datos de menor resolución espacial (GIMMS3g y SMN) y muestra los cambios que responden a un periodo más largo que la base de datos que tiene mayor detalle, pero que cubre un periodo temporal más corto (MODIS).

Conclusiones obtenidas sobre las tendencias en el NDVI:

8. La tendencia en los valores NDVI obtenidos a partir de la base de datos creada, muestra un aumento general del NDVI en la España peninsular y las Islas Baleares en las tres décadas analizadas.

9. La magnitud de los cambios en el NDVI ha sido diferente tanto a nivel espacial como temporal. Los cambios que responden al mayor aumento del NDVI se localizan en las áreas agrícolas y se deben a las actividades humanas, fundamentalmente resultado de la transformación de zonas de cultivo de secano en zonas de regadío; pero también están relacionados con factores climáticos como el incremento de la temperatura observado en las últimas décadas.
10. El aumento en el NDVI en las zonas montañosas se debe al abandono de las tierras y a la despoblación rural que han propiciado la revegetación de laderas y que aumente la

densidad de los bosques. Este tipo de cubierta vegetal ha mostrado el mayor aumento de NDVI en las últimas décadas.

11. La disminución de la actividad vegetal se localiza en áreas pequeñas, muy localizadas y se puede deber a factores antrópicos como el abandono de antiguos regadíos de tamaño reducido, al aumento de la aridez en algunos cultivos de cereales y olivos, a la expansión urbana alrededor de las grandes ciudades, sobre todo en el litoral, y a la degradación de los suelos por sobrepastoreo o intensificación de las prácticas agrarias.
12. Se ha observado un aumento de la actividad vegetal durante las últimas décadas en algunas zonas donde las temperaturas y la demanda evaporativa atmosférica también ha aumentado, cosa que sorprende porque ambas variables suelen ser limitantes de la actividad vegetal. Investigar si las concentraciones de CO2 en la atmósfera han influido en ese aumento sería una línea de investigación futura a tener en cuenta.

Respecto a la relación entre los valores NDVI y el crecimiento radial de los árboles:

13. Las mayores correlaciones positivas y significativas entre la variabilidad interanual del NDVI y el crecimiento secundario, medido gracias a los índices de crecimiento de los anillos de los árboles (TRWi), y en los diferentes bosques analizados, se encuentran en largos períodos de acumulación del NDVI (6 – 10 meses).
14. Independientemente del tipo de bosque, una alta PPB favorece al crecimiento secundario en los bosques.
15. La magnitud de las correlaciones entre el NDVI y el crecimiento de los anillos de los árboles es bastante similar entre diferentes tipos de bosque.
16. Las respuestas del crecimiento secundario forestal a las escalas temporales del NDVI son diversas espacial y temporalmente.
17. Existen patrones dominantes en cuanto a la relación NDVI y TRWi en especies arbóreas perennifolias de las regiones semiáridas y subhúmedas, y también en las especies de roble de las zonas secas mediterráneas, teniendo en cuenta un NDVI acumulado a 10 meses. También se da otro patrón de relación con un NDVI acumulado

a 8 meses, en especies frondosas de hoja ancha. El tercer patrón está representado por los bosques de *A. alba* en los Pirineos. Y el cuarto patrón también representa a los bosques pirenaicos de *A. alba* y *F. sylvatica*.

Por último, las conclusiones respecto a la actividad vegetal y las sequías:

18. La actividad de la vegetación en la España peninsular y las Islas Baleares ha estado fuertemente determinada por las variaciones interanuales de la sequía en las últimas tres décadas según la relación analizada entre el NDVI y el SPEI.
19. La componente estacional influye en el NDVI. La relación entre la actividad vegetal y la sequía es más marcada en verano, cuando la temperatura es más alta, y fundamentalmente en los bosques, que presentan una máxima actividad durante esta estación.
20. Se han encontrado diferencias estacionales en la respuesta del NDVI a la sequía y en la magnitud de la correlación, en función del tipo de cubierta.
21. Se observa que los cultivos herbáceos presentan una mayor correlación entre el NDVI y el SPEI que la mayoría de los tipos de vegetación natural. Esto es debido a una mayor adaptación por parte de la vegetación natural, a que tienen sistemas radiculares más profundos y a que los cultivos se localizan en zonas más secas que la vegetación natural.
22. Existen correlaciones significativas entre la distribución espacial de la aridez y la sensibilidad del NDVI a la sequía, sobre todo en primavera y otoño.
23. La sensibilidad del NDVI a la sequía no está tan controlada por la aridez, en el caso de los bosques, en verano.
24. En diferentes tipos de coberturas de suelo, bajo distintas condiciones ambientales, la sensibilidad del NDVI al SPEI muestra correlaciones similares durante los meses de verano.
25. La respuesta del NDVI a la sequía depende de la escala temporal en la que se mide esa sequía. Esto es probablemente debido a las diferentes estrategias morfológicas,

fisiológicas y fenológicas de los diferentes tipos de vegetación que responden de manera distinta.

26. En la España peninsular y las Islas Baleares, el NDVI responde al SPEI en escalas temporales de 10 meses de forma media, aunque hay diferencias dependiendo el tipo de suelo, ya que las coberturas herbáceas responden a escalas temporales más cortas que los bosques.
27. Las condiciones climáticas registradas durante periodos más largos también influyen en la respuesta a la sequía por parte de la vegetación.
28. Los bosques mixtos responden a escalas temporales más cortas del SPEI que la vegetación natural.

References

Abrams MD, Schultz JC, Kleiner KW. 1990. Ecophysiological responses in mesic versus xeric hardwood species to an early-season drought in central Pennsylvania. *Forest Science* **36**(4): 970–981.

Ainsworth EA, Long SP. 2005. What have we learned from 15 years of free-air CO<inf>2</inf>enrichment (FACE)? A meta-analytic review of the responses of photosynthesis, canopy properties and plant production to rising CO<inf>2</inf>. *New Phytologist* **165**(2): 351–372. DOI: 10.1111/j.1469-8137.2004.01224.x.

Alcaraz-Segura D, Liras E, Tabik S, Paruelo J, Cabello J. 2010. Evaluating the consistency of the 1982-1999 NDVI trends in the Iberian Peninsula across four time-series derived from the AVHRR sensor: LTDR, GIMMS3g, FASIR, and PAL-II. *Sensors* **10**(2): 1291–1314. DOI: 10.3390/s100201291.

Alla AQ, Pasho E, Marku V. 2017. Growth variability and contrasting climatic responses of two Quercus macrolepis stands from Southern Albania. *Trees - Structure and Function* **31**(5): 1491–1504. DOI: 10.1007/s00468-017-1564-0.

Allen CD, Breshears DD, McDowell NG. 2015. On underestimation of global vulnerability to tree mortality and forest die-off from hotter drought in the Anthropocene. *Ecosphere* **6**(8). DOI: 10.1890/ES15-00203.1.

Allen CD, Macalady AK, Chenchouni H, Bachelet D, McDowell N, Vennetier M, Kitzberger T, Rigling A, Breshears DD, Hogg EH (T. ., Gonzalez P, Fensham R, Zhang Z, Castro J, Demidova N, Lim J-H, Allard G, Running SW, Semerci A, Cobb N. 2010. A global overview of drought and heat-induced tree mortality reveals emerging climate change risks for forests. *Forest Ecology and Management* **259**(4): 660–684. DOI: 10.1016/j.foreco.2009.09.001.

Allen RG, Pereira LS, Raes D, Smith M. 1998. No Title. *Crop Evapotranspiration: Guidelines for Computing Crop Water Requirements*.

Álvaro F, Isidro J, Villegas D, García del Moral LF, Royo C. 2008. Old and modern durum wheat varieties from Italy and Spain differ in main spike components. *Field Crops Research* **106**(1): 86–93. DOI: 10.1016/j.fcr.2007.11.003.

Améztegui A, Brotons L, Coll L. 2010. Land-use changes as major drivers of mountain pine (Pinus uncinata Ram.) expansion in the Pyrenees. *Global Ecology and Biogeography* **19**(5): 632–641. DOI: 10.1111/j.1466-8238.2010.00550.x.

Ameztegui A, Coll L, Brotons L, Ninot JM. 2016. Land-use legacies rather than climate change are driving the recent upward shift of the mountain tree line in the Pyrenees. *Global Ecology and Biogeography* **25**(3): 263–273. DOI: 10.1111/geb.12407.

Anyamba A, Tucker CJ. 2005. Analysis of Sahelian vegetation dynamics using NOAA-AVHRR NDVI data from 1981-2003. *Journal of Arid Environments* **63**(3): 596–614. DOI: 10.1016/j.jaridenv.2005.03.007.

Arino O, Vermote E, Spaventa V. 1997. Operational atmospheric correction of landsat TM imagery. *Earth Observation Quarterly* (56): 32–35.

Arzac A, García-Cervigón AI, Vicente-Serrano SM, Loidi J, Olano JM. 2016. Phenological shifts in climatic response of secondary growth allow Juniperus sabina L. to cope with altitudinal and temporal climate variability. *Agricultural and Forest Meteorology* **217**. DOI: 10.1016/j.agrformet.2015.11.011.

Asseng S, Ewert F, Martre P, Rötter RP, Lobell DB, Cammarano D, Kimball BA, Ottman MJ, Wall GW, White JW, Reynolds MP, Alderman PD, Prasad PVV, Aggarwal PK, Anothai J, Basso B, Biernath C, Challinor AJ, De Sanctis G, Doltra J, Fereres E, Garcia-Vila M, Gayler S, Hoogenboom G, Hunt LA, Izaurralde RC, Jabloun M, Jones CD, Kersebaum KC, Koehler A-K, Müller C, Naresh Kumar S, Nendel C, O'leary G, Olesen JE, Palosuo T, Priesack E, Eyshi Rezaei E, Ruane AC, Semenov MA, Shcherbak I, Stöckle C, Stratonovitch P, Streck T, Supit I, Tao F, Thorburn PJ, Waha K, Wang E, Wallach D, Wolf J, Zhao Z, Zhu Y. 2015. Rising temperatures reduce global wheat production. *Nature Climate Change* **5**(2): 143–147. DOI: 10.1038/nclimate2470.

Austin RB, Cantero-Martínez C, Arrúe JL, Playán E, Cano-Marcellán P. 1998. Yield-rainfall relationships in cereal cropping systems in the Ebro river valley of Spain. *European Journal of Agronomy* **8**(3–4): 239–248. DOI: 10.1016/S1161-0301(97)00063-4.

Azorin-Molina C, Baena-Calatrava R, Echave-Calvo I, Connell BH, Vicente-Serrano SM, López-Moreno JI. 2013. A daytime over land algorithm for computing AVHRR convective cloud climatologies for the Iberian Peninsula and the Balearic Islands. *International Journal of Climatology* **33**(9). DOI: 10.1002/joc.3572.

Babst F, Bouriaud O, Alexander R, Trouet V, Frank D. 2014a. Toward consistent measurements of carbon accumulation: A multi-site assessment of biomass and basal area increment across Europe. *Dendrochronologia* **32**(2): 153–161. DOI: 10.1016/j.dendro.2014.01.002.

Babst F, Bouriaud O, Papale D, Gielen B, Janssens IA, Nikinmaa E, Ibrom A, Wu J, Bernhofer C, Köstner B, Grünwald T, Seufert G, Ciais P, Frank D. 2014b. Above-ground woody carbon sequestration measured from tree rings is coherent with net ecosystem productivity at five eddy-covariance sites. *New Phytologist* **201**(4): 1289–1303. DOI: 10.1111/nph.12589.

Bachmair S, Kohn I, Stahl K. 2015. Exploring the link between drought indicators and impacts. *Natural Hazards and Earth System Sciences* **15**(6): 1381–1397. DOI: 10.5194/nhess-15-1381-2015.

Bachmair S, Tanguy M, Hannaford J, Stahl K. 2018. How well do meteorological indicators represent agricultural and forest drought across Europe? *Environmental Research Letters* **13**(3). DOI: 10.1088/1748-9326/aaafda.

Baena-Calatrava R. 2002. Georreferenciación automática de imágenes NOAA-AVHRR. University of Jaen.

Bailing M, Zhiyong L, Cunzhu L, Lixin W, Chengzhen J, Fuxiang B, Chao J. 2018. Temporal and spatial heterogeneity of drought impact on vegetation growth on the Inner Mongolian Plateau. *Rangeland Journal* **40**(2): 113–128. DOI: 10.1071/RJ16097.

Baldi G, Nosetto MD, Aragón R, Aversa F, Paruelo JM, Jobbágy EG. 2008. Long-term satellite NDVI data sets: Evaluating their ability to detect ecosystem functional changes in South America. *Sensors* **8**(9): 5397–5425. DOI: 10.3390/s8095397.

Baldocchi DD, Xu L, Kiang N. 2004. How plant functional-type, weather, seasonal drought, and soil physical properties alter water and energy fluxes of an oak-grass savanna and an annual grassland. *Agricultural and Forest Meteorology* **123**(1–2): 13–39. DOI: 10.1016/j.agrformet.2003.11.006.

Barber VA, Juday GP, Finney BP. 2000. Reduced growth of Alaskan white spruce in the twentieth century from temperature-induced drought stress. *Nature* **405**(6787): 668–673. DOI: 10.1038/35015049.

Barbosa HA, Huete AR, Baethgen WE. 2006. A 20-year study of NDVI variability over the Northeast Region of Brazil. *Journal of Arid Environments* **67**(2): 288–307. DOI: 10.1016/j.jaridenv.2006.02.022.

Baret F, Guyot G. 1991. Potentials and limits of vegetation indices for LAI and APAR assessment. *Remote Sensing of Environment* **35**(2–3): 161–173. DOI: 10.1016/0034-4257(91)90009-U.

Barker LJ, Hannaford J, Chiverton A, Svensson C. 2016. From meteorological to hydrological drought using standardised indicators. *Hydrology and Earth System Sciences* **20**(6): 2483–2505. DOI: 10.5194/hess-20-2483-2016.

Batllori E, Gutiérrez E. 2008. Regional tree line dynamics in response to global change in the Pyrenees. *Journal of Ecology* **96**(6): 1275–1288. DOI: 10.1111/j.1365-2745.2008.01429.x.

Beck HE, McVicar TR, van Dijk AIJM, Schellekens J, de Jeu RAM, Bruijnzeel LA. 2011. Global evaluation of four AVHRR-NDVI data sets: Intercomparison and assessment against Landsat imagery. *Remote Sensing of Environment* **115**(10): 2547–2563. DOI: 10.1016/j.rse.2011.05.012.

Beck PSA, Goetz SJ. 2011. Satellite observations of high northern latitude vegetation productivity changes between 1982 and 2008: Ecological variability and regional differences. *Environmental Research Letters* **6**(4). DOI: 10.1088/1748-9326/6/4/045501.

Berg A, Sheffield J, Milly PCD. 2017. Divergent surface and total soil moisture projections under global warming. *Geophysical Research Letters* **44**(1): 236–244. DOI: 10.1002/2016GL071921.

Bergeron O, Margolis HA, Black TA, Coursolle C, Dunn AL, Barr AG, Wofsy SC. 2007. Comparison of carbon dioxide fluxes over three boreal black spruce forests in Canada. *Global Change Biology* **13**(1): 89–107. DOI: 10.1111/j.1365-2486.2006.01281.x.

Berner LT, Beck PSA, Bunn AG, Goetz SJ. 2013. Plant response to climate change along the forest-tundra ecotone in northeastern Siberia. *Global Change Biology* **19**(11): 3449–3462. DOI: 10.1111/gcb.12304.

Bhuiyan C, Singh RP, Kogan FN. 2006. Monitoring drought dynamics in the Aravalli region (India) using different indices based on ground and remote sensing data. *International Journal of Applied Earth Observation and Geoinformation* **8**(4): 289–302. DOI: 10.1016/j.jag.2006.03.002.

Bhuyan U, Zang C, Vicente-Serrano SM, Menzel A. 2017. Exploring relationships among tree-ring growth, climate variability, and seasonal leaf activity on varying timescales and spatial resolutions. *Remote Sensing* **9**(6). DOI: 10.3390/rs9060526.

Boulouf Lugo J, Deslauriers A, Rossi S. 2012. Duration of xylogenesis in black spruce lengthened between 1950 and 2010. *Annals of Botany* **110**(6): 1099–1108. DOI: 10.1093/aob/mcs175.

Breshears DD, Cobb NS, Rich PM, Price KP, Allen CD, Balice RG, Romme WH, Kastens JH, Floyd

ML, Belnap J, Anderson JJ, Myers OB, Meyer CW. 2005. Regional vegetation die-off in response to global-change-type drought. *Proceedings of the National Academy of Sciences of the United States of America* **102**(42): 15144–15148. DOI: 10.1073/pnas.0505734102.

Brown ME, Pinzón JE, Didan K, Morisette JT, Tucker CJ. 2006. Evaluation of the consistency of Long-term NDVI time series derived from AVHRR, SPOT-vegetation, SeaWiFS, MODIS, and landsat ETM+ sensors. *IEEE Transactions on Geoscience and Remote Sensing* **44**(7): 1787–1793. DOI: 10.1109/TGRS.2005.860205.

Camarero JJ, Bigler C, Linares JC, Gil-Pelegrín E. 2011. Synergistic effects of past historical logging and drought on the decline of Pyrenean silver fir forests. *Forest Ecology and Management* **262**(5): 759–769. DOI: 10.1016/j.foreco.2011.05.009.

Camarero JJ, Gazol A, Sangüesa-Barreda G, Cantero A, Sánchez-Salguero R, Sánchez-Miranda A, Granda E, Serra-Maluquer X, Ibáñez R. 2018. Forest growth responses to drought at short- and long-term scales in Spain: Squeezing the stress memory from tree rings. *Frontiers in Ecology and Evolution* **6**(FEB). DOI: 10.3389/fevo.2018.00009.

Camarero JJ, Gazol A, Sangüesa-Barreda G, Oliva J, Vicente-Serrano SM. 2015. To die or not to die: Early warnings of tree dieback in response to a severe drought. *Journal of Ecology* **103**(1). DOI: 10.1111/1365-2745.12295.

Camarero JJ, Olano JM, Parras A. 2010. Plastic bimodal xylogenesis in conifers from continental Mediterranean climates. *New Phytologist* **185**(2): 471–480. DOI: 10.1111/j.1469-8137.2009.03073.x.

Carlson TN, Ripley DA. 1997. On the relation between NDVI, fractional vegetation cover, and leaf area index. *Remote Sensing of Environment* **62**(3): 241–252. DOI: 10.1016/S0034-4257(97)00104-1.

Carnicer J, Coll M, Ninyerola M, Pons X, Sánchez G, Peñuelas J. 2011. Widespread crown condition decline, food web disruption, and amplified tree mortality with increased climate change-type drought. *Proceedings of the National Academy of Sciences of the United States of America* **108**(4): 1474–1478. DOI: 10.1073/pnas.1010070108.

Castro-Díez P, Villar-Salvador P, Pérez-Rontomé C, Maestro-Martínez M, Montserrat-Martí G. 1997. Leaf morphology and leaf chemical composition in three Quercus (Fagaceae) species along a rainfall gradient in NE Spain. *Trees - Structure and Function* **11**(3): 127–134. DOI: 10.1007/s004680050068.

Changnon SA, Easterling WE. 1989. MEASURING DROUGHT IMPACTS: THE ILLINOIS CASE. *JAWRA Journal of the American Water Resources Association* **25**(1): 27–42. DOI: 10.1111/j.1752-1688.1989.tb05663.x.

Chaves MM, Maroco JP, Pereira JS. 2003. Understanding plant responses to drought - From genes to the whole plant. *Functional Plant Biology* **30**(3): 239–264. DOI: 10.1071/FP02076.

Ciais P, Reichstein M, Viovy N, Granier A, Ogée J, Allard V, Aubinet M, Buchmann N, Bernhofer C, Carrara A, Chevallier F, De Noblet N, Friend AD, Friedlingstein P, Grünwald T, Heinesch B, Keronen P, Knohl A, Krinner G, Loustau D, Manca G, Matteucci G, Miglietta F, Ourcival JM, Papale D, Pilegaard K, Rambal S, Seufert G, Soussana JF, Sanz MJ, Schulze ED, Vesala T, Valentini R. 2005. Europe-wide reduction in primary productivity caused by the heat and drought in 2003. *Nature* **437**(7058): 529–533. DOI: 10.1038/nature03972.

Cihlar J, St.-Laurent L, Dyer JA. 1991. Relation between the normalized difference vegetation index and ecological variables. *Remote Sensing of Environment* **35**(2–3): 279–298. DOI: 10.1016/0034-4257(91)90018-2.

Contreras S, Hunink JE. 2015. Drought effects on rainfed agriculture using standardized indices: A case study in SE Spain. *Drought: Research and Science-Policy Interfacing - Proceedings of the International Conference on Drought: Research and Science-Policy Interfacing*, 65–70.

Coulthard BL, Touchan R, Anchukaitis KJ, Meko DM, Sivrikaya F. 2017. Tree growth and vegetation activity at the ecosystem-scale in the eastern Mediterranean. *Environmental Research Letters* **12**(8). DOI: 10.1088/1748-9326/aa7b26.

Čufar K, Prislan P, De Luis M, Gričar J. 2008. Tree-ring variation, wood formation and phenology of beech (Fagus sylvatica) from a representative site in Slovenia, SE Central Europe. *Trees - Structure and Function* **22**(6): 749–758. DOI: 10.1007/s00468-008-0235-6.

Cuny HE, Rathgeber CBK, Frank D, Fonti P, Makinen H, Prislan P, Rossi S, Del Castillo EM, Campelo F, Vavrčík H, Camarero JJ, Bryukhanova MV, Jyske T, Gricar J, Gryc V, De Luis M, Vieira J, Cufar K, Kirdyanov AV, Oberhuber W, Treml V, Huang J-G, Li X, Swidrak I, Deslauriers A, Liang E, Nojd P, Gruber A, Nabais C, Morin H, Krause C, King G, Fournier M. 2015. Woody biomass production lags stem-girth increase by over one month in coniferous forests. *Nature Plants* **1**: 1–6. DOI: 10.1038/nplants.2015.160.

Dardel C, Kergoat L, Hiernaux P, Mougin E, Grippa M, Tucker CJ. 2014. Re-greening Sahel: 30 years of

remote sensing data and field observations (Mali, Niger). *Remote Sensing of Environment* **140**: 350–364. DOI: 10.1016/j.rse.2013.09.011.

De Keersmaecker W, Lhermitte S, Hill MJ, Tits L, Coppin P, Somers B. 2017. Assessment of regional vegetation response to climate anomalies: A case study for australia using GIMMS3g NDVI time series between 1982 and 2006. *Remote Sensing* **9**(1). DOI: 10.3390/rs9010034.

del Barrio G, Puigdefabregas J, Sanjuan ME, Stellmes M, Ruiz A. 2010. Assessment and monitoring of land condition in the Iberian Peninsula, 1989-2000. *Remote Sensing of Environment* **114**(8): 1817–1832. DOI: 10.1016/j.rse.2010.03.009.

del Castillo J, Voltas J, Ferrio JP. 2015. Carbon isotope discrimination, radial growth, and NDVI share spatiotemporal responses to precipitation in Aleppo pine. *Trees - Structure and Function* **29**(1): 223–233. DOI: 10.1007/s00468-014-1106-y.

Díaz-Delgado R, Lloret F, Pons X, Terradas J. 2002. Satellite evidence of decreasing resilience in mediterranean plant communities after recurrent wildfires. *Ecology* **83**(8): 2293–2303. DOI: 10.1890/0012-9658(2002)083[2293:SEODRI]2.0.CO;2.

Donohue RJ, Roderick ML, McVicar TR, Farquhar GD. 2013. Impact of CO<inf>2</inf> fertilization on maximum foliage cover across the globe's warm, arid environments. *Geophysical Research Letters* **40**(12): 3031–3035. DOI: 10.1002/grl.50563.

Fensholt R, Proud SR. 2012. Evaluation of Earth Observation based global long term vegetation trends - Comparing GIMMS3g and MODIS global NDVI time series. *Remote Sensing of Environment* **119**: 131–147. DOI: 10.1016/j.rse.2011.12.015.

Fensholt R, Rasmussen K, Nielsen TT, Mbow C. 2009. Evaluation of earth observation based long term vegetation trends - Intercomparing NDVI time series trend analysis consistency of Sahel from AVHRR GIMMS3g, Terra MODIS and SPOT VGT data. *Remote Sensing of Environment* **113**(9): 1886–1898. DOI: 10.1016/j.rse.2009.04.004.

Fischer EM, Seneviratne SI, Vidale PL, Lüthi D, Schär C. 2007. Soil moisture-atmosphere interactions during the 2003 European summer heat wave. *Journal of Climate* **20**(20): 5081–5099. DOI: 10.1175/JCLI4288.1.

Fritts HC. 1976. No Title. *Tree Rings and Climate*.

Gallardo M, Martínez-Vega J. 2016. Three decades of land-use changes in the region of Madrid and how they relate to territorial planning. *European Planning Studies* **24**(5): 1016–1033. DOI: 10.1080/09654313.2016.1139059.

García-Haro FJ, Campos-Taberner M, Sabater N, Belda F, Moreno A, Gilabert MA, Martínez B, Pérez-Hoyos A, Meliá J. 2014. Vegetation vulnerability to drought in Spain | Vulnerabilidad de la vegetación a la sequía en España. *Revista de Teledeteccion* (42): 29–37. DOI: 10.4995/raet.2014.2283.

Garcia-Ruiz JM, Lasanta-Martinez T. 1990. Land-use changes in the Spanish Pyrenees. *Mountain Research & Development* **10**(3): 267–279. DOI: 10.2307/3673606.

García-Ruiz JM, Lasanta T, Ruiz-Flano P, Ortigosa L, White S, González C, Martí C. 1996. Land-use changes and sustainable development in mountain areas: A case study in the Spanish Pyrenees. *Landscape Ecology* **11**(5): 267–277. DOI: 10.1007/BF02059854.

García-Ruiz JM, López-Moreno JI, Vicente-Serrano SM, Lasanta-Martínez T, Beguería S. 2011. Mediterranean water resources in a global change scenario. *Earth-Science Reviews* **105**(3–4). DOI: 10.1016/j.earscirev.2011.01.006.

Gazol A, Camarero JJ, Anderegg WRL, Vicente-Serrano SM. 2017. Impacts of droughts on the growth resilience of Northern Hemisphere forests. *Global Ecology and Biogeography* **26**(2). DOI: 10.1111/geb.12526.

Gazol A, Camarero JJ, Vicente-Serrano SM, Sánchez-Salguero R, Gutiérrez E, de Luis M, Sangüesa-Barreda G, Novak K, Rozas V, Tíscar PA, Linares JC, Martín-Hernández N, Martínez del Castillo E, Ribas M, García-González I, Silla F, Camisón A, Génova M, Olano JM, Longares LA, Hevia A, Tomás-Burguera M, Galván JD. 2018. Forest resilience to drought varies across biomes. *Global Change Biology* **24**(5). DOI: 10.1111/gcb.14082.

Gessner U, Naeimi V, Klein I, Kuenzer C, Klein D, Dech S. 2013. The relationship between precipitation anomalies and satellite-derived vegetation activity in Central Asia. *Global and Planetary Change* **110**: 74–87. DOI: 10.1016/j.gloplacha.2012.09.007.

Giner C, Martínez B, Gilabert MA, Alcaraz-Segura D. 2012. Trends in vegetation greenness and gross primary production in Spain (2000-2009) | Tendencias en el verdor de la vegetación y en la producción primaria bruta de las áreas forestales en la España peninsular (2000-2009). *Revista de Teledeteccion* (38): 51–64.

Giorgi F, Lionello P. 2008. Climate change projections for the Mediterranean region. *Global and Planetary Change* **63**(2–3): 90–104. DOI: 10.1016/j.gloplacha.2007.09.005.

González-Alonso F, Casanova JL. 1997. Application of NOAA-AVHRR images for the validation and risk assessment of natural disasters in Spain. *Remote Sensing '96*. Balkema: Rotterdam, 227–233.

Gonzalez-Hidalgo JC, Peña-Angulo D, Brunetti M, Cortesi N. 2016. Recent trend in temperature evolution in Spanish mainland (1951–2010): From warming to hiatus. *International Journal of Climatology* **36**(6): 2405–2416. DOI: 10.1002/joc.4519.

González-Hidalgo JC, Vicente-Serrano SM, Peña-Angulo D, Salinas C, Tomas-Burguera M, Beguería S. 2018. High-resolution spatio-temporal analyses of drought episodes in the western Mediterranean basin (Spanish mainland, Iberian Peninsula). *Acta Geophysica* **66**(3). DOI: 10.1007/s11600-018-0138-x.

Gough CM, Vogel CS, Schmid HP, Su H-B, Curtis PS. 2008. Multi-year convergence of biometric and meteorological estimates of forest carbon storage. *Agricultural and Forest Meteorology* **148**(2): 158–170. DOI: 10.1016/j.agrformet.2007.08.004.

Gouveia CM, Bastos A, Trigo RM, Dacamara CC. 2012. Drought impacts on vegetation in the pre- and post-fire events over Iberian Peninsula. *Natural Hazards and Earth System Science* **12**(10): 3123–3137. DOI: 10.5194/nhess-12-3123-2012.

Gouveia CM, Páscoa P, Russo A, Trigo RM. 2016. Land degradation trend assessment over iberia during 1982-2012 | Evaluación de la tendencia a la degradación del suelo en Iberia durante 1982-2012. *Cuadernos de Investigacion Geografica* **42**(1): 89–112. DOI: 10.18172/cig.2808.

Gouveia CM, Trigo RM, Beguería S, Vicente-Serrano SM. 2017. Drought impacts on vegetation activity in the Mediterranean region: An assessment using remote sensing data and multi-scale drought indicators. *Global and Planetary Change* **151**. DOI: 10.1016/j.gloplacha.2016.06.011.

Granier A, Reichstein M, Bréda N, Janssens IA, Falge E, Ciais P, Grünwald T, Aubinet M, Berbigier P, Bernhofer C, Buchmann N, Facini O, Grassi G, Heinesch B, Ilvesniemi H, Keronen P, Knohl A, Köstner B, Lagergren F, Lindroth A, Longdoz B, Loustau D, Mateus J, Montagnani L, Nys C, Moors E, Papale D, Peiffer M, Pilegaard K, Pita G, Pumpanen J, Rambal S, Rebmann C, Rodrigues A, Seufert G, Tenhunen J, Vesala T, Wang Q. 2007. Evidence for soil water control on carbon and water dynamics in European forests during the extremely dry year: 2003. *Agricultural and Forest Meteorology* **143**(1–2): 123–145. DOI: 10.1016/j.agrformet.2006.12.004.

Grissino-Mayer HD, Fritts HC. 1997. The International Tree-Ring Data Bank: An enhanced global database serving the global scientific community. *Holocene* **7**(2): 235–238. DOI: 10.1177/095968369700700212.

Gu Y, Brown JF, Verdin JP, Wardlow B. 2007. A five-year analysis of MODIS NDVI and NDWI for grassland drought assessment over the central Great Plains of the United States. *Geophysical Research Letters* **34**(6). DOI: 10.1029/2006GL029127.

Gutman G. 1989. On the relationship between monthly mean and maximum-value composite normalized vegetation indices. *International Journal of Remote Sensing* **10**(8): 1317–1325. DOI: 10.1080/01431168908903970.

Gutman G, Masek JG. 2012. Long-term time series of the Earth's land-surface observations from space. *International Journal of Remote Sensing* **33**(15): 4700–4719. DOI: 10.1080/01431161.2011.638341.

Gutman GG. 1991. Vegetation indices from AVHRR: An update and future prospects. *Remote Sensing of Environment* **35**(2–3): 121–136. DOI: 10.1016/0034-4257(91)90005-Q.

Hair JF, Anderson RE, Tatham RL, Black WC. 1995. No Title. *Multivariate Data Analysis*.

Hayles LA, Gutiérrez E, Macias M, Ribas M, Bosch O, Camarero JJ. 2007. Climate increases regional tree-growth variability in Iberian pine forests. *Global Change Biology* **13**(7): 804–815. DOI: 10.1111/j.1365-2486.2007.01322.x.

Herrmann SM, Anyamba A, Tucker CJ. 2005. Recent trends in vegetation dynamics in the African Sahel and their relationship to climate. *Global Environmental Change* **15**(4): 394–404. DOI: 10.1016/j.gloenvcha.2005.08.004.

Herrmann SM, Didan K, Barreto-Munoz A, Crimmins MA. 2016. Divergent responses of vegetation cover in Southwestern US ecosystems to dry and wet years at different elevations. *Environmental Research Letters* **11**(12). DOI: 10.1088/1748-9326/11/12/124005.

Heumann BW, Seaquist JW, Eklundh L, Jönsson P. 2007. AVHRR derived phenological change in the Sahel and Soudan, Africa, 1982-2005. *Remote Sensing of Environment* **108**(4): 385–392. DOI: 10.1016/j.rse.2006.11.025.

Hill J, Stellmes M, Udelhoven T, Röder A, Sommer S. 2008. Mediterranean desertification and land degradation. Mapping related land use change syndromes based on satellite observations. *Global and Planetary Change* **64**(3–4): 146–157. DOI: 10.1016/j.gloplacha.2008.10.005.

Hirschi M, Seneviratne SI, Alexandrov V, Boberg F, Boroneant C, Christensen OB, Formayer H, Orlowsky B, Stepanek P. 2011. Observational evidence for soil-moisture impact on hot extremes in southeastern Europe. *Nature Geoscience* **4**(1): 17–21. DOI: 10.1038/ngeo1032.

Holben BN. 1986. Characteristics of maximum-value composite images from temporal AVHRR data. *International Journal of Remote Sensing* **7**(11): 1417–1434. DOI: 10.1080/01431168608948945.

Holmes RL. 1983. Computer-assisted quality control in tree-ring dating and measurement. *Tree-Ring Bulletin* **44**: 69–75.

Huberty CJ. 1994. No Title. *Applied Discriminant Analysis*.

Huete A, Didan K, Miura T, Rodriguez EP, Gao X, Ferreira LG. 2002. Overview of the radiometric and biophysical performance of the MODIS vegetation indices. *Remote Sensing of Environment* **83**(1–2): 195–213. DOI: 10.1016/S0034-4257(02)00096-2.

Huxman TE, Smith MD, Fay PA, Knapp AK, Shaw MR, Lolk ME, Smith SD, Tissue DT, Zak JC, Weltzin JF, Pockman WT, Sala OE, Haddad BM, Harte J, Koch GW, Schwinning S, Small EE, Williams DG. 2004. Convergence across biomes to a common rain-use efficiency. *Nature* **429**(6992): 651–654. DOI: 10.1038/nature02561.

Iglesias E, Garrido A, Gómez-Ramos A. 2003. Evaluation of drought management in irrigated areas. *Agricultural Economics* **29**(2): 211–229. DOI: 10.1016/S0169-5150(03)00084-7.

Ivits E, Horion S, Fensholt R, Cherlet M. 2014. Drought footprint on European ecosystems between 1999 and 2010 assessed by remotely sensed vegetation phenology and productivity. *Global Change Biology* **20**(2): 581–593. DOI: 10.1111/gcb.12393.

Jenkins JC, Chojnacky DC, Heath LS, Birdsey RA. 2003. National-scale biomass estimators for United States tree species. *Forest Science* **49**(1): 12–35.

Ji L, Peters AJ. 2003. Assessing vegetation response to drought in the northern Great Plains using vegetation and drought indices. *Remote Sensing of Environment* **87**(1): 85–98. DOI: 10.1016/S0034-4257(03)00174-3.

Jiang N, Zhu W, Zheng Z, Chen G, Fan D. 2013. A comparative analysis between GIMSS NDVIg and NDVI3g for monitoring vegetation activity change in the Northern Hemisphere during 1982-2008. *Remote Sensing* **5**(8): 4031–4044. DOI: 10.3390/rs5084031.

Julien Y, Sobrino JA, Mattar C, Ruescas AB, Jiménez-Muñoz JC, Sòria G, Hidalgo V, Atitar M, Franch B, Cuenca J. 2011. Temporal analysis of normalized difference vegetation index (NDVI) and land surface temperature (LST) parameters to detect changes in the Iberian land cover between 1981 and 2001. *International Journal of Remote Sensing* **32**(7): 2057–2068. DOI: 10.1080/01431161003762363.

Kagawa A, Sugimoto A, Yamashita K, Abe H. 2005. Temporal photosynthetic carbon isotope signatures revealed in a tree ring through ^{13}CO<inf>2</inf> pulse-labelling. *Plant, Cell and Environment* **28**(7): 906–915. DOI: 10.1111/j.1365-3040.2005.01343.x.

Kalnay E, Kanamitsu M, Kistler R, Collins W, Deaven D, Gandin L, Iredell M, Saha S, White G, Woollen J, Zhu Y, Chelliah M, Ebisuzaki W, Higgins W, Janowiak J, Mo KC, Ropelewski C, Wang J, Leetmaa A, Reynolds R, Jenne R, Joseph D. 1996. The NCEP/NCAR 40-year reanalysis project. *Bulletin of the American Meteorological Society* **77**(3): 437–471. DOI: 10.1175/1520-0477(1996)077<0437:TNYRP>2.0.CO;2.

Kaufman YJ, Wald AE, Remer LA, Gao B-C, Li R-R, Flynn L. 1997. MODIS 2.1-μm channel - correlation with visible reflectance for use in remote sensing of aerosol. *IEEE Transactions on Geoscience and Remote Sensing* **35**(5): 1286–1298. DOI: 10.1109/36.628795.

Kaufmann RK, D'Arrigo RD, Laskowski C, Myneni RB, Zhou L, Davi NK. 2004. The effect of growing season and summer greenness on northern forests. *Geophysical Research Letters* **31**(9). DOI: 10.1029/2004GL019608.

Kaufmann RK, D'Arrigo RD, Paletta LF, Tian HQ, Jolly WM, Myneni RB. 2008. Identifying climatic controls on ring width: The timing of correlations between tree rings and NDVI. *Earth Interactions* **12**(14): 1–14. DOI: 10.1175/2008EI263.1.

Khorchani M, Vicente-Serrano SM, Azorin-Molina C, Garcia M, Martin-Hernandez N, Peña-Gallardo M, El Kenawy A, Domínguez-Castro F. 2018. Trends in LST over the peninsular Spain as derived from the AVHRR imagery data. *Global and Planetary Change* **166**. DOI: 10.1016/j.gloplacha.2018.04.006.

Knipling EB. 1970. Physical and physiological basis for the reflectance of visible and near-infrared radiation from vegetation. *Remote Sensing of Environment* **1**(3): 155–159. DOI: 10.1016/S0034-4257(70)80021-9.

Kogan F, Vargas M, Guo W. 2011. *Comparison of AVHRR-Based Global Data Records*. *NATO Science for Peace and Security Series C: Environmental Security*. DOI: 10.1007/978-90-481-9618-0_30.

Kogan FN. 1997. Global Drought Watch from Space. *Bulletin of the American Meteorological Society*

78(4): 621–636. DOI: 10.1175/1520-0477(1997)078<0621:GDWFS>2.0.CO;2.

Koslowsky, D., Billing, H., Friedrich K. 2005. MEDOKADS: a long-term data set for detection and monitoring of desertification risks in the Mediterranean. *Remote sensing and geoinformation in the assessment and monitoring of land degradation and desertification*. Trier, Germany, 191–198.

Kraus C, Zang C, Menzel A. 2016. Elevational response in leaf and xylem phenology reveals different prolongation of growing period of common beech and Norway spruce under warming conditions in the Bavarian Alps. *European Journal of Forest Research* **135**(6): 1011–1023. DOI: 10.1007/s10342-016-0990-7.

Krause K, Cherubini P, Bugmann H, Schleppi P. 2012. Growth enhancement of Picea abies trees under long-term, low-dose N addition is due to morphological more than to physiological changes. *Tree Physiology* **32**(12): 1471–1481. DOI: 10.1093/treephys/tps109.

Kuemmerle T, Levers C, Erb K, Estel S, Jepsen MR, Müller D, Plutzar C, Stürck J, Verkerk PJ, Verburg PH, Reenberg A. 2016. Hotspots of land use change in Europe. *Environmental Research Letters* **11**(6). DOI: 10.1088/1748-9326/11/6/064020.

Lasanta-Martínez T, Vicente-Serrano SM, Cuadrat-Prats JM. 2005. Mountain Mediterranean landscape evolution caused by the abandonment of traditional primary activities: A study of the Spanish Central Pyrenees. *Applied Geography* **25**(1). DOI: 10.1016/j.apgeog.2004.11.001.

Lasanta T. 2009. Functional changes in the Irrigation at the Ebro bassin: A survey of the role of Irrigation through time | Cambios de función en los regadios de la cuenca del ebro: Un análisis del papel de los regadíos a lo largo del tiempo. *Boletin de la Asociacion de Geografos Espanoles* (50).

Lasanta T, Arnáez J, Pascual N, Ruiz-Flaño P, Errea MP, Lana-Renault N. 2017. Space–time process and drivers of land abandonment in Europe. *Catena* **149**: 810–823. DOI: 10.1016/j.catena.2016.02.024.

Lasanta T, Marín-Yaseli ML. 2007. Effects of European common agricultural policy and regional policy on the socioeconomic development of the Central Pyrenees, Spain. *Mountain Research and Development* **27**(2): 130–137. DOI: 10.1659/mrd.0840.

Lasanta T, Vicente-Serrano SM. 2007. Cambios en la cubierta vegetal en el pirineo aragonés en los últimos 50 años. *Pirineos* (162).

Lasanta T, Vicente-Serrano SM. 2012. Complex land cover change processes in semiarid Mediterranean regions: An approach using Landsat images in northeast Spain. *Remote Sensing of Environment* **124**. DOI: 10.1016/j.rse.2012.04.023.

Latifovic R, Pouliot D, Dillabaugh C. 2012. Identification and correction of systematic error in NOAA AVHRR long-term satellite data record. *Remote Sensing of Environment* **127**: 84–97. DOI: 10.1016/j.rse.2012.08.032.

Latifovic R, Trishchenko AP, Chen J, Park WB, Khlopenkov KV, Fernandes R, Pouliot D, Ungureanu C, Luo Y, Wang S, Davidson A, Cihlar J. 2005. Generating historical AVHRR 1 km baseline satellite data records over Canada suitable for climate change studies. *Canadian Journal of Remote Sensing* **31**(5): 324–346. DOI: 10.5589/m05-024.

Leavitt SW, Chase TN, Rajagopalan B, Lee E, Lawrence PJ. 2008. Southwestern U.S. tree-ring carbon isotope indices as a possible proxy for reconstruction of greenness of vegetation. *Geophysical Research Letters* **35**(12). DOI: 10.1029/2008GL033894.

Lecina S, Isidoro D, Playán E, Aragüés R. 2010. Irrigation modernization and water conservation in Spain: The case of Riegos del Alto Aragón. *Agricultural Water Management* **97**(10): 1663–1675. DOI: 10.1016/j.agwat.2010.05.023.

Liang E, Eckstein D, Liu H. 2009. Assessing the recent grassland greening trend in a long-term context based on tree-ring analysis: A case study in North China. *Ecological Indicators* **9**(6): 1280–1283. DOI: 10.1016/j.ecolind.2009.02.007.

Liang S, Fang H, Chen M. 2001. Atmospheric correction of Landsat ETM+ land surface imagery-Part I: Methods. *IEEE Transactions on Geoscience and Remote Sensing* **39**(11): 2490–2498. DOI: 10.1109/36.964986.

Liu N, Harper RJ, Dell B, Liu S, Yu Z. 2017. Vegetation dynamics and rainfall sensitivity for different vegetation types of the Australian continent in the dry period 2002–2010. *Ecohydrology* **10**(2). DOI: 10.1002/eco.1811.

Liu WT, Kogan FN. 1996. Monitoring regional drought using the vegetation condition index. *International Journal of Remote Sensing* **17**(14): 2761–2782. DOI: 10.1080/01431169608949106.

Lloret F, Lobo A, Estevan H, Maisongrande P, Vayreda J, Terradas J. 2007. Woody plant richness and NDVI response to drought events in Catalonian (northeastern Spain) forests. *Ecology* **88**(9): 2270–2279. DOI: 10.1890/06-1195.1.

Lobell DB, Hammer GL, Chenu K, Zheng B, Mclean G, Chapman SC. 2015. The shifting influence of drought and heat stress for crops in northeast Australia. *Global Change Biology* **21**(11): 4115–4127. DOI: 10.1111/gcb.13022.

Lopatin E, Kolström T, Spiecker H. 2006. Determination of forest growth trends in Komi Republic (northwestern Russia): Combination of tree-ring analysis and remote sensing data. *Boreal Environment Research* **11**(5): 341–353.

López-Moreno JI, Beguería S, García-Ruiz JM. 2004. The management of a large Mediterranean reservoir: Storage regimens of the Yesa Reservoir, Upper Aragon River basin, Central Spanish Pyrenees. *Environmental Management* **34**(4): 508–515. DOI: 10.1007/s00267-003-0249-1.

López-Moreno JI, Vicente-Serrano SM, Zabalza J, Beguería S, Lorenzo-Lacruz J, Azorin-Molina C, Morán-Tejeda E. 2013. Hydrological response to climate variability at different time scales: A study in the Ebro basin. *Journal of Hydrology* **477**: 175–188. DOI: 10.1016/j.jhydrol.2012.11.028.

Lorenzo-Lacruz J, Moŕan-Tejeda E, Vicente-Serrano SM, Ĺopez-Moreno JI. 2013. Streamflow droughts in the Iberian Peninsula between 1945 and 2005: Spatial and temporal patterns. *Hydrology and Earth System Sciences* **17**(1). DOI: 10.5194/hess-17-119-2013.

Lorenzo-Lacruz J, Vicente-Serrano SM, López-Moreno JI, Beguería S, García-Ruiz JM, Cuadrat JM. 2010. The impact of droughts and water management on various hydrological systems in the headwaters of the Tagus River (central Spain). *Journal of Hydrology* **386**(1–4). DOI: 10.1016/j.jhydrol.2010.01.001.

Lotsch A, Friedl MA, Anderson BT, Tucker CJ. 2003. Coupled vegetation-precipitation variability observed from satellite and climate records. *Geophysical Research Letters* **30**(14). DOI: 10.1029/2003GL017506.

Ma X, Huete A, Moran S, Ponce-Campos G, Eamus D. 2015. Abrupt shifts in phenology and vegetation productivity under climate extremes. *Journal of Geophysical Research: Biogeosciences* **120**(10): 2036–2052. DOI: 10.1002/2015JG003144.

Macias M, Andreu L, Bosch O, Camarero JJ, Gutiérrez E. 2006. Increasing aridity is enhancing silver fir (Abies alba Mill.) water stress in its south-western distribution limit. *Climatic Change* **79**(3–4): 289–313. DOI: 10.1007/s10584-006-9071-0.

Malmström CM, Thompson MV, Juday GP, Los SO, Randerson JT, Field CB. 1997. Interannual variation in global-scale net primary production: Testing model estimates. *Global Biogeochemical Cycles* **11**(3): 367–392. DOI: 10.1029/97GB01419.

Malo AR, Nicholson SE. 1990. A study of rainfall and vegetation dynamics in the African Sahel using normalized difference vegetation index. *Journal of Arid Environments* **19**(1): 1–24.

Marraccini E, Debolini M, Moulery M, Abrantes P, Bouchier A, Chéry J-P, Sanz Sanz E, Sabbatini T, Napoleone C. 2015. Common features and different trajectories of land cover changes insix Western Mediterranean urban regions. *Applied Geography* **62**: 347–356. DOI: 10.1016/j.apgeog.2015.05.004.

Martínez-Fernández J, Ceballos A. 2003. Temporal Stability of Soil Moisture in a Large-Field Experiment in Spain. *Soil Science Society of America Journal* **67**(6): 1647–1656.

Martínez-Fernández J, Ruiz-Benito P, Zavala MA. 2015. Recent land cover changes in Spain across biogeographical regions and protection levels: Implications for conservation policies. *Land Use Policy* **44**: 62–75. DOI: 10.1016/j.landusepol.2014.11.021.

Martinez del Castillo E, García-Martin A, Longares Aladrén LA, de Luis M. 2015. Evaluation of forest cover change using remote sensing techniques and landscape metrics in Moncayo Natural Park (Spain). *Applied Geography* **62**: 247–255. DOI: 10.1016/j.apgeog.2015.05.002.

McDowell N, Pockman WT, Allen CD, Breshears DD, Cobb N, Kolb T, Plaut J, Sperry J, West A, Williams DG, Yepez EA. 2008. Mechanisms of plant survival and mortality during drought: Why do some plants survive while others succumb to drought? *New Phytologist* **178**(4): 719–739. DOI: 10.1111/j.1469-8137.2008.02436.x.

McKee TB, Doesken NJ, Kleist J. 1993. The relationship of drought frequency and duration to time scales. *Eighth Conf. on Applied Climatology* 179–184.

Milich L, Weiss E. 1997. Characterization of the sahel: Implications of correctly calculating interannual coefficients of variation (CoVs) from GAC NDVI values. *International Journal of Remote Sensing* **18**(18): 3749–3759. DOI: 10.1080/014311697216603.

Militino AF, Ugarte MD, Pérez-Goya U. 2018. *Detecting Change-Points in the Time Series of Surfaces Occupied by Pre-defined NDVI Categories in Continental Spain from 1981 to 2015*. *Studies in Systems, Decision and Control*. DOI: 10.1007/978-3-319-73848-2_28.

Molina AJ, del Campo AD. 2012. The effects of experimental thinning on throughfall and stemflow: A contribution towards hydrology-oriented silviculture in Aleppo pine plantations. *Forest Ecology*

and Management **269**: 206–213. DOI: 10.1016/j.foreco.2011.12.037.
Montserrat-Martí G, Camarero JJ, Palacio S, Pérez-Rontomé C, Milla R, Albuixech J, Maestro M. 2009. Summer-drought constrains the phenology and growth of two coexisting Mediterranean oaks with contrasting leaf habit: Implications for their persistence and reproduction. *Trees - Structure and Function* **23**(4): 787–799. DOI: 10.1007/s00468-009-0320-5.
Moreno MV, Conedera M, Chuvieco E, Pezzatti GB. 2014. Fire regime changes and major driving forces in Spain from 1968 to 2010. *Environmental Science and Policy* **37**: 11–22. DOI: 10.1016/j.envsci.2013.08.005.
Mu Q, Zhao M, Kimball JS, McDowell NG, Running SW. 2013. A remotely sensed global terrestrial drought severity index. *Bulletin of the American Meteorological Society* **94**(1): 83–98. DOI: 10.1175/BAMS-D-11-00213.1.
Mühlbauer S, Costa AC, Caetano M. 2016. A spatiotemporal analysis of droughts and the influence of North Atlantic Oscillation in the Iberian Peninsula based on MODIS imagery. *Theoretical and Applied Climatology* **124**(3–4): 703–721. DOI: 10.1007/s00704-015-1451-9.
Mukherjee S, Mishra A, Trenberth KE. 2018. Climate Change and Drought: a Perspective on Drought Indices. *Current Climate Change Reports* **4**(2): 145–163. DOI: 10.1007/s40641-018-0098-x.
Myneni RB, Hall FG, Sellers PJ, Marshak AL. 1995. Interpretation of spectral vegetation indexes. *IEEE Transactions on Geoscience and Remote Sensing* **33**(2): 481–486. DOI: 10.1109/36.377948.
Nagaraja Rao CR, Chen J. 1995. Inter-satellite calibration linkages for the visible and near-infared channels of the advanced very high resolution radiometer on the NOAA-7,-9, and-ii spacecraft. *International Journal of Remote Sensing* **16**(11): 1931–1942. DOI: 10.1080/01431169508954530.
Nemani RR, Keeling CD, Hashimoto H, Jolly WM, Piper SC, Tucker CJ, Myneni RB, Running SW. 2003. Climate-driven increases in global terrestrial net primary production from 1982 to 1999. *Science* **300**(5625): 1560–1563. DOI: 10.1126/science.1082750.
Newberry TL. 2010. Effect of climatic variability on $\delta^{13}C$ and tree-ring growth in piñon pine (Pinus edulis). *Trees - Structure and Function* **24**(3): 551–559. DOI: 10.1007/s00468-010-0426-9.
Nicholson SE, Davenport ML, Malo AR. 1990. A comparison of the vegetation response to rainfall in the Sahel and East Africa, using normalized difference vegetation index from NOAA AVHRR. *Climatic Change* **17**(2–3): 209–241. DOI: 10.1007/BF00138369.
Okin GS, Dong C, Willis KS, Gillespie TW, MacDonald GM. 2018. The Impact of Drought on Native Southern California Vegetation: Remote Sensing Analysis Using MODIS-Derived Time Series. *Journal of Geophysical Research: Biogeosciences* **123**(6): 1927–1939. DOI: 10.1029/2018JG004485.
Ortigosa LM, Garcia-Ruiz JM, Gil-Pelegrin E. 1990. Land reclamation by reforestation in the Central Pyrenees. *Mountain Research & Development* **10**(3): 281–288. DOI: 10.2307/3673607.
Orwig DA, Abrams MD. 1997. Variation in radial growth responses to drought among species, site, and canopy strata. *Trees - Structure and Function* **11**(8): 474–484. DOI: 10.1007/s004680050110.
Ouaidrari H, El Saleous N, Vermote EF, Townshend JR, Goward SN. 2003. AVHRR Land Pathfinder II (ALP II) data set: Evaluation and inter-comparison with other data sets. *International Journal of Remote Sensing* **24**(1): 135–142. DOI: 10.1080/01431160305006.
Palazón A, Aragonés L, López I. 2016. Evaluation of coastal management: Study case in the province of Alicante, Spain. *Science of the Total Environment* **572**: 1184–1194. DOI: 10.1016/j.scitotenv.2016.08.032.
Páscoa P, Gouveia CM, Russo A, Trigo RM. 2017. The role of drought on wheat yield interannual variability in the Iberian Peninsula from 1929 to 2012. *International Journal of Biometeorology* **61**(3): 439–451. DOI: 10.1007/s00484-016-1224-x.
Pasho E, Alla AQ. 2015. Climate impacts on radial growth and vegetation activity of two co-existing Mediterranean pine species. *Canadian Journal of Forest Research* **45**(12): 1748–1756. DOI: 10.1139/cjfr-2015-0146.
Pasho E, Camarero JJ, de Luis M, Vicente-Serrano SM. 2011. Impacts of drought at different time scales on forest growth across a wide climatic gradient in north-eastern Spain. *Agricultural and Forest Meteorology* **151**(12). DOI: 10.1016/j.agrformet.2011.07.018.
Pausas JG. 2004. Changes in fire and climate in the eastern Iberian Peninsula (Mediterranean Basin). *Climatic Change* **63**(3): 337–350. DOI: 10.1023/B:CLIM.0000018508.94901.9c.
Pausas JG, Fernández-Muñoz S. 2012. Fire regime changes in the Western Mediterranean Basin: From fuel-limited to drought-driven fire regime. *Climatic Change* **110**(1–2): 215–226. DOI: 10.1007/s10584-011-0060-6.
Peco B, Ortega M, Levassor C. 1998. Similarity between seed bank and vegetation in Mediterranean grassland: A predictive model. *Journal of Vegetation Science* **9**(6): 815–828. DOI:

10.2307/3237047.
Peguero-Pina JJ, Camarero JJ, Abadía A, Martín E, González-Cascón R, Morales F, Gil-Pelegrín E. 2007. Physiological performance of silver-fir (Abies alba Mill.) populations under contrasting climates near the south-western distribution limit of the species. *Flora: Morphology, Distribution, Functional Ecology of Plants* **202**(3): 226–236. DOI: 10.1016/j.flora.2006.06.004.
Peña-Gallardo M, SM V-S, Domínguez-Castro F, Quiring S, Svoboda M, Beguería S, Hannaford J. 2018a. Effectiveness of drought indices in identifying impacts on major crops across the USA . *Climate Research* **75**(3): 221–240.
Peña-Gallardo M, Vicente-Serrano SM, Camarero JJ, Gazol A, Sánchez-Salguero R, Domínguez-Castro F, El Kenawy A, Beguería-Portugés S, Gutiérrez E, de Luis M, Sangüesa-Barreda G, Novak K, Rozas V, Tíscar PA, Linares JC, del Castillo E, Ribas Matamoros M, García-González I, Silla F, Camisón Á, Génova M, Olano JM, Longares LA, Hevia A, Galván JD. 2018b. Drought Sensitiveness on Forest Growth in Peninsular Spain and the Balearic Islands. *Forests* **9**(9).
Peñuelas J, Sardans J, Filella I, Estiarte M, Llusià J, Ogaya R, Carnicer J, Bartrons M, Rivas-Ubach A, Grau O, Peguero G, Margalef O, Pla-Rabés S, Stefanescu C, Asensio D, Preece C, Liu L, Verger A, Rico L, Barbeta A, Achotegui-Castells A, Gargallo-Garriga A, Sperlich D, Farré-Armengol G, Fernández-Martínez M, Liu D, Zhang C, Urbina I, Camino M, Vives M, Nadal-Sala D, Sabaté S, Gracia C, Terradas J. 2018. Assessment of the impacts of climate change on Mediterranean terrestrial ecosystems based on data from field experiments and long-term monitored field gradients in Catalonia. *Environmental and Experimental Botany* **152**: 49–59. DOI: 10.1016/j.envexpbot.2017.05.012.
Peterson TC, Easterling DR, Karl TR, Groisman P, Nicholls N, Plummer N, Torok S, Auer I, Boehm R, Gullet D, Vincent L, Heino R, Tuomenvirta H, Mestre O, Szentimrey T, Salinger J, Førland EJ, Hanssen-Bauer I, Alexandersson H, Jones P, Parker D. 1998. Homogeneity adjustments of in situ atmospheric climate data: A review. *International Journal of Climatology* **18**(13): 1493–1517. DOI: 10.1002/(SICI)1097-0088(19981115)18:13<1493::AID-JOC329>3.0.CO;2-T.
Pinilla V. 2006. The development of irrigated agriculture in twentieth-century Spain: A case study of the Ebro basin. *Agricultural History Review* **54**(1): 122–141.
Pinzon JE, Tucker CJ. 2014. A non-stationary 1981-2012 AVHRR NDVI<inf>3g</inf>time series. *Remote Sensing* **6**(8): 6929–6960. DOI: 10.3390/rs6086929.
Poulter B, Pederson N, Liu H, Zhu Z, D'Arrigo R, Ciais P, Davi N, Frank D, Leland C, Myneni R, Piao S, Wang T. 2013. Recent trends in Inner Asian forest dynamics to temperature and precipitation indicate high sensitivity to climate change. *Agricultural and Forest Meteorology* **178**–**179**: 31–45. DOI: 10.1016/j.agrformet.2012.12.006.
Poyatos R, Latron J, Llorens P. 2003. Land use and land cover change after agricultural abandonment: The case of a Mediterranean Mountain area (Catalan Pre-Pyrenees). *Mountain Research and Development* **23**(4): 362–368. DOI: 10.1659/0276-4741(2003)023[0362:LUALCC]2.0.CO;2.
Quarmby NA, Milnes M, Hindle TL, Silleos N. 1993. The use of multi-temporal NDVI measurements from AVHRR data for crop yield estimation and prediction. *International Journal of Remote Sensing* **14**(2): 199–210. DOI: 10.1080/01431169308904332.
Quiring SM, Ganesh S. 2010. Evaluating the utility of the Vegetation Condition Index (VCI) for monitoring meteorological drought in Texas. *Agricultural and Forest Meteorology* **150**(3): 330–339. DOI: 10.1016/j.agrformet.2009.11.015.
Quiroga S, Iglesias A. 2009. A comparison of the climate risks of cereal, citrus, grapevine and olive production in Spain. *Agricultural Systems* **101**(1–2): 91–100. DOI: 10.1016/j.agsy.2009.03.006.
Rao CRN, Chen J. 1999. Revised post-launch calibration of the visible and near-infrared channels of the Advanced Very High Resolution Radiometer (AVHRR) on the NOAA-14 spacecraft. *International Journal of Remote Sensing* **20**(18): 3485–3491. DOI: 10.1080/014311699211147.
Reichstein M, Ciais P, Papale D, Valentini R, Running S, Viovy N, Cramer W, Granier A, Ogée J, Allard V, Aubinet M, Bernhofer C, Buchmann N, Carrara A, Grünwald T, Heimann M, Heinesch B, Knohl A, Kutsch W, Loustau D, Manca G, Matteucci G, Miglietta F, Ourcival JM, Pilegaard K, Pumpanen J, Rambal S, Schaphoff S, Seufert G, Soussana J-F, Sanz M-J, Vesala T, Zhao M. 2007. Reduction of ecosystem productivity and respiration during the European summer 2003 climate anomaly: A joint flux tower, remote sensing and modelling analysis. *Global Change Biology* **13**(3): 634–651. DOI: 10.1111/j.1365-2486.2006.01224.x.
Restaino CM, Peterson DL, Littell J. 2016. Increased water deficit decreases Douglas fir growth throughout western US forests. *Proceedings of the National Academy of Sciences of the United States of America* **113**(34): 9557–9562. DOI: 10.1073/pnas.1602384113.
Rhee J, Im J, Carbone GJ. 2010. Monitoring agricultural drought for arid and humid regions using multi-sensor remote sensing data. *Remote Sensing of Environment* **114**(12): 2875–2887. DOI:

10.1016/j.rse.2010.07.005.
Riaño D, Chuvieco E, Salas J, Aguado I. 2003. Assessment of different topographic corrections in landsat-TM data for mapping vegetation types (2003). *IEEE Transactions on Geoscience and Remote Sensing* **41**(5 PART 1): 1056–1061. DOI: 10.1109/TGRS.2003.811693.
Richardson AD, Carbone MS, Keenan TF, Czimczik CI, Hollinger DY, Murakami P, Schaberg PG, Xu X. 2013. Seasonal dynamics and age of stemwood nonstructural carbohydrates in temperate forest trees. *New Phytologist* **197**(3): 850–861. DOI: 10.1111/nph.12042.
Richman MB. 1986. Rotation of principal components. *Journal of Climatology* **6**(3): 293–335. DOI: 10.1002/joc.3370060305.
Rozas V, Camarero JJ, Sangüesa-Barreda G, Souto M, García-González I. 2015. Summer drought and ENSO-related cloudiness distinctly drive Fagus sylvatica growth near the species rear-edge in northern Spain. *Agricultural and Forest Meteorology* **201**: 153–164. DOI: 10.1016/j.agrformet.2014.11.012.
Russi L, Cocks PS, Roberts EH. 1992. Seed bank dynamics in a Mediterranean grassland. *Journal of Applied Ecology* **29**(3): 763–771. DOI: 10.2307/2404486.
Sanchez-Garcia M, Álvaro F, Martín-Sánchez JA, Sillero JC, Escribano J, Royo C. 2012. Breeding effects on the genotype×environment interaction for yield of bread wheat grown in Spain during the 20th century. *Field Crops Research* **126**: 79–86. DOI: 10.1016/j.fcr.2011.10.001.
Sánchez-Salguero R, Camarero JJ, Carrer M, Gutiérrez E, Alla AQ, Andreu-Hayles L, Hevia A, Koutavas A, Martínez-Sancho E, Nola P, Papadopoulos A, Pasho E, Toromani E, Carreira JA, Linares JC. 2017. Climate extremes and predicted warming threaten Mediterranean Holocene firs forests refugia. *Proceedings of the National Academy of Sciences of the United States of America* **114**(47): E10142–E10150. DOI: 10.1073/pnas.1708109114.
Sánchez-Salguero R, Camarero JJ, Dobbertin M, Fernández-Cancio T, Vilà-Cabrera A, Manzanedo RD, Zavala MA, Navarro-Cerrillo RM. 2013. Contrasting vulnerability and resilience to drought-induced decline of densely planted vs. natural rear-edge Pinus nigra forests. *Forest Ecology and Management* **310**: 956–967. DOI: 10.1016/j.foreco.2013.09.050.
Sanjuán Y, Arnáez J, Beguería S, Lana-Renault N, Lasanta T, Gómez-Villar A, Álvarez-Martínez J, Coba-Pérez P, García-Ruiz JM. 2018. Woody plant encroachment following grazing abandonment in the subalpine belt: a case study in northern Spain. *Regional Environmental Change* **18**(4): 1103–1115. DOI: 10.1007/s10113-017-1245-y.
Scaini A, Sánchez N, Vicente-Serrano SM, Martínez-Fernández J. 2015. SMOS-derived soil moisture anomalies and drought indices: A comparative analysis using in situ measurements. *Hydrological Processes* **29**(3). DOI: 10.1002/hyp.10150.
Schultz PA, Halpert MS. 1995. Global analysis of the relationships among a vegetation index, precipitation and land surface temperature. *International Journal of Remote Sensing* **16**(15): 2755–2777. DOI: 10.1080/01431169508954590.
Serra P, Pons X, Saurí D. 2008. Land-cover and land-use change in a Mediterranean landscape: A spatial analysis of driving forces integrating biophysical and human factors. *Applied Geography* **28**(3): 189–209. DOI: 10.1016/j.apgeog.2008.02.001.
Serra P, Vera A, Tulla AF, Salvati L. 2014. Beyond urban-rural dichotomy: Exploring socioeconomic and land-use processes of change in Spain (1991-2011). *Applied Geography* **55**: 71–81. DOI: 10.1016/j.apgeog.2014.09.005.
Skomarkova MV, Vaganov EA, Mund M, Knohl A, Linke P, Boerner A, Schulze E-D. 2006. Inter-annual and seasonal variability of radial growth, wood density and carbon isotope ratios in tree rings of beech (Fagus sylvatica) growing in Germany and Italy. *Trees - Structure and Function* **20**(5): 571–586. DOI: 10.1007/s00468-006-0072-4.
Slayback DA, Pinzon JE, Los SO, Tucker CJ. 2003. Northern hemisphere photosynthetic trends 1982-99. *Global Change Biology* **9**(1): 1–15. DOI: 10.1046/j.1365-2486.2003.00507.x.
Sona NT, Chen CF, Chen CR, Chang LY, Minh VQ. 2012. Monitoring agricultural drought in the lower mekong basin using MODIS NDVI and land surface temperature data. *International Journal of Applied Earth Observation and Geoinformation* **18**(1): 417–427. DOI: 10.1016/j.jag.2012.03.014.
Song Y, Ma M, Veroustraete F. 2010. Comparison and conversion of AVHRR GIMMS3g and SPOT VEGETATION NDVI data in China. *International Journal of Remote Sensing* **31**(10): 2377–2392. DOI: 10.1080/01431160903002409.
Stagge JH, Kohn I, Tallaksen LM, Stahl K. 2015. Modeling drought impact occurrence based on meteorological drought indices in Europe. *Journal of Hydrology* **530**: 37–50. DOI: 10.1016/j.jhydrol.2015.09.039.
Stellmes M, Röder A, Udelhoven T, Hill J. 2013. Mapping syndromes of land change in Spain with

remote sensing time series, demographic and climatic data. *Land Use Policy* **30**(1): 685–702. DOI: 10.1016/j.landusepol.2012.05.007.

Stellmes M, Udelhoven T, Röder A, Sonnenschein R, Hill J. 2010. Dryland observation at local and regional scale - Comparison of Landsat TM/ETM+ and NOAA AVHRR time series. *Remote Sensing of Environment* **114**(10): 2111–2125. DOI: 10.1016/j.rse.2010.04.016.

Stoy PC, Richardson AD, Baldocchi DD, Katul GG, Stanovick J, Mahecha MD, Reichstein M, Detto M, Law BE, Wohlfahrt G, Arriga N, Campos J, McCaughey JH, Montagnani L, Paw U KT, Sevanto S, Williams M. 2009. Biosphere-atmosphere exchange of CO<inf>2</inf>in relation to climate: A cross-biome analysis across multiple time scales. *Biogeosciences* **6**(10): 2297–2312. DOI: 10.5194/bg-6-2297-2009.

Tarnavsky E, Garrigues S, Brown ME. 2008. Multiscale geostatistical analysis of AVHRR, SPOT-VGT, and MODIS global NDVI products. *Remote Sensing of Environment* **112**(2): 535–549. DOI: 10.1016/j.rse.2007.05.008.

Terres J-M, Scacchiafichi LN, Wania A, Ambar M, Anguiano E, Buckwell A, Coppola A, Gocht A, Källström HN, Pointereau P, Strijker D, Visek L, Vranken L, Zobena A. 2015. Farmland abandonment in Europe: Identification of drivers and indicators, and development of a composite indicator of risk. *Land Use Policy* **49**: 20–34. DOI: 10.1016/j.landusepol.2015.06.009.

Tognetti R, Cherubini P, Marchi S, Raschi A. 2007. Leaf traits and tree rings suggest different water-use and carbon assimilation strategies by two co-occurring Quercus species in a Mediterranean mixed-forest stand in Tuscany, Italy. *Tree Physiology* **27**(12): 1741–1751. DOI: 10.1093/treephys/27.12.1741.

Trishchenko AP. 2009. Effects of spectral response function on surface reflectance and NDVI measured with moderate resolution satellite sensors: Extension to AVHRR NOAA-17, 18 and METOP-A. *Remote Sensing of Environment* **113**(2): 335–341. DOI: 10.1016/j.rse.2008.10.002.

Trishchenko AP, Cihlar J, Li Z. 2002. Effects of spectral response function on surface reflectance and NDVI measured with moderate resolution satellite sensors. *Remote Sensing of Environment* **81**(1): 1–18. DOI: 10.1016/S0034-4257(01)00328-5.

Tucker CJ. 1979. Red and photographic infrared linear combinations for monitoring vegetation. *Remote Sensing of Environment* **8**(2): 127–150. DOI: 10.1016/0034-4257(79)90013-0.

Tucker CJ, Pinzon JE, Brown ME, Slayback DA, Pak EW, Mahoney R, Vermote EF, El Saleous N. 2005. An extended AVHRR 8-km NDVI dataset compatible with MODIS and SPOT vegetation NDVI data. *International Journal of Remote Sensing* **26**(20): 4485–4498. DOI: 10.1080/01431160500168686.

Tucker CJ, Vanpraet C, Boerwinkel E, Gaston A. 1983. Satellite remote sensing of total dry matter production in the Senegalese Sahel. *Remote Sensing of Environment* **13**(6): 461–474. DOI: 10.1016/0034-4257(83)90053-6.

Udelhoven T, Stellmes M, del Barrio G, Hill J. 2009. Assessment of rainfall and NDVI anomalies in Spain (1989-1999) using distributed lag models. *International Journal of Remote Sensing* **30**(8): 1961–1976. DOI: 10.1080/01431160802546829.

Vaganov EA, Hughes MK, Kirdyanov AV, Schweingruber FH, Silkin PP. 1999. Influence of snowfall and melt timing on tree growth in subarctic Eurasia. *Nature* **400**(6740): 149–151. DOI: 10.1038/22087.

Van Leeuwen WJD, Casady GM, Neary DG, Bautista S, Alloza JA, Carmel Y, Wittenberg L, Malkinson D, Orr BJ. 2010. Monitoring post-wildfire vegetation response with remotely sensed time-series data in Spain, USA and Israel. *International Journal of Wildland Fire* **19**(1): 75–93. DOI: 10.1071/WF08078.

Vayreda J, Martinez-Vilalta J, Gracia M, Canadell JG, Retana J. 2016. Anthropogenic-driven rapid shifts in tree distribution lead to increased dominance of broadleaf species. *Global Change Biology* **22**(12): 3984–3995. DOI: 10.1111/gcb.13394.

Verbesselt J, Hyndman R, Newnham G, Culvenor D. 2010. Detecting trend and seasonal changes in satellite image time series. *Remote Sensing of Environment* **114**(1): 106–115. DOI: 10.1016/j.rse.2009.08.014.

Vermote EF, El Saleous NZ, Justice CO. 2002. Atmospheric correction of MODIS data in the visible to middle infrared: First results. *Remote Sensing of Environment* **83**(1–2): 97–111. DOI: 10.1016/S0034-4257(02)00089-5.

Vermote EF, Tanré D, Deuzé JL, Herman M, Morcrette J-J. 1997. Second simulation of the satellite signal in the solar spectrum, 6s: an overview. *IEEE Transactions on Geoscience and Remote Sensing* **35**(3): 675–686. DOI: 10.1109/36.581987.

Vicente-Serrano SM. 2006. Spatial and temporal analysis of droughts in the Iberian Peninsula (1910-2000). *Hydrological Sciences Journal* **51**(1). DOI: 10.1623/hysj.51.1.83.

Vicente-Serrano SM. 2007. Evaluating the impact of drought using remote sensing in a Mediterranean, Semi-arid Region. *Natural Hazards* **40**(1). DOI: 10.1007/s11069-006-0009-7.

Vicente-Serrano SM, Azorin-Molina C, Sanchez-Lorenzo A, Morán-Tejeda E, Lorenzo-Lacruz J, Revuelto J, López-Moreno JI, Espejo F. 2014a. Temporal evolution of surface humidity in Spain: Recent trends and possible physical mechanisms. *Climate Dynamics* **42**(9–10). DOI: 10.1007/s00382-013-1885-7.

Vicente-Serrano SM, Azorin-Molina C, Sanchez-Lorenzo A, Revuelto J, López-Moreno JI, González-Hidalgo JC, Moran-Tejeda E, Espejo F. 2014b. Reference evapotranspiration variability and trends in Spain, 1961-2011. *Global and Planetary Change* **121**. DOI: 10.1016/j.gloplacha.2014.06.005.

Vicente-Serrano SM, Azorin-Molina C, Sanchez-Lorenzo A, Revuelto J, Morán-Tejeda E, Lõpez-Moreno JI, Espejo F. 2014c. Sensitivity of reference evapotranspiration to changes in meteorological parameters in Spain (1961-2011). *Water Resources Research* **50**(11). DOI: 10.1002/2014WR015427.

Vicente-Serrano SM, Beguería S. 2016. Comment on "Candidate distributions for climatological drought indices (SPI and SPEI)" by James H. Stagge et al. *International Journal of Climatology* **36**(4). DOI: 10.1002/joc.4474.

Vicente-Serrano SM, Beguería S, Lasanta T. 2006a. Spatial diversity of vegetal activity in abandoned fields of the central Spanish Pyrenees: Analysis of the processes of succession by means of Landsat imagery (1984-2001). *Pirineos* (161).

Vicente-Serrano SM, Beguería S, López-Moreno JI. 2010. A multiscalar drought index sensitive to global warming: The standardized precipitation evapotranspiration index. *Journal of Climate* **23**(7). DOI: 10.1175/2009JCLI2909.1.

Vicente-Serrano SM, Beguería S, López-Moreno JI. 2011. Comment on Characteristics and trends in various forms of the Palmer Drought Severity Index (PDSI) during 1900-2008 by Aiguo Dai. *Journal of Geophysical Research Atmospheres* **116**(19).

Vicente-Serrano SM, Beguería S, Lorenzo-Lacruz J, Camarero JJ, López-Moreno JI, Azorin-Molina C, Revuelto J, Morán-Tejeda E, Sanchez-Lorenzo A. 2012a. Performance of drought indices for ecological, agricultural, and hydrological applications. *Earth Interactions* **16**(10). DOI: 10.1175/2012EI000434.1.

Vicente-Serrano SM, Cabello D, Tomás-Burguera M, Martín-Hernández N, Beguería S, Azorin-Molina C, Kenawy AE. 2015a. Drought variability and land degradation in semiarid regions: Assessment using remote sensing data and drought indices (1982-2011). *Remote Sensing* **7**(4). DOI: 10.3390/rs70404391.

Vicente-Serrano SM, Camarero JJ, Azorin-Molina C. 2014d. Diverse responses of forest growth to drought time-scales in the Northern Hemisphere. *Global Ecology and Biogeography* **23**(9). DOI: 10.1111/geb.12183.

Vicente-Serrano SM, Camarero JJ, Olano JM, Martín-Hernández N, Peña-Gallardo M, Tomás-Burguera M, Gazol A, Azorin-Molina C, Bhuyan U, El Kenawy A. 2016. Diverse relationships between forest growth and the Normalized Difference Vegetation Index at a global scale. *Remote Sensing of Environment* **187**. DOI: 10.1016/j.rse.2016.10.001.

Vicente-Serrano SM, Camarero JJ, Zabalza J, Sangüesa-Barreda G, López-Moreno JI, Tague CL. 2015b. Evapotranspiration deficit controls net primary production and growth of silver fir: Implications for Circum-Mediterranean forests under forecasted warmer and drier conditions. *Agricultural and Forest Meteorology* **206**. DOI: 10.1016/j.agrformet.2015.02.017.

Vicente-Serrano SM, Cuadrat-Prats JM, Romo A. 2006b. Aridity influence on vegetation patterns in the middle Ebro Valley (Spain): Evaluation by means of AVHRR images and climate interpolation techniques. *Journal of Arid Environments* **66**(2). DOI: 10.1016/j.jaridenv.2005.10.021.

Vicente-Serrano SM, Gouveia C, Camarero JJ, Beguería S, Trigo R, López-Moreno JI, Azorín-Molina C, Pasho E, Lorenzo-Lacruz J, Revuelto J, Morán-Tejeda E, Sanchez-Lorenzo A. 2013. Response of vegetation to drought time-scales across global land biomes. *Proceedings of the National Academy of Sciences of the United States of America* **110**(1). DOI: 10.1073/pnas.1207068110.

Vicente-Serrano SM, Heredia-Laclaustra A. 2004. NAO influence on NDVI trends in the Iberian peninsula (1982-2000). *International Journal of Remote Sensing* **25**(14). DOI: 10.1080/01431160410001685009.

Vicente-Serrano SM, Lasanta T, Romo A. 2004. Analysis of spatial and temporal evolution of vegetation cover in the Spanish central pyrenees: Role of human management. *Environmental Management* **34**(6). DOI: 10.1007/s00267-003-0022-5.

Vicente-Serrano SM, Lopez-Moreno J-I, Beguería S, Lorenzo-Lacruz J, Sanchez-Lorenzo A, García-Ruiz JM, Azorin-Molina C, Morán-Tejeda E, Revuelto J, Trigo R, Coelho F, Espejo F. 2014e.

Evidence of increasing drought severity caused by temperature rise in southern Europe. *Environmental Research Letters* **9**(4). DOI: 10.1088/1748-9326/9/4/044001.

Vicente-Serrano SM, Rodríguez-Camino E, Domínguez-Castro F, El Kenawy A, Azorín-Molina C. 2017a. An updated review on recent trends in observational surface atmospheric variables and their extremes over Spain. *Cuadernos de Investigacion Geografica* **43**(1). DOI: 10.18172/cig.3134.

Vicente-Serrano SM, Tomas-Burguera M, Beguería S, Reig F, Latorre B, Peña-Gallardo M, Luna MY, Morata A, González-Hidalgo JC. 2017b. A High Resolution Dataset of Drought Indices for Spain. *Data* **2**(3).

Vicente-Serrano SM, Zouber A, Lasanta T, Pueyo Y. 2012b. Dryness is accelerating degradation of vulnerable shrublands in semiarid mediterranean environments. *Ecological Monographs* **82**(4). DOI: 10.1890/11-2164.1.

Viedma O, Moity N, Moreno JM. 2015. Changes in landscape fire-hazard during the second half of the 20th century: Agriculture abandonment and the changing role of driving factors. *Agriculture, Ecosystems and Environment* **207**: 126–140. DOI: 10.1016/j.agee.2015.04.011.

Wan Z, Wang P, Li X. 2004. Using MODIS Land Surface Temperature and Normalized Difference Vegetation Index products for monitoring drought in the southern Great Plains, USA. *International Journal of Remote Sensing* **25**(1): 61–72. DOI: 10.1080/0143116031000115328.

Wang J, Rich PM, Price KP. 2003. Temporal responses of NDVI to precipitation and temperature in the central Great Plains, USA. *International Journal of Remote Sensing* **24**(11): 2345–2364. DOI: 10.1080/01431160210154812.

Wylie BK, Meyer DJ, Tieszen LL, Mannel S. 2002. Satellite mapping of surface biophysical parameters at the biome scale over the North American grasslands a case study. *Remote Sensing of Environment* **79**(2–3): 266–278. DOI: 10.1016/S0034-4257(01)00278-4.

Yang S, Meng D, Li X, Wu X. 2018. Multi-scale responses of vegetation changes relative to the SPEI meteorological drought index in North China in 2001-2014. *Shengtai Xuebao/ Acta Ecologica Sinica* **38**(3): 1028–1039. DOI: 10.5846/stxb201611242398.

Yin H, Udelhoven T, Fensholt R, Pflugmacher D, Hostert P. 2012. How normalized difference vegetation index (NDVI) trends from advanced very high resolution radiometer (AVHRR) and système probatoire d'observation de la terre vegetation (SPOT VGT) time series differ in agricultural areas: An inner mongolian case study. *Remote Sensing* **4**(11): 3364–3389. DOI: 10.5829/idosi.mejsr.2012.12.3.64113.

Zavala MA, Espelta JM, Retana J. 2000. Constraints and trade-offs in Mediterranean plant communities: The case of holm oak-Aleppo pine forests. *Botanical Review* **66**(1): 119–149. DOI: 10.1007/BF02857785.

Zhang Q, Kong D, Singh VP, Shi P. 2017. Response of vegetation to different time-scales drought across China: Spatiotemporal patterns, causes and implications. *Global and Planetary Change* **152**: 1–11. DOI: 10.1016/j.gloplacha.2017.02.008.

Zhao M, Geruo A, Velicogna I, Kimball JS. 2017. Satellite observations of regional drought severity in the continental United States using GRACE-based terrestrial water storage changes. *Journal of Climate* **30**(16): 6297–6308. DOI: 10.1175/JCLI-D-16-0458.1.

Zhao M, Running SW. 2010. Drought-induced reduction in global terrestrial net primary production from 2000 through 2009. *Science* **329**(5994): 940–943. DOI: 10.1126/science.1192666.

Zhao X, Wei H, Liang S, Zhou T, He B, Tang B, Wu D. 2015. Responses of natural vegetation to different stages of extreme drought during 2009-2010 in Southwestern China. *Remote Sensing* **7**(10): 14039–14054. DOI: 10.3390/rs71014039.

Zhou L, Tucker CJ, Kaufmann RK, Slayback D, Shabanov NV, Myneni RB. 2001. Variations in northern vegetation activity inferred from satellite data of vegetation index during 1981 to 1999. *Journal of Geophysical Research Atmospheres* **106**(D17): 20069–20083. DOI: 10.1029/2000JD000115.

Zweifel R, Eugster W, Etzold S, Dobbertin M, Buchmann N, Häsler R. 2010. Link between continuous stem radius changes and net ecosystem productivity of a subalpine Norway spruce forest in the Swiss Alps. *New Phytologist* **187**(3): 819–830. DOI: 10.1111/j.1469-8137.2010.03301.x.

SUPPLEMENTARY MATERIAL

List of supplementary figures

List of supplementary tables

Supplementary Figures and tables

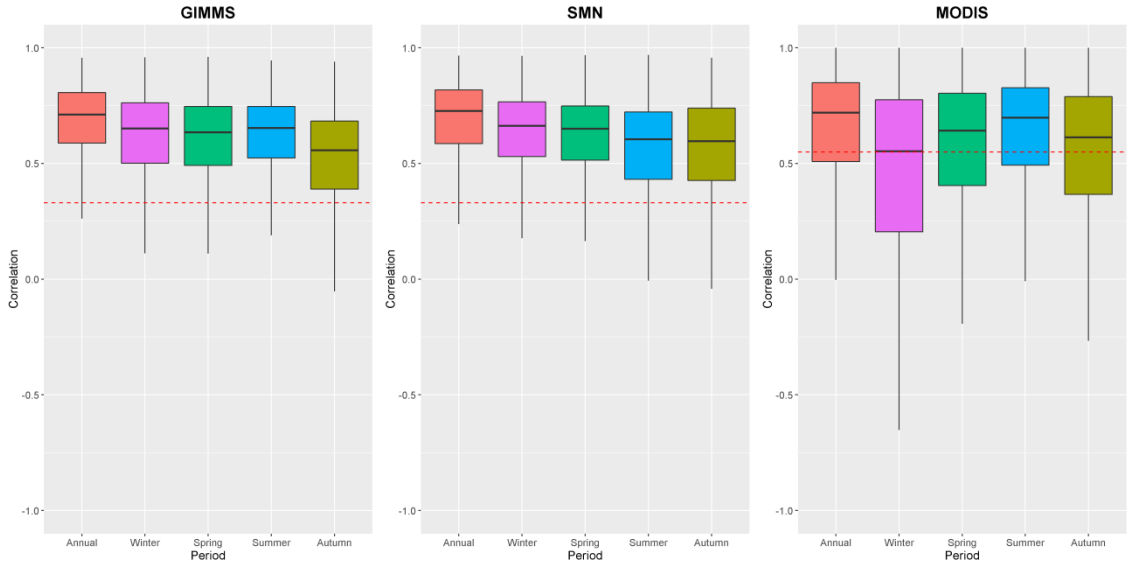

Supplementary Figure 1. Box plots showing the annual and seasonal Pearson's correlation between the Sp_1km_NDVI and the other NDVI datasets. Dashed red line indicate the significant values ($p < 0.5$).

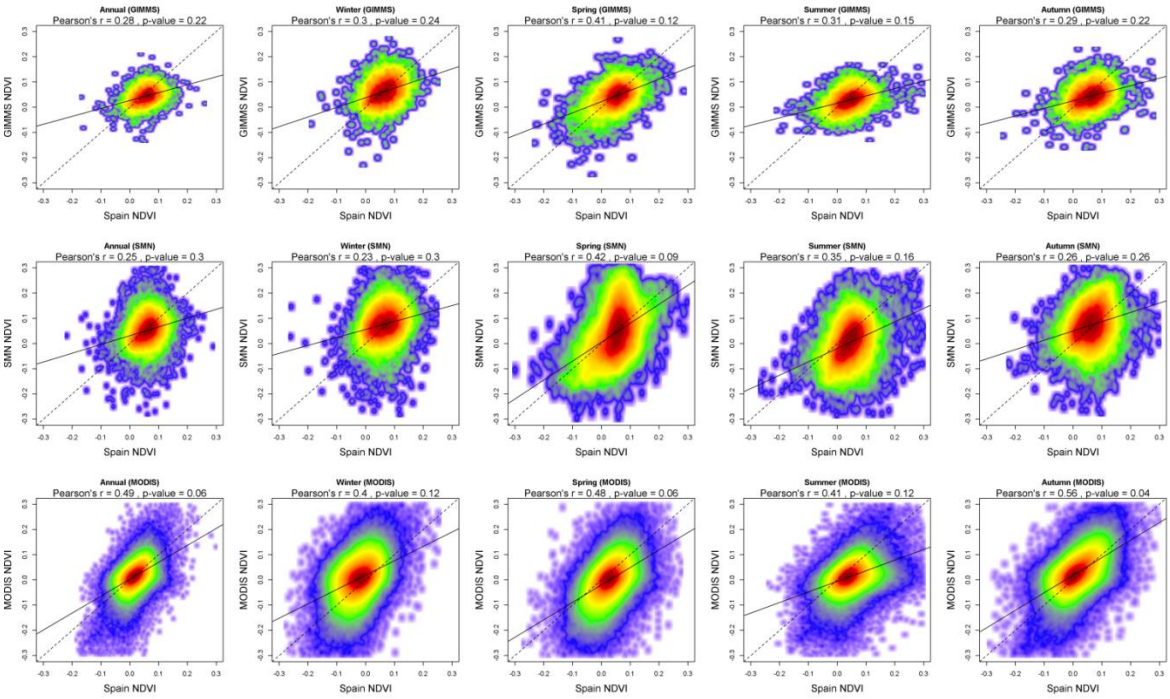

Supplementary Figure 2. Spatial relationship between the seasonal and annual NDVI magnitude of change between the Sp_1km_NDVI and the rest of datasets. Given the high number of points the signification of correlation was obtained by means of 1000 random samples of 30 cases from which correlations and p-values were obtained. The final signification was assessed by means of the average of the obtained p-values.

	Sp_1km_NDVI vs. GIMMS				Sp_1km_NDVI vs. SMN				Sp_1km_NDVI vs. MODIS			
Annual	Neg. (<0.05)	Neg. (no sign.)	Pos. (no sign.)	Pos. (<0.05)	Neg. (<0.05)	Neg. (no sign.)	Pos. (no sign.)	Pos. (<0.05)	Neg. (<0.05)	Neg. (no sign.)	Pos. (no sign.)	Pos. (<0.05)
Neg. (<0.05)	0.12	0.17	0.29	0.25	0.07	0.00	0.16	3.39	0.25	0.74	0.48	0.04
Neg. (no sign.)	0.27	0.63	1.25	1.55	0.02	0.09	0.47	8.71	1.27	11.54	9.88	0.84
Pos. (no sign.)	0.64	1.67	4.09	8.26	0.02	0.27	1.31	27.20	0.99	14.28	40.47	5.56
Pos. (<0.05)	0.60	2.44	15.82	61.89	0.09	0.53	3.52	54.15	0.13	1.60	7.59	4.17
Winter	Neg. (<0.05)	Neg. (no sign.)	Pos. (no sign.)	Pos. (<0.05)	Neg. (<0.05)	Neg. (no sign.)	Pos. (no sign.)	Pos. (<0.05)	Neg. (<0.05)	Neg. (no sign.)	Pos. (no sign.)	Pos. (<0.05)
Neg. (<0.05)	0.07	0.10	0.17	0.08	0.08	0.13	0.16	0.09	0.49	5.39	3.96	0.32
Neg. (no sign.)	0.21	0.64	1.10	1.40	0.17	0.57	1.37	1.89	1.66	28.79	29.21	2.31
Pos. (no sign.)	0.29	2.04	6.71	10.92	0.54	1.34	5.83	14.93	0.28	6.25	17.31	2.61
Pos. (<0.05)	0.47	2.72	18.29	54.75	0.64	2.27	11.87	58.12	0.01	0.15	0.74	0.40
Spring	Neg. (<0.05)	Neg. (no sign.)	Pos. (no sign.)	Pos. (<0.05)	Neg. (<0.05)	Neg. (no sign.)	Pos. (no sign.)	Pos. (<0.05)	Neg. (<0.05)	Neg. (no sign.)	Pos. (no sign.)	Pos. (<0.05)
Neg. (<0.05)	1.01	0.99	0.71	0.39	1.81	0.70	0.29	0.28	0.01	0.17	0.18	0.02
Neg. (no sign.)	1.02	2.35	2.87	2.26	3.48	2.36	1.36	1.38	0.35	4.79	5.19	0.72
Pos. (no sign.)	0.86	3.16	10.07	11.08	5.37	6.90	5.44	7.43	1.26	16.75	17.97	2.49
Pos. (<0.05)	0.72	3.40	18.17	40.89	3.25	7.37	11.04	41.52	0.21	2.88	2.78	0.37
Summer	Neg. (<0.05)	Neg. (no sign.)	Pos. (no sign.)	Pos. (<0.05)	Neg. (<0.05)	Neg. (no sign.)	Pos. (no sign.)	Pos. (<0.05)	Neg. (<0.05)	Neg. (no sign.)	Pos. (no sign.)	Pos. (<0.05)
Neg. (<0.05)	0.40	0.80	0.65	0.18	1.03	0.49	0.24	0.17	0.11	0.19	0.07	0.00
Neg. (no sign.)	0.81	4.32	3.98	2.05	6.12	2.26	1.20	1.18	0.72	5.96	3.00	0.12
Pos. (no sign.)	0.97	6.58	11.84	9.16	10.13	7.23	5.35	6.14	1.30	21.68	40.44	2.24
Pos. (<0.05)	0.99	4.98	16.89	35.34	8.98	10.78	13.24	25.42	0.32	4.75	15.66	3.35
Autumn	Neg. (<0.05)	Neg. (no sign.)	Pos. (no sign.)	Pos. (<0.05)	Neg. (<0.05)	Neg. (no sign.)	Pos. (no sign.)	Pos. (<0.05)	Neg. (<0.05)	Neg. (no sign.)	Pos. (no sign.)	Pos. (<0.05)
Neg. (<0.05)	0.34	0.43	0.33	0.29	0.25	0.34	0.37	0.59	0.36	2.03	1.43	0.14
Neg. (no sign.)	0.61	1.38	1.87	2.31	0.33	0.71	1.44	2.87	1.14	14.22	17.92	1.98
os. (no sign.)	0.93	2.31	5.66	7.50	0.49	1.52	3.85	11.66	0.40	7.56	35.19	8.33
0.05)	0.94	4.94	20.97	49.14	1.81	5.10	13.53	55.11	0.03	0.67	4.82	3.62

Supplementary Table 1. Contingency tables showing the relationship between the sign and signification of the NDVI trends between the Sp_1km_NDVI and the other three NDVI datasets.

	Annual	Winter	Spring	Summer	Autumn
GIMMS	0.32	0.28	0.47	0.44	0.34
SMN	0.46	0.27	0.52	0.41	0.19
MODIS	0.43	0.31	0.37	0.37	0.45

Supplementary Table 2: Coefficients of contingency obtained between the spatial distribution of trend categories.

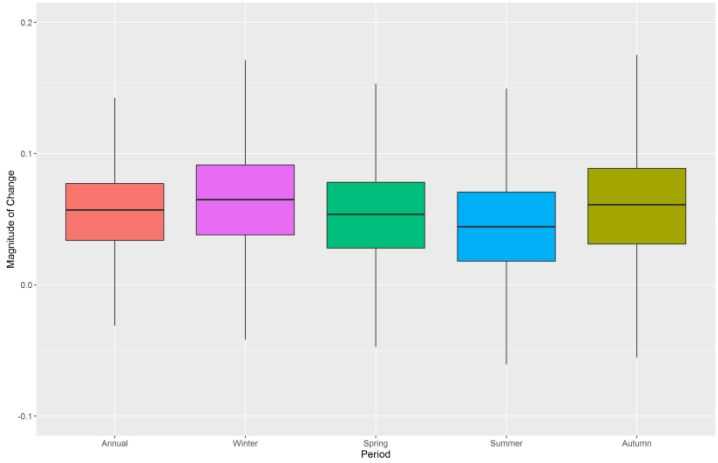

Supplementary Figure 3: Box-plot showing the annual and seasonal NDVI magnitude of change.

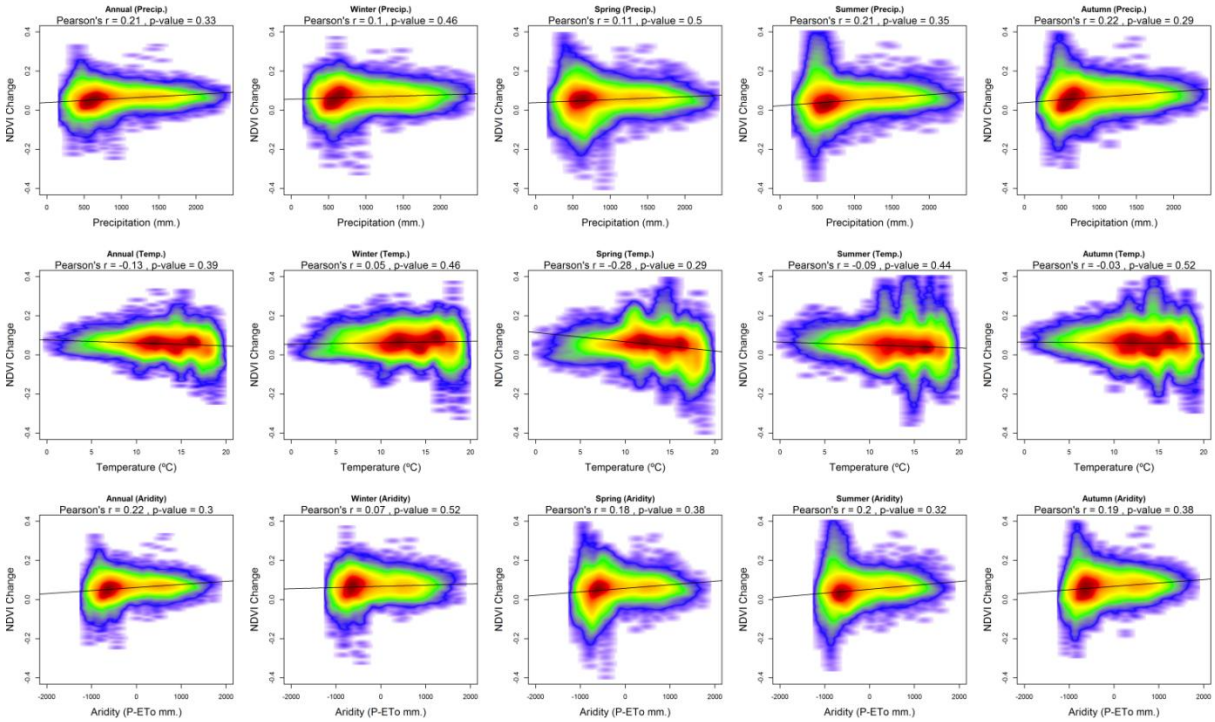

Supplementary Figure 4. Scatterplots showing the relationship between the NDVI magnitude of change and the average climate conditions (precipitation, temperature and aridity) at seasonal and annual scales.

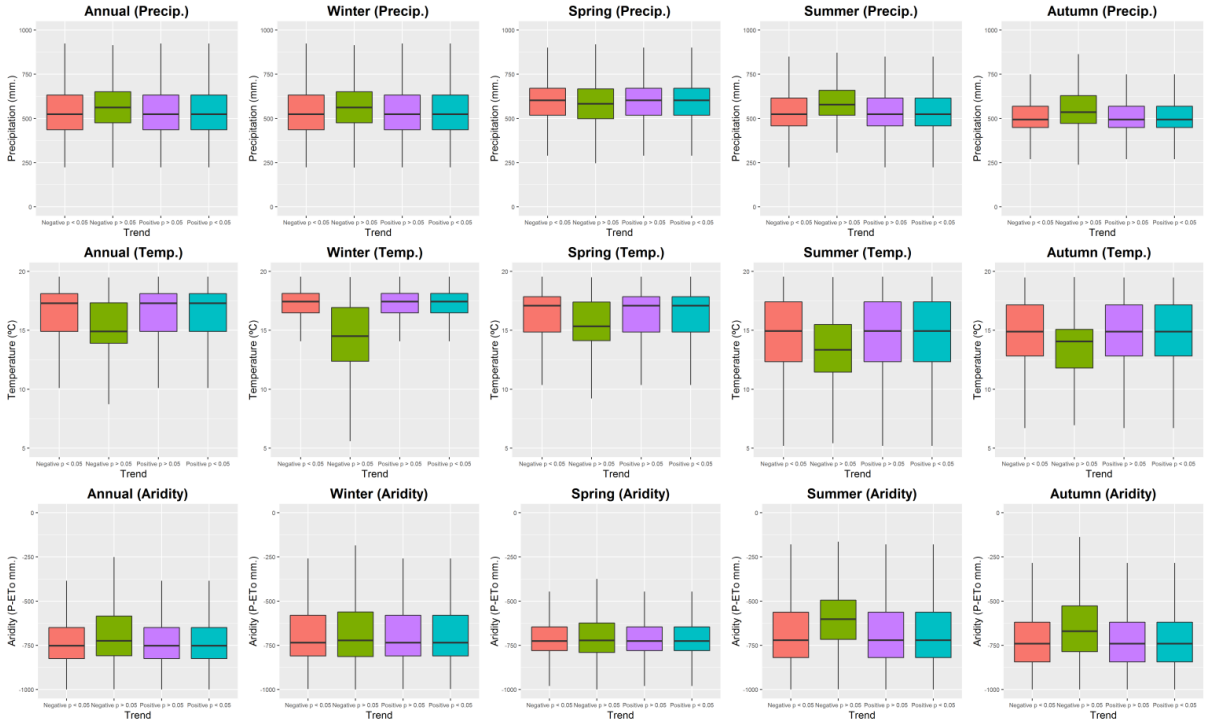

Supplementary Figure 5. Box plots showing the values for precipitation, temperature and aridity corresponding to the recorded seasonal and annual NDVI trends.

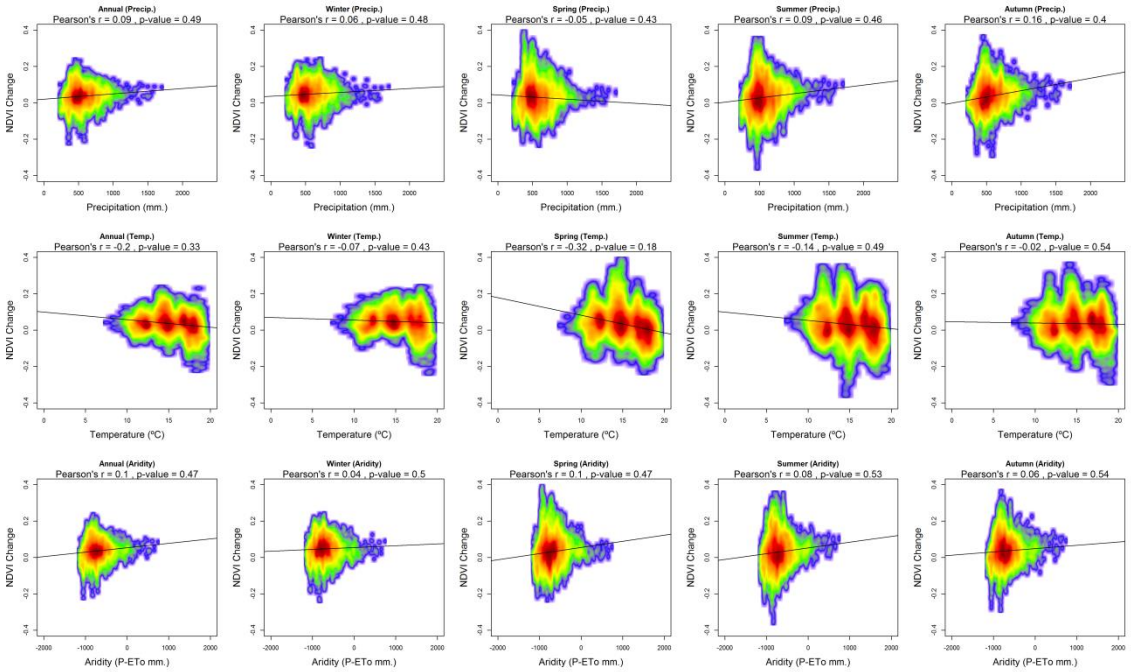

Supplementary Figure 6: Scatterplots showing the relationship between the NDVI magnitude of change and the average climate conditions (precipitation, temperature and aridity) at seasonal and annual scales. Irrigated Lands

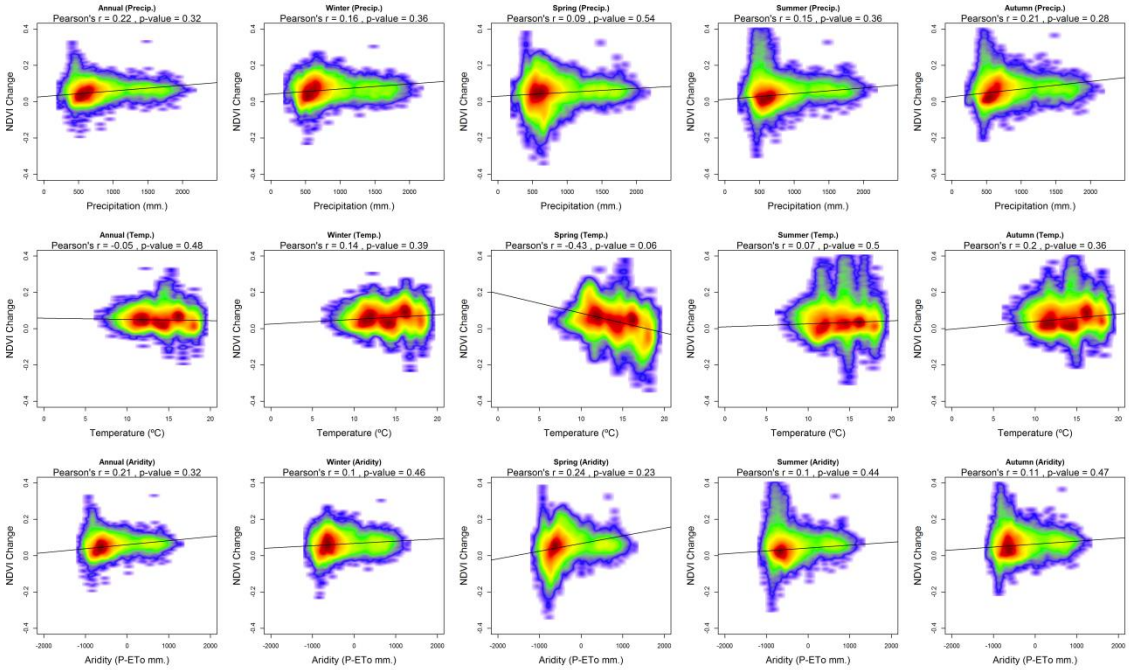

Supplementary Figure 7: Scatterplots showing the relationship between the NDVI magnitude of change and the average climate conditions (precipitation, temperature and aridity) at seasonal and annual scales. Arable dry lands

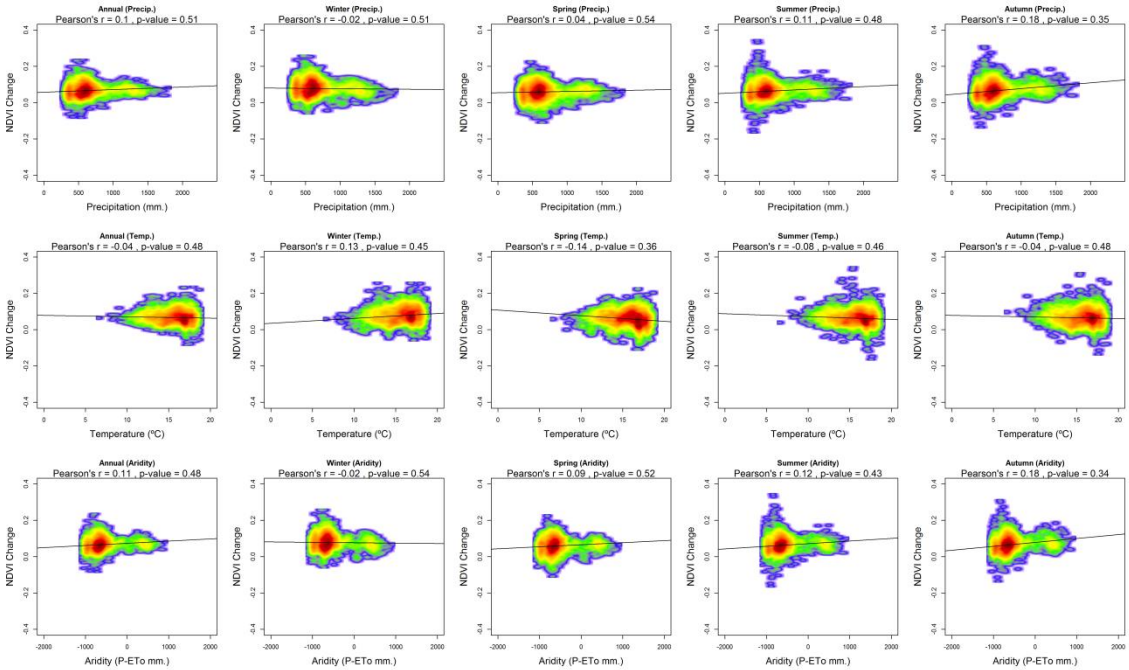

Supplementary Figure 8: Scatterplots showing the relationship between the NDVI magnitude of change and the average climate conditions (precipitation, temperature and aridity) at seasonal and annual scales. Fruit trees

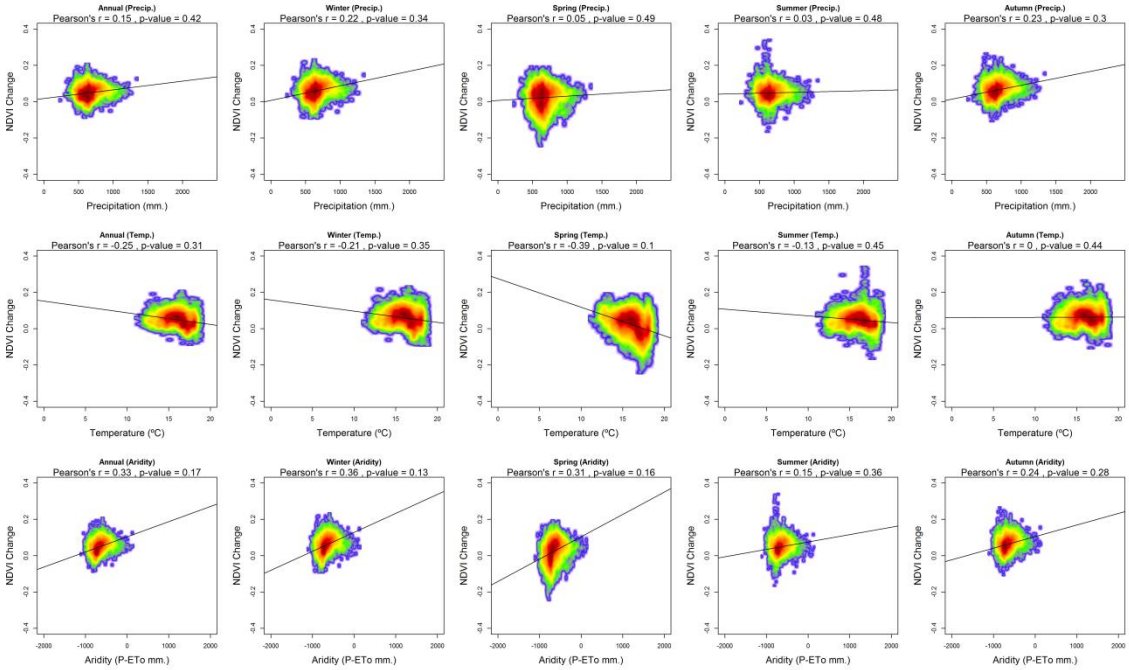

Supplementary Figure 9: Scatterplots showing the relationship between the NDVI magnitude of change and the average climate conditions (precipitation, temperature and aridity) at seasonal and annual scales. Olive groves

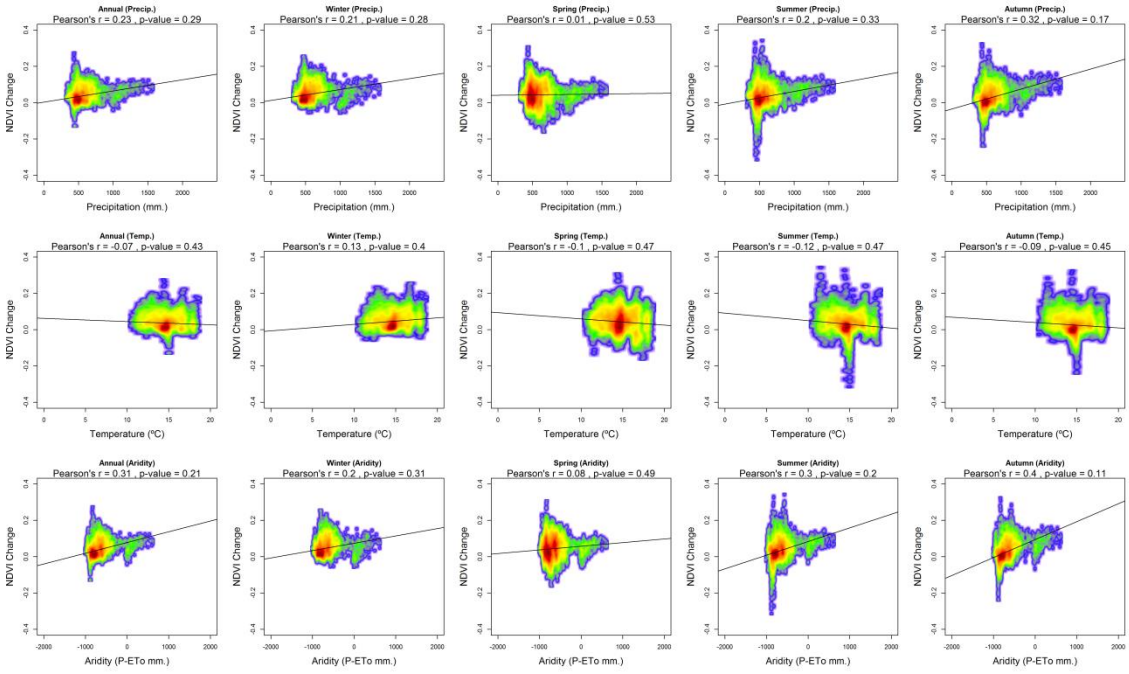

Supplementary Figure 10: Scatterplots showing the relationship between the NDVI magnitude of change and the average climate conditions (precipitation, temperature and aridity) at seasonal and annual scales. Vineyards

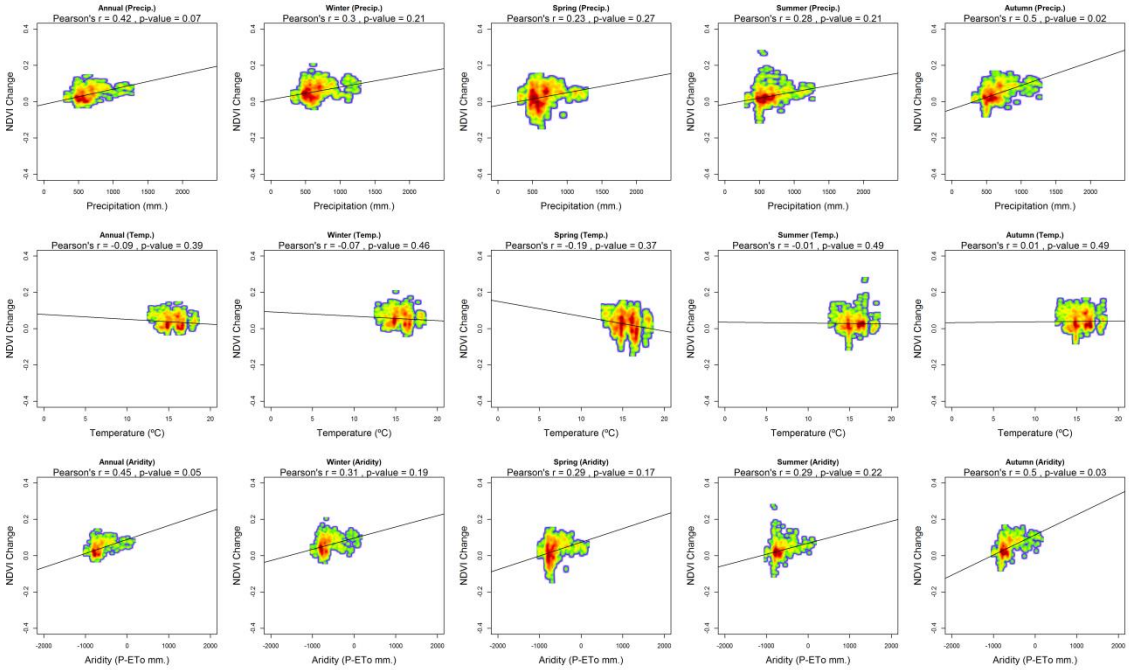

Supplementary Figure 11: Scatterplots showing the relationship between the NDVI magnitude of change and the average climate conditions (precipitation, temperature and aridity) at seasonal and annual scales. Vineyards-Olive groves

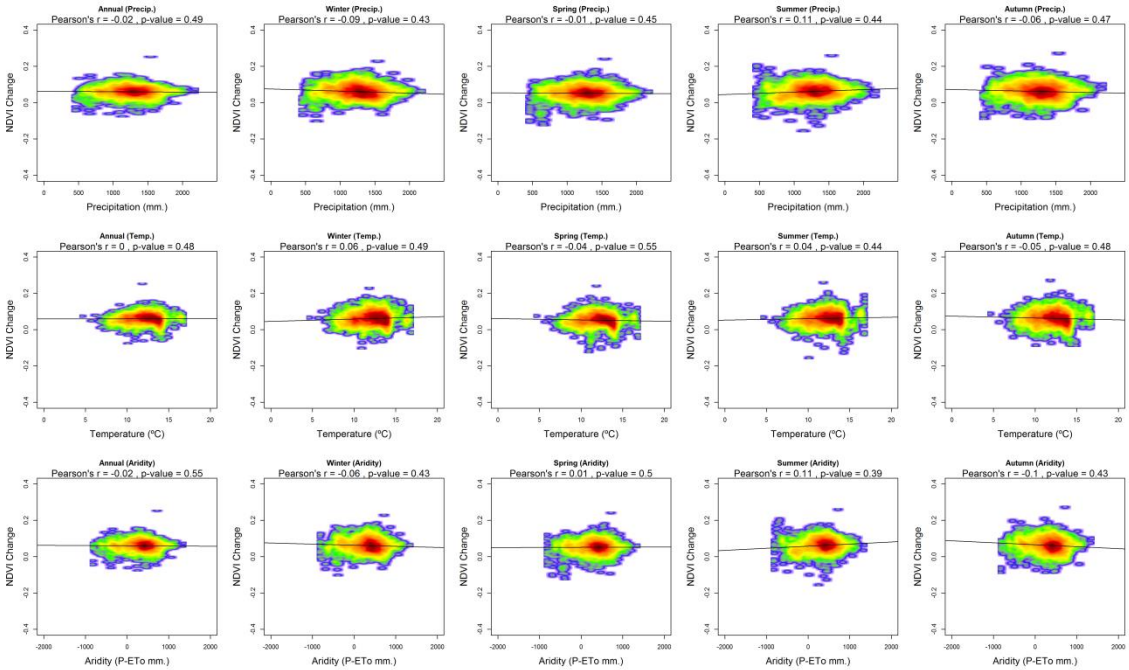

Supplementary Figure 12: Scatterplots showing the relationship between the NDVI magnitude of change and the average climate conditions (precipitation, temperature and aridity) at seasonal and annual scales. Grasslands

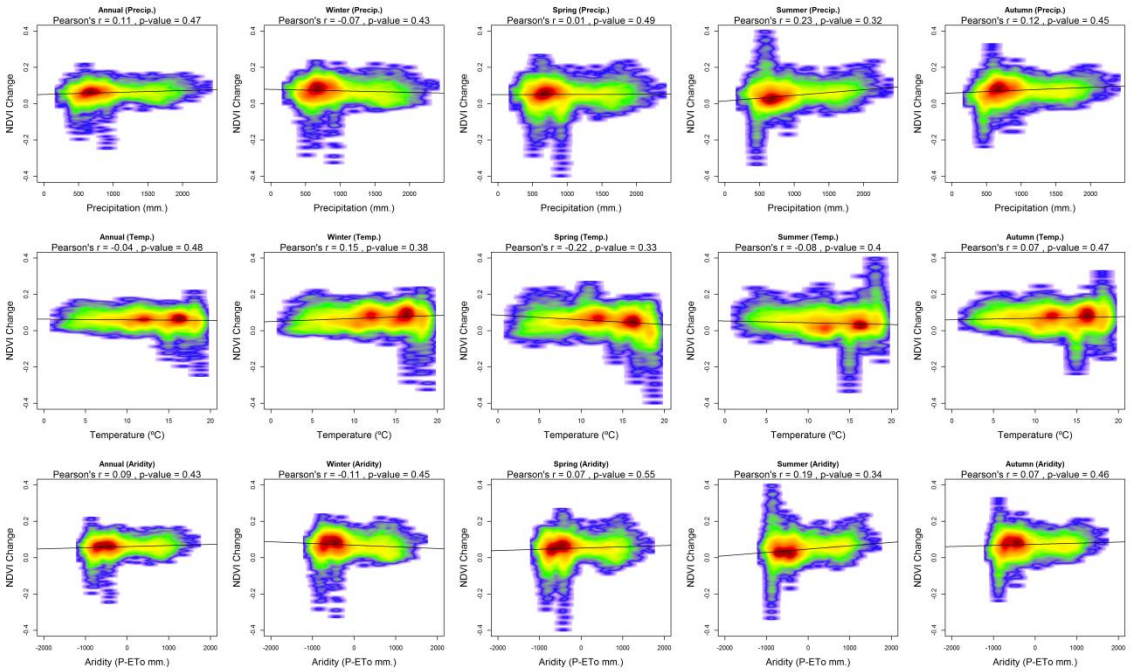

Supplementary Figure 13: Scatterplots showing the relationship between the NDVI magnitude of change and the average climate conditions (precipitation, temperature and aridity) at seasonal and annual scales. Pastures

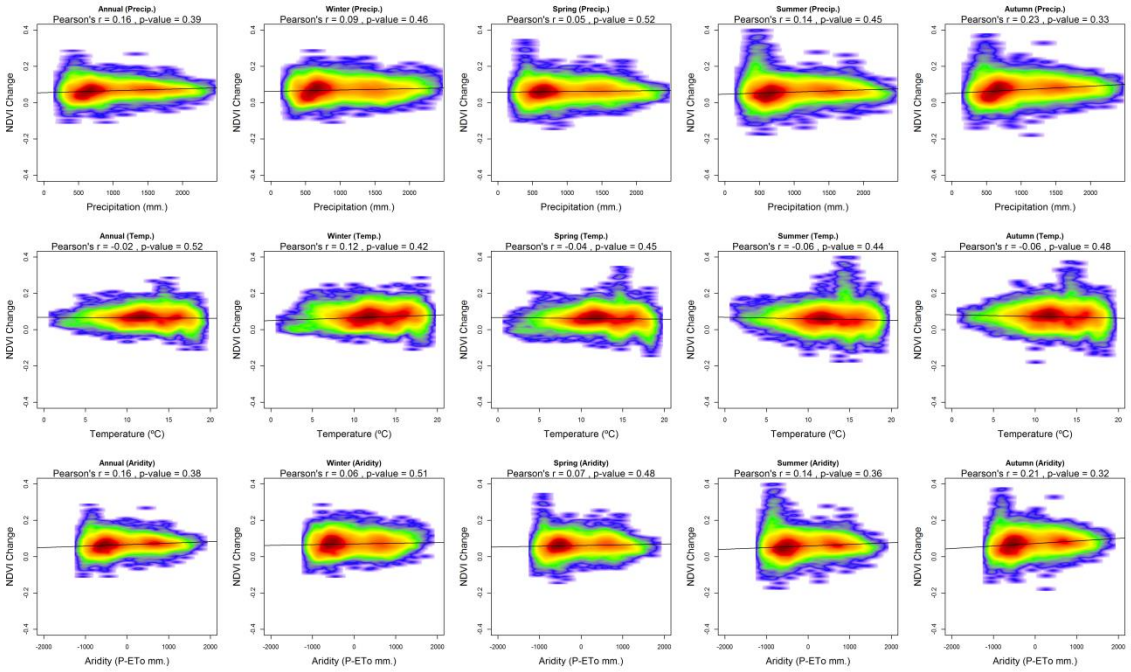

Supplementary Figure 14: Scatterplots showing the relationship between the NDVI magnitude of change and the average climate conditions (precipitation, temperature and aridity) at seasonal and annual scales. Shrubs

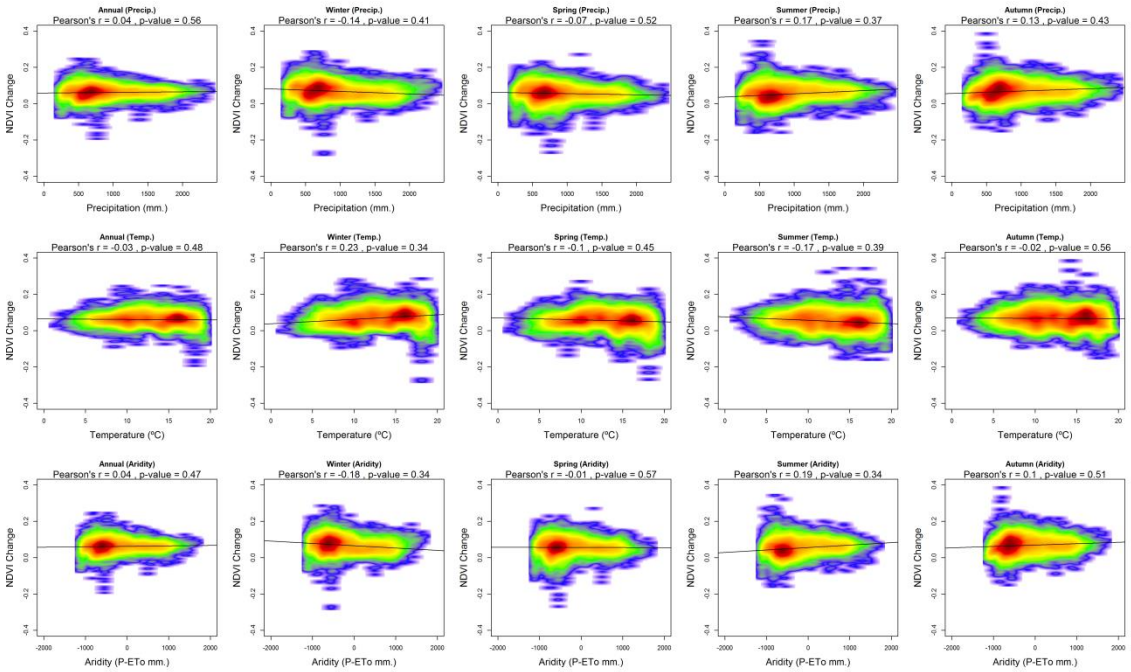

Supplementary Figure15: Scatterplots showing the relationship between the NDVI magnitude of change and the average climate conditions (precipitation, temperature and aridity) at seasonal and annual scales. Pastures-Shrubs

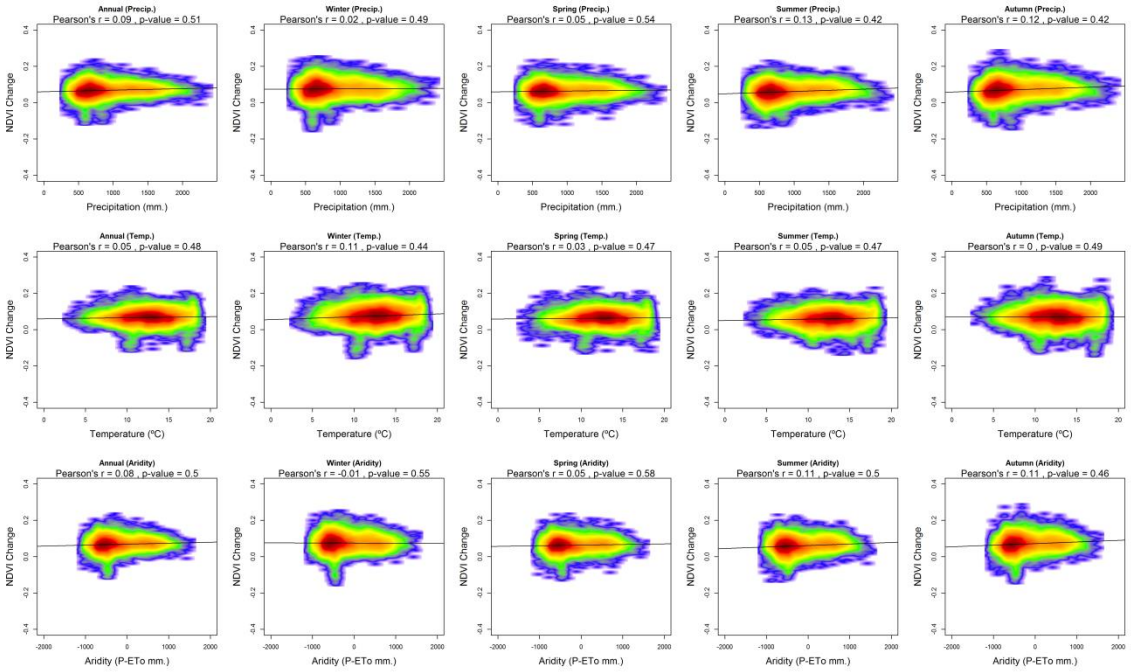

Supplementary Figure 16: Scatterplots showing the relationship between the NDVI magnitude of change and the average climate conditions (precipitation, temperature and aridity) at seasonal and annual scales. Coniferous forests

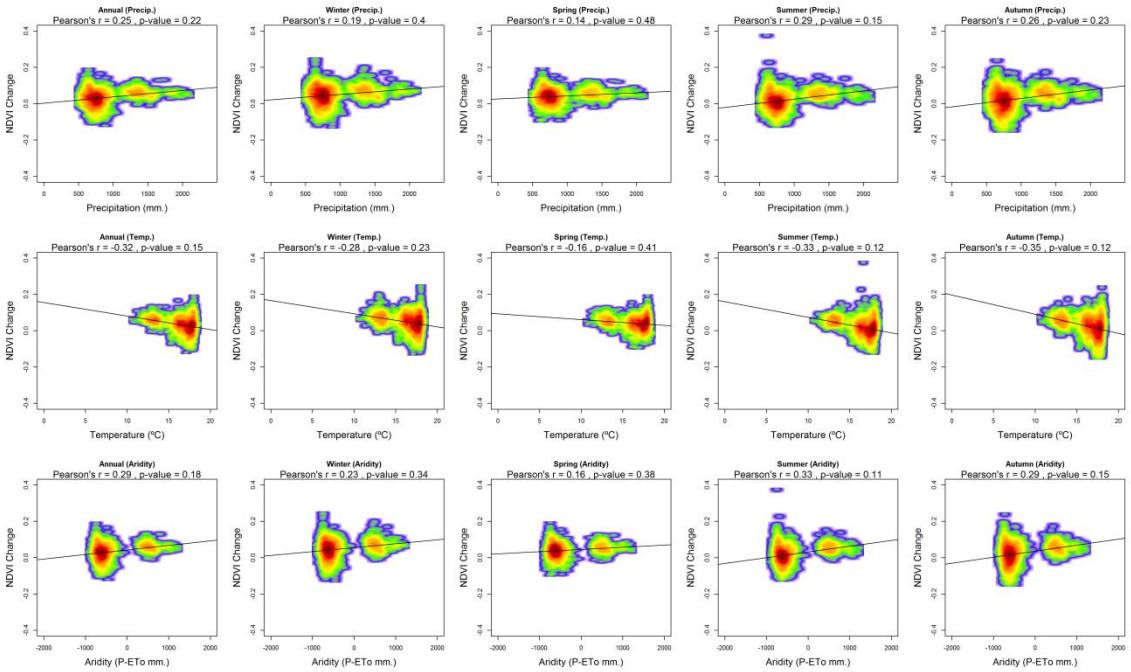

Supplementary Figure 17: Scatterplots showing the relationship between the NDVI magnitude of change and the average climate conditions (precipitation, temperature and aridity) at seasonal and annual scales. Eucalyptus

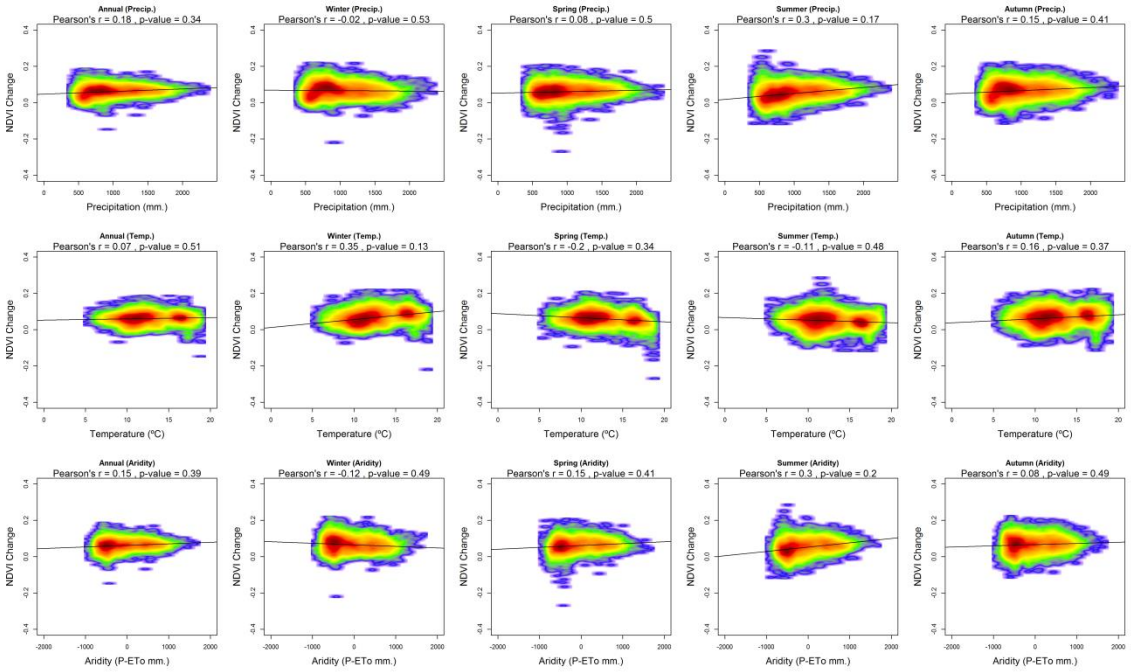

Supplementary Figure 18: Scatterplots showing the relationship between the NDVI magnitude of change and the average climate conditions (precipitation, temperature and aridity) at seasonal and annual scales. Leaf forests

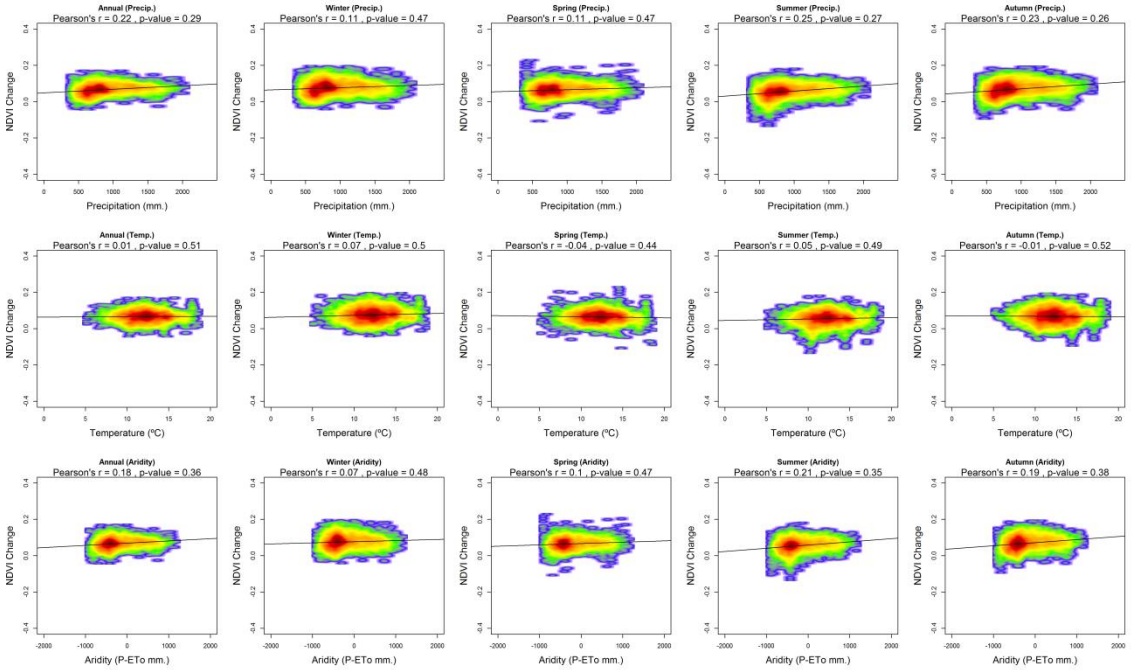

Supplementary Figure 19: Scatterplots showing the relationship between the NDVI magnitude of change and the average climate conditions (precipitation, temperature and aridity) at seasonal and annual scales. Mixed forests

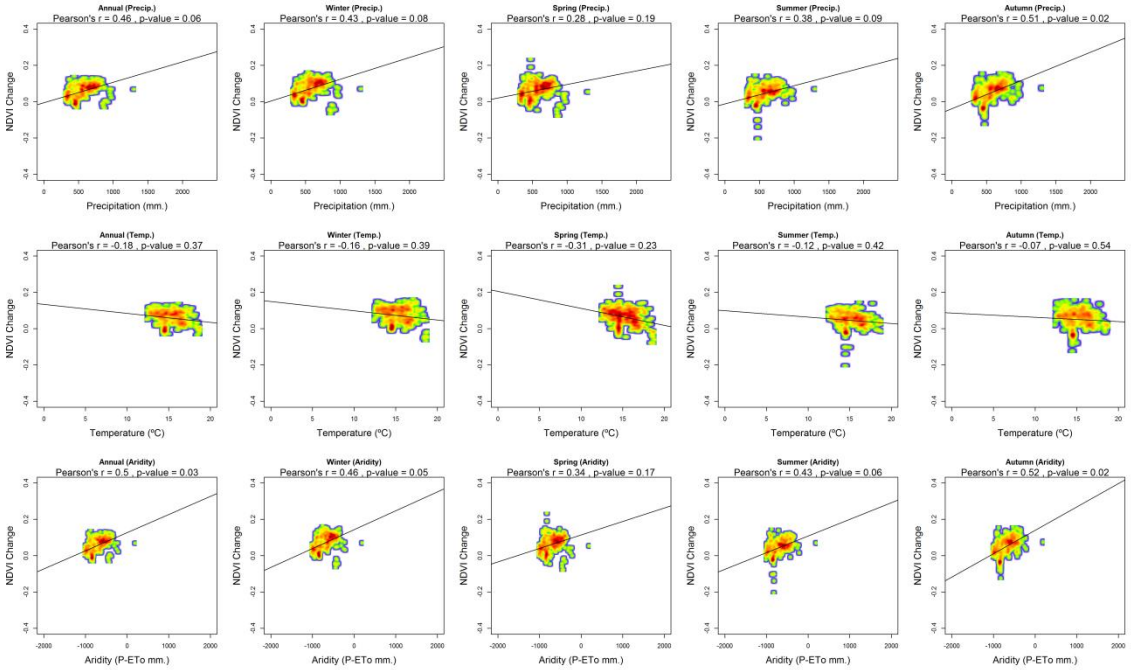

Supplementary Figure 20: Scatterplots showing the relationship between the NDVI magnitude of change and the average climate conditions (precipitation, temperature and aridity) at seasonal and annual scales. Vineyards-Fruit trees.

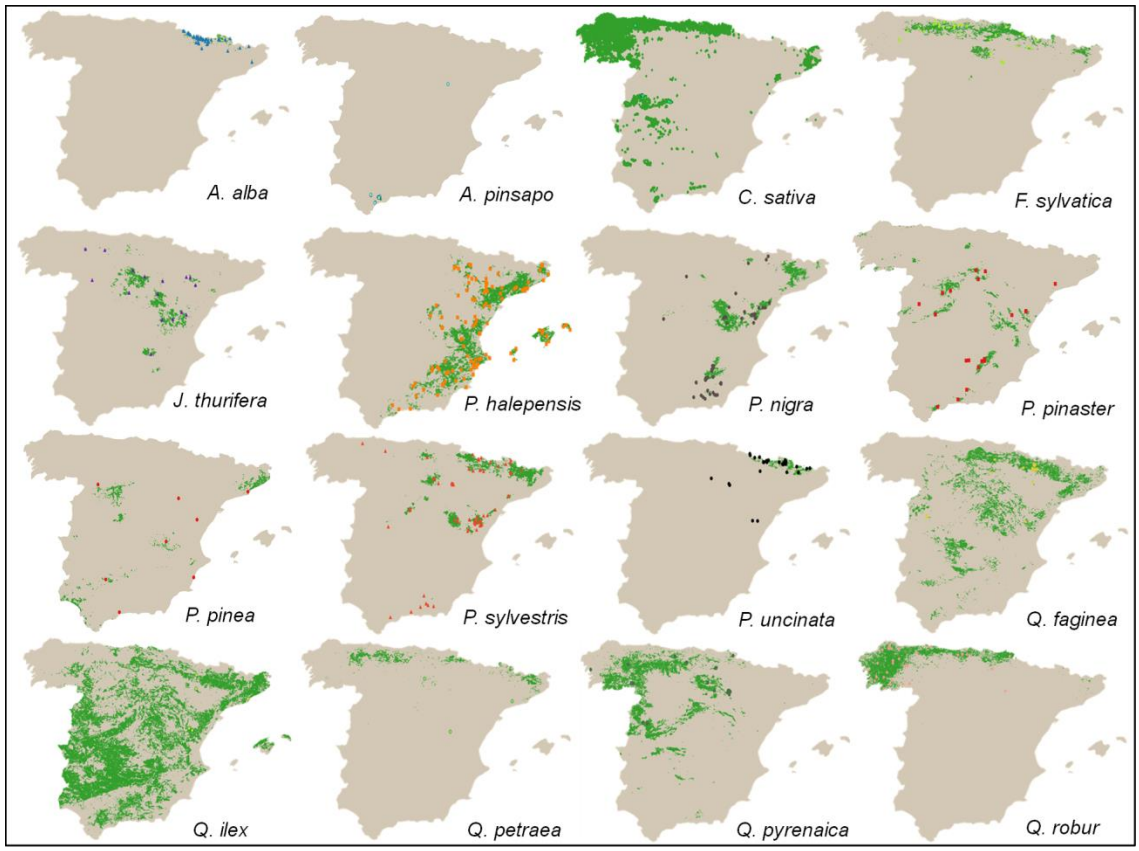

Supplementary Figure 21. Maps showing the distribution areas of the forests sampled in Spain considering the distribution of the 16 studied tree species. Symbols show sampled sites and green patches show the distribution area of each species. See site characteristics in Table 1.

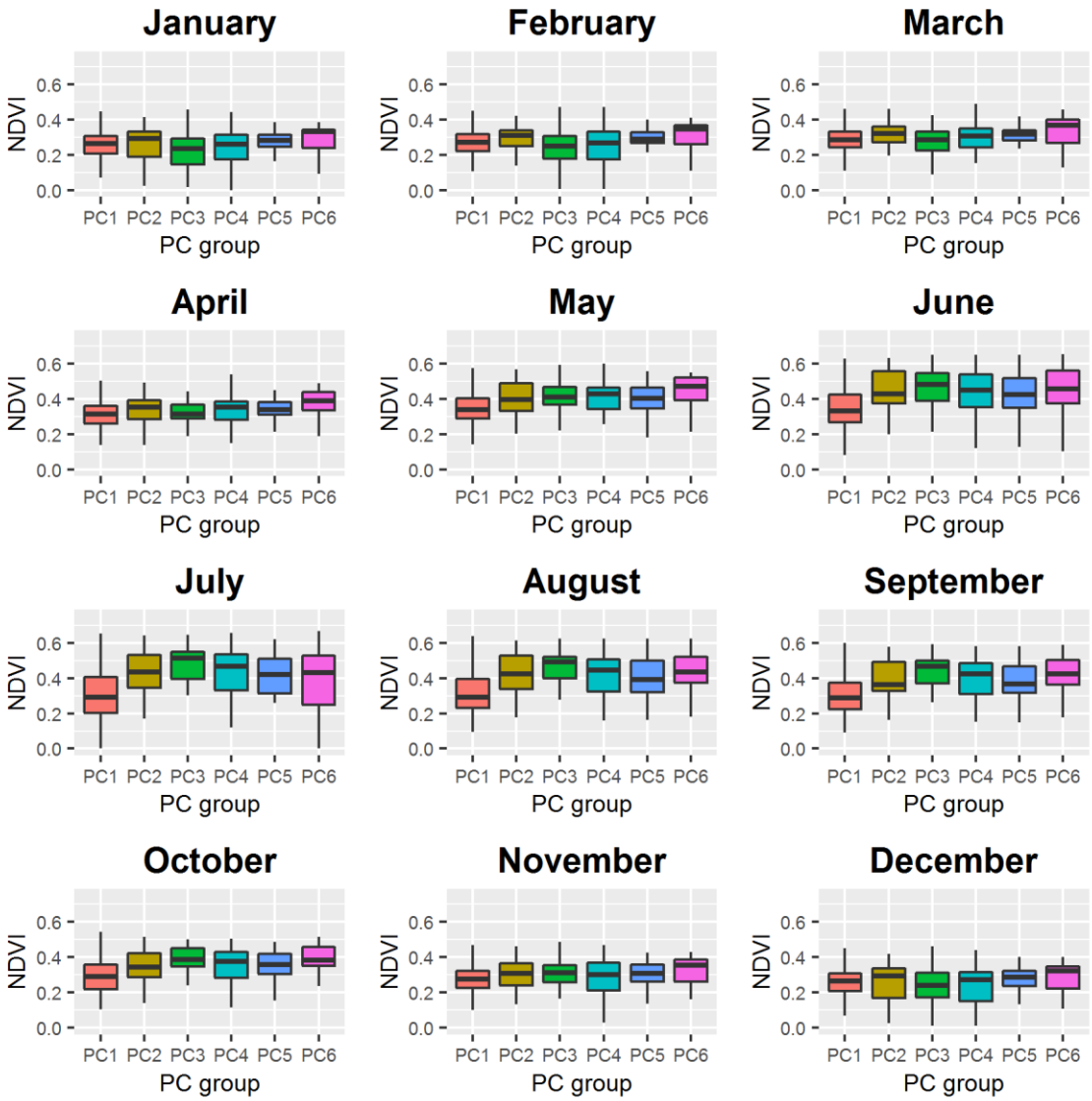

Supplementary Figure 22. Box-plots showing the monthly average values of NDVI corresponding to each PC.

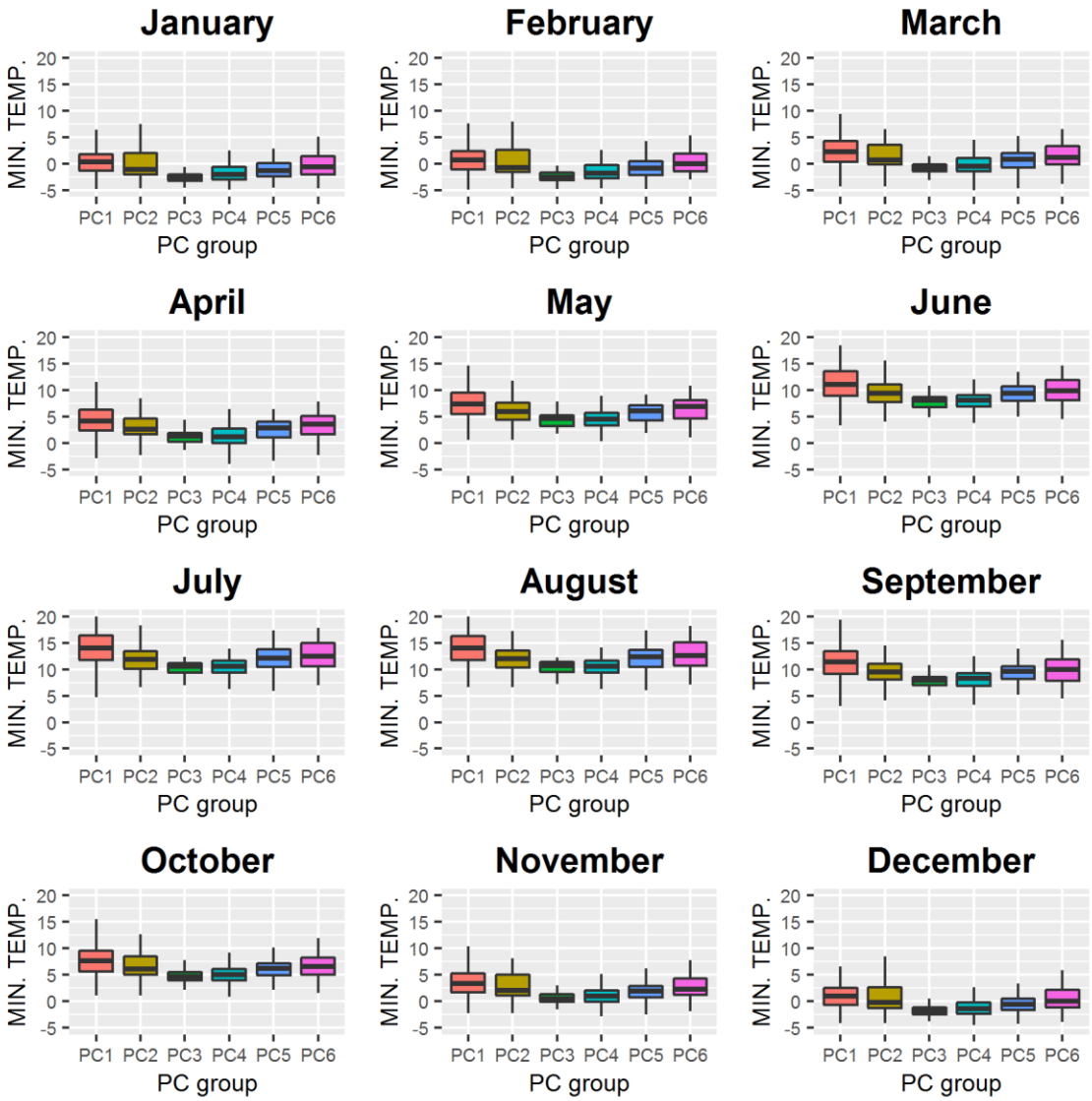

Supplementary Figure 23. Box-plots showing the monthly average values of minimum air temperature (C°) corresponding to each PC.

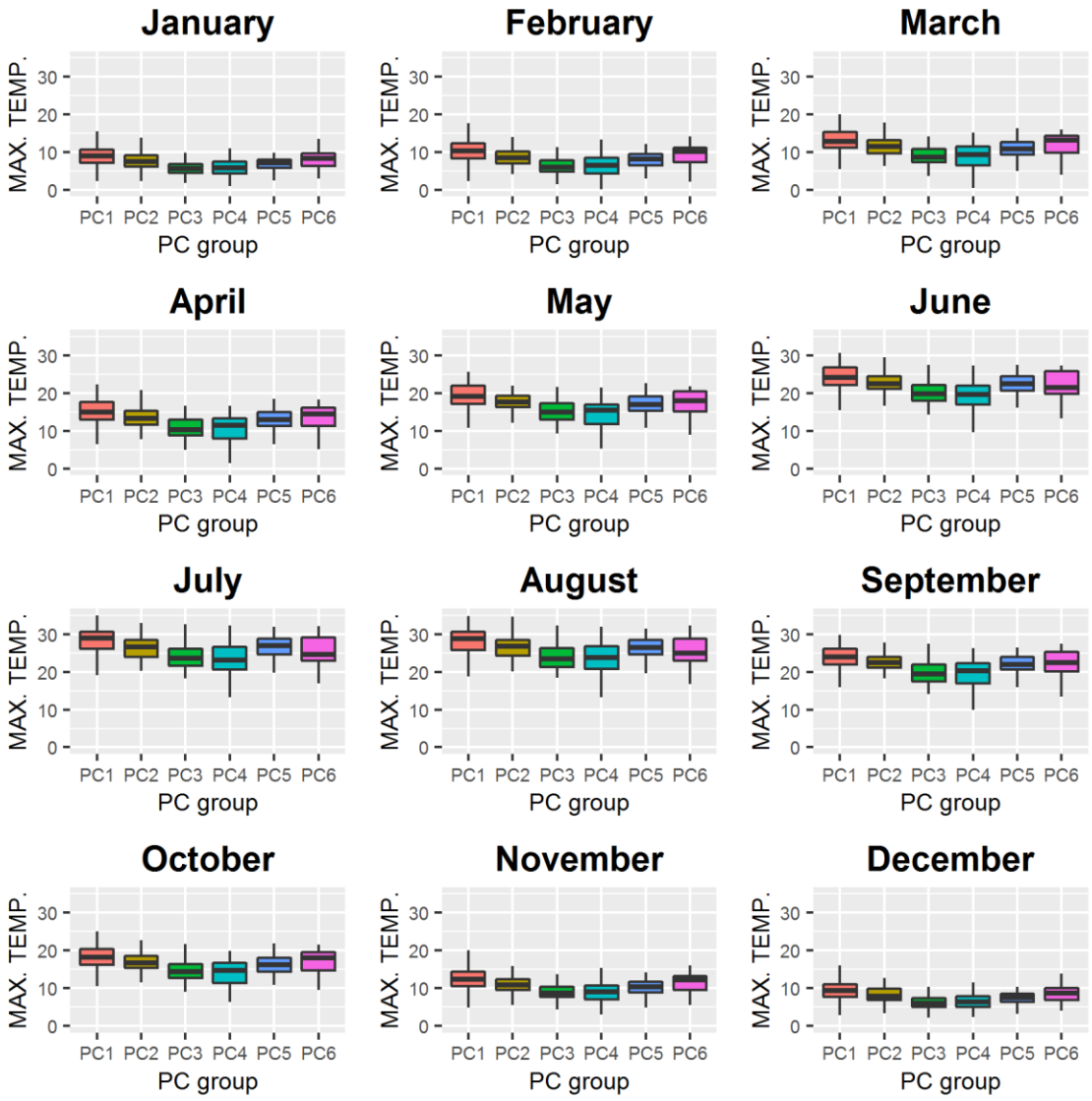

Supplementary Figure 24. Box-plot showing the monthly average values of maximum air temperature (C°) corresponding to each PC.

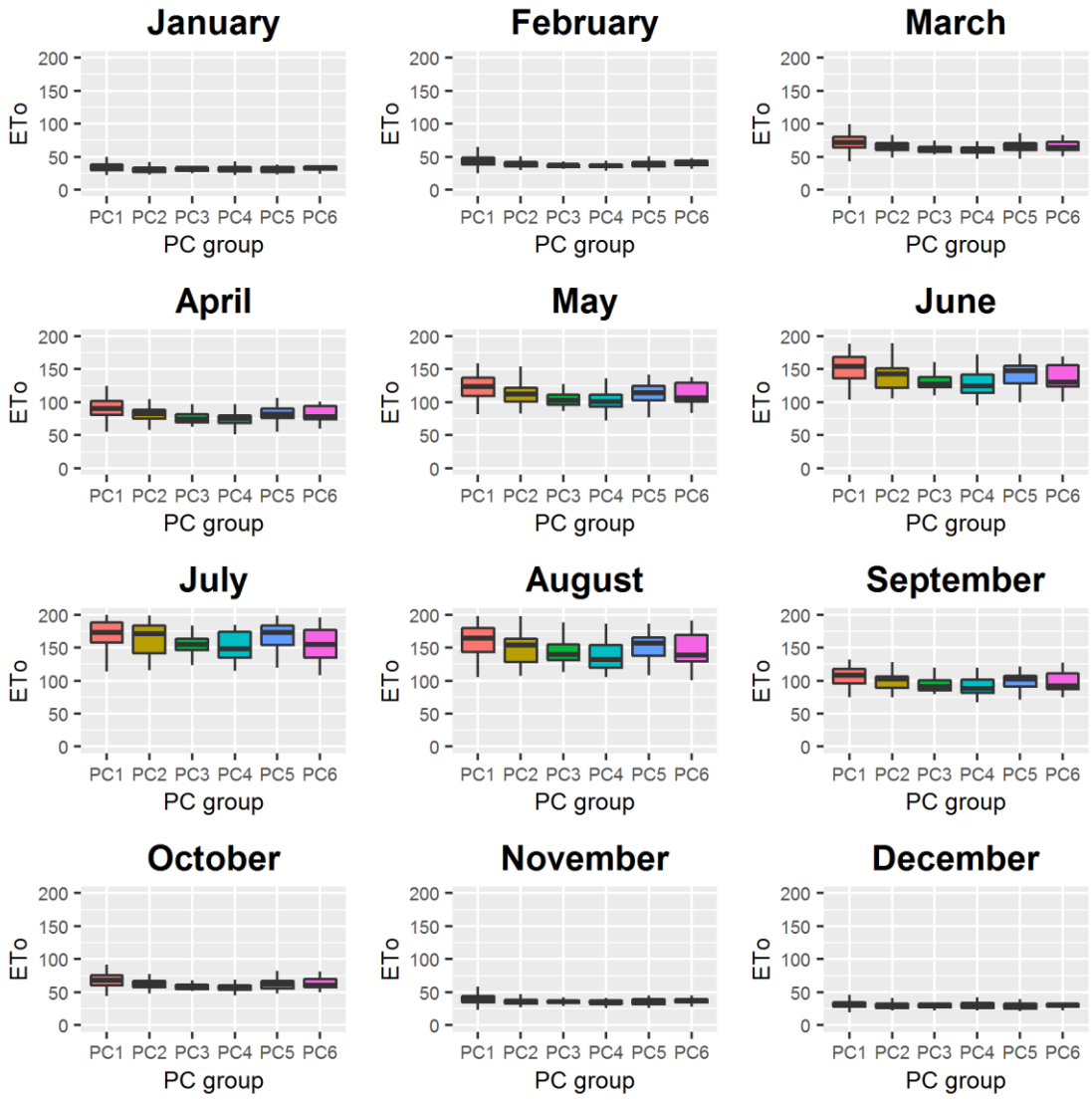

Supplementary Figure 25. Box-plots showing the monthly average values of ETo (mm) corresponding to each PC.

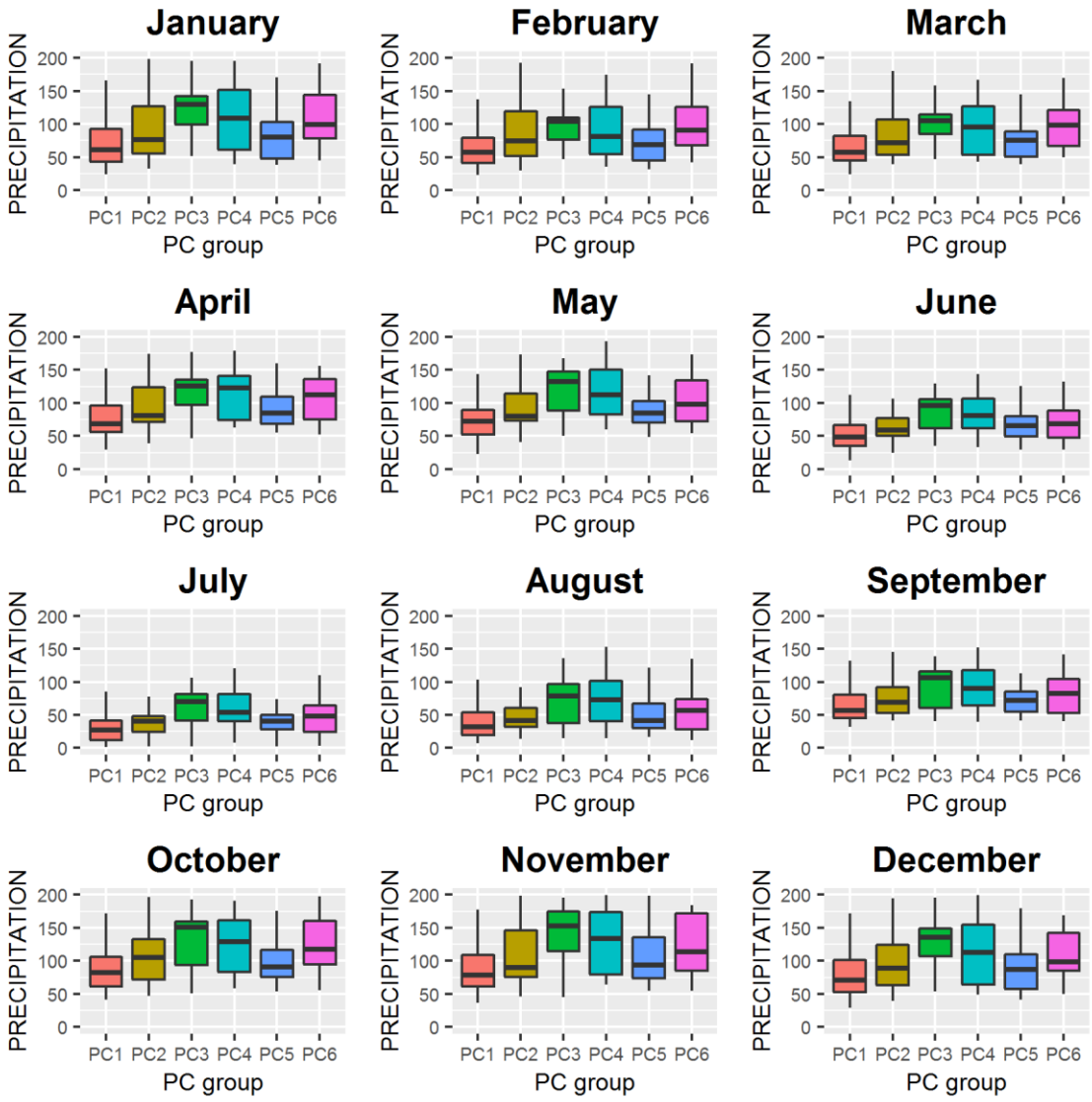

Supplementary Figure 26. Box-plots showing the monthly average values of precipitation (mm) corresponding to each PC.

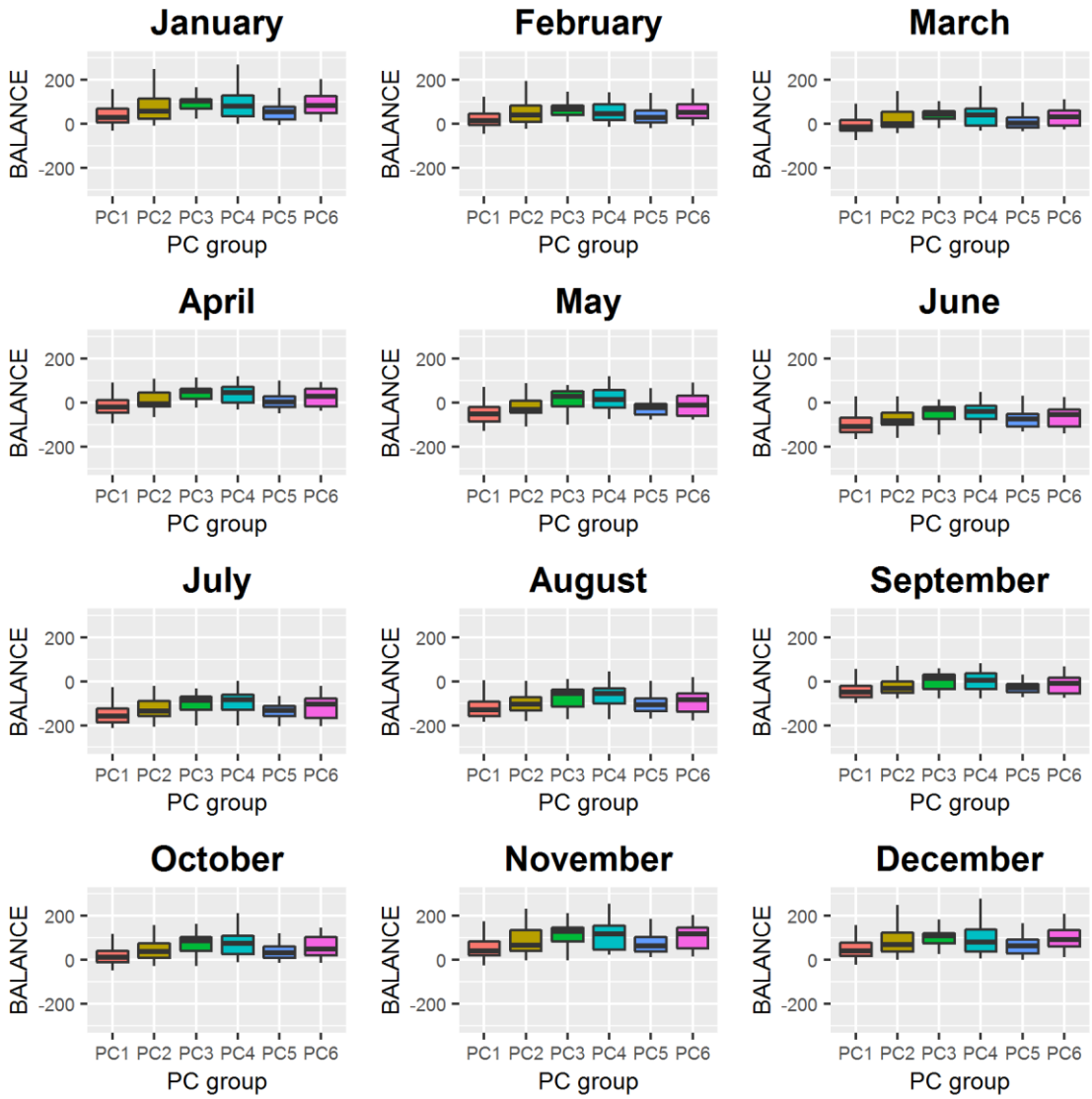

Supplementary Figure 27. Box-plots showing the monthly average values of climatic balance (mm) corresponding to each PC.

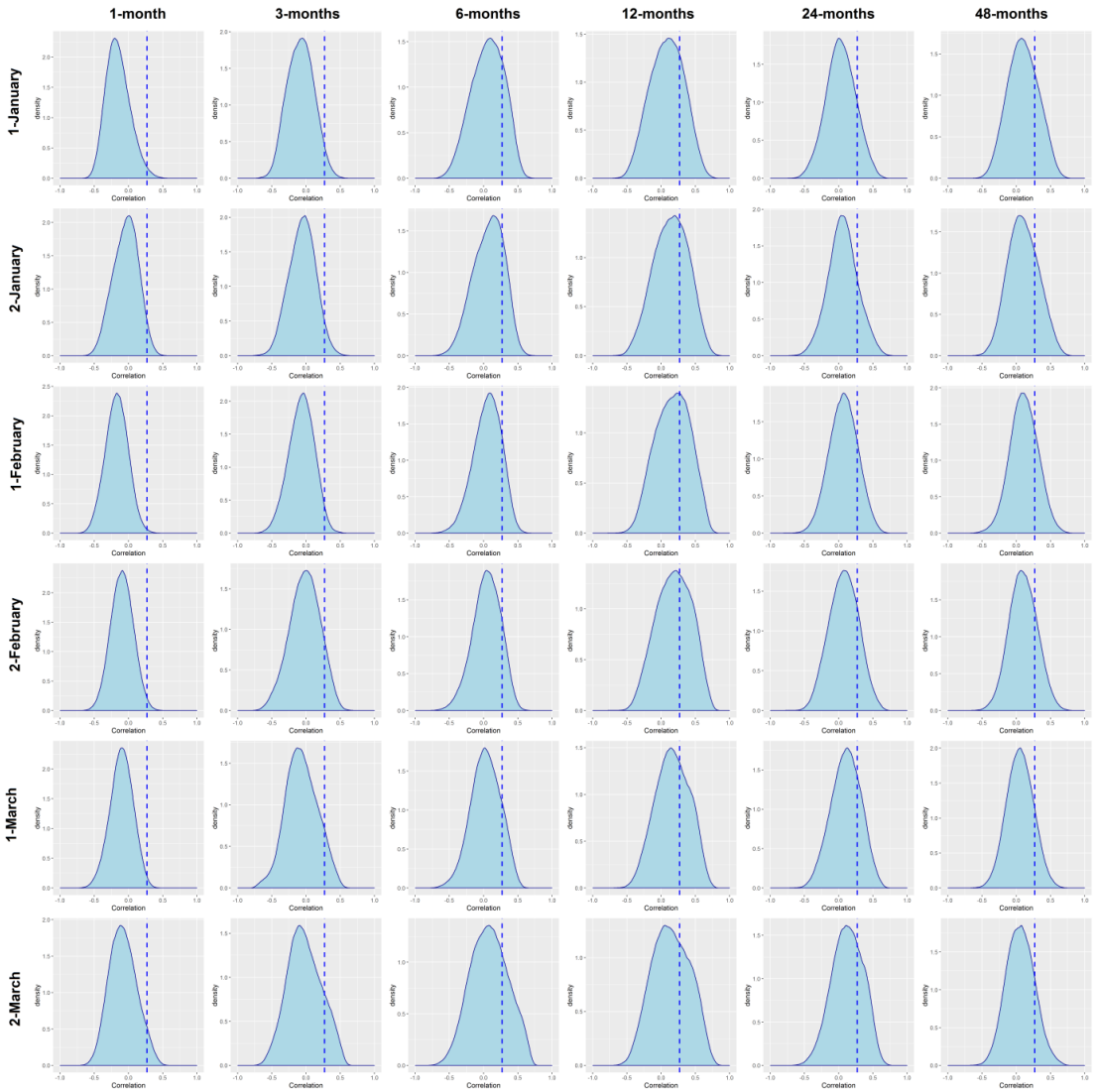

Supplementary Figure 28: Density plots summarizing the maximum correlations found between the sNDVI and the SPEI (January-March). Vertical dashed line represents the threshold for significant correlations ($p < 0.05$).

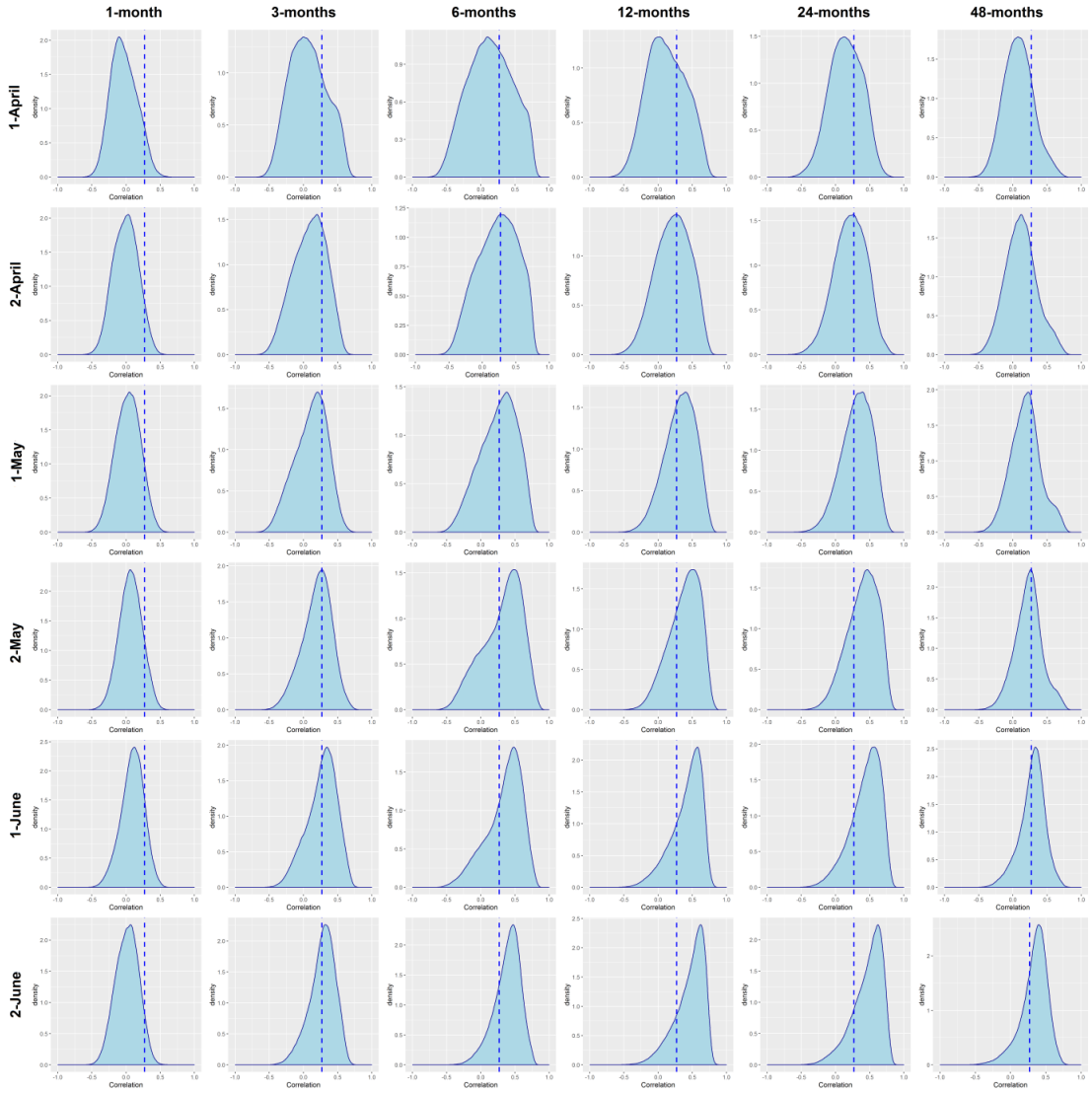

Supplementary Figure 29: Density plots summarizing the maximum correlations found between the sNDVI and the SPEI (April-June). Vertical dashed line represents the threshold for significant correlations ($p < 0.05$).

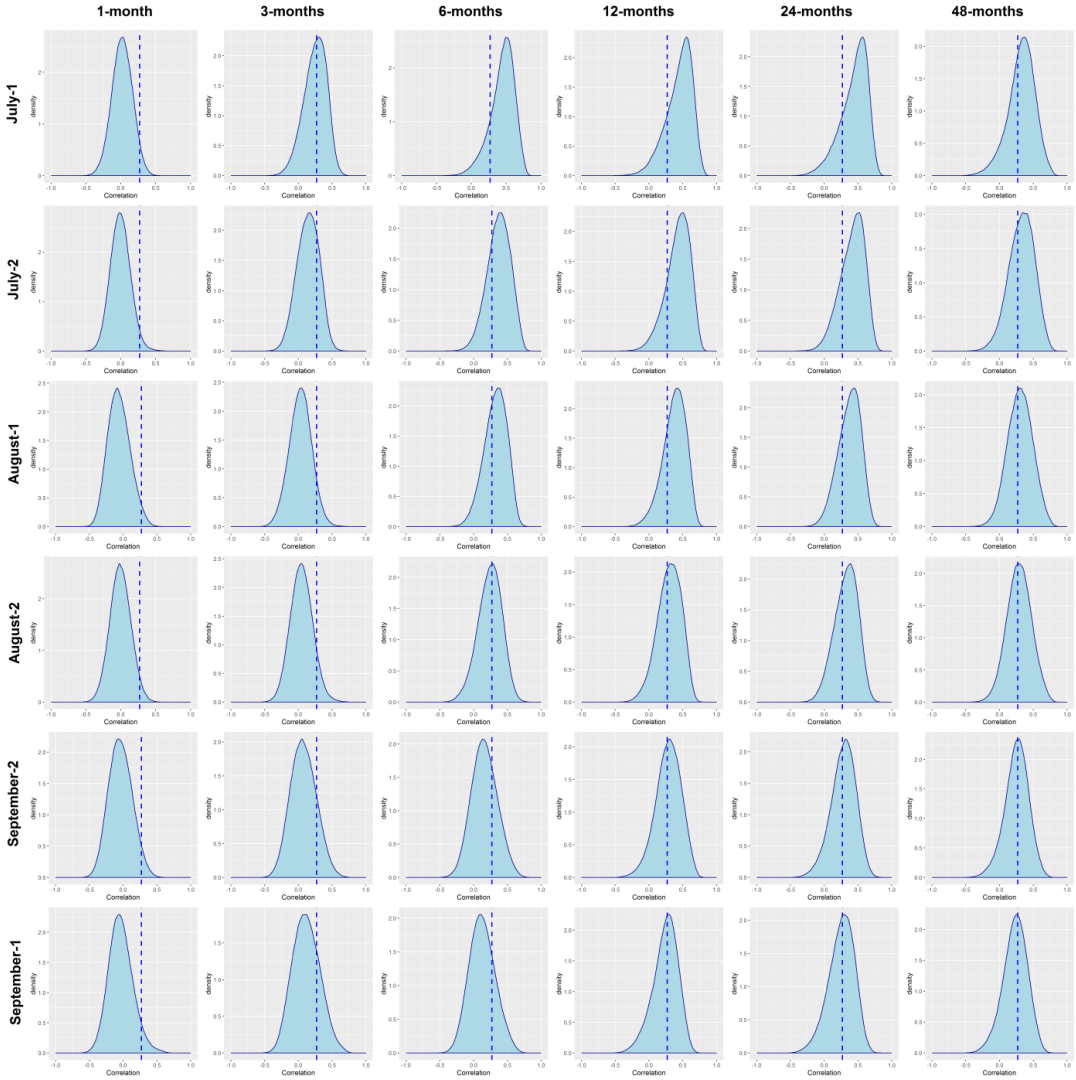

Supplementary Figure 30: Density plots summarizing the maximum correlations found between the sNDVI and the SPEI (July-September). Vertical dashed line represents the threshold for significant correlations ($p < 0.05$).

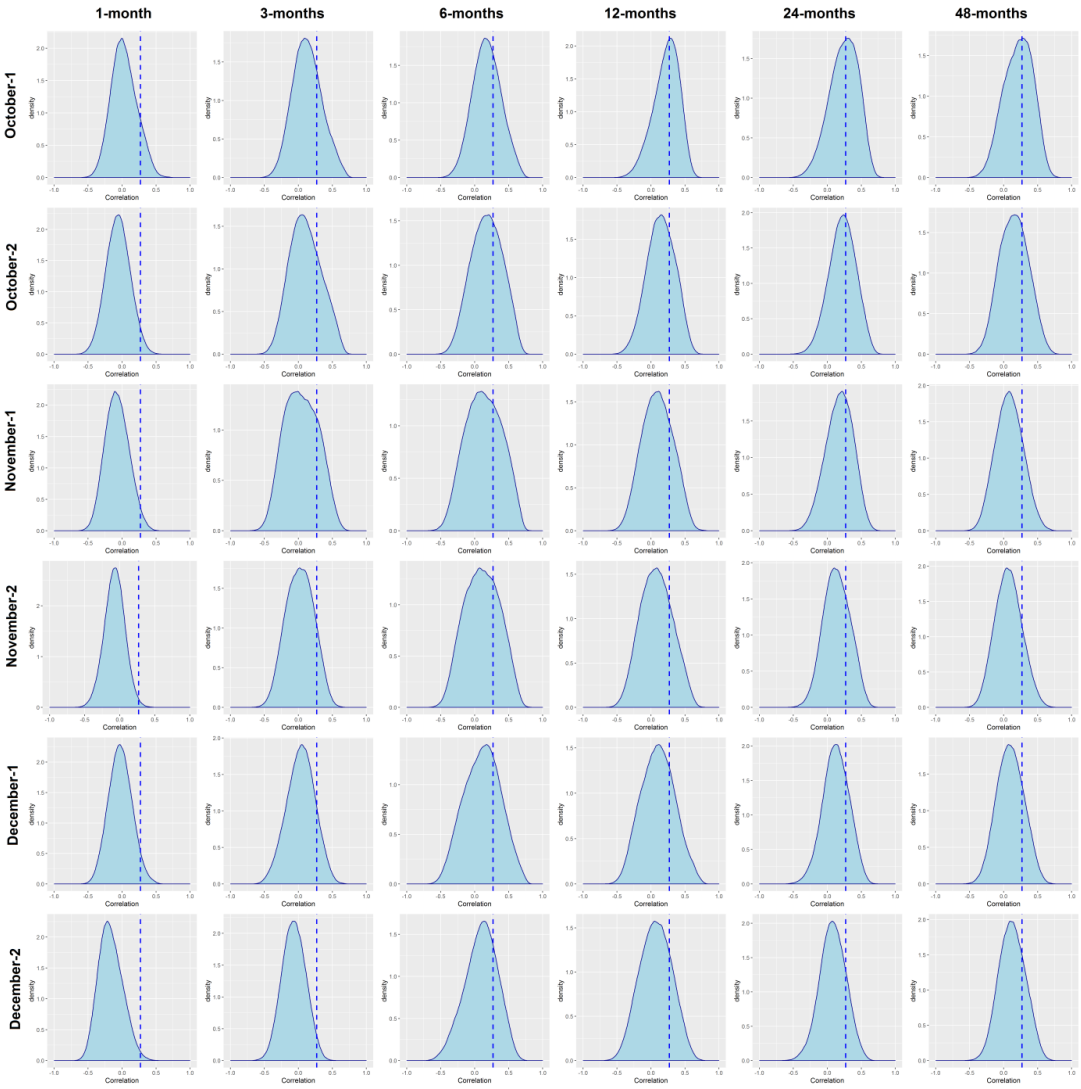

Supplementary Figure 31: Density plots summarizing the maximum correlations found between the sNDVI and the SPEI (October-December). Vertical dashed line represents the threshold for significant correlations ($p < 0.05$).

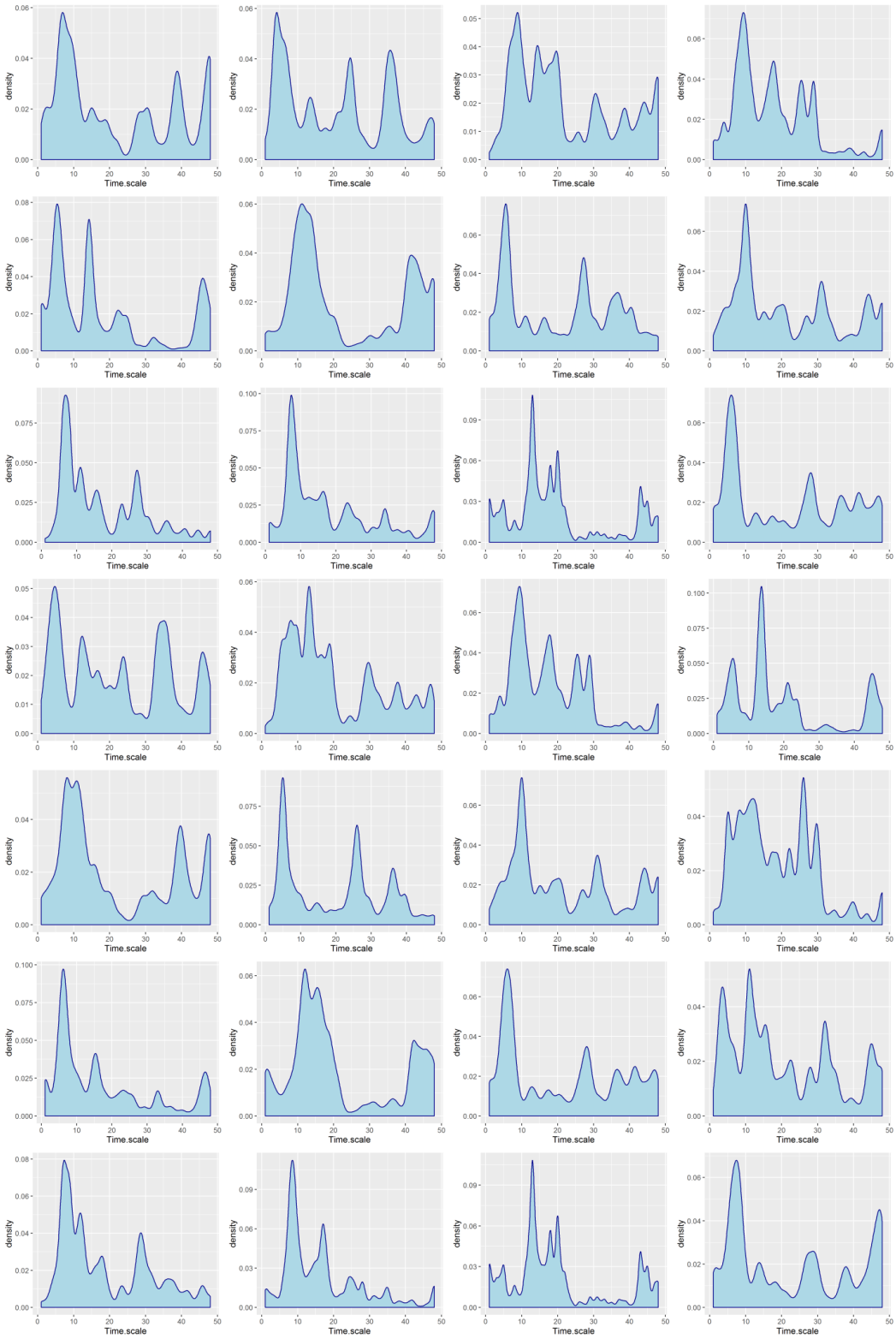

Supplementary Figure 32: Density plots showing the SPEI time scale at which the maximum correlation between sNDVI and SPEI is recorded for the different 24 semi-monthly periods.

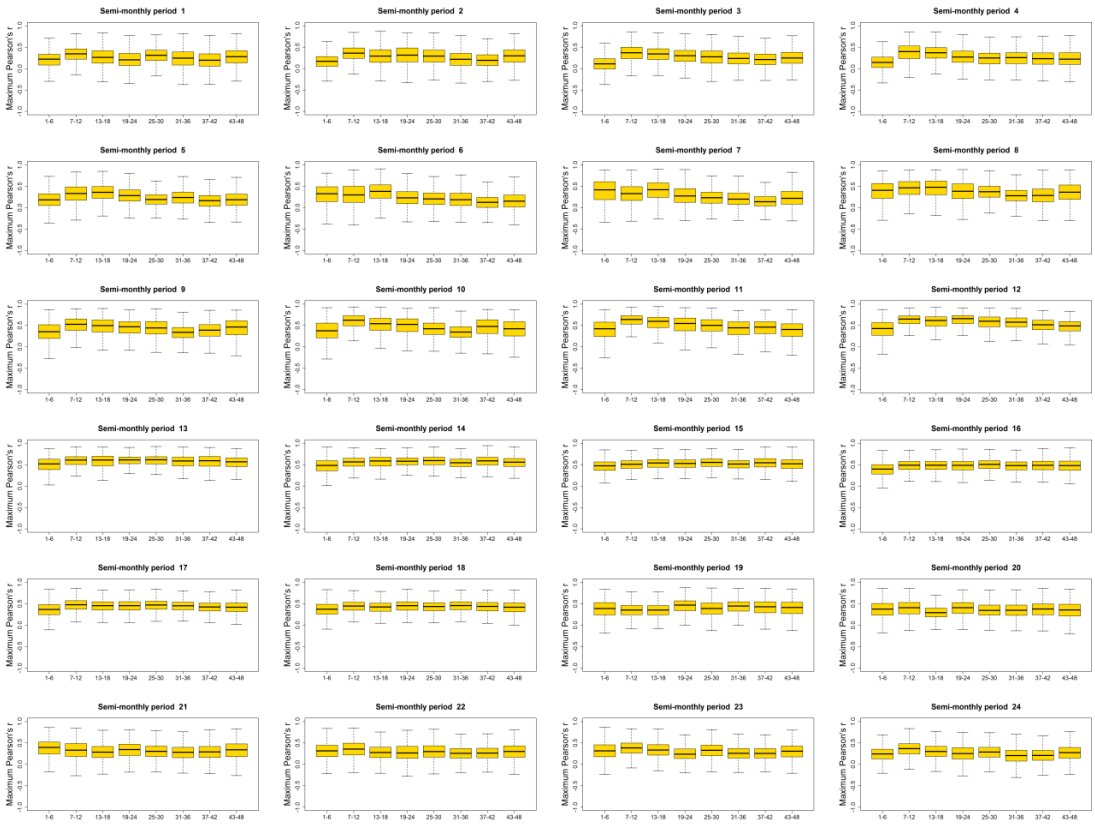

Supplementary Figure 33: Boxplots showing the maximum sNDVI vs. SPEI correlation as a function of the different SPEI time-scales.

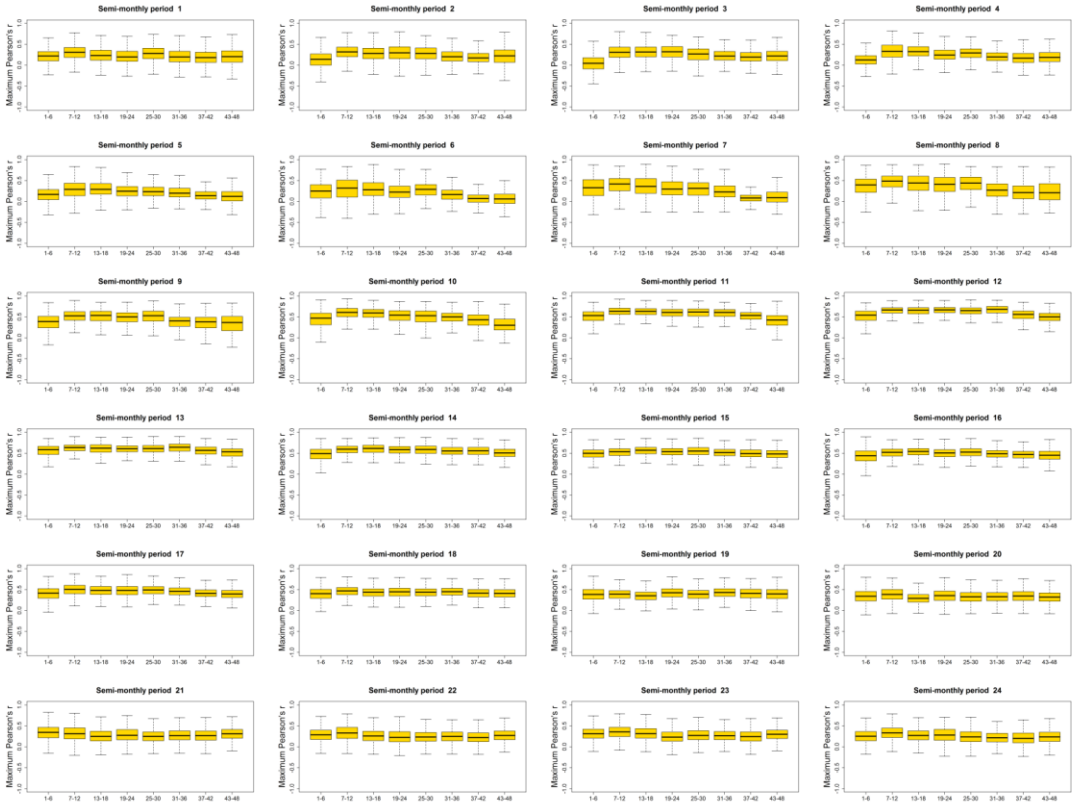

Supplementary Figure 34: Boxplots showing the maximum sNDVI vs. SPEI correlation as a function of the different SPEI time-scales. Non-irrigated arable lands

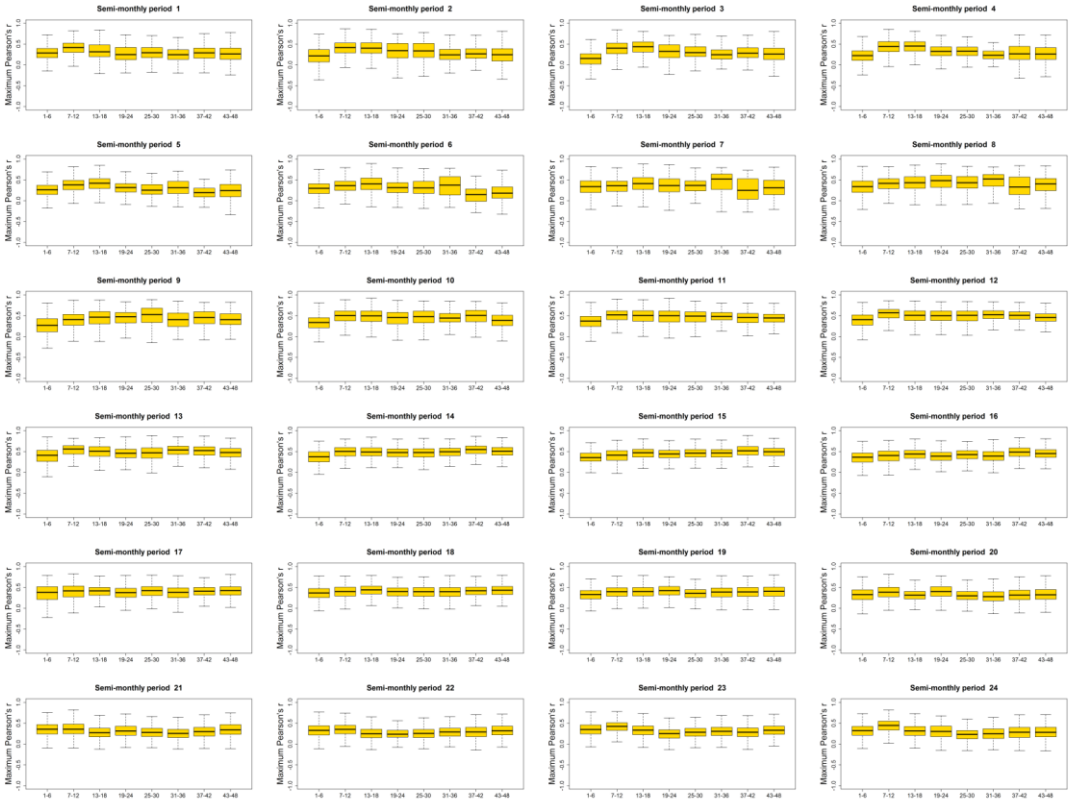

Supplementary Figure 35: Boxplots showing the maximum sNDVI vs. SPEI correlation as a function of the different SPEI time-scales. Irrigated lands

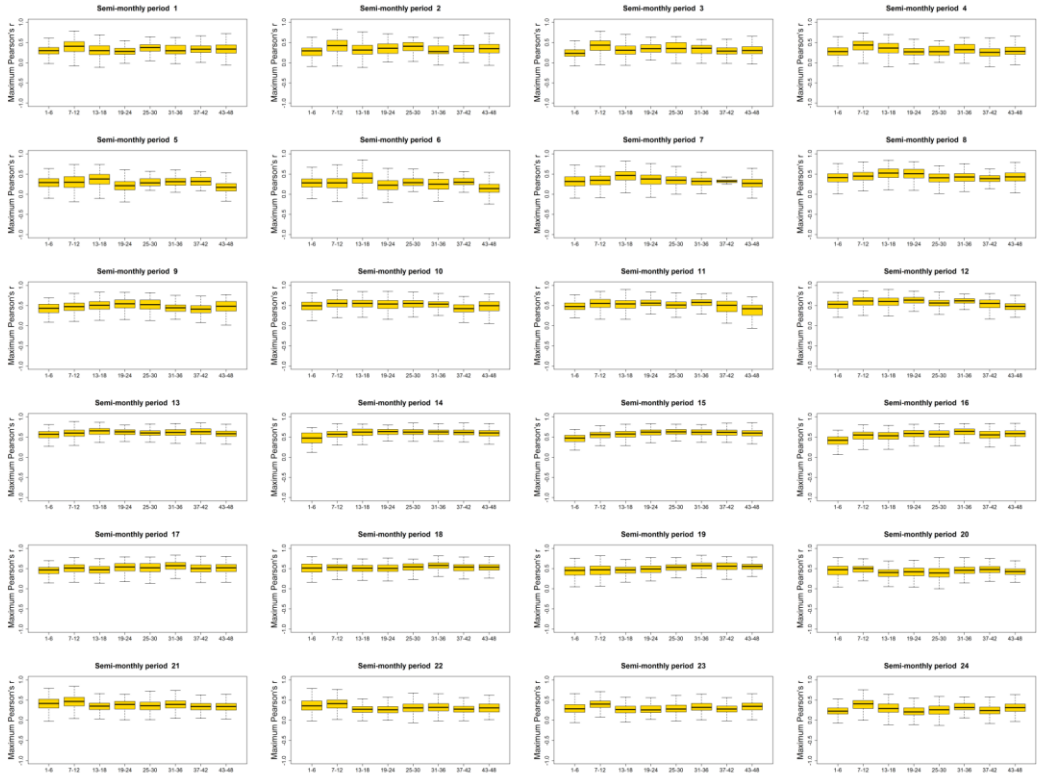

Supplementary Figure 36: Boxplots showing the maximum sNDVI vs. SPEI correlation as a function of the different SPEI time-scales. Vineyards

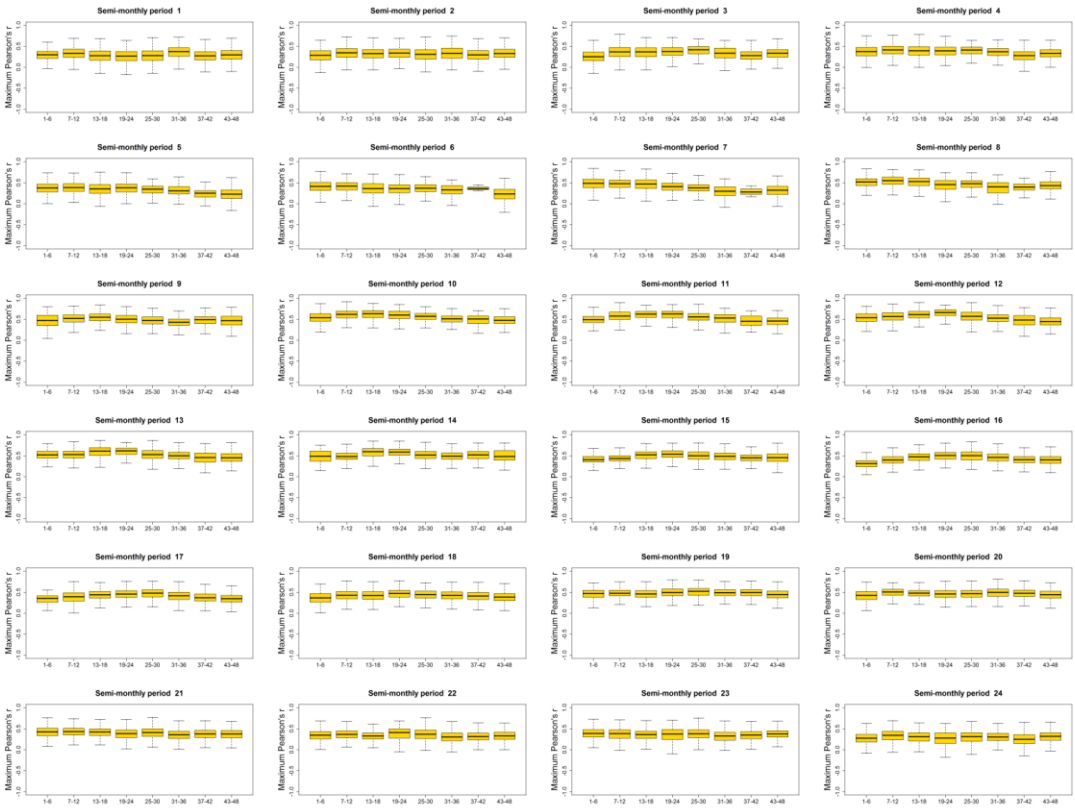

Supplementary Figure 37: Boxplots showing the maximum sNDVI vs. SPEI correlation as a function of the different SPEI time-scales. Olive groves.

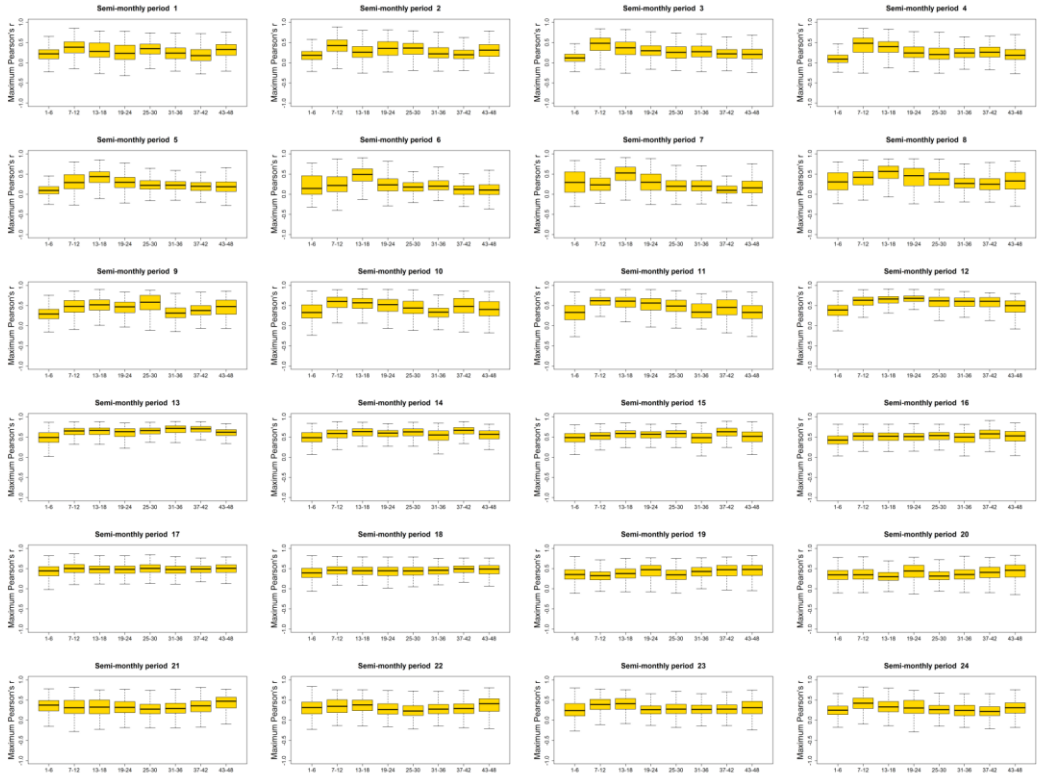

Supplementary Figure 38: Boxplots showing the maximum sNDVI vs. SPEI correlation as a function of the different SPEI time-scales. Mixed agriculture/natural vegetation

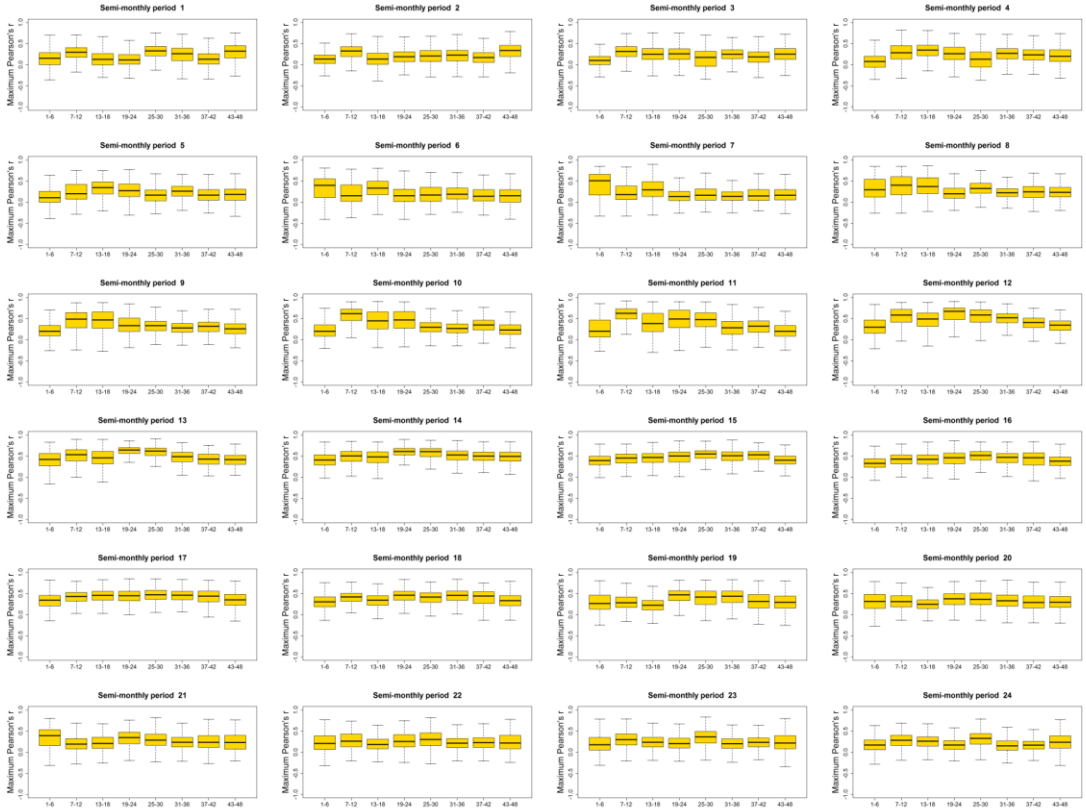

Supplementary Figure 39: Boxplots showing the maximum sNDVI vs. SPEI correlation as a function of the different SPEI time-scales. Broad-leaved forests

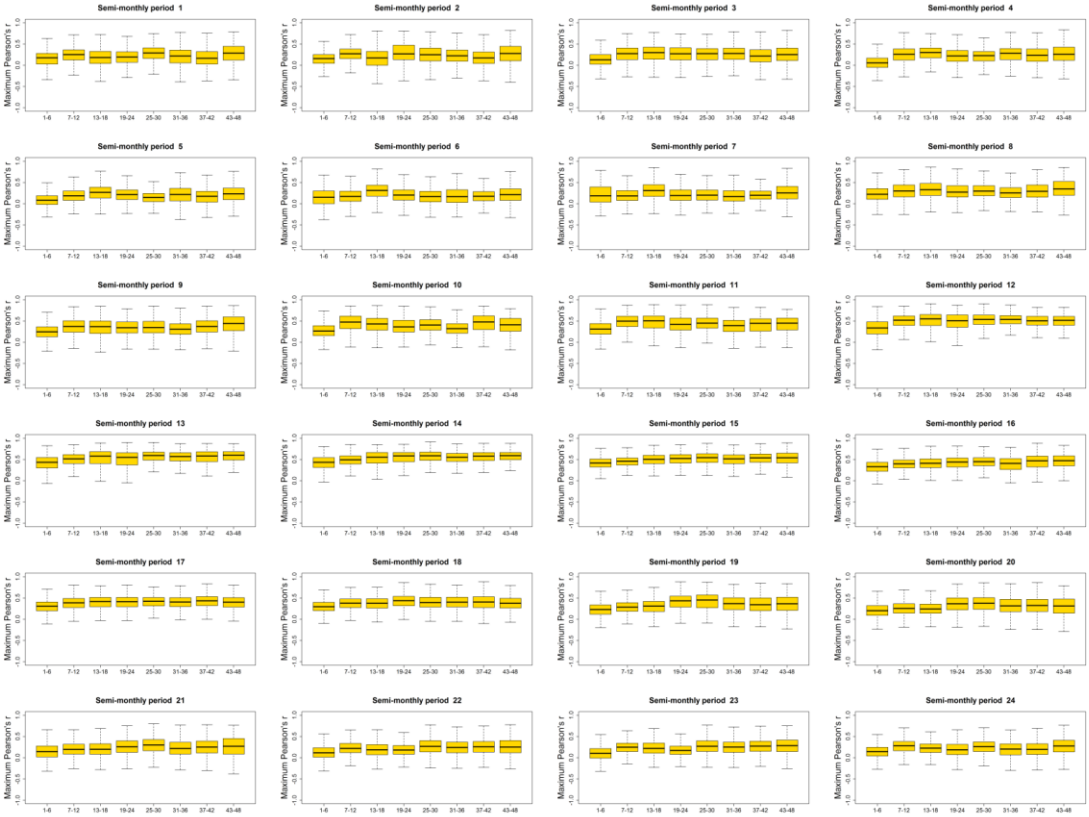

Supplementary Figure 40: Boxplots showing the maximum sNDVI vs. SPEI correlation as a function of the different SPEI time-scales. Coniferous forests

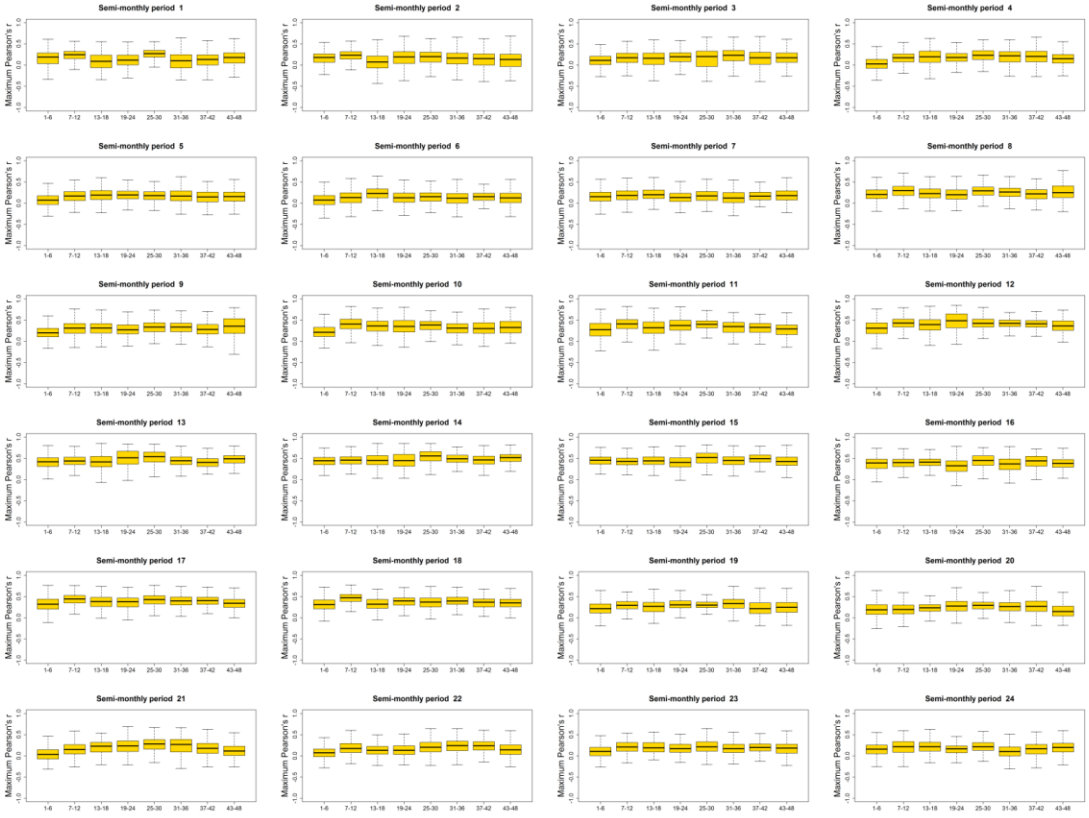

Supplementary Figure 41: Boxplots showing the maximum sNDVI vs. SPEI correlation as a function of the different SPEI time-scales. Mixed forests

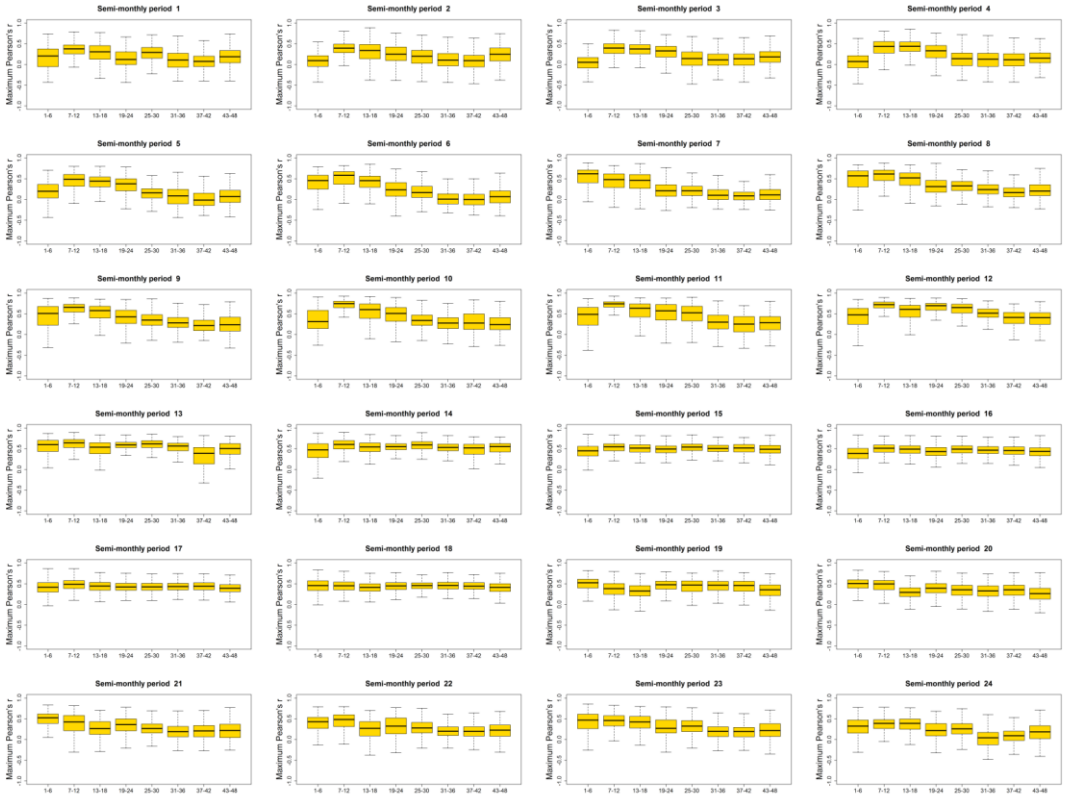

Supplementary Figure 42: Boxplots showing the maximum sNDVI vs. SPEI correlation as a function of the different SPEI time-scales. Natural grassland

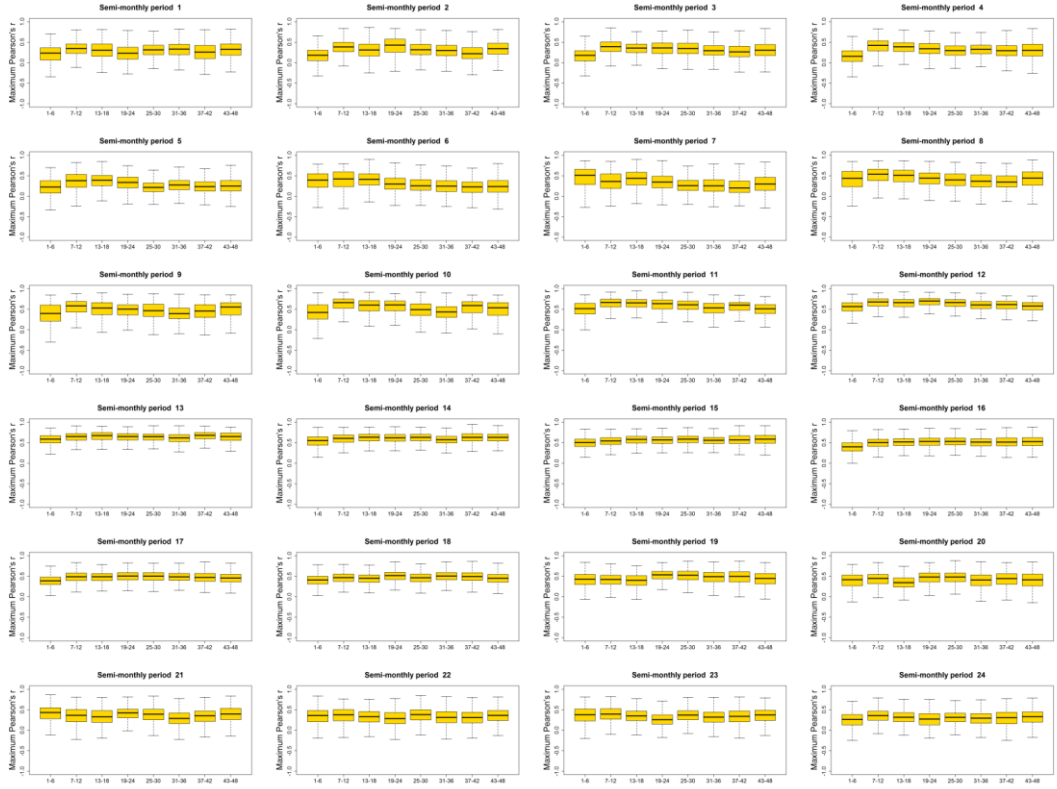

Supplementary Figure 43: Boxplots showing the maximum sNDVI vs. SPEI correlation as a function of the different SPEI time-scales. Sclerophillous vegetation

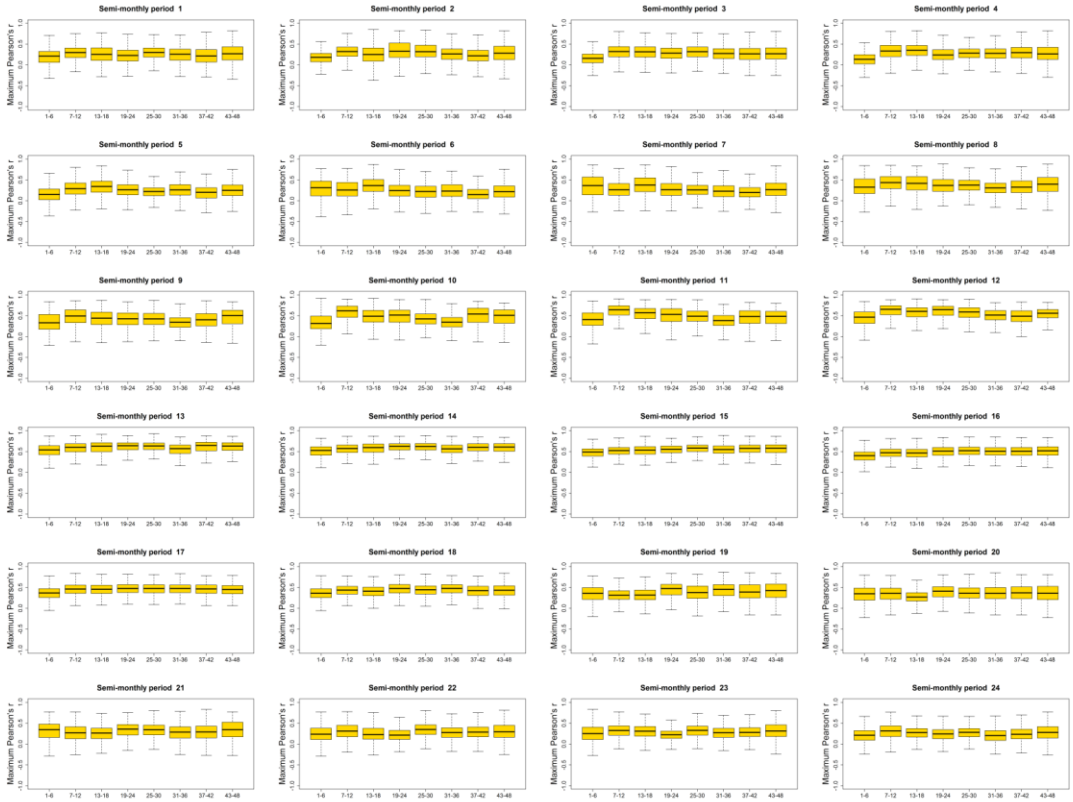

Supplementary Figure 44: Boxplots showing the maximum sNDVI vs. SPEI correlation as a function of the different SPEI time-scales. Transition wood-scrub.

	Negative ($p < 0.05$)	Negative ($p > 0.05$)	Positive ($p > 0.05$)	Positive ($p < 0.05$)
1st Jan	0.1	7.9	47.1	44.9
2nd Jan	0.5	7.8	43.6	48.2
1st Feb	0.2	7.3	43.2	49.3
2sd Feb	0.0	6.1	45.2	48.6
1st Mar	0.0	9.5	48.2	42.2
2sd Mar	0.3	13.0	44.0	42.7
1st Apr	0.0	8.6	35.5	55.9
2sd Apr	0.0	4.7	25.3	69.9
1st May	0.0	1.0	13.7	85.3
2sd May	0.0	0.3	7.2	92.5
1st Jun	0.0	0.1	2.4	97.5
2sd Jun	0.0	0.0	1.3	98.7
1st Jul	0.0	0.0	1.8	98.2
2sd Jul	0.0	0.0	2.3	97.7
1st Aug	0.0	0.0	3.5	96.4
2sd Aug	0.0	0.1	5.6	94.2
1st Sep	0.0	0.2	9.7	90.1
2sd Sep	0.0	0.2	12.7	87.1
1st Oct	0.0	0.5	22.0	77.5
2sd Oct	0.0	1.1	35.9	63.1
1st Nov	0.0	3.1	42.7	54.2
2sd Nov	0.0	3.5	48.5	47.9
1st Dec	0.0	1.9	40.6	57.5
2sd Dec	0.0	4.1	45.8	50.1

Supplementary Table 3: Percentage of the total surface area in Spain showing positive or negative, significant or non-significant Pearson's r correlations between the sNDVI and the SPEI. Non-irrigated arable lands.

	Negative ($p < 0.05$)	Negative ($p > 0.05$)	Positive ($p > 0.05$)	Positive ($p < 0.05$)
1st Jan	0.0	4.0	32.5	63.5
2nd Jan	0.2	5.1	28.0	66.7
1st Feb	0.3	4.4	27.1	68.2
2sd Feb	0.1	2.8	26.1	71.0
1st Mar	0.0	3.3	31.7	65.0
2sd Mar	0.0	4.4	32.8	62.8
1st Apr	0.0	3.5	30.7	65.8
2sd Apr	0.0	3.0	26.3	70.7
1st May	0.0	2.6	24.7	72.7
2sd May	0.0	1.6	16.9	81.5
1st Jun	0.0	1.0	14.4	84.7
2sd Jun	0.0	0.3	11.0	88.7
1st Jul	0.0	0.3	12.0	87.6
2sd Jul	0.0	0.1	9.8	90.1
1st Aug	0.0	0.2	11.6	88.2
2sd Aug	0.0	0.7	17.2	82.1
1st Sep	0.0	1.1	22.1	76.7
2sd Sep	0.0	0.5	20.8	78.7
1st Oct	0.0	0.8	25.8	73.4
2sd Oct	0.0	2.3	35.5	62.2
1st Nov	0.0	1.8	37.0	61.2
2sd Nov	0.0	2.0	40.6	57.3
1st Dec	0.0	1.1	30.6	68.3
2sd Dec	0.0	2.2	32.3	65.4

Supplementary Table 4: Percentage of the total surface area in Spain showing positive or negative, significant or non-significant Pearson's r correlations between the sNDVI and the SPEI. Irrigated lands

	Negative ($p < 0.05$)	Negative ($p > 0.05$)	Positive ($p > 0.05$)	Positive ($p < 0.05$)
1st Jan	0.0	1.6	32.4	66.1
2nd Jan	0.0	1.2	29.3	69.4
1st Feb	0.0	1.1	35.4	63.5
2sd Feb	0.0	0.9	37.0	62.1
1st Mar	0.0	3.8	44.8	51.4
2sd Mar	0.0	6.3	41.2	52.4
1st Apr	0.0	1.0	33.1	65.9
2sd Apr	0.0	0.2	14.1	85.7
1st May	0.0	0.1	9.0	90.9
2sd May	0.0	0.1	4.4	95.5
1st Jun	0.0	0.1	5.3	94.6
2sd Jun	0.0	0.0	1.7	98.3
1st Jul	0.0	0.0	0.9	99.1
2sd Jul	0.0	0.0	0.6	99.4
1st Aug	0.0	0.0	0.8	99.2
2sd Aug	0.0	0.0	1.9	98.1
1st Sep	0.0	0.0	4.1	95.9
2sd Sep	0.0	0.0	2.7	97.3
1st Oct	0.0	0.1	5.0	94.9
2sd Oct	0.0	0.2	11.3	88.5
1st Nov	0.0	0.2	22.7	77.1
2sd Nov	0.0	0.4	40.3	59.4
1st Dec	0.0	0.5	40.1	59.3
2sd Dec	0.0	1.8	45.3	52.9

Supplementary Table 5: Percentage of the total surface area in Spain showing positive or negative, significant or non-significant Pearson's r correlations between the sNDVI and the SPEI. Vineyards

	Negative ($p < 0.05$)	Negative ($p > 0.05$)	Positive ($p > 0.05$)	Positive ($p < 0.05$)
1st Jan	0.0	2.9	43.1	54.0
2nd Jan	0.0	1.6	36.4	61.9
1st Feb	0.0	1.5	31.7	66.8
2sd Feb	0.0	0.6	24.2	75.2
1st Mar	0.0	1.5	28.0	70.5
2sd Mar	0.0	1.5	23.0	75.5
1st Apr	0.0	0.6	11.9	87.5
2sd Apr	0.0	0.2	5.7	94.2
1st May	0.0	0.1	4.6	95.3
2sd May	0.0	0.0	1.2	98.8
1st Jun	0.0	0.0	0.9	99.1
2sd Jun	0.0	0.0	1.7	98.3
1st Jul	0.0	0.0	2.7	97.3
2sd Jul	0.0	0.0	2.6	97.4
1st Aug	0.0	0.0	4.7	95.2
2sd Aug	0.0	0.1	10.9	89.1
1st Sep	0.0	0.1	20.2	79.7
2sd Sep	0.0	0.0	12.6	87.4
1st Oct	0.0	0.0	4.5	95.5
2sd Oct	0.0	0.1	6.8	93.1
1st Nov	0.0	0.2	16.4	83.4
2sd Nov	0.0	0.5	31.2	68.3
1st Dec	0.0	0.5	23.4	76.1
2sd Dec	0.0	1.8	39.6	58.6

Supplementary Table 6: Percentage of the total surface area in Spain showing positive or negative, significant or non-significant Pearson's r correlations between the sNDVI and the SPEI. Olive groves.

	Negative ($p < 0.05$)	Negative ($p > 0.05$)	Positive ($p > 0.05$)	Positive ($p < 0.05$)
1st Jan	0.0	7.7	39.1	53.1
2nd Jan	0.0	5.7	39.7	54.6
1st Feb	0.0	5.6	39.0	55.3
2sd Feb	0.0	6.6	37.4	55.9
1st Mar	0.0	6.9	38.7	54.4
2sd Mar	0.1	12.3	34.4	53.1
1st Apr	0.0	9.6	34.1	56.3
2sd Apr	0.0	4.0	28.9	67.0
1st May	0.0	0.9	20.5	78.5
2sd May	0.0	0.8	15.8	83.4
1st Jun	0.0	1.6	15.1	83.3
2sd Jun	0.0	0.6	9.5	89.9
1st Jul	0.0	0.1	5.4	94.5
2sd Jul	0.0	0.0	4.2	95.8
1st Aug	0.0	0.0	5.4	94.6
2sd Aug	0.0	0.1	8.8	91.1
1st Sep	0.0	0.6	9.4	89.9
2sd Sep	0.0	0.4	15.6	83.9
1st Oct	0.0	1.0	26.4	72.5
2sd Oct	0.0	1.3	32.1	66.6
1st Nov	0.0	4.5	37.6	57.9
2sd Nov	0.0	4.9	42.2	52.9
1st Dec	0.0	4.1	41.0	54.9
2sd Dec	0.0	4.1	39.9	56.0

Supplementary Table 7: Percentage of the total surface area in Spain showing positive or negative, significant or non-significant Pearson's r correlations between the sNDVI and the SPEI. Mixed agriculture/natural vegetation

	Negative ($p < 0.05$)	Negative ($p > 0.05$)	Positive ($p > 0.05$)	Positive ($p < 0.05$)
1st Jan	0.2	15.9	45.5	38.4
2nd Jan	0.2	12.3	49.5	38.0
1st Feb	0.2	11.3	47.5	41.0
2sd Feb	0.1	13.2	44.3	42.3
1st Mar	0.1	13.6	46.7	39.7
2sd Mar	0.2	17.9	41.8	40.1
1st Apr	0.0	12.6	45.3	42.0
2sd Apr	0.0	5.8	42.5	51.7
1st May	0.0	3.3	33.1	63.5
2sd May	0.0	2.6	29.1	68.3
1st Jun	0.0	4.7	25.2	70.2
2sd Jun	0.0	1.9	18.9	79.2
1st Jul	0.0	1.0	13.5	85.5
2sd Jul	0.0	0.2	11.5	88.4
1st Aug	0.0	0.1	14.1	85.8
2sd Aug	0.0	0.4	21.0	78.6
1st Sep	0.0	1.6	20.9	77.5
2sd Sep	0.0	1.7	28.9	69.5
1st Oct	0.0	4.4	37.2	58.3
2sd Oct	0.0	2.9	39.2	57.9
1st Nov	0.0	7.0	43.6	49.4
2sd Nov	0.0	8.1	47.7	44.2
1st Dec	0.0	9.0	46.0	45.0
2sd Dec	0.1	8.8	51.0	40.1

Supplementary Table 8: Percentage of the total surface area in Spain showing positive or negative, significant or non-significant Pearson's r correlations between the sNDVI and the SPEI. Broad-leaved forests

	Negative ($p < 0.05$)	Negative ($p > 0.05$)	Positive ($p > 0.05$)	Positive ($p < 0.05$)
1st Jan	0.4	15.9	46.0	37.7
2nd Jan	0.6	15.1	47.0	37.3
1st Feb	0.3	11.3	45.2	43.3
2sd Feb	0.2	12.1	45.5	42.2
1st Mar	0.3	14.2	51.1	34.5
2sd Mar	0.2	14.0	48.4	37.3
1st Apr	0.0	10.2	48.7	41.1
2sd Apr	0.0	4.8	42.2	53.0
1st May	0.0	2.9	32.7	64.4
2sd May	0.0	1.4	27.2	71.4
1st Jun	0.0	1.5	19.9	78.6
2sd Jun	0.0	0.8	13.6	85.6
1st Jul	0.0	0.3	9.6	90.0
2sd Jul	0.0	0.1	7.2	92.7
1st Aug	0.0	0.1	8.2	91.7
2sd Aug	0.0	0.5	20.3	79.2
1st Sep	0.0	1.6	26.4	72.0
2sd Sep	0.0	0.9	31.3	67.8
1st Oct	0.0	3.7	37.9	58.3
2sd Oct	0.0	5.6	42.8	51.7
1st Nov	0.1	10.8	47.3	41.8
2sd Nov	0.1	9.5	51.2	39.2
1st Dec	0.1	9.5	48.0	42.3
2sd Dec	0.3	10.8	49.2	39.8

Supplementary Table 9: Percentage of the total surface area in Spain showing positive or negative, significant or non-significant Pearson's r correlations between the sNDVI and the SPEI. Coniferous forests

	Negative ($p < 0.05$)	Negative ($p > 0.05$)	Positive ($p > 0.05$)	Positive ($p < 0.05$)
1st Jan	0.9	19.6	53.6	25.9
2nd Jan	1.8	18.4	55.6	24.2
1st Feb	1.5	17.2	55.5	25.8
2sd Feb	0.1	17.8	59.8	22.2
1st Mar	0.1	16.4	62.9	20.7
2sd Mar	0.8	20.8	60.1	18.3
1st Apr	0.0	12.7	62.7	24.6
2sd Apr	0.0	5.4	50.4	44.2
1st May	0.0	3.5	39.4	57.0
2sd May	0.0	1.7	31.3	66.9
1st Jun	0.0	2.8	26.0	71.2
2sd Jun	0.0	1.9	20.5	77.6
1st Jul	0.0	0.4	14.4	85.1
2sd Jul	0.0	0.0	9.7	90.2
1st Aug	0.0	0.1	10.6	89.2
2sd Aug	0.0	0.8	21.5	77.6
1st Sep	0.0	0.9	24.8	74.3
2sd Sep	0.0	0.9	27.4	71.7
1st Oct	0.0	4.1	47.2	48.6
2sd Oct	0.0	6.0	52.8	41.2
1st Nov	0.1	13.4	47.3	39.1
2sd Nov	0.1	12.4	57.6	29.9
1st Dec	0.1	11.9	64.8	23.2
2sd Dec	0.2	13.4	61.4	25.0

Supplementary Table 10: Percentage of the total surface area in Spain showing positive or negative, significant or non-significant Pearson's r correlations between the sNDVI and the SPEI. Mixed forests

	Negative ($p < 0.05$)	Negative ($p > 0.05$)	Positive ($p > 0.05$)	Positive ($p < 0.05$)
1st Jan	1.7	16.2	34.3	47.8
2nd Jan	2.0	13.1	33.2	51.7
1st Feb	1.2	11.5	33.4	54.0
2sd Feb	1.0	11.8	29.5	57.7
1st Mar	1.4	12.2	27.6	58.8
2sd Mar	0.5	13.3	26.5	59.7
1st Apr	0.0	9.1	25.7	65.2
2sd Apr	0.0	2.7	23.2	74.1
1st May	0.0	2.2	16.5	81.3
2sd May	0.0	1.8	13.7	84.4
1st Jun	0.0	2.5	10.7	86.7
2sd Jun	0.0	1.8	7.8	90.4
1st Jul	0.1	1.4	6.5	92.0
2sd Jul	0.0	0.8	6.0	93.1
1st Aug	0.0	0.1	6.8	93.1
2sd Aug	0.0	0.2	10.8	88.9
1st Sep	0.0	0.2	12.4	87.3
2sd Sep	0.0	0.2	13.7	86.0
1st Oct	0.0	1.4	18.9	79.7
2sd Oct	0.0	1.7	22.4	75.9
1st Nov	0.0	6.5	26.7	66.8
2sd Nov	0.2	6.7	32.0	61.1
1st Dec	0.3	7.6	28.7	63.4
2sd Dec	1.3	10.8	36.2	51.8

Supplementary Table 11: Percentage of the total surface area in Spain showing positive or negative, significant or non-significant Pearson's r correlations between the sNDVI and the SPEI. Natural grassland

	Negative ($p < 0.05$)	Negative ($p > 0.05$)	Positive ($p > 0.05$)	Positive ($p < 0.05$)
1st Jan	0.1	7.8	37.4	54.7
2nd Jan	0.1	6.2	36.9	56.8
1st Feb	0.1	4.3	35.6	60.0
2sd Feb	0.0	4.0	33.1	62.9
1st Mar	0.1	5.0	37.8	57.2
2sd Mar	0.1	5.7	34.2	60.0
1st Apr	0.0	5.0	29.8	65.1
2sd Apr	0.0	1.8	21.5	76.7
1st May	0.0	1.1	15.1	83.8
2sd May	0.0	0.4	9.4	90.2
1st Jun	0.0	0.1	4.0	95.9
2sd Jun	0.0	0.0	1.8	98.1
1st Jul	0.0	0.0	1.2	98.8
2sd Jul	0.0	0.0	1.2	98.8
1st Aug	0.0	0.0	2.2	97.8
2sd Aug	0.0	0.1	5.7	94.2
1st Sep	0.0	0.2	8.8	91.1
2sd Sep	0.0	0.2	10.7	89.2
1st Oct	0.0	0.6	15.8	83.6
2sd Oct	0.0	0.9	21.4	77.8
1st Nov	0.0	3.1	28.6	68.3
2sd Nov	0.0	3.2	33.7	63.2
1st Dec	0.0	2.8	31.5	65.8
2sd Dec	0.0	4.7	37.4	57.8

Supplementary Table 12: Percentage of the total surface area in Spain showing positive or negative, significant or non-significant Pearson's r correlations between the sNDVI and the SPEI. Sclerophillous vegetation

	Negative ($p < 0.05$)	Negative ($p > 0.05$)	Positive ($p > 0.05$)	Positive ($p < 0.05$)
1st Jan	0.1	11.7	44.0	44.1
2nd Jan	0.2	9.9	44.1	45.9
1st Feb	0.1	6.8	43.4	49.6
2sd Feb	0.1	6.5	42.6	50.8
1st Mar	0.1	8.1	45.0	46.9
2sd Mar	0.2	10.1	42.9	46.8
1st Apr	0.0	7.7	40.2	52.1
2sd Apr	0.0	2.9	30.3	66.8
1st May	0.0	1.9	23.1	75.0
2sd May	0.0	0.9	17.4	81.7
1st Jun	0.0	0.8	11.7	87.5
2sd Jun	0.0	0.5	7.3	92.2
1st Jul	0.0	0.1	3.7	96.2
2sd Jul	0.0	0.0	2.6	97.3
1st Aug	0.0	0.0	3.9	96.1
2sd Aug	0.0	0.1	8.9	91.0
1st Sep	0.0	0.3	13.4	86.3
2sd Sep	0.0	0.2	18.9	80.9
1st Oct	0.0	1.5	28.5	70.0
2sd Oct	0.0	2.5	33.0	64.5
1st Nov	0.0	5.3	37.1	57.6
2sd Nov	0.0	4.7	43.3	52.0
1st Dec	0.0	4.5	42.8	52.7
2sd Dec	0.1	7.0	46.8	46.1

Supplementary Table 13: Percentage of the total surface area in Spain showing positive or negative, significant or non-significant Pearson's r correlations between the sNDVI and the SPEI. Transition wood-scrub.

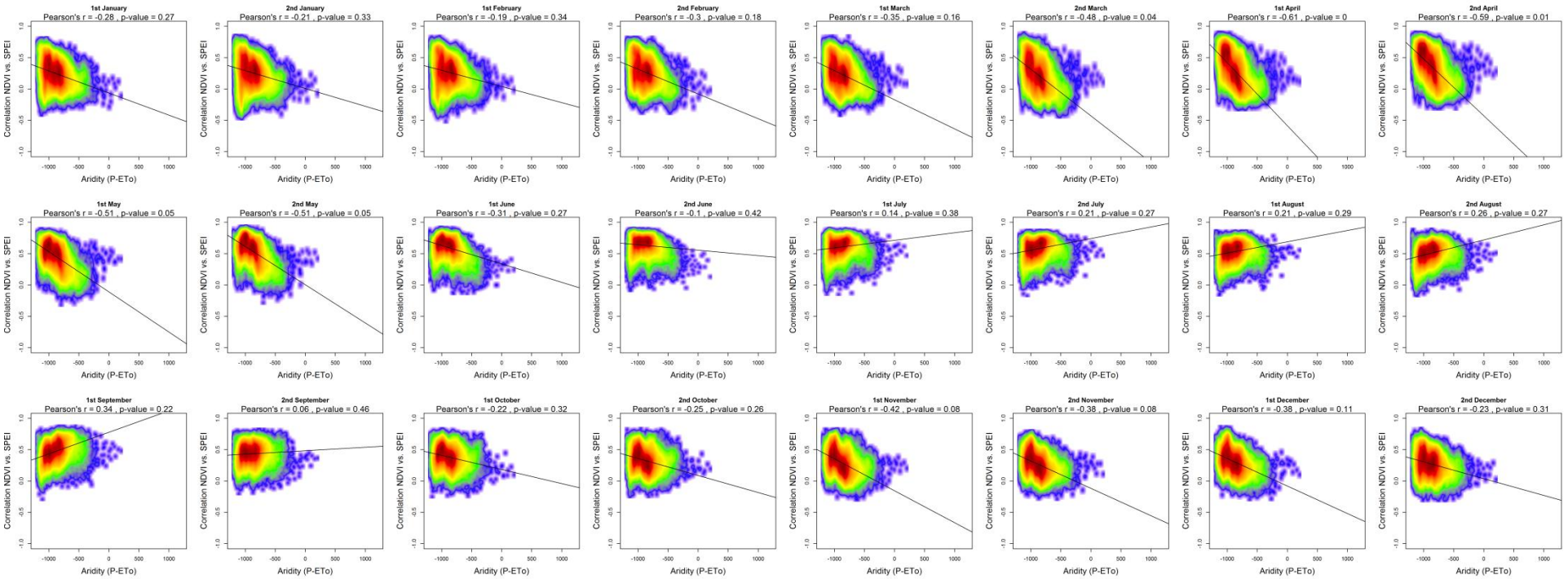

Supplementary Figure 45: Relationship between the average aridity (P-ETo) and the maximum correlations obtained between NDVI and the SPEI during the 24 semi-monthly periods of the year. Non Irrigated arable lands. Given the high number of points the signification of correlation was obtained by means of 1000 random samples of 30 cases from which correlations and p-values were obtained. The final signification was assessed by means of the average of the obtained p-values.

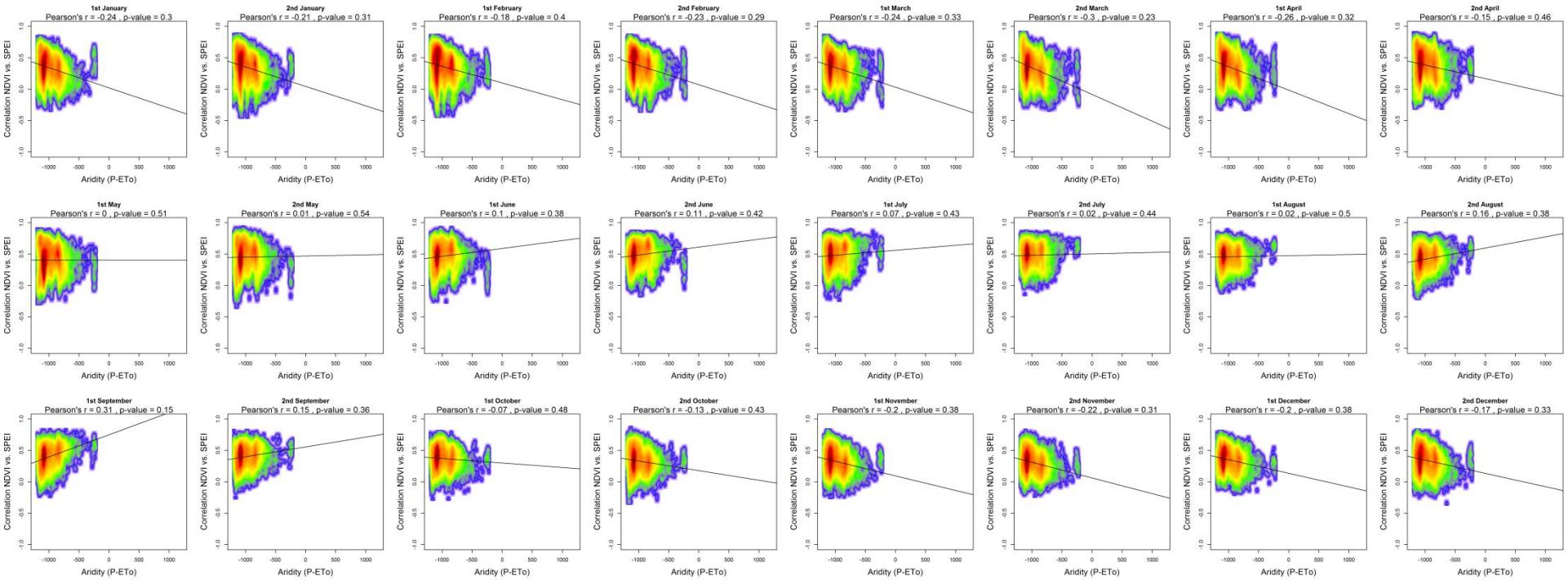

Supplementary Figure 46: Relationship between the average aridity (P-ETo) and the maximum correlations obtained between NDVI and the SPEI during the 24 semi-monthly periods of the year. Irrigated lands. Given the high number of points the signification of correlation was obtained by means of 1000 random samples of 30 cases from which correlations and p-values were obtained. The final signification was assessed by means of the average of the obtained p-values.

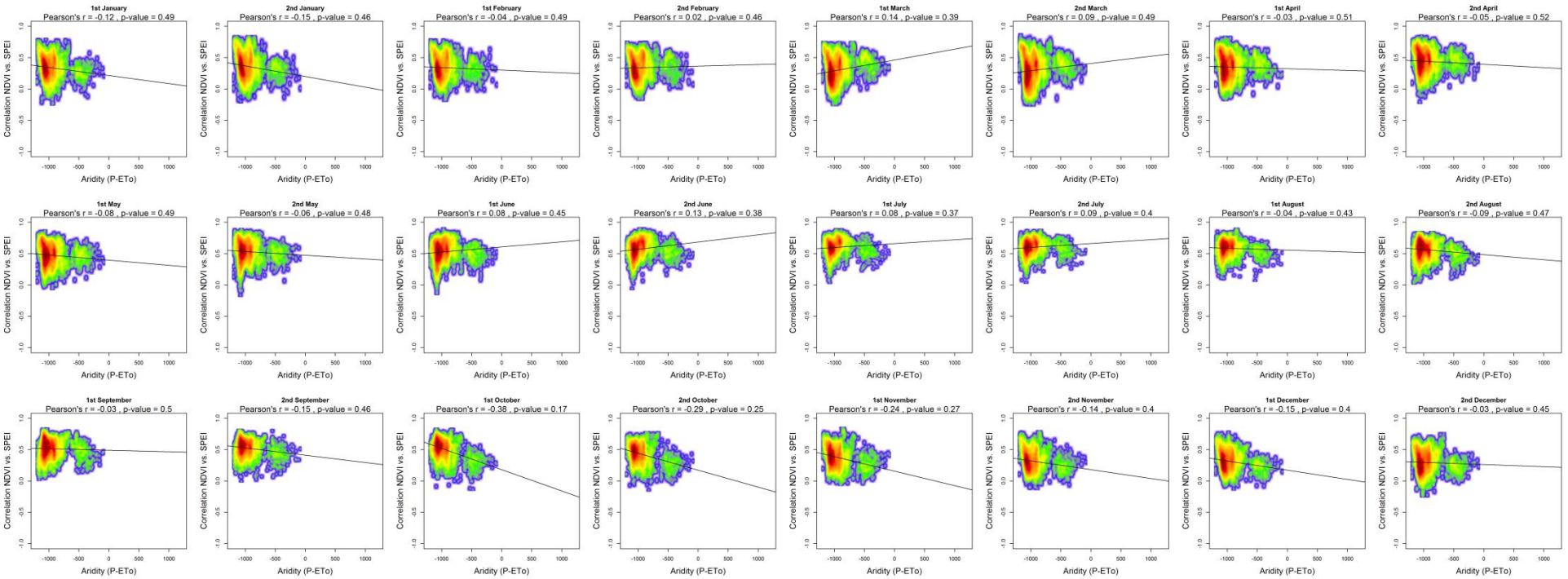

Supplementary Figure 47: Relationship between the average aridity (P-ETo) and the maximum correlations obtained between NDVI and the SPEI during the 24 semi-monthly periods of the year. Vineyards. Given the high number of points the signification of correlation was obtained by means of 1000 random samples of 30 cases from which correlations and p-values were obtained. The final signification was assessed by means of the average of the obtained p-values.

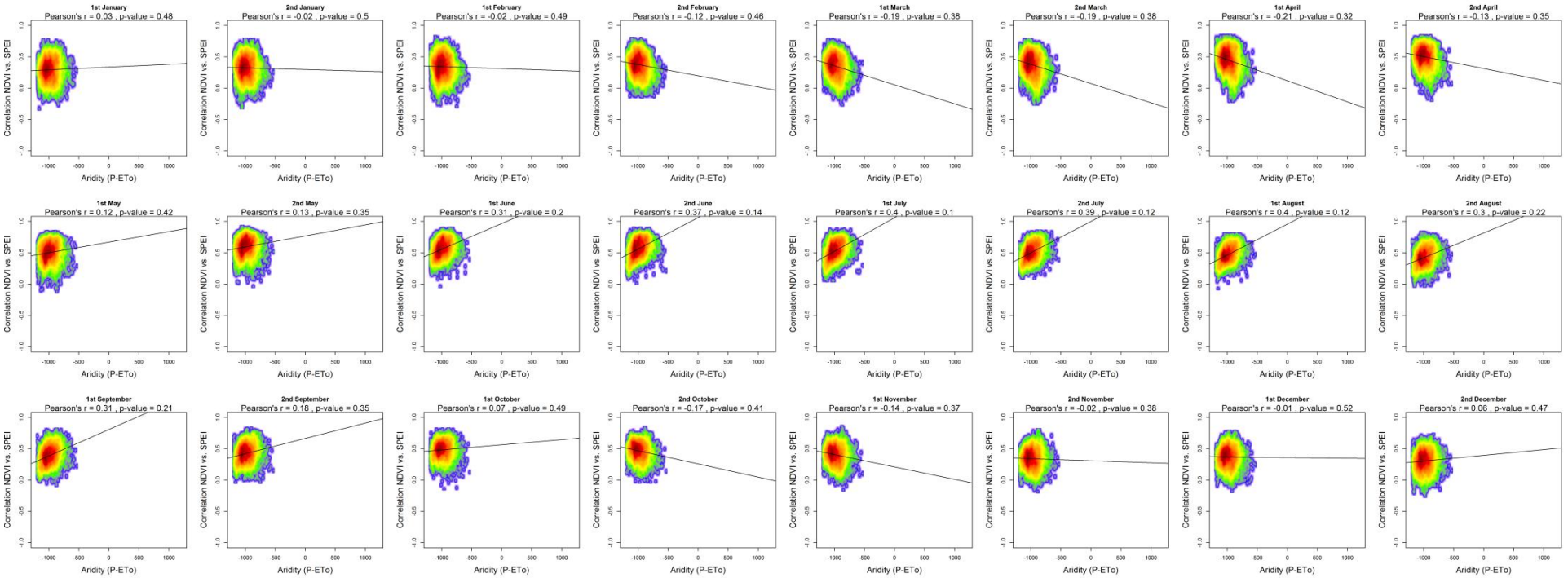

Supplementary Figure 48: Relationship between the average aridity (P-ETo) and the maximum correlations obtained between NDVI and the SPEI during the 24 semi-monthly periods of the year. Olive groves. Given the high number of points the signification of correlation was obtained by means of 1000 random samples of 30 cases from which correlations and p-values were obtained. The final signification was assessed by means of the average of the obtained p-values.

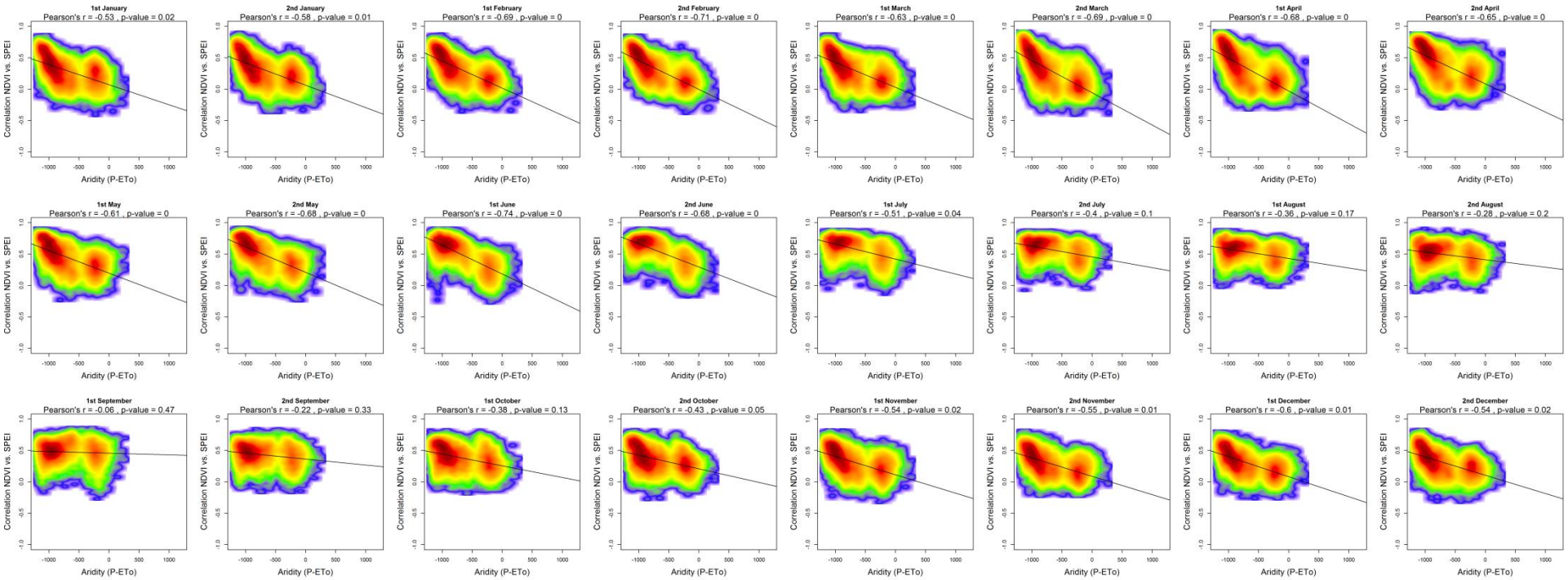

Supplementary Figure 49: Relationship between the average aridity (P-ETo) and the maximum correlations obtained between NDVI and the SPEI during the 24 semi-monthly periods of the year. Mixed agriculture/natural vegetation. Given the high number of points the signification of correlation was obtained by means of 1000 random samples of 30 cases from which correlations and p-values were obtained. The final signification was assessed by means of the average of the obtained p-values.

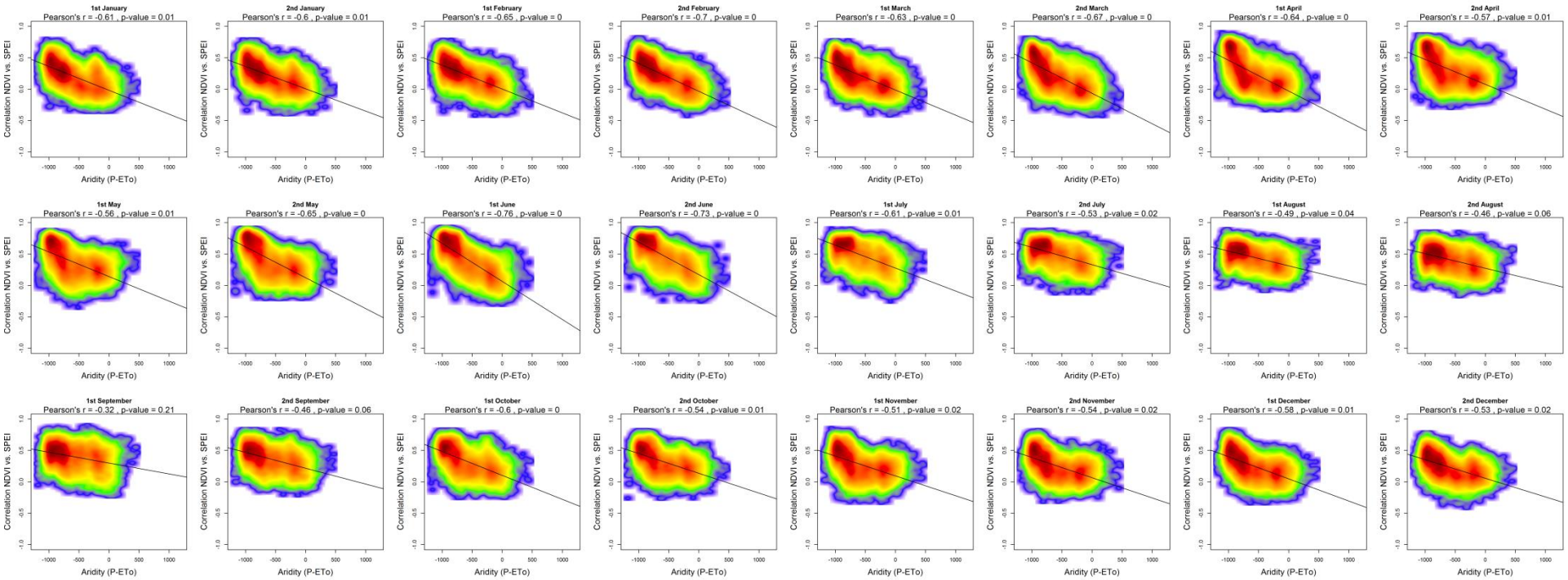

Supplementary Figure 50: Relationship between the average aridity (P-ETo) and the maximum correlations obtained between NDVI and the SPEI during the 24 semi-monthly periods of the year. Broad-leaved forests. Given the high number of points the signification of correlation was obtained by means of 1000 random samples of 30 cases from which correlations and p-values were obtained. The final signification was assessed by means of the average of the obtained p-values.

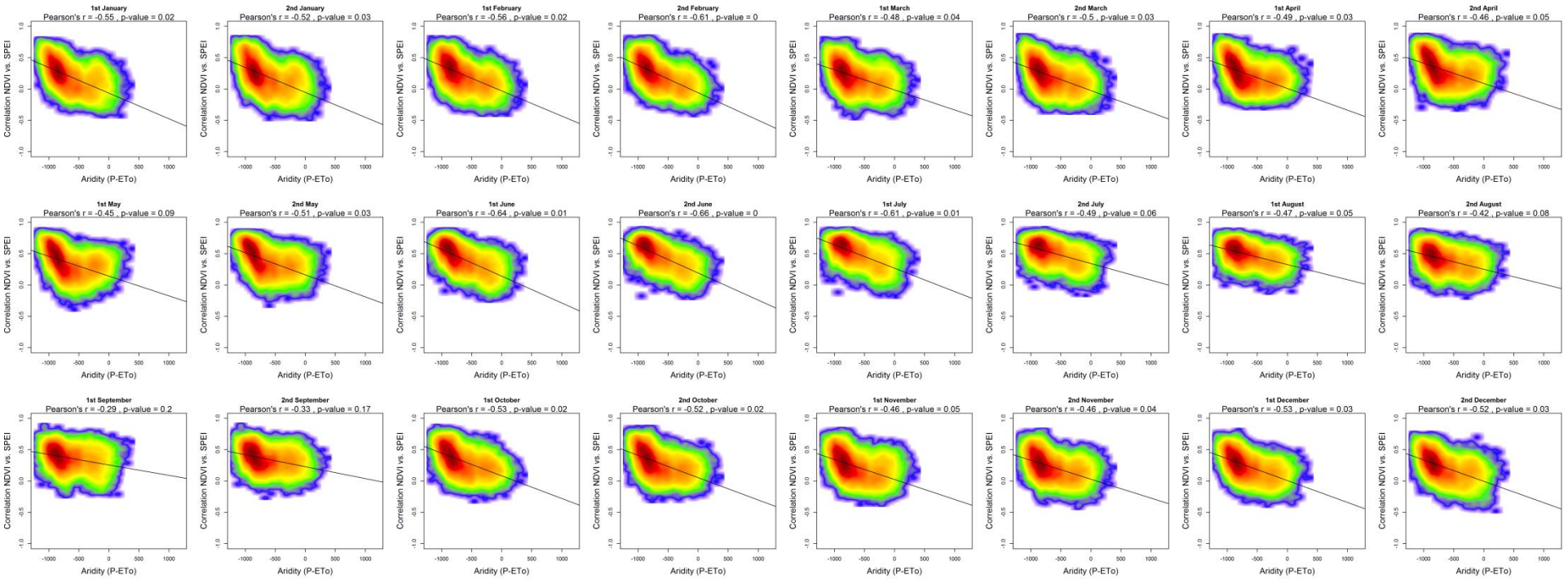

Supplementary Figure 51: Relationship between the average aridity (P-ETo) and the maximum correlations obtained between NDVI and the SPEI during the 24 semi-monthly periods of the year. Coniferous forests. Given the high number of points the signification of correlation was obtained by means of 1000 random samples of 30 cases from which correlations and p-values were obtained. The final signification was assessed by means of the average of the obtained p-values.

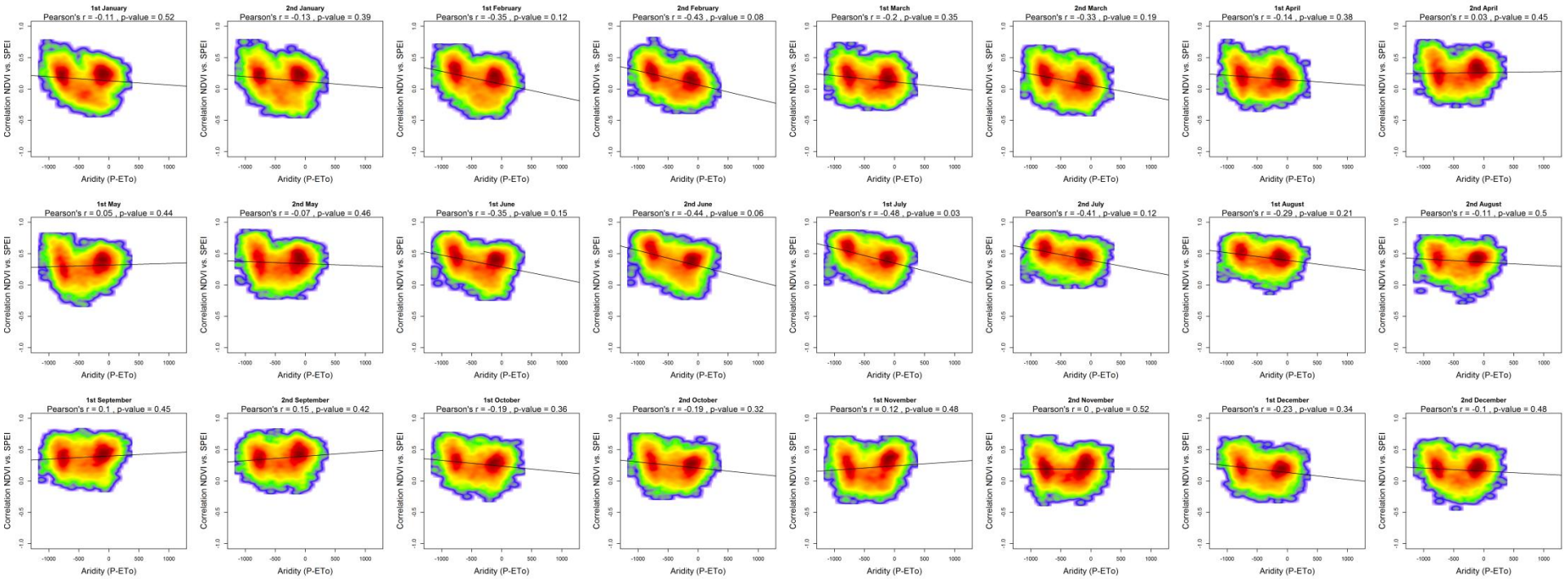

Supplementary Figure 52: Relationship between the average aridity (P-ETo) and the maximum correlations obtained between NDVI and the SPEI during the 24 semi-monthly periods of the year. Mixed forests. Given the high number of points the signification of correlation was obtained by means of 1000 random samples of 30 cases from which correlations and p-values were obtained. The final signification was assessed by means of the average of the obtained p-values.

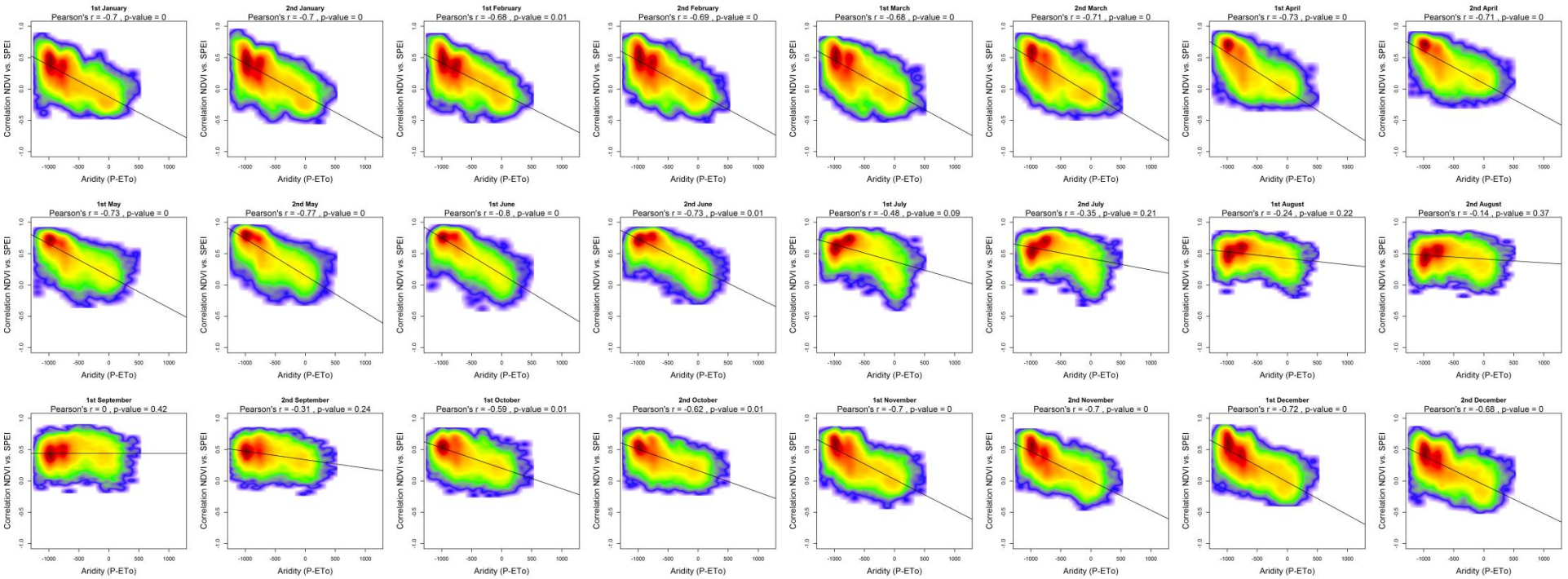

Supplementary Figure 53: Relationship between the average aridity (P-ETo) and the maximum correlations obtained between NDVI and the SPEI during the 24 semi-monthly periods of the year. Natural grasslands. Given the high number of points the signification of correlation was obtained by means of 1000 random samples of 30 cases from which correlations and p-values were obtained. The final signification was assessed by means of the average of the obtained p-values.

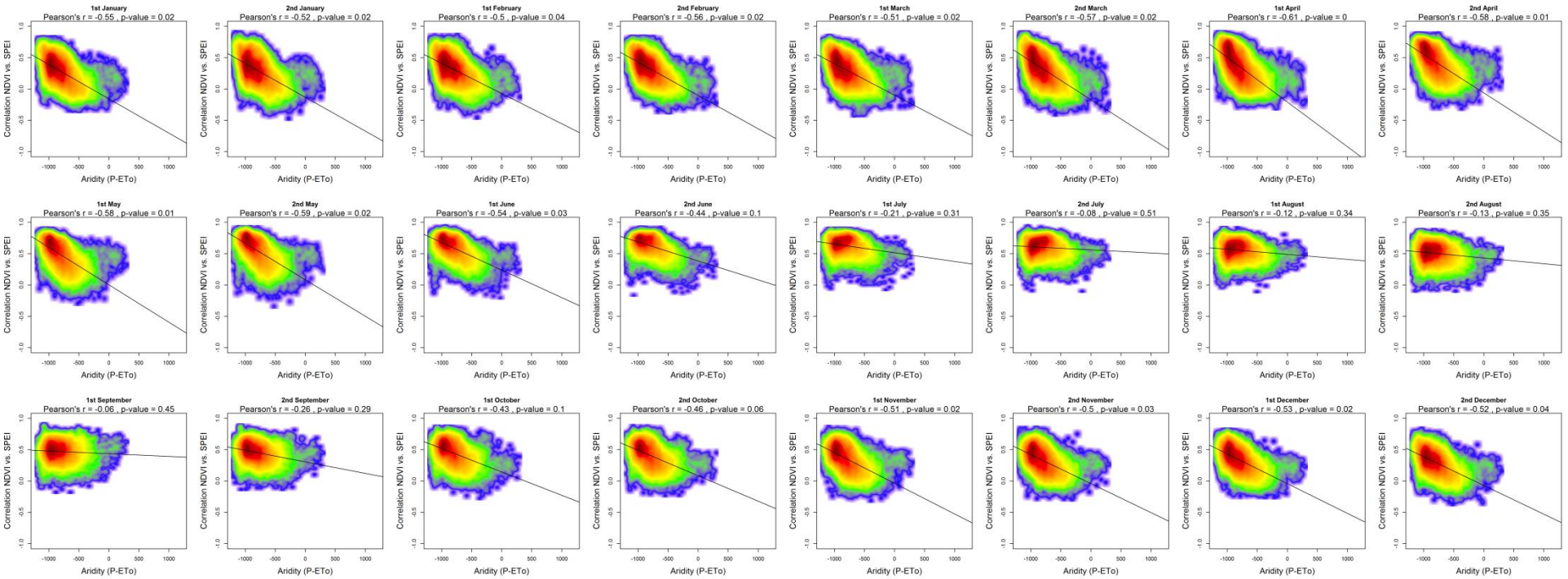

Supplementary Figure 54: Relationship between the average aridity (P-ETo) and the maximum correlations obtained between NDVI and the SPEI during the 24 semi-monthly periods of the year. Sclerophillous vegetation. Given the high number of points the signification of correlation was obtained by means of 1000 random samples of 30 cases from which correlations and p-values were obtained. The final signification was assessed by means of the average of the obtained p-values.

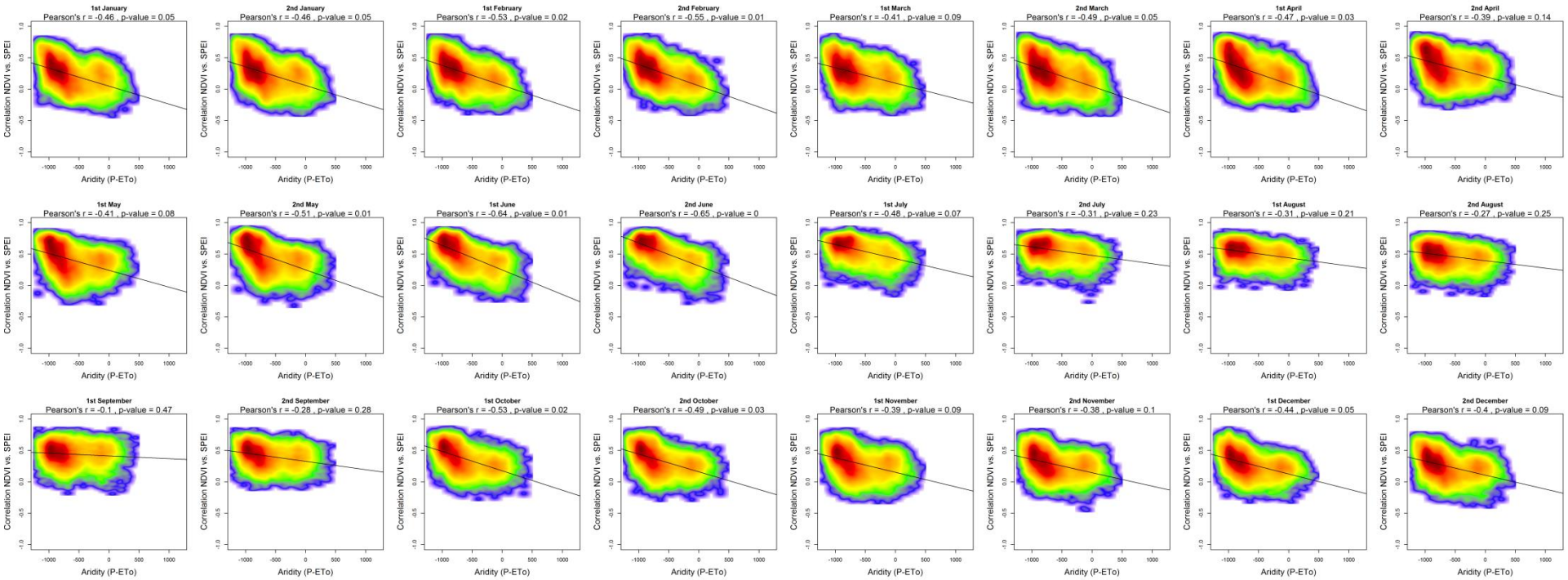

Supplementary Figure 55: Relationship between the average aridity (P-ETo) and the maximum correlations obtained between NDVI and the SPEI during the 24 semi-monthly periods of the year. Transition wood-scrub. Given the high number of points the signification of correlation was obtained by means of 1000 random samples of 30 cases from which correlations and p-values were obtained. The final signification was assessed by means of the average of the obtained p-values.

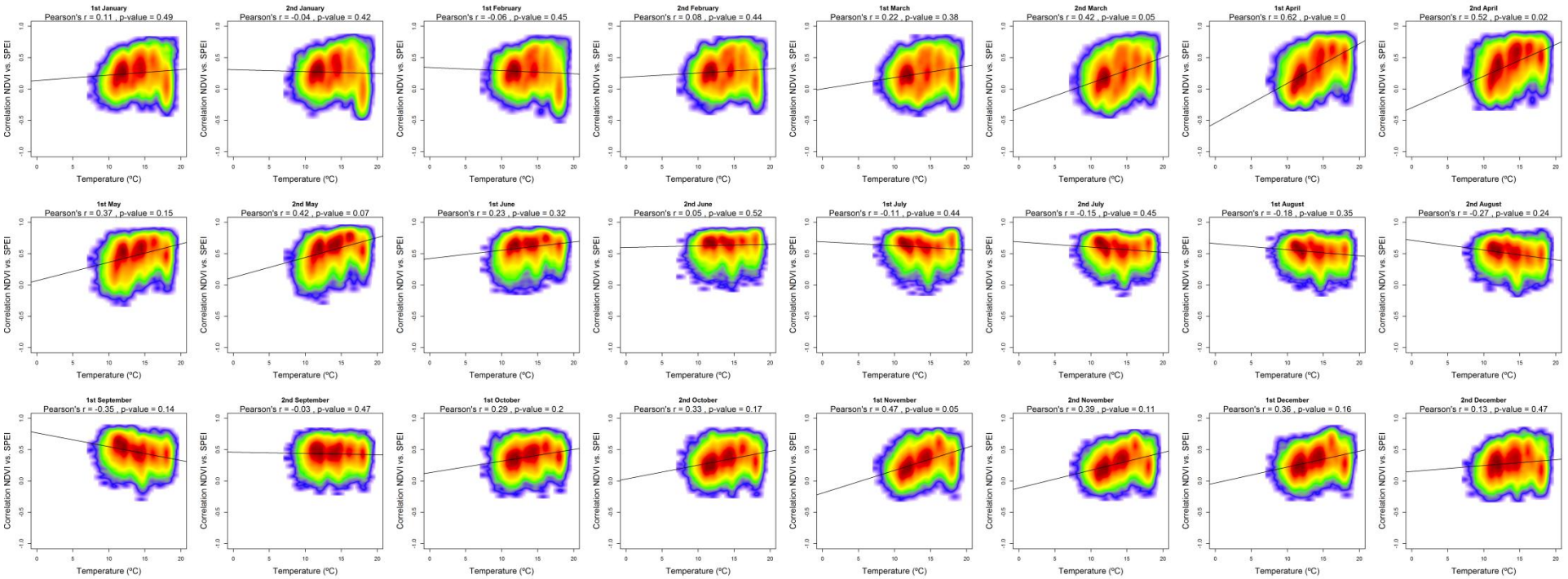

Supplementary Figure 56: Relationship between the average temperature and the maximum correlations obtained between NDVI and the SPEI during the 24 semi-monthly periods of the year. Non Irrigated arable lands. Given the high number of points the signification of correlation was obtained by means of 1000 random samples of 30 cases from which correlations and p-values were obtained. The final signification was assessed by means of the average of the obtained p-values.

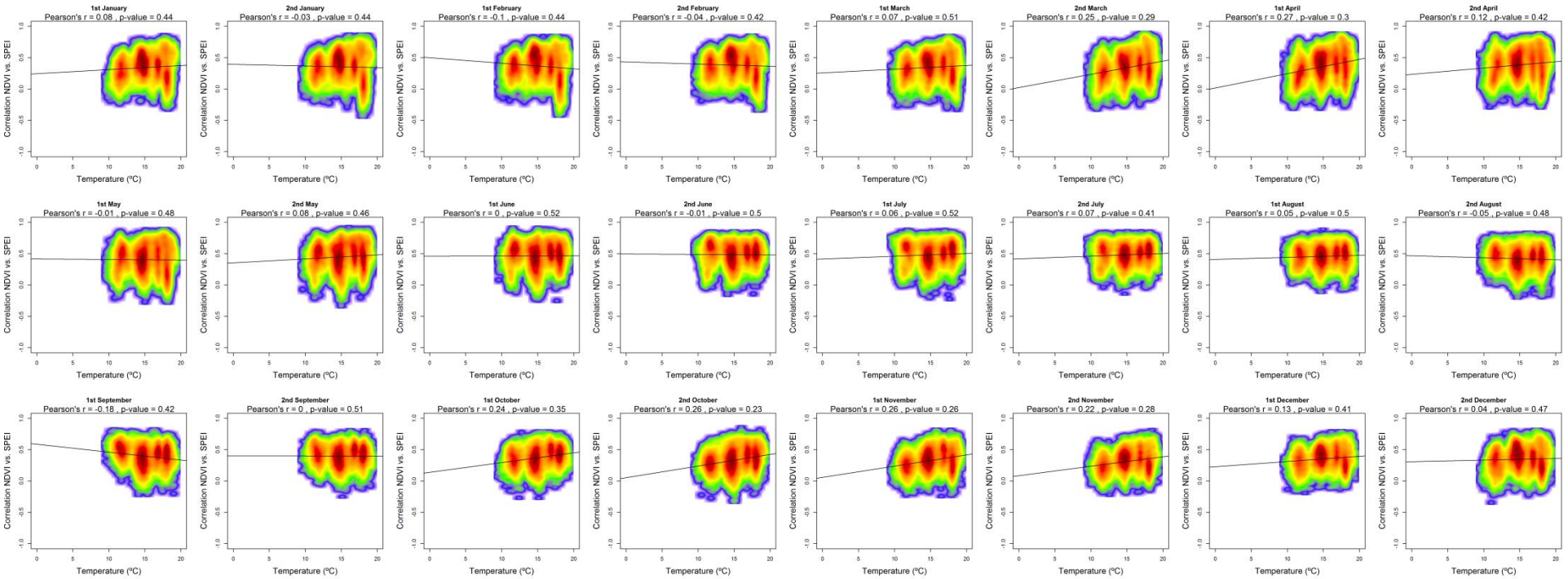

Supplementary Figure 57: Relationship between the average temperature and the maximum correlations obtained between NDVI and the SPEI during the 24 semi-monthly periods of the year. Irrigated lands. Given the high number of points the signification of correlation was obtained by means of 1000 random samples of 30 cases from which correlations and p-values were obtained. The final signification was assessed by means of the average of the obtained p-values.

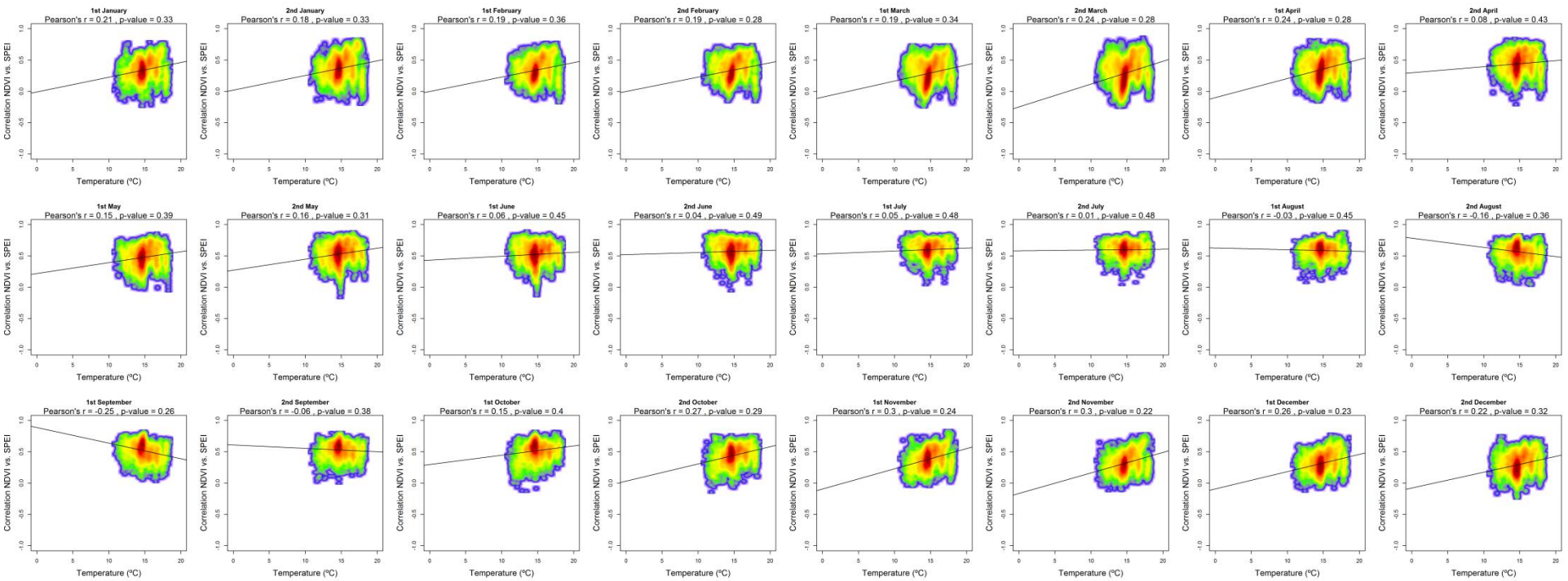

Supplementary Figure 58: Relationship between the average temperature and the maximum correlations obtained between NDVI and the SPEI during the 24 semi-monthly periods of the year. Vineyeards. Given the high number of points the signification of correlation was obtained by means of 1000 random samples of 30 cases from which correlations and p-values were obtained. The final signification was assessed by means of the average of the obtained p-values.

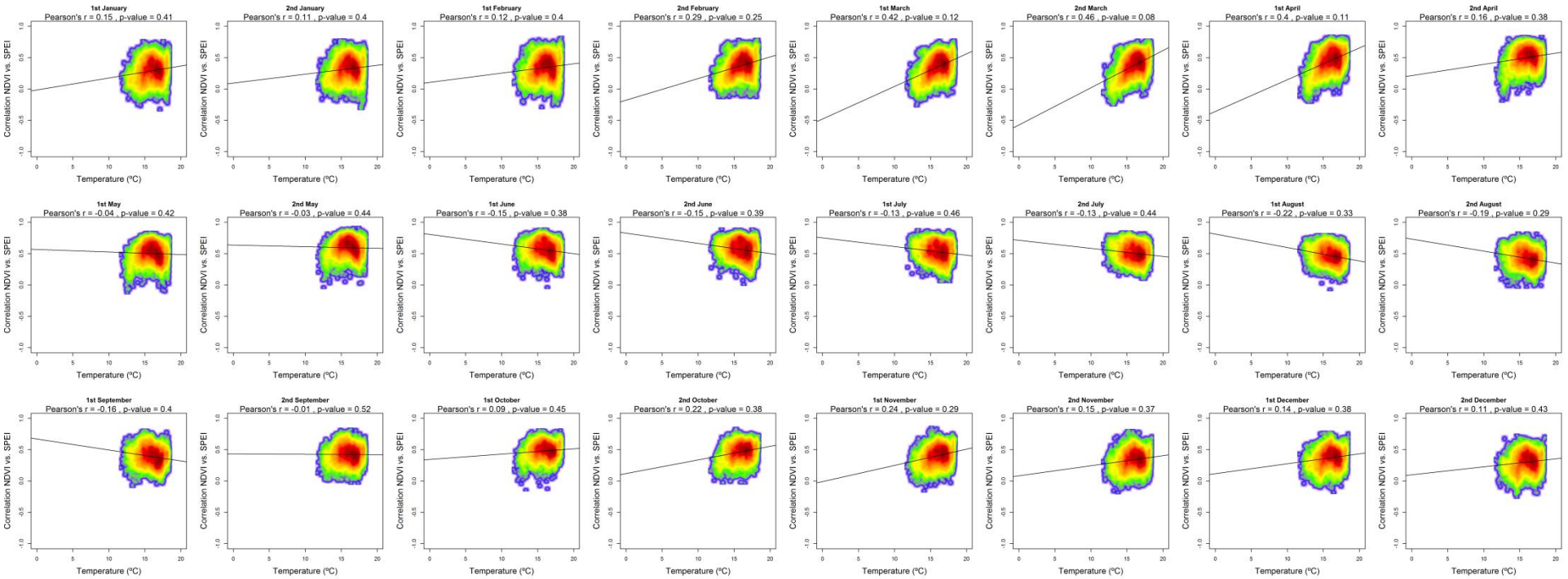

Supplementary Figure 59: Relationship between the average temperature and the maximum correlations obtained between NDVI and the SPEI during the 24 semi-monthly periods of the year. Olive groves. Given the high number of points the signification of correlation was obtained by means of 1000 random samples of 30 cases from which correlations and p-values were obtained. The final signification was assessed by means of the average of the obtained p-values.

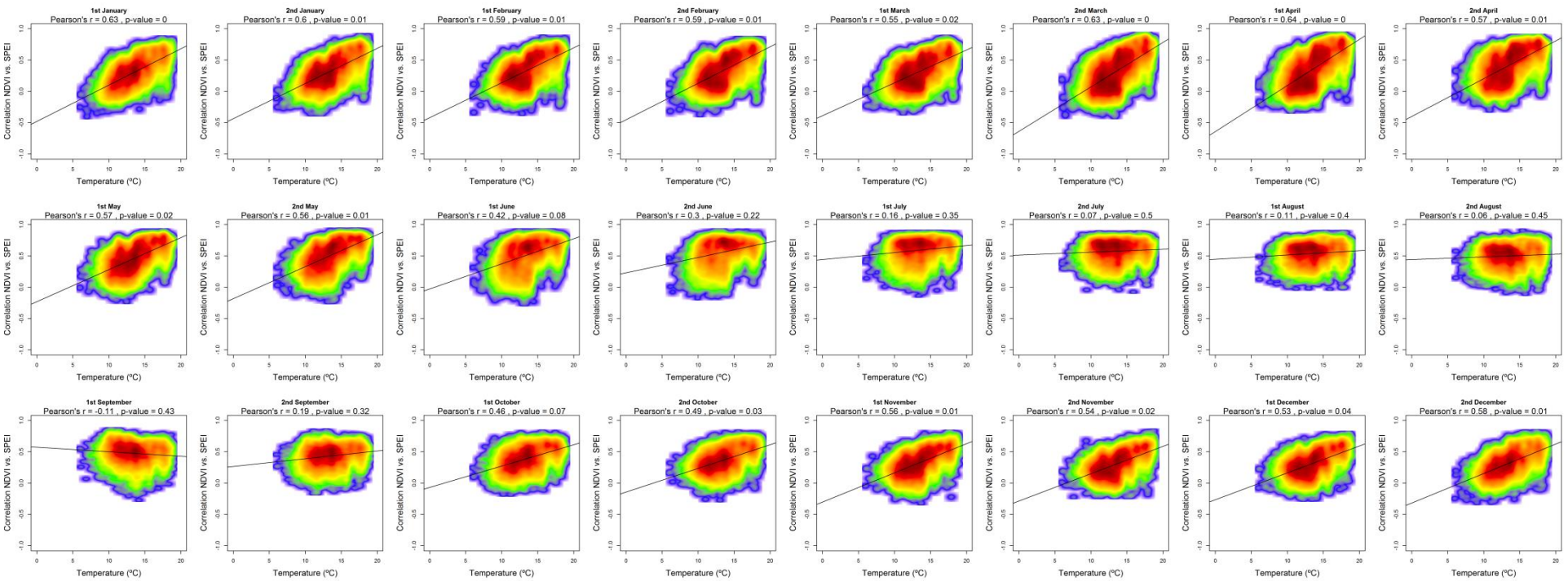

Supplementary Figure 60: Relationship between the average temperature and the maximum correlations obtained between NDVI and the SPEI during the 24 semi-monthly periods of the year. Mixed agriculture/natural vegetation. Given the high number of points the signification of correlation was obtained by means of 1000 random samples of 30 cases from which correlations and p-values were obtained. The final signification was assessed by means of the average of the obtained p-values.

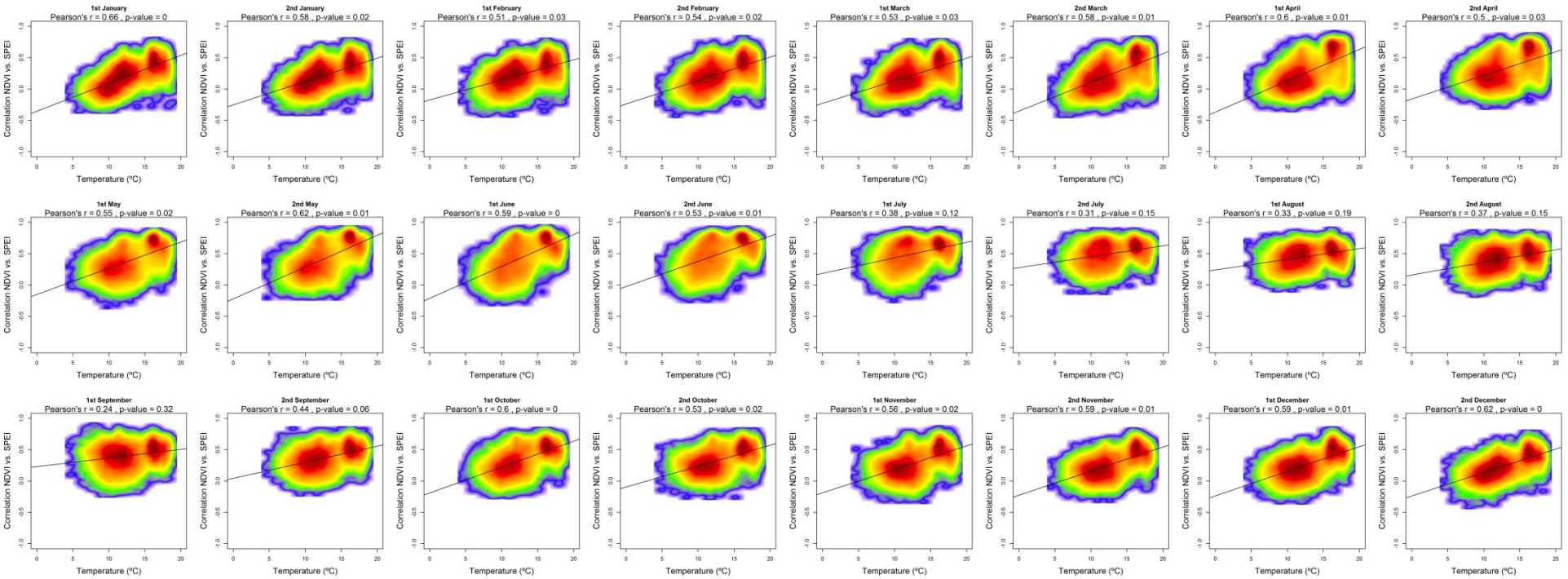

Supplementary Figure 61: Relationship between the average temperature and the maximum correlations obtained between NDVI and the SPEI during the 24 semi-monthly periods of the year. Broad-leaved forests. Given the high number of points the signification of correlation was obtained by means of 1000 random samples of 30 cases from which correlations and p-values were obtained. The final signification was assessed by means of the average of the obtained p-values.

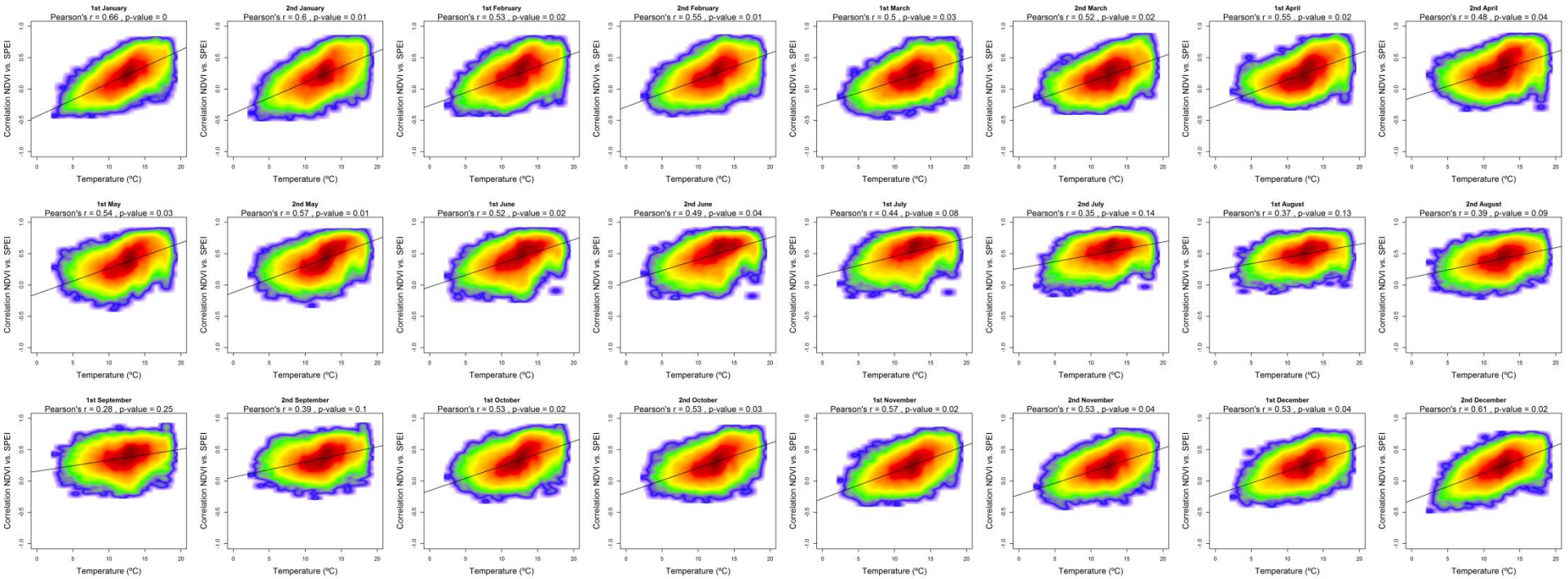

Supplementary Figure 62: Relationship between the average temperature and the maximum correlations obtained between NDVI and the SPEI during the 24 semi-monthly periods of the year. Coniferous forests. Given the high number of points the signification of correlation was obtained by means of 1000 random samples of 30 cases from which correlations and p-values were obtained. The final signification was assessed by means of the average of the obtained p-values.

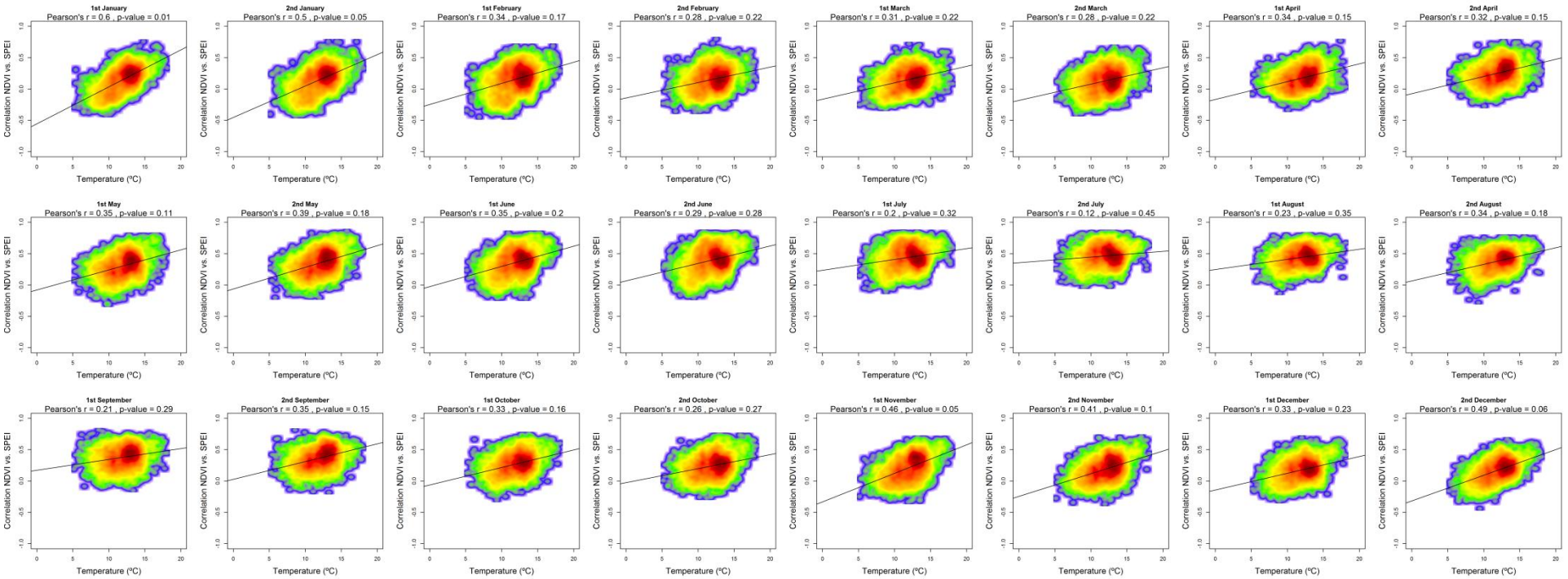

Supplementary Figure 63: Relationship between the average temperature and the maximum correlations obtained between NDVI and the SPEI during the 24 semi-monthly periods of the year. Mixed forests. Given the high number of points the signification of correlation was obtained by means of 1000 random samples of 30 cases from which correlations and p-values were obtained. The final signification was assessed by means of the average of the obtained p-values.

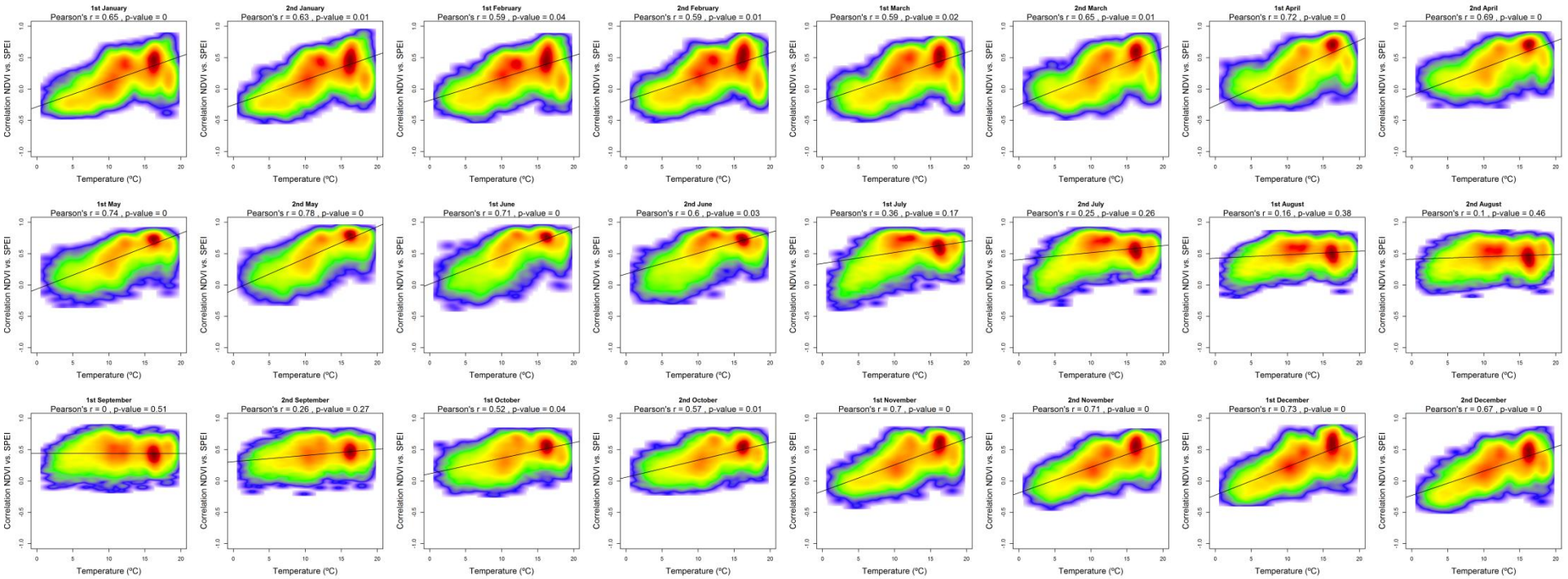

Supplementary Figure 64: Relationship between the average temperature and the maximum correlations obtained between NDVI and the SPEI during the 24 semi-monthly periods of the year. Natural grasslands. Given the high number of points the signification of correlation was obtained by means of 1000 random samples of 30 cases from which correlations and p-values were obtained. The final signification was assessed by means of the average of the obtained p-values.

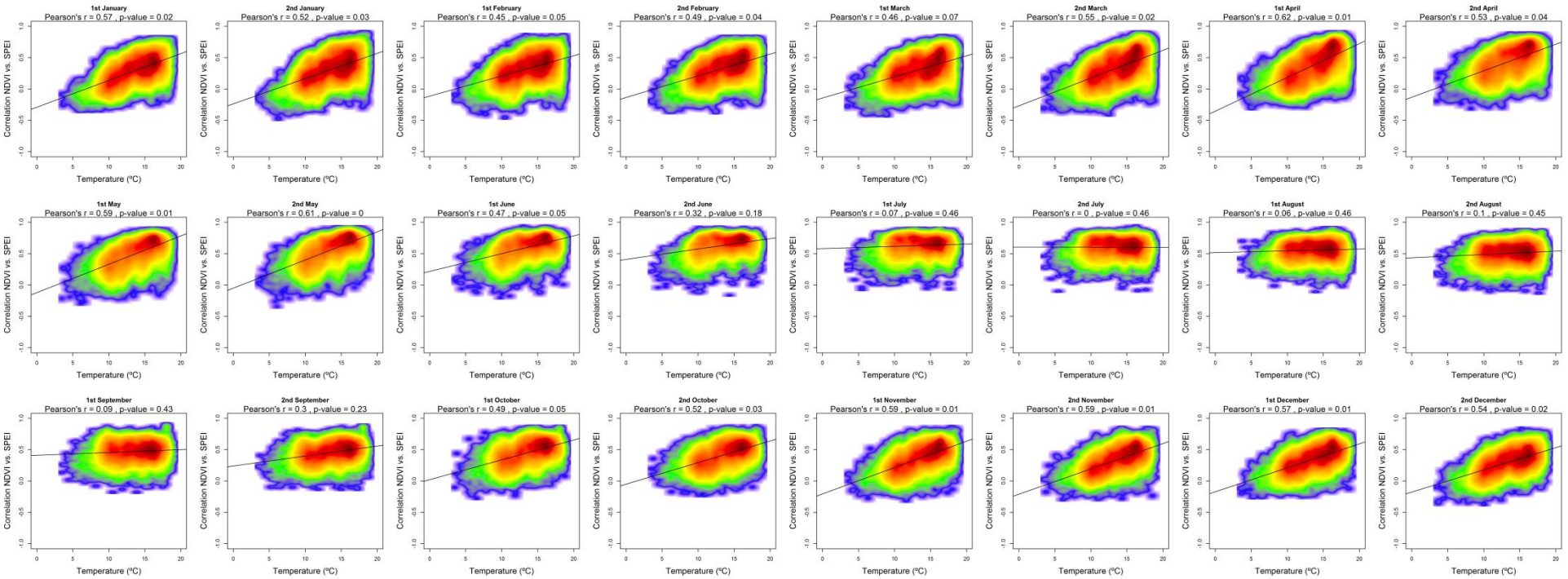

Supplementary Figure 65: Relationship between the average temperature and the maximum correlations obtained between NDVI and the SPEI during the 24 semi-monthly periods of the year. Sclerophillous vegetation. Given the high number of points the signification of correlation was obtained by means of 1000 random samples of 30 cases from which correlations and p-values were obtained. The final signification was assessed by means of the average of the obtained p-values.

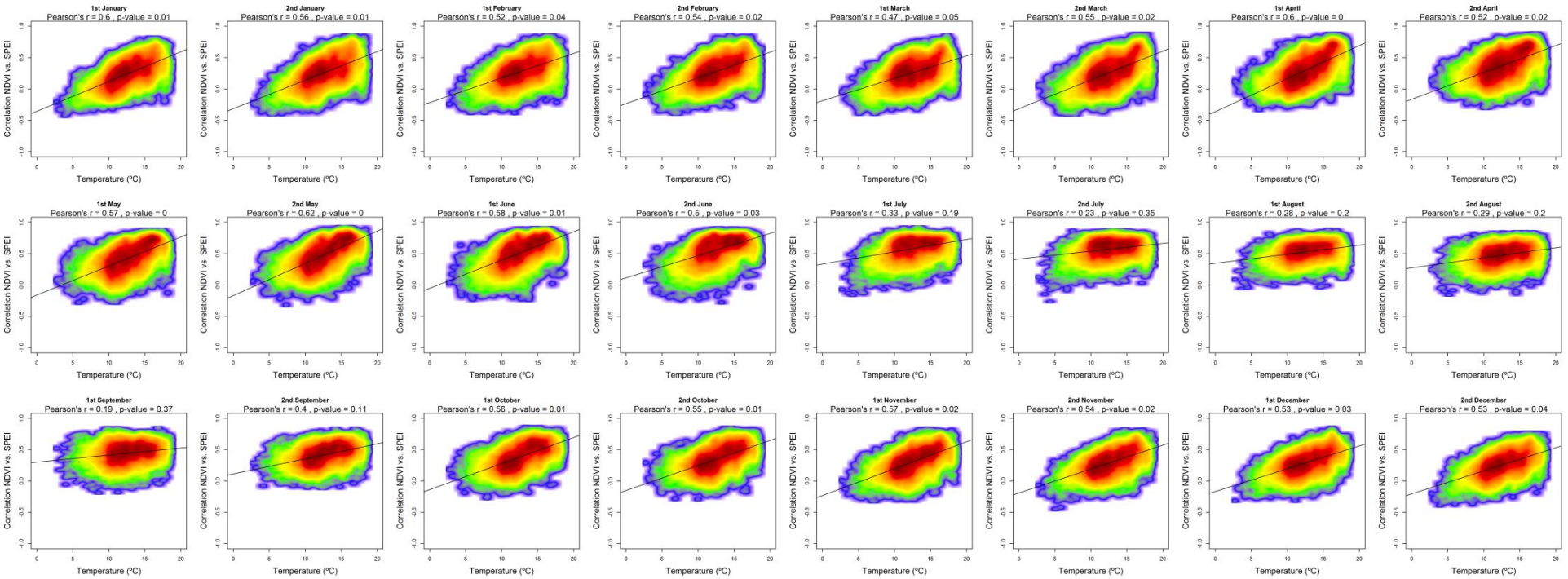

Supplementary Figure 66: Relationship between the average temperature and the maximum correlations obtained between NDVI and the SPEI during the 24 semi-monthly periods of the year. Transition wood-scrub. Given the high number of points the signification of correlation was obtained by means of 1000 random samples of 30 cases from which correlations and p-values were obtained. The final signification was assessed by means of the average of the obtained p-values.

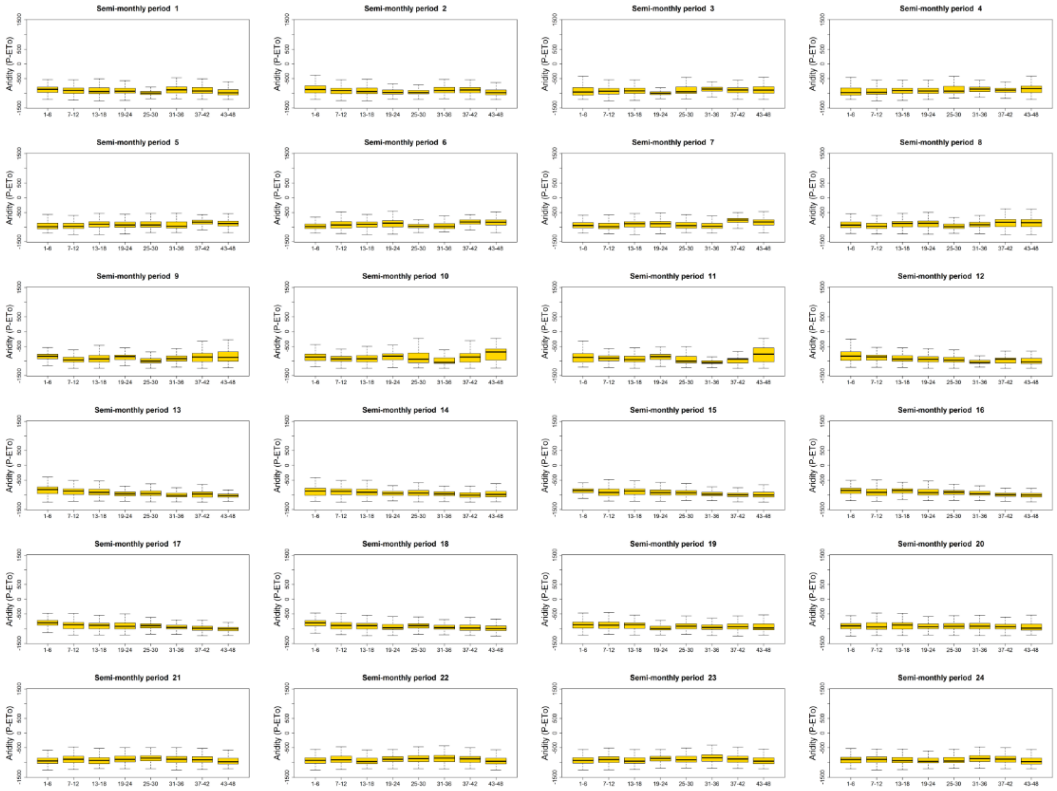

Supplementary Figure 67: Box-plots showing the values of aridity (P-ETo) for areas showing maximum correlation between SPEI and sNDVI on different time scales. Non irrigated arable lands.

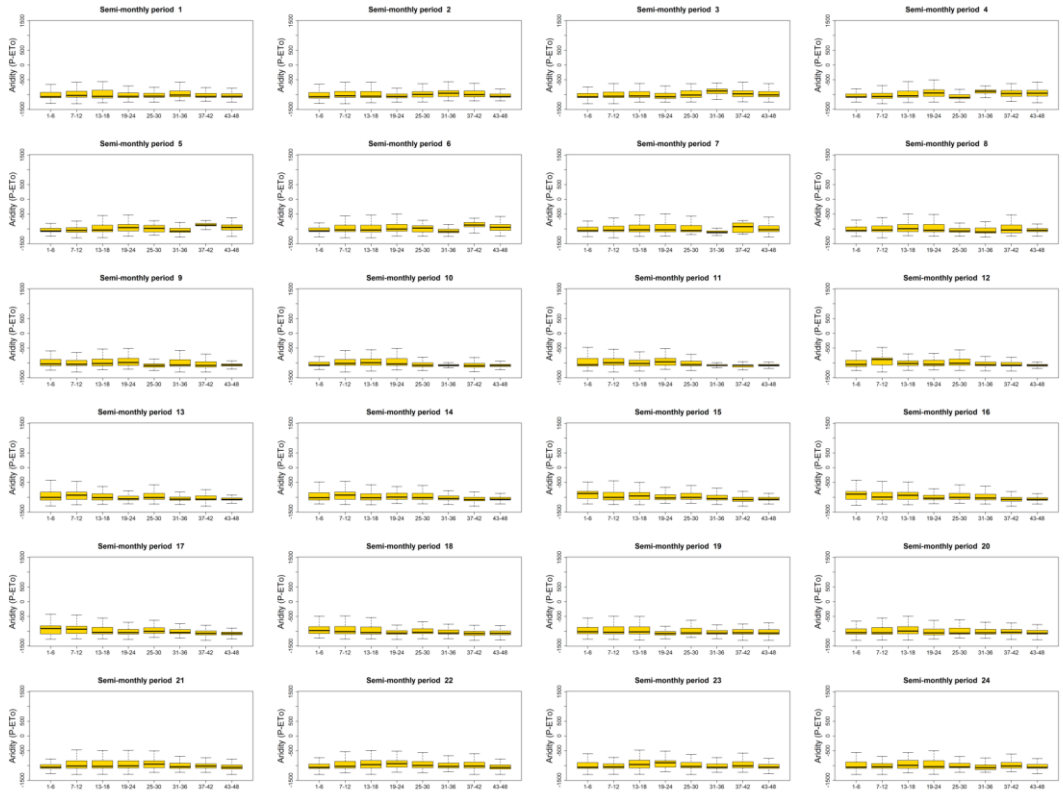

Supplementary Figure 68: Box-plots showing the values of aridity (P-ETo) for areas showing maximum correlation between SPEI and sNDVI on different time scales. Irrigated lands.

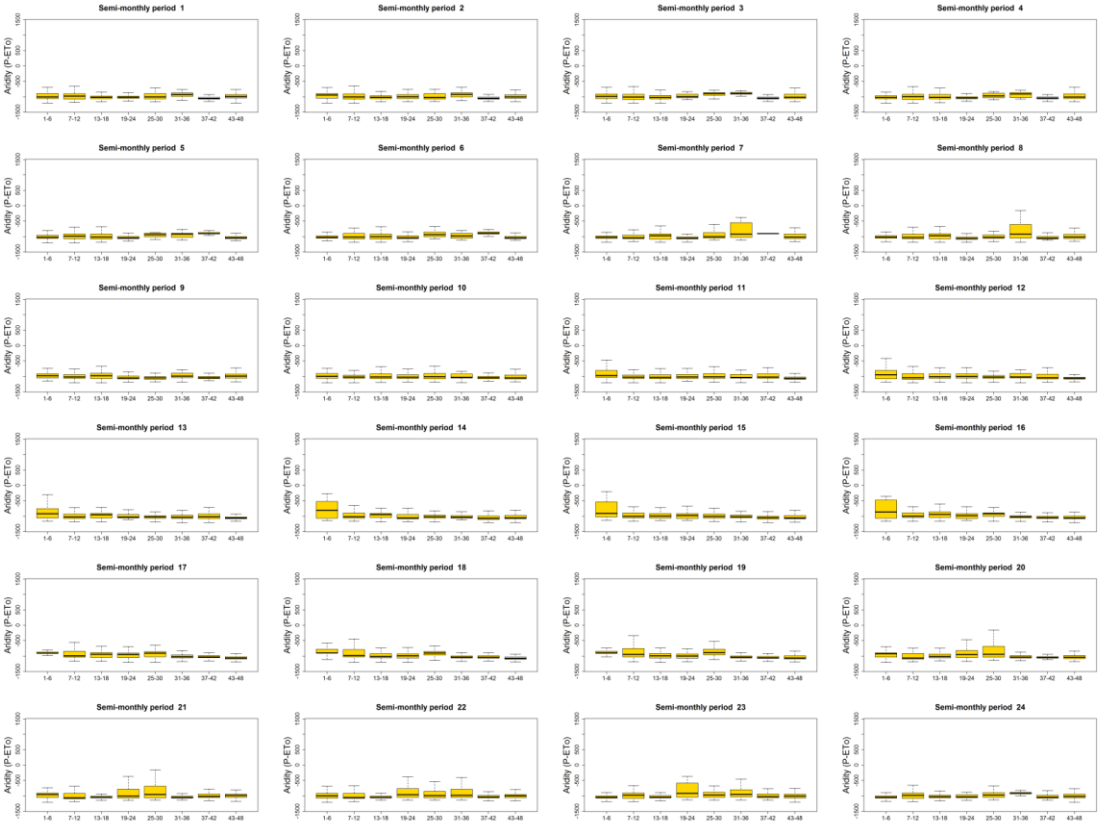

Supplementary Figure 69: Box-plots showing the values of aridity (P-ETo) for areas showing maximum correlation between SPEI and sNDVI on different time scales. Vineyards.

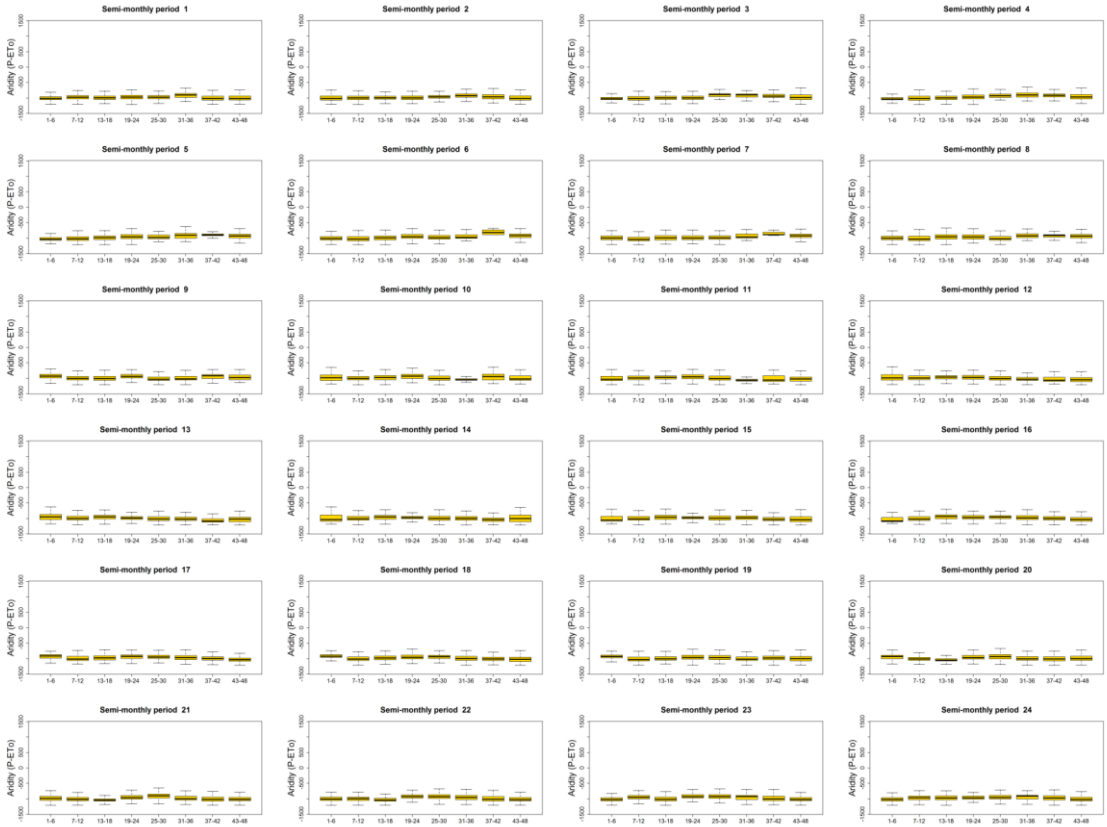

Supplementary Figure 70: Box-plots showing the values of aridity (P-ETo) for areas showing maximum correlation between SPEI and sNDVI on different time scales. Olive groves.

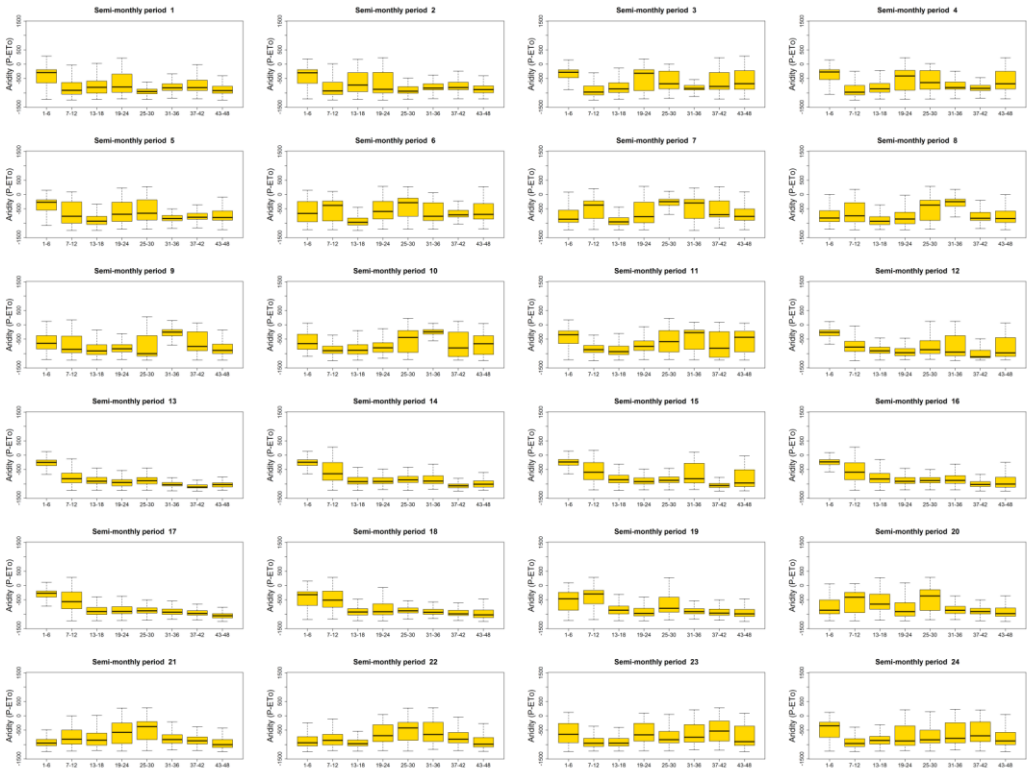

Supplementary Figure 71: Box-plots showing the values of aridity (P-ETo) for areas showing maximum correlation between SPEI and sNDVI on different time scales. Mixed agriculture/natural vegetation.

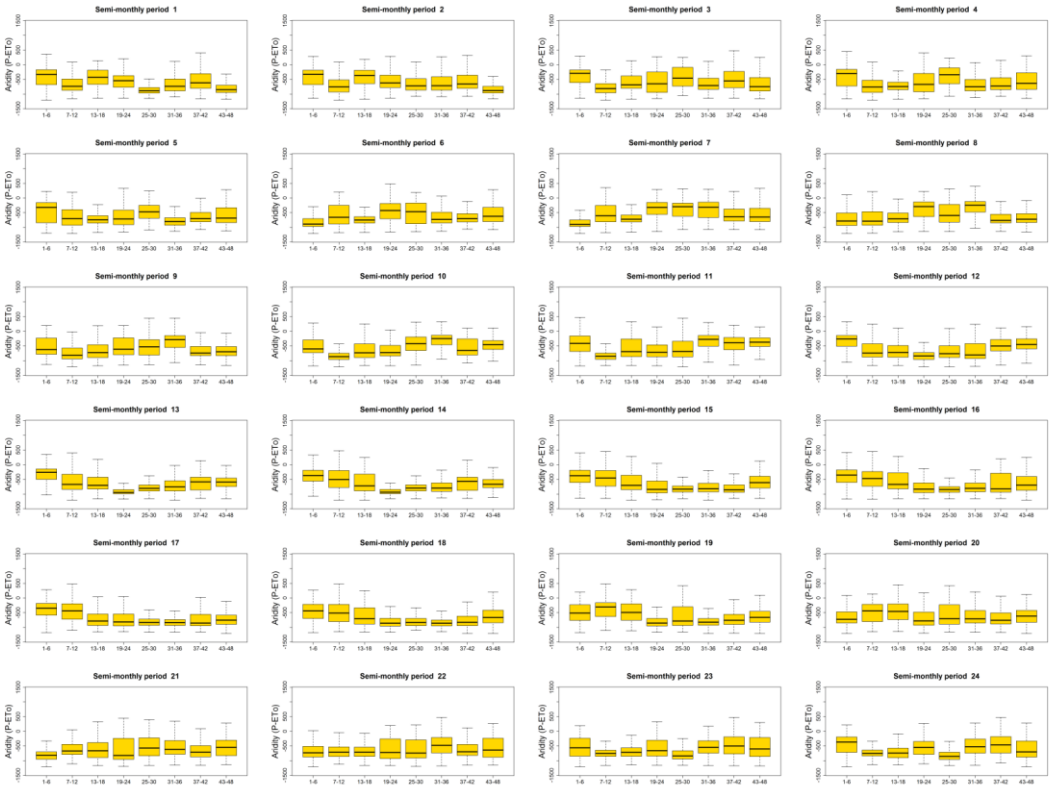

Supplementary Figure 72: Box-plots showing the values of aridity (P-ETo) for areas showing maximum correlation between SPEI and sNDVI on different time scales. Broad-leaved forests.

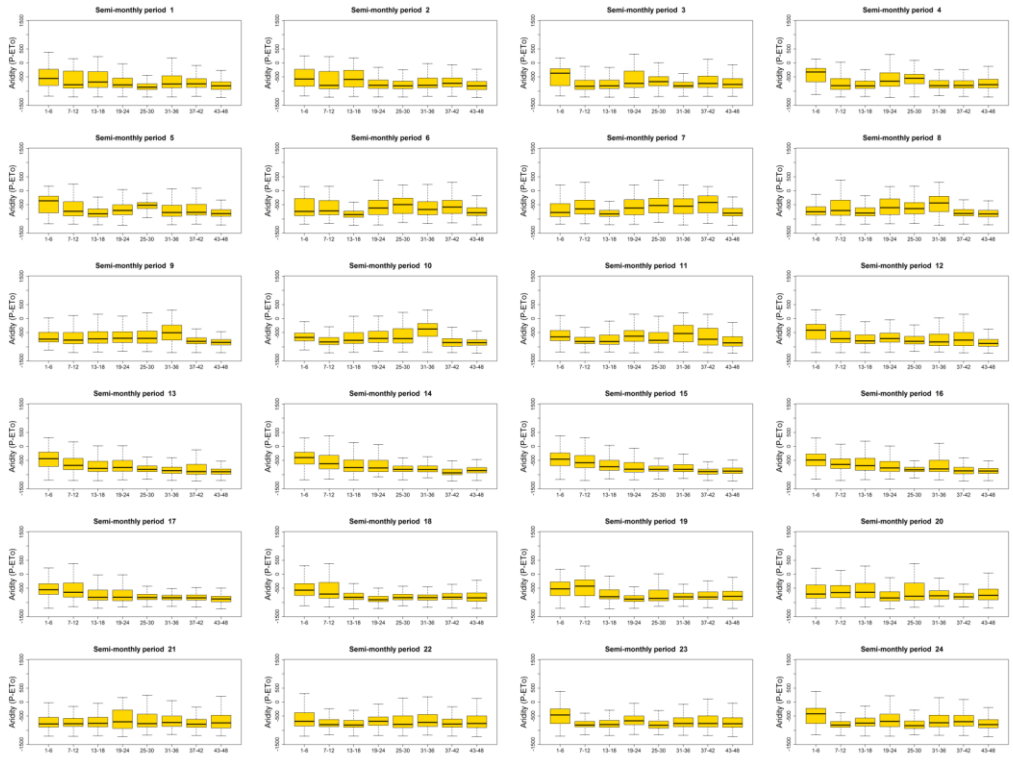

Supplementary Figure 73: Box-plots showing the values of aridity (P-ETo) for areas showing maximum correlation between SPEI and sNDVI on different time scales. Coniferous forests.

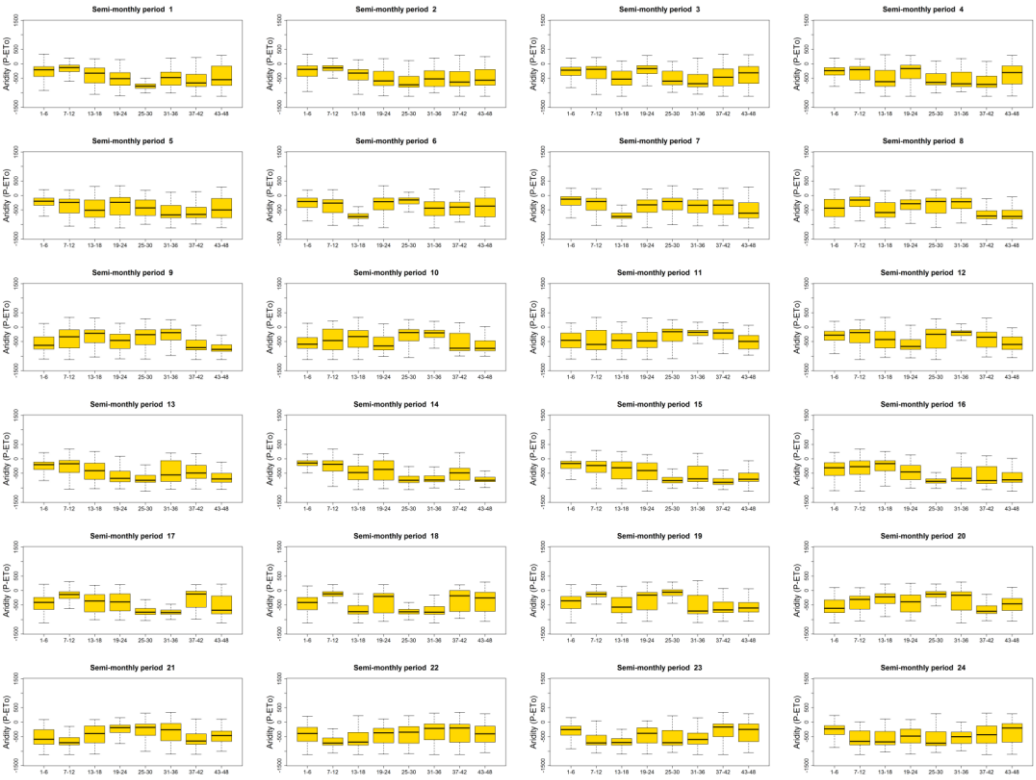

Supplementary Figure 74: Box-plots showing the values of aridity (P-ETo) for areas showing maximum correlation between SPEI and sNDVI on different time scales. Mixed forests.

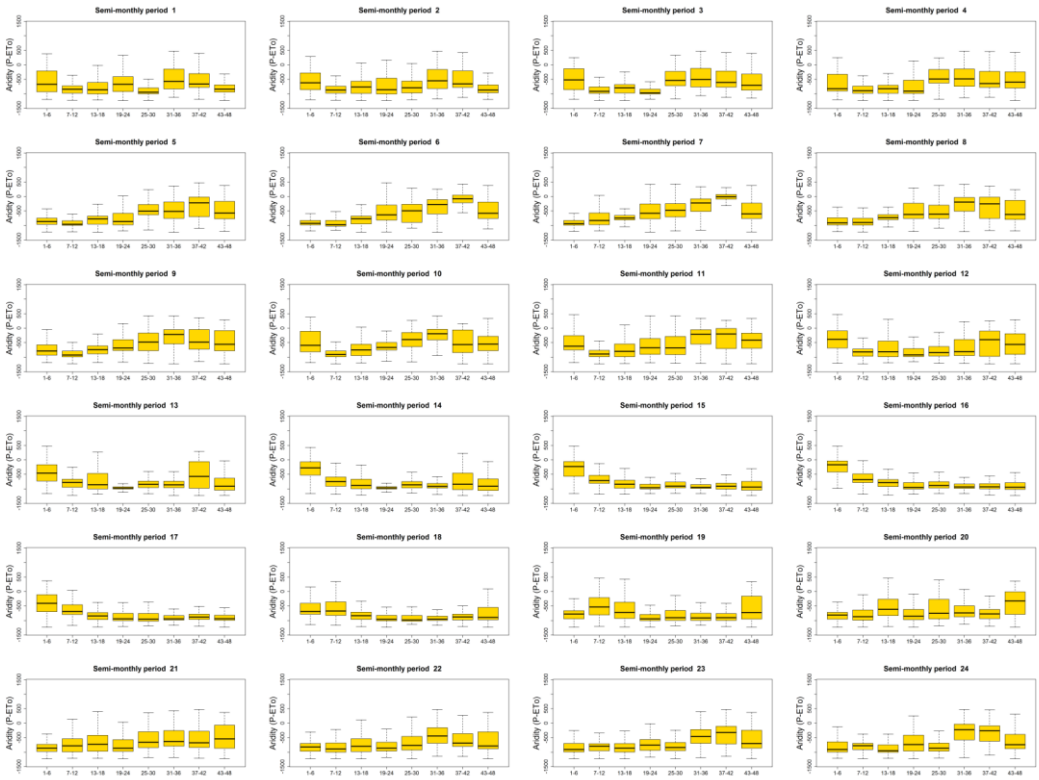

Supplementary Figure 75: Box-plots showing the values of aridity (P-ETo) for areas showing maximum correlation between SPEI and sNDVI on different time scales. Natural grassland.

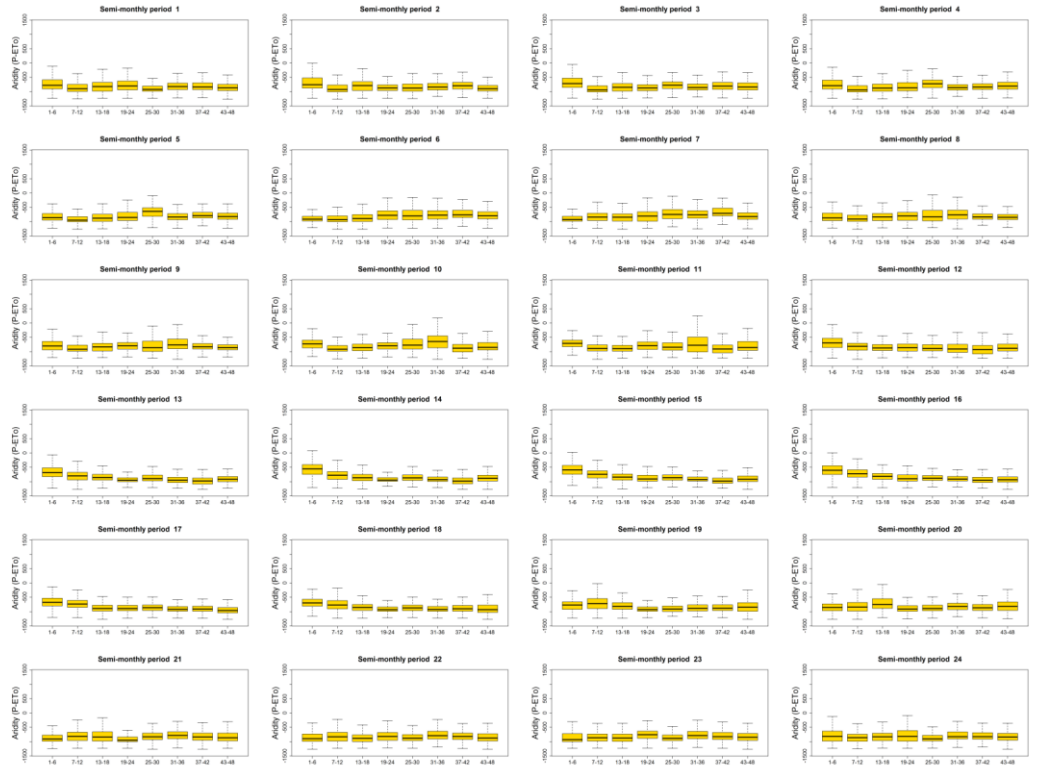

Supplementary Figure 76: Box-plots showing the values of aridity (P-ETo) for areas showing maximum correlation between SPEI and sNDVI on different time scales. Sclerophillous vegetation.

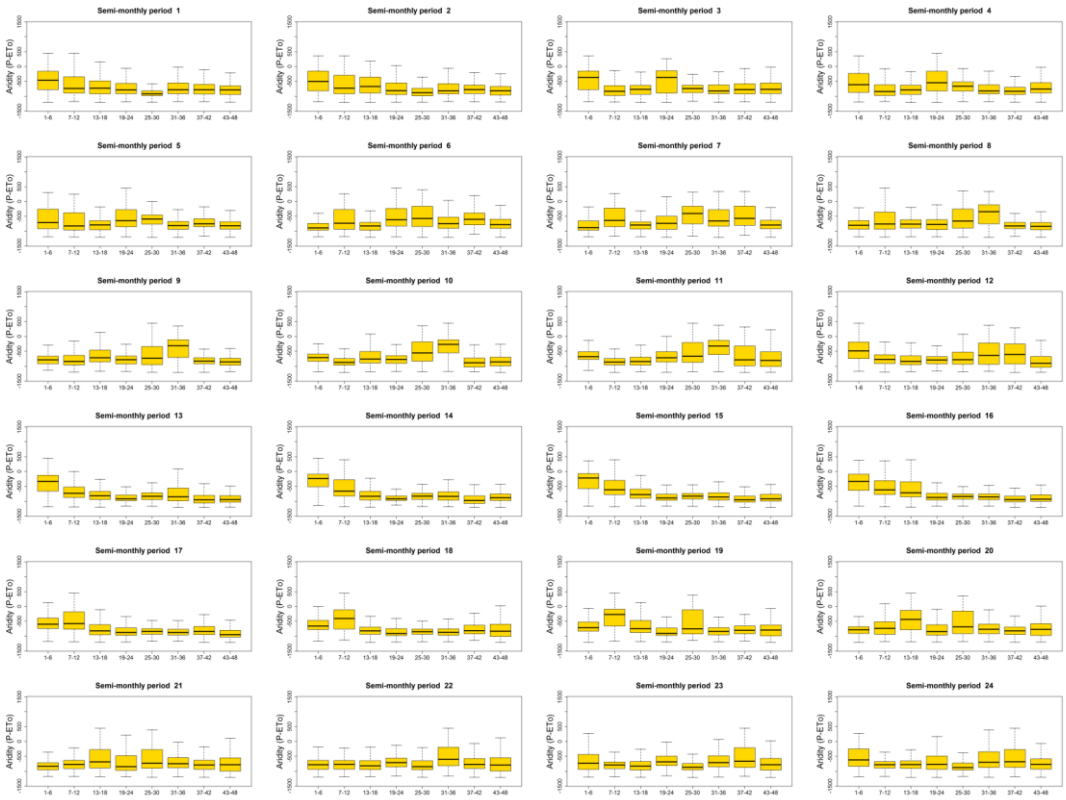

Supplementary Figure 77: Box-plots showing the values of aridity (P-ETo) for areas showing maximum correlation between SPEI and sNDVI on different time scales. Transition wood-scrub.

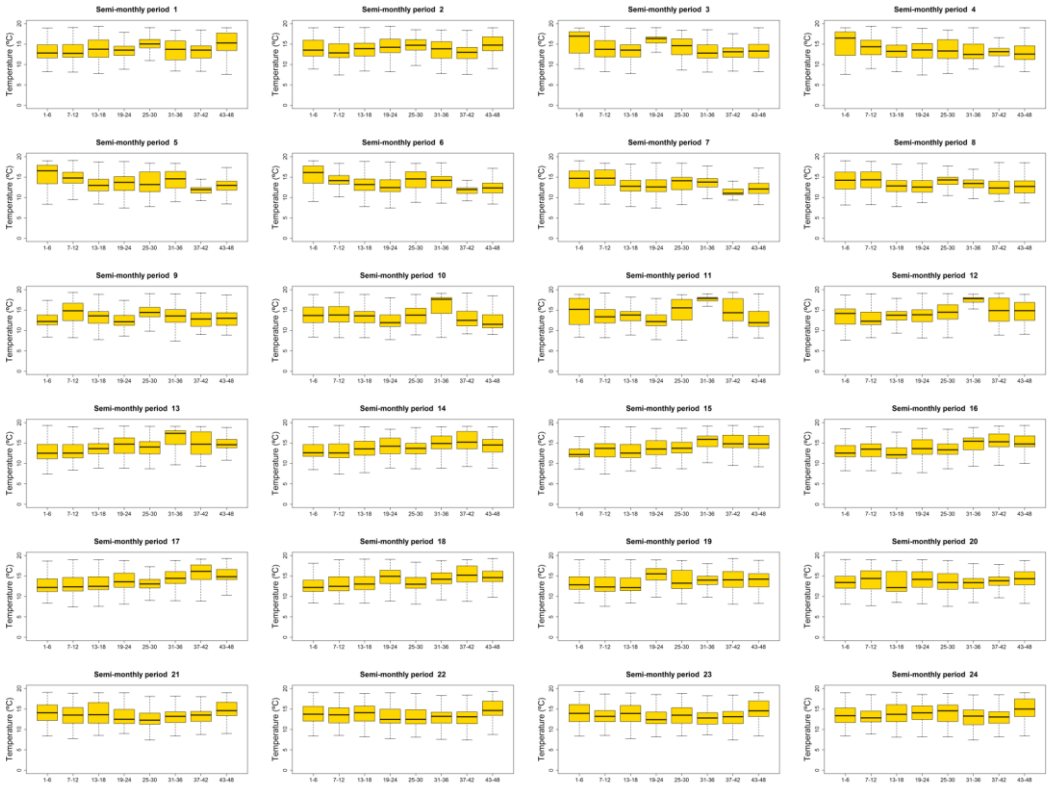

Supplementary Figure 78: Box-plots showing the values of average air temperature for areas showing maximum correlation between SPEI and sNDVI on different time scales. Non irrigated arable lands.

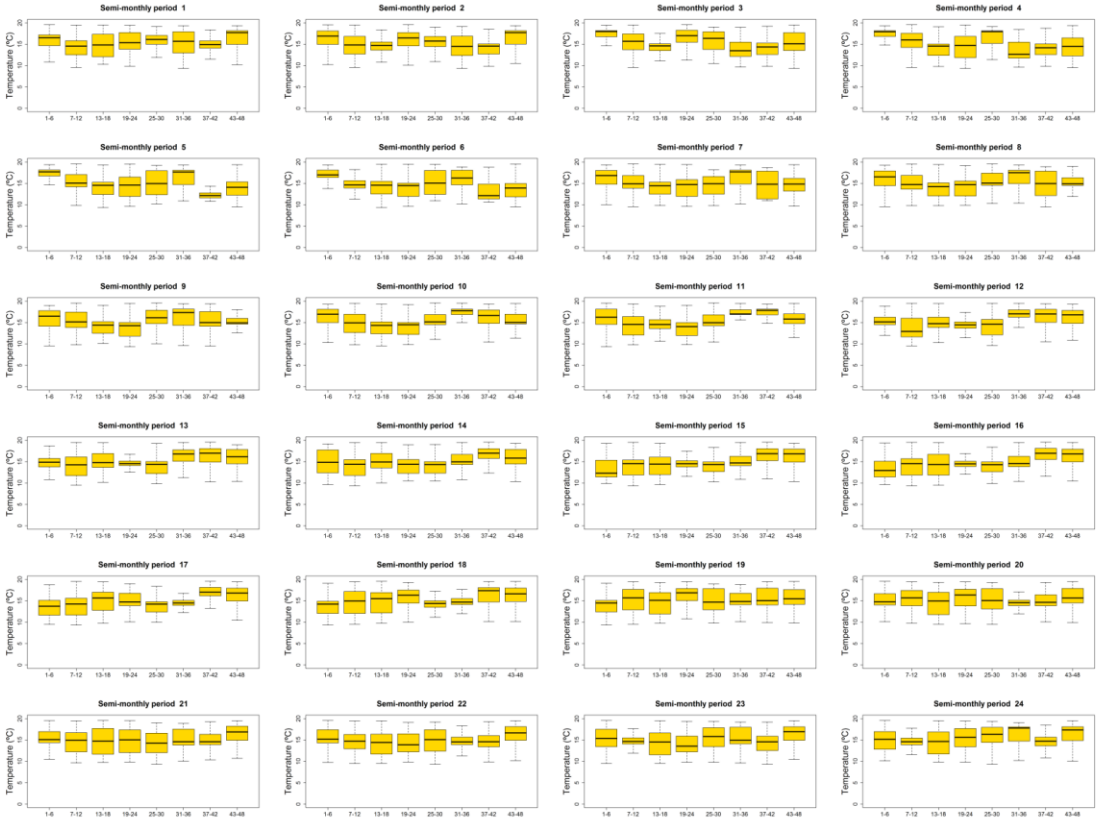

Supplementary Figure 79: Box-plots showing the values of average air temperature for areas showing maximum correlation between SPEI and sNDVI on different time scales. Irrigated lands.

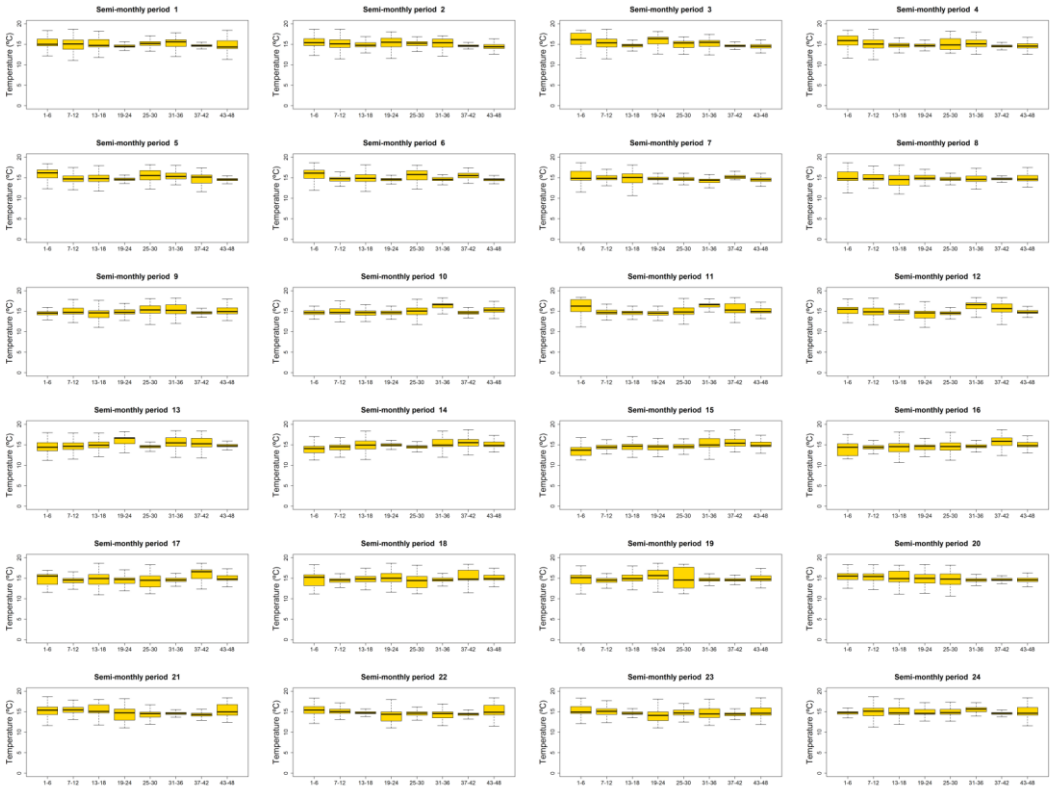

Supplementary Figure 80: Box-plots showing the values of average air temperature for areas showing maximum correlation between SPEI and sNDVI on different time scales. Vineyards.

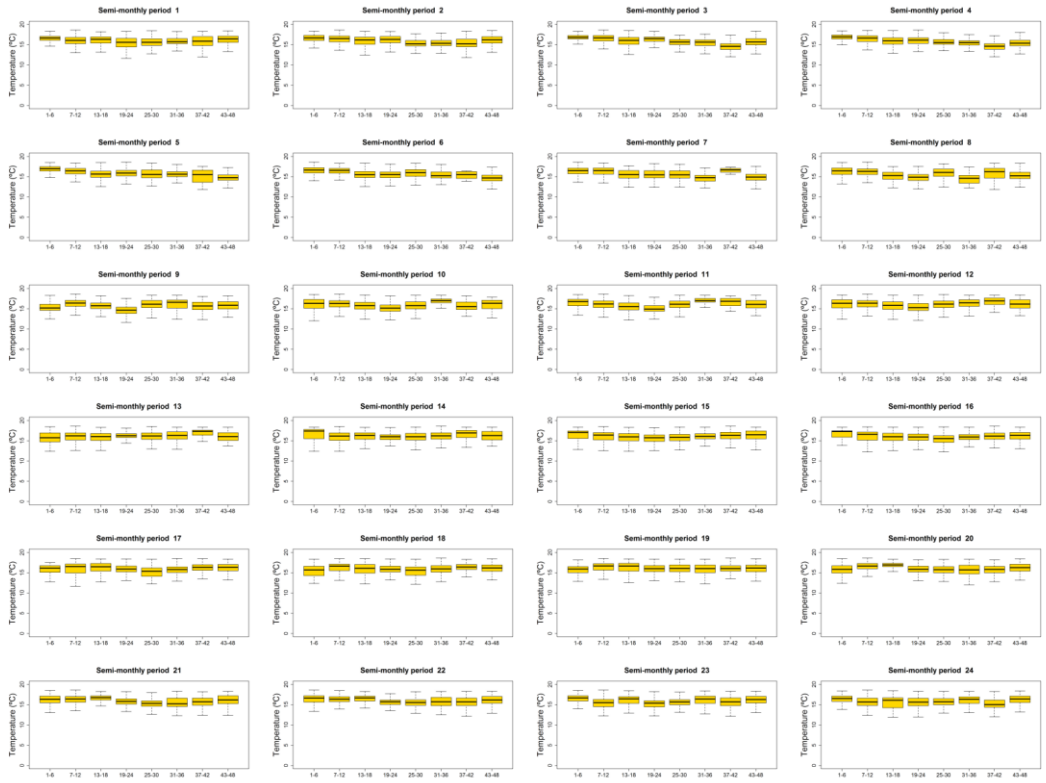

Supplementary Figure 81: Box-plots showing the values of average air temperature for areas showing maximum correlation between SPEI and sNDVI on different time scales. Olive groves.

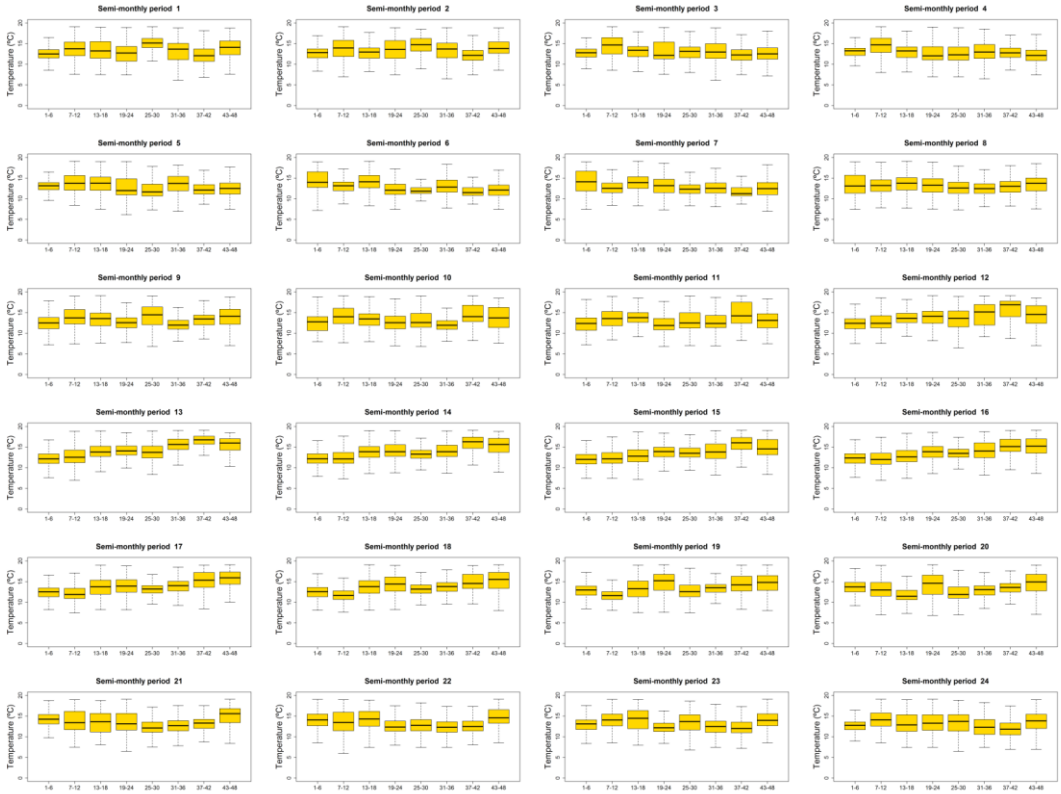

Supplementary Figure 82: Box-plots showing the values of average air temperature for areas showing maximum correlation between SPEI and sNDVI on different time scales. Mixed agriculture/natural vegetation.

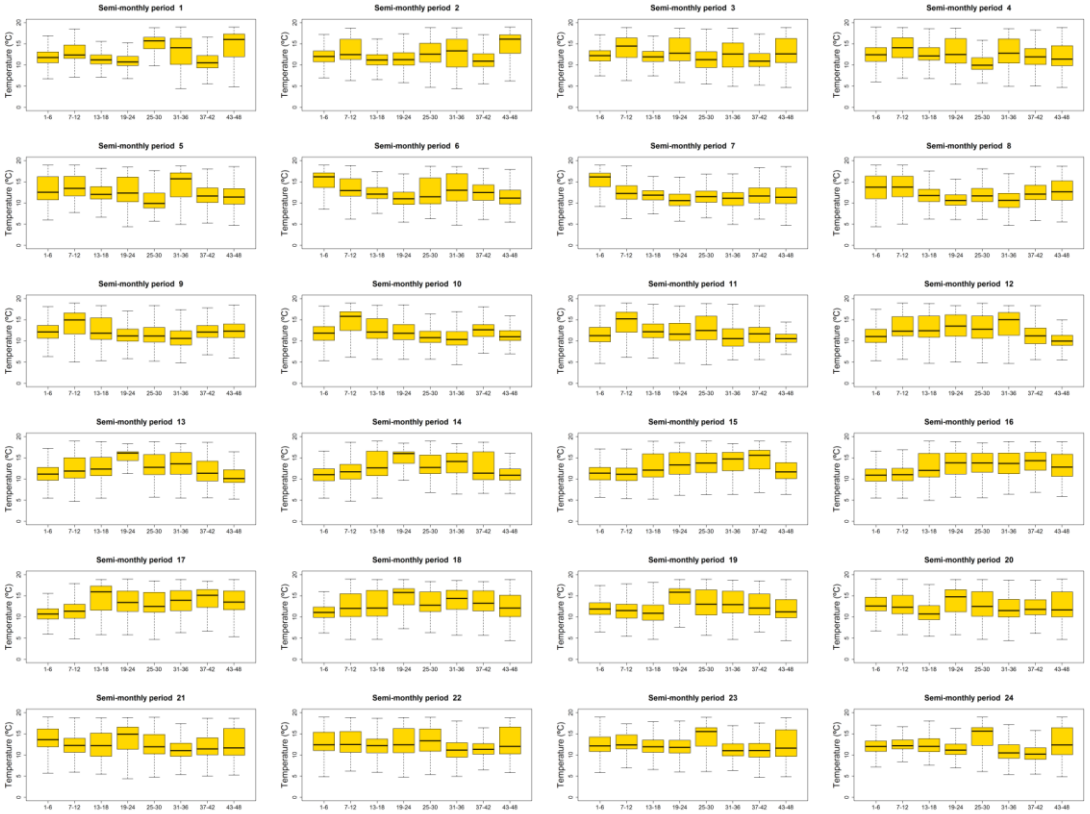

Supplementary Figure 83: Box-plots showing the values of average air temperature for areas showing maximum correlation between SPEI and sNDVI on different time scales. Broad-leaved forests.

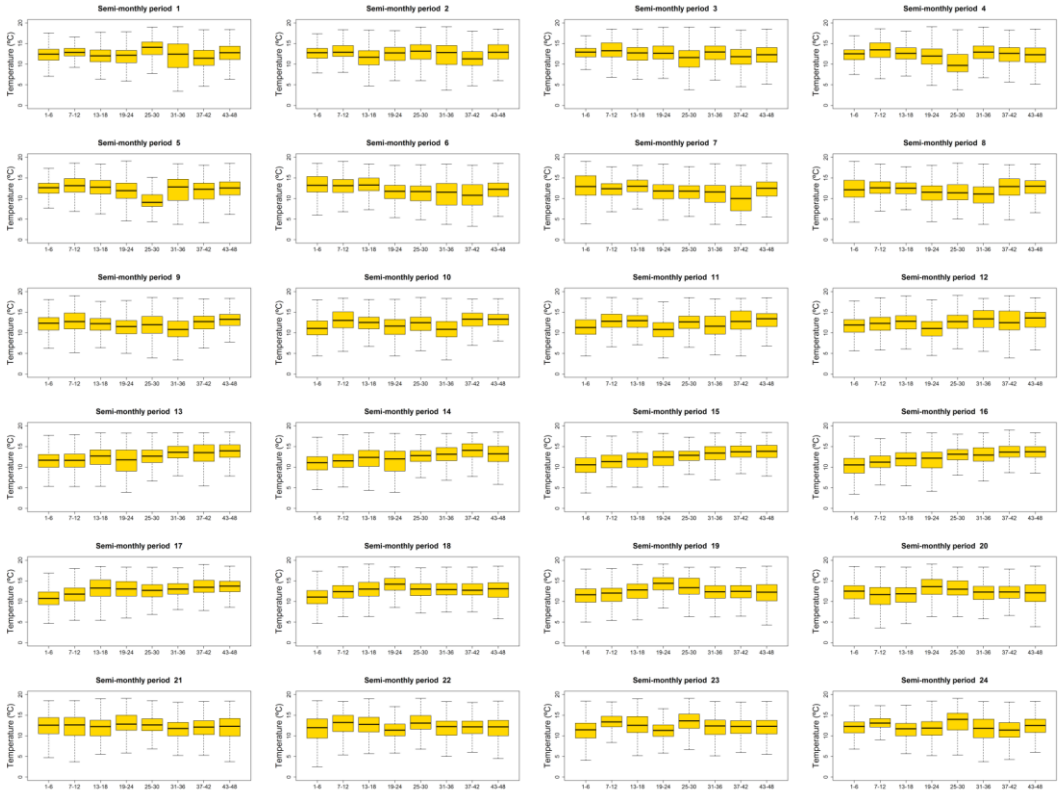

Supplementary Figure 84: Box-plots showing the values of average air temperature for areas showing maximum correlation between SPEI and sNDVI on different time scales. Coniferous forests.

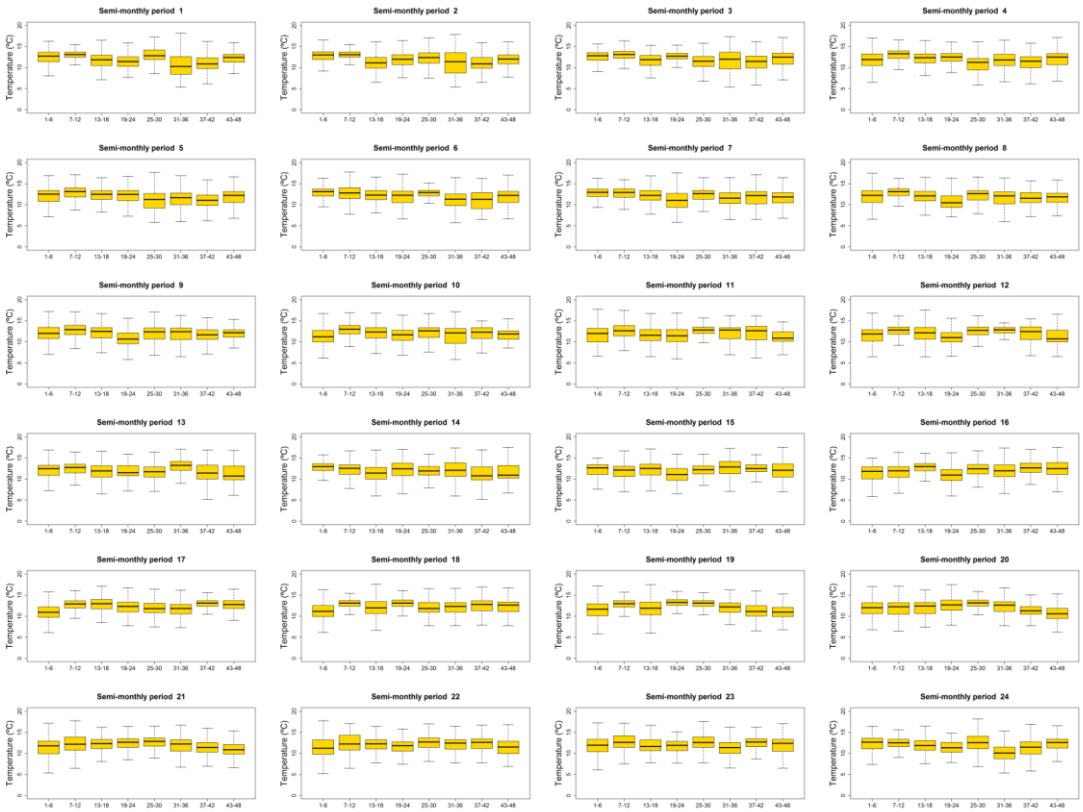

Supplementary Figure 85: Box-plots showing the values of average air temperature for areas showing maximum correlation between SPEI and sNDVI on different time scales. Mixed forests.

Supplementary Figure 86: Box-plots showing the values of average air temperature for areas showing maximum correlation between SPEI and sNDVI on different time scales. Natural grassland.

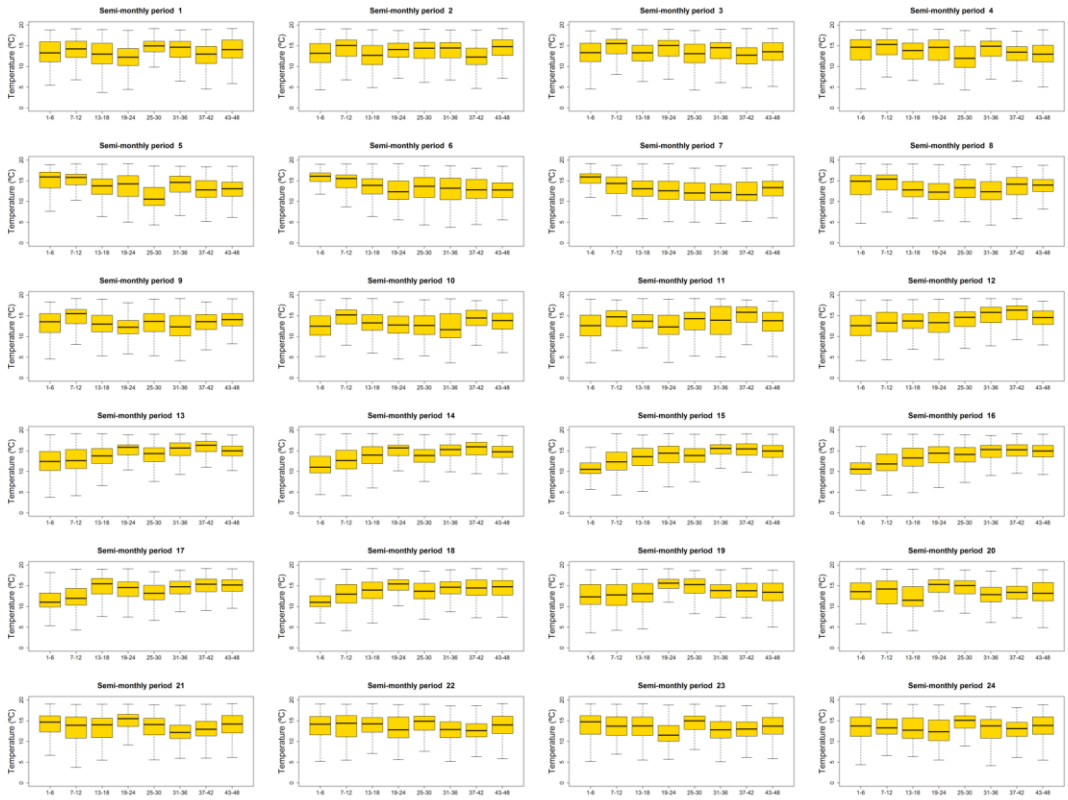

Supplementary Figure 87: Box-plots showing the values of average air temperature for areas showing maximum correlation between SPEI and sNDVI on different time scales. Sclerophillous vegetation.

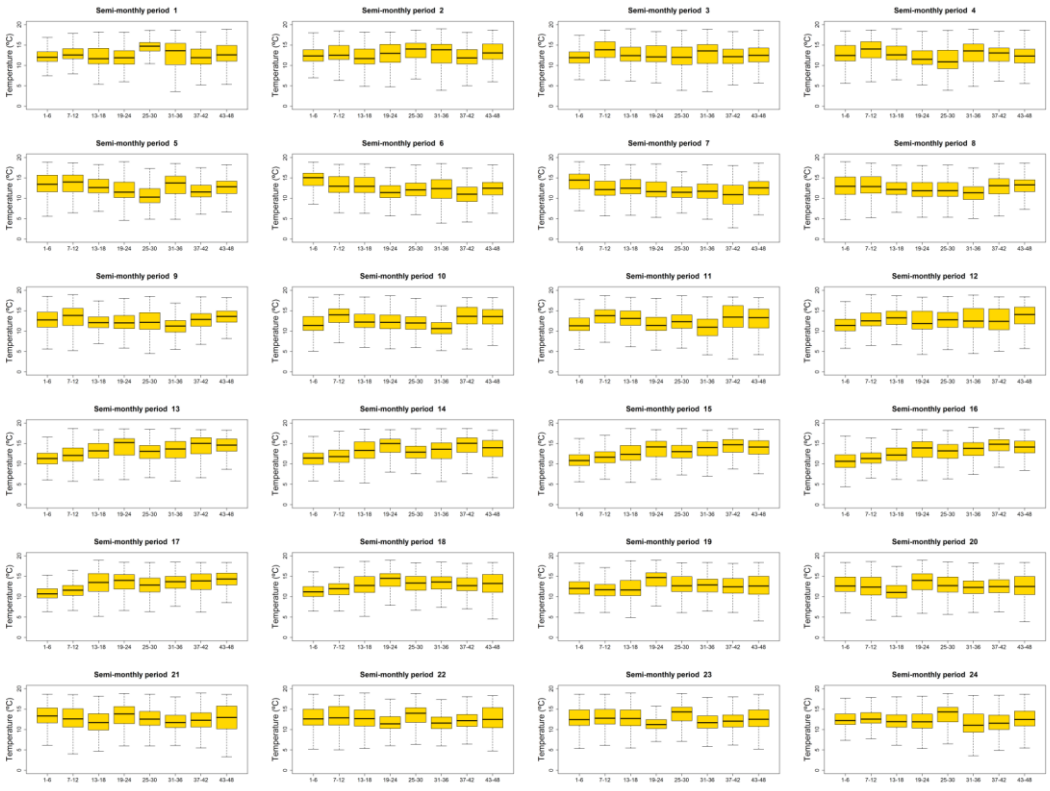

Supplementary Figure 88: Box-plots showing the values of average air temperature for areas showing maximum correlation between SPEI and sNDVI on different time scales. Transition wood-scrub.